

FAULT TOLERANT FLIGHT CONTROL APPLICATIONS FOR A FIXED  
WING UAV USING LINEAR AND NONLINEAR APPROACHES

A THESIS SUBMITTED TO  
THE GRADUATE SCHOOL OF NATURAL AND APPLIED SCIENCES  
OF  
MIDDLE EAST TECHNICAL UNIVERSITY

BY

BURAK ERGÖÇMEN

IN PARTIAL FULFILLMENT OF THE REQUIREMENTS  
FOR  
THE DEGREE OF MASTER OF SCIENCE  
IN  
AEROSPACE ENGINEERING

JANUARY 2019



Approval of the thesis:

**FAULT TOLERANT FLIGHT CONTROL APPLICATIONS FOR A FIXED  
WING UAV USING LINEAR AND NONLINEAR APPROACHES**

submitted by **BURAK ERGÖÇMEN** in partial fulfillment of the requirements for the degree of **Master of Science in Aerospace Engineering Department, Middle East Technical University** by,

Prof. Dr. Halil Kalıpçılar  
Dean, Graduate School of **Natural and Applied Sciences**

\_\_\_\_\_

Prof. Dr. İsmail H. Tuncer  
Head of Department, **Aerospace Engineering**

\_\_\_\_\_

Assoc. Prof. Dr. İlkay Yavrucuk  
Supervisor, **Aerospace Engineering Dept., METU**

\_\_\_\_\_

**Examining Committee Members:**

Prof. Dr. D. Funda Kurtuluş  
Aerospace Engineering Dept., METU

\_\_\_\_\_

Assoc. Prof. Dr. İlkay Yavrucuk  
Aerospace Engineering Dept., METU

\_\_\_\_\_

Prof. Dr. M. Kemal Leblebicioğlu  
Electrical and Electronic Engineering Dept., METU

\_\_\_\_\_

Assist. Prof. Dr. Ali Türker Kutay  
Aerospace Engineering Dept., METU

\_\_\_\_\_

Assist. Prof. Dr. Volkan Nalbantoğlu  
School of Civil Aviation, Atılım University

\_\_\_\_\_

Date: 21.01.2019

**I hereby declare that all information in this document has been obtained and presented in accordance with academic rules and ethical conduct. I also declare that, as required by these rules and conduct, I have fully cited and referenced all material and results that are not original to this work.**

Name, Surname: Burak Ergöçmen

Signature:

## ABSTRACT

### **FAULT TOLERANT FLIGHT CONTROL APPLICATIONS FOR A FIXED WING UAV USING LINEAR AND NONLINEAR APPROACHES**

Ergöçmen, Burak  
Master of Science, Aerospace Engineering  
Supervisor: Assoc. Prof. Dr. İlkey Yavrucuk

January 2019, 200 pages

Control surface or actuator faults or failures in any flight, lead to system-induced loss of control in flight (LOC-I) and results can be fatal. In this thesis, to prevent these accidents, an active fault-tolerant flight control (FTFC) is proposed. The system consists of the nonlinear control technique, state-dependent Riccati equation (SDRE) and linear controller techniques. Besides, examples for emergency cases; control surface damage, degradation, stuck and turbulence are studied for different levels. In addition, if there is a problem with regard to the construction of the state-dependent coefficient (SDC) matrices for SDRE controller, the solution is to change to a Linear Quadratic Regulator (LQR) and Linear Quadratic Tracking (LQT). To prevent these emergencies, a Reconfigure Mechanism (RM) sends signals in real-time to the SDRE controller to slow down or accelerate the control surface movement or change to LQR/LQT controller to prevent LOC-I. Comparative figures are given to illustrate the effectiveness of the hybrid controller architecture.

Keywords: Fault Tolerant Flight Control, UAV, SDRE, LQR, LQT

## ÖZ

### **DOĞRUSAL VE DOĞRUSAL OLMAYAN YAKLAŞIMLARI KULLANARAK SABİT KANATLI İHA İÇİN HATA TOLERANSLI UÇUŞ KONTROL UYGULAMALARI**

Ergöçmen, Burak  
Yüksek Lisans, Havacılık ve Uzay Mühendisliği  
Tez Danışmanı: Doç. Dr. İlkey Yavrucuk

Ocak 2019, 200 sayfa

Herhangi bir uçuşta, kontrol yüzeyi ya da akçuatör arızaları, sistem ile ilgili uçuşta kontrol kaybına yol açar ve sonuçlar ölümcül olabilir. Bu tezde, bu kazaları önlemek için, aktif hata toleranslı uçuş kontrolü (HTUK) kullanılmaktadır. Sistem, doğrusal olmayan kontrol tekniği, Duruma Bağlı Riccati Denklemi (DBRD) ve doğrusal kontrol tekniklerinden oluşur. Ayrıca, acil durumlar için örnekler; kontrol yüzeyi hasarı, indirgemesi, sıkışması ve türbülans, farklı düzeylerde incelenmiştir. Ek olarak, DBRD kontrolcüsü için duruma bağlı katsayı (SDC) matrislerinin yapımı ile ilgili bir sorun varsa, çözüm Doğrusal Karesel Düzenleyici (DKD) ve Doğrusal Karesel Referans İzleyicisine (DKİ) değişim olacaktır. Bu acil durumları önlemek için, bir Yeniden Yapılandırma Mekanizması (YM), kontrol yüzey hareketini yavaşlatmak, hızlandırmak veya uçuşta kontrol kaybını (UKK) önlemek için DKD/DKİ kontrolcüsüne geçmek için DBRD kontrolcüsüne gerçek zamanlı olarak sinyaller gönderir. Karşılaştırmalı şekiller, hibrid hata toleranslı uçuş kontrolcüsünün etkinliğini göstermek için verilmiştir.

Anahtar Kelimeler: Hata Toleranslı Uçuş Kontrolü, İHA, Duruma Bağlı Riccati Denklemi, Doğrusal Karesel Düzenleyici, Doğrusal Karesel Referans İzleyici

to my son, my daughter, my wife, my mother and my father

## ACKNOWLEDGMENTS

I would like to express my deepest and sincerest gratitude to my thesis supervisor, Assoc. Prof. Dr. İlkey Yavrucuk for his encouragements, advices, guidance, and helpfulness throughout this research work.

I would like to thank to my beloved wife Feride who strongly supported and motivated me and i thank for her love with all my heart. She, my son and my daughter give me a joy of life. I sincerely thank to my mother, Kamuran, and my father Kenan for their unique support and trust. I feel fortunate to have such a magnificent family.

I would like to express my sincere thanks to one of my best friend Kemal Öksüz. Especially during writing thesis, his support is valuable for me.

I work in a magnificent business environment. I special thank to my superior, Lieutenant Colonel Tarhan Doğan for his support and motivation to attend the courses. Besides, all personnel of Aircraft Flight Training Unit for their support and motivation.

## TABLE OF CONTENTS

ABSTRACT . . . . .	v
ÖZ . . . . .	vii
ACKNOWLEDGMENTS . . . . .	x
TABLE OF CONTENTS . . . . .	xi
LIST OF TABLES . . . . .	xix
LIST OF FIGURES . . . . .	xxi
LIST OF ABBREVIATIONS . . . . .	xxxiii
CHAPTERS	
1 INTRODUCTION . . . . .	1
1.1 Motivation of the Thesis . . . . .	1
1.2 The aim of the Thesis . . . . .	2
1.3 Introduction to FTC . . . . .	3
1.4 Faults/Failures Classification . . . . .	5
1.4.1 Faults/Failures In terms of Location . . . . .	5
1.4.2 Faults/Failures In terms of Time . . . . .	8
1.4.3 Faults/Failures In terms of a Way . . . . .	8
1.5 Literature Survey on Fault-Tolerant Control . . . . .	9
1.5.1 Passive Fault-Tolerant Control Systems (PFTCS) . . . . .	10

1.5.2	Active Fault-Tolerant Control Systems (AFTCS)	11
1.6	Literature Survey on the UAV Model	17
1.7	Contents of the Thesis	18
1.8	Contribution of the Thesis	20
2	DYNAMICS AND MATHEMATICAL MODELLING	23
2.1	Reference Frames and Coordinate Systems	23
2.2	6-DOF Equations of Motion	25
2.3	Other Equations	31
2.4	The Aircraft Model	32
2.4.1	The UAV Model	32
2.4.2	The Mode Selection (MS) block	39
2.4.2.1	Modes of an Autopilot	39
2.4.2.2	Command Filters and Rate Limiters	41
2.4.3	Atmospheric Environment	43
2.4.4	Flight Control Computer	43
2.4.5	Actuators Model	44
2.4.6	FDI/FDD	44
2.4.7	Reconfiguration Mechanism	44
2.5	Faulty and Damaged Aircraft Model	45
2.5.1	Fault Injection Block	46
2.5.2	Damaged and Faulty UAV Model	48
2.5.2.1	Faulty Control Surface Actuator	48
2.5.2.2	Faulty Engine Actuator	50

	2.5.2.3	Damaged Control Surfaces . . . . .	50
	2.5.2.4	Observability and Controllability Problem in the Controller . . . . .	52
3		LINEARIZATION AND LINEAR MODEL . . . . .	53
	3.1	Trim and Linearization . . . . .	53
	3.2	Linear Model . . . . .	55
	3.2.1	General . . . . .	55
	3.2.2	Longitudinal Dynamics . . . . .	57
	3.2.3	Lateral Dynamics . . . . .	58
	3.2.4	Linear Model in MATLAB/Simulink . . . . .	59
4		LINEAR AND NONLINEAR CONTROLLERS AND RECONFIGURATION . . . . .	61
	4.1	Linear Controller-PID . . . . .	61
	4.1.1	Heading or Roll Controller . . . . .	63
	4.1.2	Altitude or Pitch Controller . . . . .	63
	4.1.3	Yaw Rate Controller . . . . .	64
	4.1.4	Speed Controller . . . . .	65
	4.2	Linear Controller-LQR and LQT . . . . .	66
	4.2.1	Mathematical Background for LQR and LQT . . . . .	66
	4.2.2	Reference Command . . . . .	66
	4.2.3	LQR and LQT Controllers . . . . .	69
	4.2.4	Results for LQR and LQT Controller . . . . .	70
	4.3	Non-linear Controller-SDRE . . . . .	75
	4.3.1	Mathematical Background for SDRE . . . . .	75

4.3.2	SDRE Controllers in the Flight Control Computer .	78
4.3.3	Reconfiguration Mechanism for SDRE . . . . .	84
4.3.3.1	Reconfiguration of $\phi$ and $\psi$ limiter . .	85
4.3.3.2	Reconfiguration of altitude limiter . .	85
4.3.3.3	Reconfiguration of $\phi$ and $\theta$ command filters . . . . .	85
4.3.3.4	Reconfiguration of $Q_1$ and $R_1$ for $K_{T-1}$	86
4.3.3.5	Reconfiguration of $Q_2$ and $R_2$ for $K_{T-2}$ and $K_{R-2}$ . . . . .	86
4.3.3.6	Reconfiguration of Reference Commands Architecture and Decreasing Airspeed for Full Engine Shut Down . . . . .	88
4.3.3.7	SDRE or LQR/LQT, and control deriva- tive rectifier . . . . .	89
4.3.3.8	FTC Supervisor . . . . .	90
5	RESULTS FOR ACTUATOR STUCK, DEGRADATION AND FOR DAMAGED CONTROL SURFACE . . . . .	95
5.1	Emergency Case-1 Control Surface Actuator Degradation . .	95
5.1.1	Aileron Degradation . . . . .	95
5.1.1.1	The 3rd Level Degradation Without Reconfiguration . . . . .	95
5.1.1.2	The 3rd Level Degradation With Re- configuration . . . . .	97
5.1.1.3	The 4th Level Degradation Without Reconfiguration . . . . .	99
5.1.1.4	The 4th Level Degradation With Re- configuration . . . . .	101
5.1.2	Elevator Degradation . . . . .	103

5.1.2.1	The 3rd Level Degradation Without Reconfiguration . . . . .	103
5.1.2.2	The 3rd Level Degradation With Reconfiguration . . . . .	105
5.1.3	Rudder Degradation . . . . .	107
5.1.3.1	The 3rd Level Degradation Without Reconfiguration . . . . .	107
5.1.3.2	The 3rd Level Degradation With Reconfiguration . . . . .	109
5.1.3.3	The 4th Level Degradation Without Reconfiguration . . . . .	111
5.1.3.4	The 4th Level Degradation With Reconfiguration . . . . .	112
5.2	Emergency Case-2 Control Surface Actuator Stuck . . . . .	114
5.2.1	Aileron Stuck . . . . .	114
5.2.1.1	0.5 Degree Stuck Without Reconfiguration . . . . .	115
5.2.1.2	0.5 Degree Stuck With Reconfiguration	116
5.2.2	Elevator Stuck . . . . .	118
5.2.3	Rudder Stuck . . . . .	119
5.2.3.1	20 Degree Stuck Without Reconfiguration . . . . .	119
5.2.3.2	20 Degree Stuck With Reconfiguration	120
5.2.3.3	40 Degree Stuck With Reconfiguration	122
5.3	Emergency Case-3 Control Surface Damage . . . . .	124
5.3.1	Aileron Damage . . . . .	124
5.3.1.1	The 3rd Level Damage Without Reconfiguration . . . . .	124

5.3.1.2	The 3rd Level Damage With Reconfiguration . . . . .	126
5.3.1.3	The 4th level Damage Without Reconfiguration . . . . .	128
5.3.1.4	The 4th level Damage With Reconfiguration . . . . .	130
5.3.2	Elevator Damage . . . . .	132
5.3.2.1	The 3rd Level Damage Without Reconfiguration . . . . .	132
5.3.2.2	The 3rd Level Damage With Reconfiguration . . . . .	134
5.3.2.3	The 4th Level Damage Without Reconfiguration . . . . .	136
5.3.2.4	The 4th Level Damage With Reconfiguration . . . . .	138
5.3.3	Rudder Damage . . . . .	140
5.3.3.1	The 3rd Level Damage Without Reconfiguration . . . . .	140
5.3.3.2	The 3rd Level Damage With Reconfiguration . . . . .	142
5.3.3.3	The 4th Level Damage Without Reconfiguration . . . . .	144
5.3.3.4	The 4th Level Damage With Reconfiguration . . . . .	145
6	RESULTS FOR OTHER EMERGENCY SITUATIONS . . . . .	149
6.1	Emergency Case-4 Engine Full Shut down :Longitudinal Controller Exchange for Reference Command . . . . .	149
6.1.1	Engine Shut down during Level flight . . . . .	149
6.1.2	Engine Shut down during Climbing . . . . .	150

6.2	Emergency Case-5 Controllability or Observability Problem . . . . .	151
6.2.1	Controllability fault (1) during climbing about Tracker Controller-2 and without reconfiguration . . . . .	152
6.2.2	Controllability fault (2) during heading change about Tracker Controller-2 and without reconfiguration . . . . .	154
6.2.3	Controllability fault (1) during climbing about Tracker Controller-2 and with reconfiguration . . . . .	156
6.2.4	Controllability fault (2) during heading change about Tracker Controller-2 and with reconfiguration . . . . .	158
6.3	Emergency Case-6 Turbulence and Wind gust . . . . .	160
6.3.1	Moderate to Severe Turbulence condition and without reconfiguration . . . . .	160
6.3.2	Moderate to Severe Turbulence condition and with reconfiguration . . . . .	162
7	CONCLUSION . . . . .	165
7.1	Conclusion . . . . .	165
7.2	Future Work . . . . .	167
	REFERENCES . . . . .	169
	APPENDICES	
A	INTRODUCTION TO FLIGHT CONTROLS . . . . .	181
A.1	Flight Controls . . . . .	181
A.2	Airbus versus Boeing Philosophies about Flight Control Computer . . . . .	185
A.3	Loss-of-Control In-Flight (LOC-I) . . . . .	188
A.4	Aircraft Accidents Related to Loss-of-Control In-Flight (LOC-I) . . . . .	189
B	COMPARISON FOR THE UAV AND PIONEER UAV . . . . .	193

B.1	The Difference With Regard to Aerodynamic Stability Derivatives Between The UAV and Pioneer UAV . . . . .	193
C	DEFINITIONS . . . . .	195
C.1	Definitions of Fault-Tolerant . . . . .	195
C.2	Definitions of Fault-Tolerant Techniques . . . . .	196
C.2.1	Redundancy . . . . .	196
C.2.2	Diversity . . . . .	199
C.2.3	Segregation . . . . .	200

## LIST OF TABLES

### TABLES

Table 2.1	Non dimensional stability derivatives. . . . .	26
Table 2.2	Stability derivatives of the UAV in the stability axis. . . . .	34
Table 2.3	Properties of the UAV . . . . .	35
Table 2.4	Properties of the UAV control surface . . . . .	36
Table 2.5	Properties of the UAV wing, horizontal and vertical stabilizer. . . . .	36
Table 2.6	Stability derivatives of Pioneer UAV in the stability axis. . . . .	37
Table 2.7	Properties of Pioneer UAV . . . . .	38
Table 3.1	Trim values from XFLR5. . . . .	54
Table 3.2	Trim values from MATLAB/Simulink Linear Analysis Toolbox. . . . .	54
Table 3.3	Longitudinal stability derivatives formula. . . . .	56
Table 3.4	Lateral stability derivatives formula. . . . .	57
Table 3.5	Longitudinal Modes. . . . .	58
Table 3.6	Lateral Modes. . . . .	59
Table 4.1	All PID values for controllers. . . . .	66
Table 4.2	Supervisor logic. . . . .	94
Table 5.1	The solution for aileron degradation at the 3rd level. . . . .	97

Table 5.2	The solution for aileron degradation at the 4th level. . . . .	101
Table 5.3	The solution for elevator degradation at the 3rd level. . . . .	105
Table 5.4	The solution for rudder degradation at the 3rd level. . . . .	109
Table 5.5	The solution for rudder degradation at the 4th level. . . . .	113
Table 5.6	The solution for aileron stuck at 0.5 degree. . . . .	117
Table 5.7	The solution for rudder stuck at 20 degrees. . . . .	121
Table 5.8	The solution for rudder stuck at 40 degrees. . . . .	123
Table 5.9	The solution for aileron damage at the 3rd level. . . . .	127
Table 5.10	The solution for aileron damage at the 4th level. . . . .	130
Table 5.11	The solution for elevator damage at the 3rd level. . . . .	134
Table 5.12	The solution for elevator damage at the 4th level. . . . .	138
Table 5.13	The solution for rudder damage at the 3rd level. . . . .	142
Table 5.14	The solution for rudder damage at the 4th level. . . . .	146
Table 6.1	The solution for Engine Full Shut down. . . . .	149
Table 6.2	The solution for controllability and observability problem during climbing. . . . .	156
Table 6.3	The solution for controllability and observability problem during heading change. . . . .	158
Table 6.4	The solution for the turbulence problem. . . . .	163
Table B.1	The Difference With Regard to Aerodynamic Stability Derivatives Between The UAV and Pioneer UAV. . . . .	193

## LIST OF FIGURES

### FIGURES

Figure 1.1 The Photo of Airbus A300B4-203(F) hit by missile, flight OO-DLL.	2
Figure 1.2 Reconfiguration process . . . . .	3
Figure 1.3 Fault-Tolerant Techniques . . . . .	4
Figure 1.4 Dependability Tree . . . . .	5
Figure 1.5 Types of actuator failures/faults. . . . .	6
Figure 1.6 Types of sensor failures/faults. . . . .	7
Figure 1.7 Faults/Failure In terms of Time. . . . .	8
Figure 1.8 Faults/Failure In terms of Way. . . . .	8
Figure 1.9 General structure for Fault-Tolerant Control System. . . . .	10
Figure 1.10 Classification of approaches to Fault-Tolerant Flight Control. . . . .	11
Figure 1.11 MRAC architecture: (a) indirect adaptive controller; and (b) direct adaptive controller. . . . .	14
Figure 1.12 Blocks for the simulation. . . . .	19
Figure 2.1 Body-fixed Reference Frame: Forces are X, Y, Z; moments are L, M, N; components of velocity are u, v, w; rates are p, q, r. . . . .	25
Figure 2.2 Forces in stability ( $X_s, Z_s$ ) and body ( $X_b, Z_b$ ) axis. . . . .	28
Figure 2.3 Process for simulation. . . . .	30

Figure 2.4	Simulation Model. . . . .	32
Figure 2.5	The UAV model in XFLR5. . . . .	33
Figure 2.6	The UAV model in Simulink. . . . .	33
Figure 2.7	Aerodynamics block. . . . .	37
Figure 2.8	The Cg and Cp calculation in the Aerodynamic Coefficients Datum. . . . .	39
Figure 2.9	The Mode Selection of the UAV. . . . .	40
Figure 2.10	Command filters in the reference command in the FCC. . . . .	42
Figure 2.11	FCC and Reference command. . . . .	44
Figure 2.12	Inside the reconfiguration mechanism. . . . .	45
Figure 2.13	Inside The Fault injection (Control surfaces and actuators). . . . .	46
Figure 2.14	Inside The Fault injection (the engine and actuator). . . . .	47
Figure 2.15	Inside The Fault injection (Flight control computer). . . . .	48
Figure 2.16	Inside control surface actuators. . . . .	49
Figure 2.17	The actuator degraded cases. . . . .	49
Figure 2.18	Inside the engine actuator. . . . .	50
Figure 2.19	Inside Aerodynamic/ Aerodynamic Coefficients of control surfaces / aileron block. . . . .	51
Figure 2.20	Aileron damage cases. . . . .	52
Figure 2.21	ARE calculator in the controller. . . . .	52
Figure 4.1	PID controller for Autopilot. . . . .	62
Figure 4.2	PID Tuner in MATLAB/Simulink. . . . .	62
Figure 4.3	Heading Controller. . . . .	63

Figure 4.4	Altitude or Pitch Controller. . . . .	64
Figure 4.5	Yaw Rate Controller. . . . .	65
Figure 4.6	Speed Controller. . . . .	65
Figure 4.7	LQR and LQT Controller. . . . .	67
Figure 4.8	Inside the reference command. . . . .	67
Figure 4.9	$\theta_{ref}$ and $\delta_t$ Controller-1. . . . .	68
Figure 4.10	$\theta_{ref}$ and $\delta_t$ Controller-2. . . . .	68
Figure 4.11	$\psi_{ref}$ Controller. . . . .	69
Figure 4.12	Altitude and vertical speed during climbing. . . . .	70
Figure 4.13	Control surface deflection during altitude change. . . . .	70
Figure 4.14	Air speed and throttle command during climbing. . . . .	71
Figure 4.15	Heading ( $\psi$ ) and roll angle ( $\phi$ ) responses during heading change. . . . .	71
Figure 4.16	Alpha and beta angle responses during heading change. . . . .	72
Figure 4.17	Altitude and Airspeed responses during heading change. . . . .	72
Figure 4.18	Control surface deflection during heading change. . . . .	72
Figure 4.19	Airspeed and throttle responses during airspeed change. . . . .	73
Figure 4.20	Altitude and alpha angle responses during airspeed change. . . . .	73
Figure 4.21	Control surface deflection during airspeed change. . . . .	73
Figure 4.22	Euler angles and altitude responses during airspeed, altitude and heading change. . . . .	74
Figure 4.23	Airspeed and throttle command responses during airspeed, altitude and heading change. . . . .	74

Figure 4.24 Alpha and beta angle responses during airspeed, altitude and heading change. . . . .	75
Figure 4.25 Control surface deflection during airspeed, altitude and heading change. . . . .	75
Figure 4.26 Mathematical methods for solving ARE. . . . .	77
Figure 4.27 SDRE Controller. . . . .	78
Figure 4.28 SDRE Calculator in the controller. . . . .	79
Figure 4.29 Controllability controller in SDRE calculator. . . . .	83
Figure 4.30 Reconfiguration Mechanism. . . . .	84
Figure 4.31 Reconfiguration of $Q_2$ and $R_2$ for $K_{T-2}$ and $K_{R-2}$ . . . . .	87
Figure 4.32 Turbulence part of the reconfiguration of $Q_2$ and $R_2$ for $K_{T-2}$ and $K_{R-2}$ . . . . .	88
Figure 4.33 Observability controller in SDRE calculator. . . . .	89
Figure 4.34 SDRE or LQR/LQT mechanism. . . . .	89
Figure 4.35 Control derivative rectifier. . . . .	90
Figure 4.36 Reconfiguration Mechanism with SDRE controller, command filters and rate limiters. . . . .	92
Figure 4.37 Summary for reconfiguration strategies. . . . .	93
Figure 5.1 Altimeter and $\theta$ , $\alpha$ responses without reconfiguration. . . . .	96
Figure 5.2 Airspeed and throttle responses without reconfiguration. . . . .	96
Figure 5.3 $\psi$ and $\phi$ responses without reconfiguration. . . . .	96
Figure 5.4 Actuator responses without reconfiguration. . . . .	97
Figure 5.5 Altimeter and $\theta$ , $\alpha$ responses with reconfiguration. . . . .	98

Figure 5.6	Airspeed and throttle responses and with reconfiguration. . . . .	98
Figure 5.7	$\psi$ and $\phi$ responses with reconfiguration. . . . .	98
Figure 5.8	Actuator responses with reconfiguration. . . . .	99
Figure 5.9	Altimeter and $\theta$ , $\alpha$ responses without reconfiguration. . . . .	99
Figure 5.10	Airspeed and throttle responses without reconfiguration. . . . .	100
Figure 5.11	$\psi$ and $\phi$ responses without reconfiguration. . . . .	100
Figure 5.12	Actuator responses without reconfiguration. . . . .	100
Figure 5.13	Altimeter and $\theta$ , $\alpha$ responses with reconfiguration. . . . .	102
Figure 5.14	Airspeed and throttle responses with reconfiguration. . . . .	102
Figure 5.15	$\psi$ and $\phi$ responses with reconfiguration. . . . .	102
Figure 5.16	Actuator responses with reconfiguration. . . . .	103
Figure 5.17	Altimeter and vertical speed responses without reconfiguration. . .	103
Figure 5.18	Airspeed and throttle responses without reconfiguration. . . . .	104
Figure 5.19	$\theta$ , $\alpha$ and $\phi$ responses without reconfiguration. . . . .	104
Figure 5.20	Actuator responses without reconfiguration. . . . .	104
Figure 5.21	Altimeter and vertical speed responses with reconfiguration. . . . .	105
Figure 5.22	Airspeed and throttle responses with reconfiguration. . . . .	106
Figure 5.23	$\theta$ , $\alpha$ and $\phi$ responses with reconfiguration. . . . .	106
Figure 5.24	Actuator responses with reconfiguration. . . . .	106
Figure 5.25	Altimeter and $\theta$ , $\alpha$ responses without reconfiguration. . . . .	107
Figure 5.26	Airspeed and throttle responses without reconfiguration. . . . .	108
Figure 5.27	$\psi$ and $\phi$ responses without reconfiguration. . . . .	108

Figure 5.28 Actuator responses without reconfiguration. . . . .	108
Figure 5.29 Altimeter and $\theta, \alpha$ responses with reconfiguration. . . . .	109
Figure 5.30 Airspeed and throttle responses with reconfiguration. . . . .	110
Figure 5.31 $\psi$ and $\phi$ responses with reconfiguration. . . . .	110
Figure 5.32 Actuator responses with reconfiguration. . . . .	110
Figure 5.33 Altimeter and $\theta, \alpha$ responses without reconfiguration. . . . .	111
Figure 5.34 Airspeed and throttle responses without reconfiguration. . . . .	111
Figure 5.35 $\psi$ and $\phi$ responses without reconfiguration. . . . .	112
Figure 5.36 Actuator responses without reconfiguration. . . . .	112
Figure 5.37 Altimeter and $\theta, \alpha$ responses with reconfiguration. . . . .	113
Figure 5.38 Airspeed and throttle responses with reconfiguration. . . . .	113
Figure 5.39 $\psi$ and $\phi$ responses with reconfiguration. . . . .	114
Figure 5.40 Actuator responses with reconfiguration. . . . .	114
Figure 5.41 Altimeter and $\theta, \alpha$ responses without reconfiguration. . . . .	115
Figure 5.42 Airspeed and throttle responses without reconfiguration. . . . .	115
Figure 5.43 $\psi$ and $\phi$ responses without reconfiguration. . . . .	116
Figure 5.44 Actuator responses without reconfiguration. . . . .	116
Figure 5.45 Altimeter and $\theta, \alpha$ responses with reconfiguration. . . . .	117
Figure 5.46 Airspeed and throttle responses with reconfiguration. . . . .	117
Figure 5.47 $\psi$ and $\phi$ responses with reconfiguration. . . . .	118
Figure 5.48 Actuator responses with reconfiguration. . . . .	118
Figure 5.49 Altimeter and $\theta, \alpha$ responses without reconfiguration. . . . .	119

Figure 5.50	Airspeed and throttle responses without reconfiguration. . . . .	119
Figure 5.51	$\psi$ and $\phi$ responses without reconfiguration. . . . .	120
Figure 5.52	Actuator responses without reconfiguration. . . . .	120
Figure 5.53	Altimeter and $\theta$ , $\alpha$ responses with reconfiguration. . . . .	121
Figure 5.54	Airspeed and throttle responses with reconfiguration. . . . .	121
Figure 5.55	$\psi$ and $\phi$ responses with reconfiguration. . . . .	122
Figure 5.56	Actuator responses with reconfiguration. . . . .	122
Figure 5.57	Altimeter and $\theta$ , $\alpha$ responses with reconfiguration. . . . .	123
Figure 5.58	Airspeed and throttle responses with reconfiguration. . . . .	123
Figure 5.59	$\psi$ and $\phi$ responses with reconfiguration. . . . .	124
Figure 5.60	Actuator responses with reconfiguration. . . . .	124
Figure 5.61	Altimeter and $\theta$ , $\alpha$ responses without reconfiguration. . . . .	125
Figure 5.62	Airspeed and throttle responses without reconfiguration. . . . .	125
Figure 5.63	$\psi$ and $\phi$ responses without reconfiguration. . . . .	126
Figure 5.64	Actuator responses without reconfiguration. . . . .	126
Figure 5.65	Altimeter and $\theta$ , $\alpha$ responses with reconfiguration. . . . .	127
Figure 5.66	Airspeed and throttle responses with reconfiguration. . . . .	127
Figure 5.67	$\psi$ and $\phi$ responses with reconfiguration. . . . .	128
Figure 5.68	Actuator responses with reconfiguration. . . . .	128
Figure 5.69	Altimeter and $\theta$ , $\alpha$ responses without reconfiguration. . . . .	129
Figure 5.70	Airspeed and throttle responses without reconfiguration. . . . .	129
Figure 5.71	$\psi$ and $\phi$ responses without reconfiguration. . . . .	129

Figure 5.72 Actuator responses without reconfiguration. . . . .	130
Figure 5.73 Altimeter and $\theta$ , $\alpha$ responses with reconfiguration. . . . .	131
Figure 5.74 Airspeed and throttle responses with reconfiguration. . . . .	131
Figure 5.75 $\psi$ and $\phi$ responses with reconfiguration. . . . .	131
Figure 5.76 Actuator responses with reconfiguration. . . . .	132
Figure 5.77 Altimeter and vertical speed responses without reconfiguration. . .	133
Figure 5.78 Airspeed and throttle responses without reconfiguration. . . . .	133
Figure 5.79 $\theta$ , $\alpha$ and $\Phi$ responses without reconfiguration. . . . .	133
Figure 5.80 Actuator responses without reconfiguration. . . . .	134
Figure 5.81 Altimeter and vertical speed responses with reconfiguration. . . . .	135
Figure 5.82 Airspeed and throttle responses with reconfiguration. . . . .	135
Figure 5.83 $\theta$ , $\alpha$ and $\phi$ responses with reconfiguration. . . . .	135
Figure 5.84 Actuator responses with reconfiguration. . . . .	136
Figure 5.85 Altimeter and vertical speed responses without reconfiguration. . .	136
Figure 5.86 Airspeed and throttle responses without reconfiguration. . . . .	137
Figure 5.87 $\theta$ , $\alpha$ and $\phi$ responses without reconfiguration. . . . .	137
Figure 5.88 Actuator responses without reconfiguration. . . . .	137
Figure 5.89 Altimeter and vertical speed responses with reconfiguration. . . . .	138
Figure 5.90 Airspeed and throttle responses with reconfiguration. . . . .	139
Figure 5.91 $\theta$ , $\alpha$ and $\phi$ responses with reconfiguration. . . . .	139
Figure 5.92 Actuator responses with reconfiguration. . . . .	139
Figure 5.93 Altimeter and $\theta$ , $\alpha$ responses without reconfiguration. . . . .	140

Figure 5.94	Airspeed and throttle responses without reconfiguration. . . . .	141
Figure 5.95	$\psi$ and $\phi$ responses without reconfiguration. . . . .	141
Figure 5.96	Actuator responses without reconfiguration. . . . .	141
Figure 5.97	Altimeter and $\theta$ , $\alpha$ responses with reconfiguration. . . . .	142
Figure 5.98	Airspeed and throttle responses with reconfiguration. . . . .	143
Figure 5.99	$\psi$ and $\phi$ responses with reconfiguration. . . . .	143
Figure 5.100	Actuator responses with reconfiguration. . . . .	143
Figure 5.101	Altimeter and $\theta$ , $\alpha$ responses without reconfiguration. . . . .	144
Figure 5.102	Airspeed and throttle responses without reconfiguration. . . . .	144
Figure 5.103	$\psi$ and $\phi$ responses without reconfiguration. . . . .	145
Figure 5.104	Actuator responses without reconfiguration. . . . .	145
Figure 5.105	Altimeter and $\theta$ , $\alpha$ responses with reconfiguration. . . . .	146
Figure 5.106	Airspeed and throttle responses with reconfiguration. . . . .	147
Figure 5.107	$\psi$ and $\phi$ responses with reconfiguration. . . . .	147
Figure 5.108	Actuator responses with reconfiguration. . . . .	147
Figure 6.1	Airspeed and altitude responses during level flight for full engine shut down. . . . .	150
Figure 6.2	Throttle command and $\alpha$ , $\theta$ responses during level flight for full engine shut down. . . . .	150
Figure 6.3	Airspeed and altimeter responses during climb for full engine shut down. . . . .	151
Figure 6.4	Throttle command and $\alpha$ and $\theta$ responses during climb for full engine shut down. . . . .	151

Figure 6.5 Altimeter and $\theta$ , $\alpha$ responses and reconfiguration for algorithm does not occur. . . . .	152
Figure 6.6 Airspeed and throttle responses and reconfiguration for algorithm does not occur. . . . .	153
Figure 6.7 Actuator responses and reconfiguration for algorithm does not occur.	153
Figure 6.8 The controller algorithm and reconfiguration for algorithm does not occur. . . . .	153
Figure 6.9 Altimeter and $\theta$ , $\alpha$ responses and reconfiguration for algorithm does not occur. . . . .	154
Figure 6.10 Airspeed and throttle responses and reconfiguration for algorithm does not occur. . . . .	154
Figure 6.11 $\psi$ and $\phi$ responses and reconfiguration for algorithm does not occur.	155
Figure 6.12 Actuator responses and reconfiguration for algorithm does not occur.	155
Figure 6.13 The controller algorithm and reconfiguration for algorithm does not occur. . . . .	155
Figure 6.14 Altimeter and $\theta$ , $\alpha$ responses and reconfiguration for algorithm occurs. . . . .	157
Figure 6.15 Airspeed and throttle responses and reconfiguration for algorithm occurs. . . . .	157
Figure 6.16 Actuator responses and reconfiguration for algorithm occurs. . . . .	157
Figure 6.17 Controller algorithm and reconfiguration for algorithm occurs. . . . .	158
Figure 6.18 Altimeter and $\theta$ , $\alpha$ responses and reconfiguration for algorithm occurs. . . . .	159
Figure 6.19 Airspeed and throttle responses and reconfiguration for algorithm occurs. . . . .	159

Figure 6.20 $\psi$ and $\phi$ responses and reconfiguration for algorithm occurs. . . . .	159
Figure 6.21 Actuator responses and reconfiguration for algorithm occurs. . . . .	160
Figure 6.22 Controller algorithm during and reconfiguration for algorithm occurs.	160
Figure 6.23 Altitude and air speed responses and reconfiguration for algorithm does not occur. . . . .	161
Figure 6.24 $\theta$ and $\alpha$ responses and reconfiguration for algorithm does not occur.	161
Figure 6.25 $\phi$ and $\psi$ responses and reconfiguration for algorithm does not occur.	162
Figure 6.26 Control surface deflection and reconfiguration for algorithm does not occur. . . . .	162
Figure 6.27 Altitude and air speed responses and reconfiguration for algorithm occurs. . . . .	163
Figure 6.28 $\theta$ and $\alpha$ responses and reconfiguration for algorithm occurs. . . . .	163
Figure 6.29 $\phi$ and $\psi$ responses and reconfiguration for algorithm occurs. . . . .	164
Figure 6.30 Control surface deflection and reconfiguration for algorithm occurs.	164
Figure A.1 Aircraft flight controls. . . . .	181
Figure A.2 Global Hawk UAV Flight Controls. . . . .	182
Figure A.3 Mechanical systems. . . . .	182
Figure A.4 Hydromechanical systems. . . . .	183
Figure A.5 Fly-by-wire systems (FBW) . . . . .	183
Figure A.6 Flight Control Computers for A320 . . . . .	186
Figure A.7 Roll Control for Airbus A320. . . . .	186
Figure A.8 Pitch Control for Airbus A320. . . . .	187
Figure A.9 Yaw Control for Airbus A320. . . . .	187

Figure A.10 Flight Control Computers for B777. . . . . 188

Figure C.1 Sensor direct (hardware) redundancy and Voting System for Sensors 197

Figure C.2 Actuator direct (hardware) redundancy for control surfaces. . . . . 198

Figure C.3 Recovery Blocks . . . . . 199

## LIST OF ABBREVIATIONS

ADC	Air Data Computer
ADIRU	Air Data Inertial Reference Unit
AFTCS	Active Fault Tolerant Control Systems
AHRS	Attitude and Heading Reference Unit
AirSTAR	Airborne Subscale Transport Aircraft Research
AI	Artificial Intelligence
ALT SEL	Altitude Select
ANDI	Adaptive Nonlinear Dynamic Inversion
ANN	Artificial Neural Network
ARE	Algebraic Riccati Equation
BFF	Body Freedom Flutter
CA	Control Allocation
CFD	Computational Fluid Dynamics
C <sub>g</sub>	Center of Gravity
COESA	Committee on Extension to the Standard Atmosphere
C <sub>p</sub>	Center of Pressure
DATCOM	Data Compendium
DCM	Direction Cosine Matrix
DFBW	Digital Fly-By-Wire
DME	Distance Measurement Equipment
DOF	Degrees of freedom
EA	Eigenstructure Assignment
EHA	Electric Actuators With Hydrostatic Transmission
ELAC	Elevator and Aileron Computers

EMA	Electric Actuators With Mechanical Transmission
FAA	Federal Aviation Administration
FAC	Rudder Control Computers
FBW	Fly-by-wire
FCC	Flight Control Computer
FDI	Fault Detection and Isolation
FDD	Fault Diagnosis and Detection
FTC	Fault Tolerant Control
FTFC	Fault Tolerant Flight Control
GA	General Aviation
GNSS	Global Navigation Satellite System
GPS	Global Positioning System
GS	Gain Scheduling
GTM	NASA Generic Transport Model
HA	Hydraulic Actuators
HD	Heading
IAS	Indicated Airspeed
ICAO	International Civil Aviation Organization
IFCS	Intelligent Flight Control System
ILS	Instrument Landing System
IRS	Inertial Reference System
IMM	Interacting Multiple Models
INS	Inertial Navigation System
IUS	Inertial Upper Stage
LLT	Lifting Line Theory
LNAV	Lateral Navigation
LQR	Linear Quadratic Regulator

LQT	Linear Quadratic Tracking
LOC-I	Loss-of-Control In-Flight
LPV	Linear Parameter Varying
LVL CHG	Level Change
MLS	Microwave Landing System
MMST	Multiple Model Switching And Tuning
MPC	Model Predictive Control
MRAC	Model Reference Adaptive Control
MS	Mode Selection
NDB	Non-directional Beacon
NDI	Nonlinear Dynamic Inversion
NED	North East Down
NTSB	National Transportation Safety Board
PCA	Propulsion Controlled Aircraft
PID	Proportional-Integral-Derivative
PFC	Primary Flight Computers
PFTCS	Passive Fault Tolerant Control Systems
RAT	Ram Air Turbine
RHC	Receding Horizon Optimal Control
RM	Reconfiguration Mechanism
SDC	State Dependent Coefficient
SDRE	State Dependent Ricatti Equation
SEC	Spoiler and Elevator Computers
SMC	Sliding Mode Control
SRFCS	Self-Repairing Flight Control System
STC	Self Tuning Control
TACAN	Tactical Air Navigation

TMR	Triple modular redundancy
UAV	Unmanned Aerial Vehicle
USAF	US Air Force
WGS	World Geodetic System
VLM	Vortex Lattice Method
VNAV	Vertical Navigation
VOR	VHF Omni-bearing Range
VS	Vertical Speed

# CHAPTER 1

## INTRODUCTION

### 1.1 Motivation of the Thesis

Flight controls are an essential component of aircraft. There are mainly two types of flight controls. These are primary and secondary flight controls. Primary flight controls are elevator, aileron, and rudder. Detailed information about flight controls are given in Appendix A.1. Flight control problems sometimes lead to loss of control in-flight (LOC-I). LOC-I refers to accidents in which the flight crew was unable to maintain control of the aircraft in flight, resulting in an unrecoverable deviation from the intended flight path [1]. It has the highest percentage for a number of fatal accidents for commercial aircraft over 5700 kg maximum take-off weight between 2010 and 2014 [2] and between 2013 and 2017 [3]. One of the cause is control component failure/fault or flight control problems in system induced LOC-I. For example, fly-by-wire flight controls have a stringent requirement, critical failure must be less than  $10^{-9}$  per flight hours [4]. However, accidents due to loss of control related to flight control malfunctions continue to occur. There are numerous airline aircraft accidents [5] and UAV accidents [6] related to Loss of Control In-flight (LOC-I). These accidents are explained in Appendix A.4. One of the accident photos is depicted in Figure 1.1.

Dependability is an important and vital feature for flight control systems. Dependability is a measure of a system's availability when required [7]. To achieve safety, availability, reliability and especially dependability; fault tolerance, fault detection and diagnosis, fault isolation are employed [8]. Regarding fault-tolerant control; redundancy, segregation, diversity, and reconfiguration is the means to achieve system

properties, explained in Appendix C.2. There are many examples and industry applications for redundancy, diversity, and segregation. Especially for large aircraft, redundant control effectors like more than one rudder, aileron and elevator are widely used. However, with respect to the reconfiguration of the controller, even if there are examples of research, further study is needed [5]. In this thesis, reconfiguration is used for fault-tolerant flight control (FTFC) to achieve dependability. The algorithm chosen for FTFC is State-Dependent Riccati Equation (SDRE). This reconfigurable controller has a Linear Quadratic Regulator (LQR), Linear Quadratic Tracking (LQT) controller as a backup.



Figure 1.1: The Photo of Airbus A300B4-203(F) hit by missile, flight OO-DLL [9].

## 1.2 The aim of the Thesis

The aim of this thesis is designing a controller to obtain control of the UAV and avoid LOC-I during an emergency. In this thesis, emergency cases consist of actuator lock in place (stuck) and loss of effectiveness (degradation), in addition to damaged control surfaces. As a limited, full engine stop case is also studied. During an emergency, reconfiguration mechanism block reconfigures SDRE controller in the flight control computer (FCC) and limiters in the mode selection (MS) block depending on

emergency cases. In the Reconfiguration mechanism block, the supervisor works as a decision maker. FDI/FDD is assumed to send a signal which consists of emergency information to the supervisor. As a result, with this process shown in Figure 1.2, the UAV can recover from the emergency case and LOC-I is prevented.

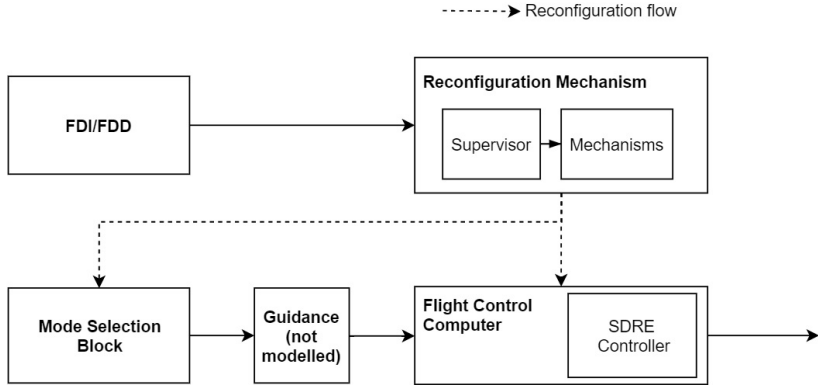


Figure 1.2: Reconfiguration process

**1.3 Introduction to FTC**

FTC is a control system which compensates faults and failures. During and after this compensation, maintaining overall stability can be ensured [8]. In other words, with the help of the FTC, the system can perform to some degree safely.

Aircraft’s fly-by-wire systems are related to Fault-Tolerant Control Systems. If the pilot control input is converted to electronic signal, flight envelope protection algorithm can be designed and the accurate control input can be calculated. It is a vital feature during emergencies.

For example in the battlefield, due to a missile hit, damages or faults can occur to the UAV or aircraft. Moreover, for civil Unmanned Aerial Vehicles (UAVs) or aircraft, flying above cities is dangerous during an emergency case. As a result, fault-tolerant flight control is extremely useful for both of these environments.

Definitions [7] about FTC are given in Appendix C.

Dependability is a vital feature for flight control systems. First, dependability is ex-

plained by six features:

1. Availability
2. Reliability
3. Safety
4. Integrity
5. Maintainability
6. Security

Dependability is strengthened by stability augmentation systems (SAS) and flight envelope protection. In this thesis, SAS is used.

Secondly, to achieve dependability, fault prevention, fault tolerance, fault removal, and fault forecasting means are preferred. As stated before, the meaning of fault tolerance is explained as the system continues to operate to some degree despite fault or faults. Fault tolerance is used vastly for flight control systems in software and hardware. Fault tolerance techniques are different for achieving dependability shown in Figure 1.3:

1. Redundancy
2. Diversity
3. Segregation [10]
4. Reconfiguration

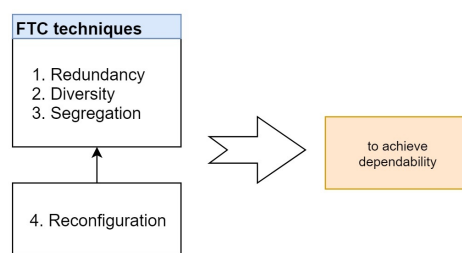


Figure 1.3: Fault-Tolerant Techniques

Fault tolerance techniques definitions are given in Appendix C.2. Reconfiguration of the flight control started to be one of the fault tolerant control techniques. In reconfiguration, the controller can be reconfigured for different types of faults or failures

to recover from an emergency. The first objective is to guarantee system stability. There are extensive studies about reconfiguration, but there is not any certification for both commercial and military aircraft [5]. In this thesis, the reconfiguration of the controller is chosen as a fault tolerant control.

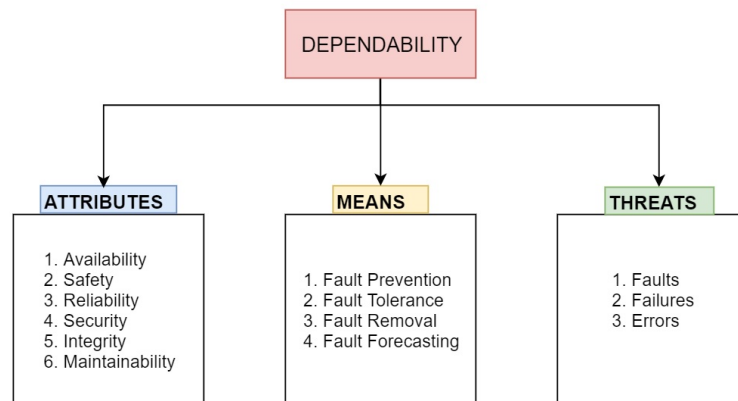


Figure 1.4: Dependability Tree

Dependability tree is shown in Figure 1.4.

## 1.4 Faults/Failures Classification

Faults/Failures can be categorized in terms of location as actuator failures/faults, sensor failures/faults and failures/faults due to a component or structural damage. They can also be categorized in terms of time as abrupt, incipient, intermittent faults/failures, in terms of way additive and multiplicative faults/failures [5]. Finally, faults also can be divided into hardware and software faults/failures.

### 1.4.1 Faults/Failures In terms of Location

**Actuator Faults/Failures:** The consequence of the actuator failures/faults is fatal as in the aircraft accidents which mentioned in Appendix A.4. Types of actuator failures/faults shown in Figure1.5 can be categorized as [11]:

1. Lock in place

2. Float
3. Runaway/Hardover
4. Loss of effectiveness

The worst scenario is runaway/hardover because it creates force and moment to prevail by other control surfaces. A deadly accident occurred in USAir flight 427 Boeing 737-300, N513AU [12] which is stated in Appendix A.4. Aircraft's rudder suddenly moved to the maximum limit and stuck there. Finally, aircraft crashed to the ground. An example accident for Loss of effectiveness is EL AL Cargo Boeing 747-200F, LY1862 [13]. Due to the disintegration of aircraft's engines, hydraulics leaked and the effectiveness of the control surfaces are degraded. An example accidents for float, are DHL Airbus A300B4-203F freighter (OO-DLL) and Japan Airlines Boeing 747SR-100 (Flight JL123) [5].

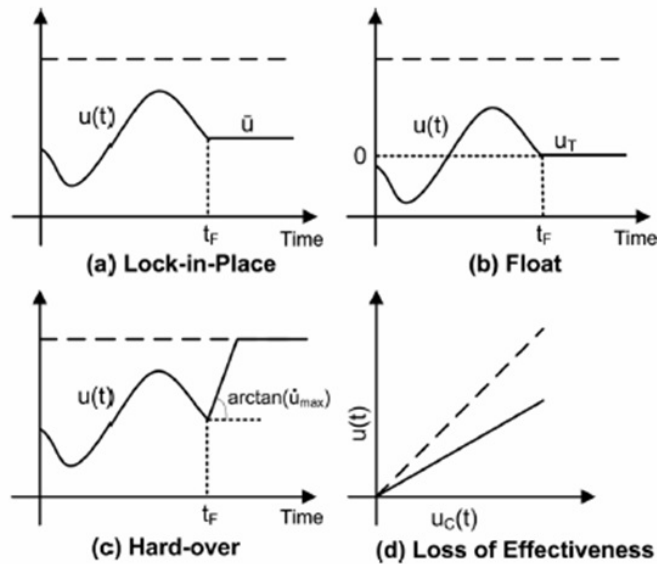


Figure 1.5: Types of actuator failures/faults [14].

**Sensor Faults/Failures:** Types of sensor failures/faults shown in Figure 1.6 can be categorized as [11]:

1. Bias
2. Freezing
3. Drift
4. Loss of accuracy

## 5. Calibration error

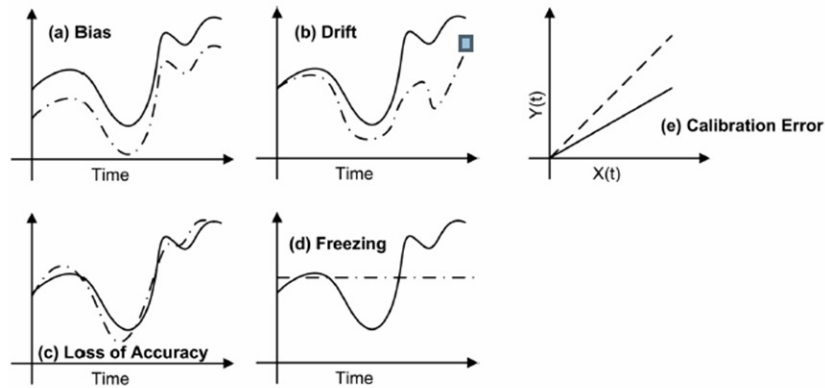


Figure 1.6: Types of sensor failures/faults [14].

Aircraft have a lot of sensors and equipment for flight and navigation instruments. For airspeed and altitude, pitot-statics system; for position, Global Navigation Satellite System (GNSS), VHF Omni-bearing Range (VOR), Distance Measurement Equipment (DME), Non-directional Beacon (NDB), Instrument Landing System (ILS) or Microwave Landing System (MLS), Tactical Air Navigation (TACAN) are used. For position and attitude, Inertial Navigation System (INS) or Inertial Reference System (IRS) is used. Generally, Inertial Reference System (IRS) is used with Air Data Computer and called Air Data Inertial Reference Unit (ADIRU). In this equipment, due to faulty sensors, position and airspeed can be erroneous. This problem can be fatal during an approach to the runway. Some of these sensors and equipment are also used for navigation in Unmanned Aerial Vehicles (UAV) [15].

**Faults/Failure Due to Component or Structural Damage:** Structural damages bring about changing cg of the aircraft, changing damping characteristics and also changing aerodynamic derivatives [11]. Normally, aircraft fly in a cg envelope but if flying out of this envelope, control surface range can be degraded. It means that in a normal flight with a too much forward cg, actuators move to the limits. Besides, it is the same in lateral cg change. More aileron command is needed to compensate for moments. Changing aerodynamics characteristic can also be compensated by elevator, aileron, rudder and throttle command. Accidents related to component or structural damage are EL AL Cargo Boeing 747-200F (LY186) [13], DHL Airbus

A300B4-203F freighter (OO-DLL) [5], United Airlines Mc-Donnell Douglas DC-10-10 (Flight UA232) [16], Japan Airlines Boeing 747SR-100 (Flight JL123) [17], American Airlines widebody Mc-Donnell Douglas DC-10-10 (Flight AA191) [18].

### 1.4.2 Faults/Failures In terms of Time

They can be categorized in terms of time as abrupt, incipient, intermittent faults/-failures shown in Figure1.7. They can be used for actuator, sensor and component faults/failures.

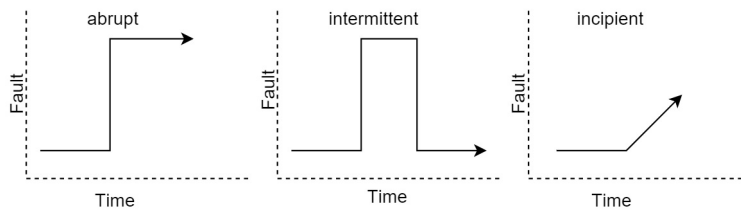


Figure 1.7: Faults/Failure In terms of Time.

### 1.4.3 Faults/Failures In terms of a Way

They can be categorized in terms of a way as an additive and multiplicative faults/-failures shown in Figure1.8. They can be used for actuator, sensor and component faults/failures.

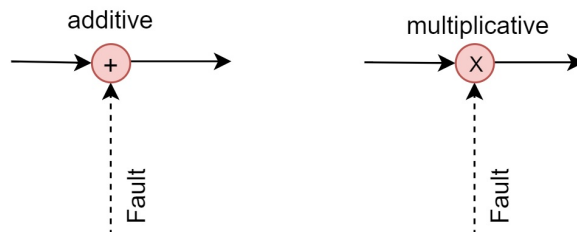


Figure 1.8: Faults/Failure In terms of Way.

## 1.5 Literature Survey on Fault-Tolerant Control

For normal operations, the controller can operate but if fault tolerance is not considered, the outcome can be fatal. To achieve dependability, there are some fault control techniques (redundancy, diversity, segregation) [10]. Reconfiguration of flight control is crucial and life-saving during emergency situations but it has not been certified yet [5]. Real applications for reconfiguration case studies are:

1. Self-Repairing Flight Control System (SRFCS)
2. Propulsion Controlled Aircraft (PCA)
3. Intelligent Flight Control System (IFCS)

NASA used F-15 HiDEC (Highly Integrated Digital Electronic Control) research aircraft for SRFCS flight test. SRFCS was tested at the NASA Ames Research Center in 1984 which was sponsored by the US Air Force (USAF). Also, NASA worked with Mc-Donnell Aircraft Company and General Electric Controls Division. The purpose in the SRFCS, in the event of failure or loss of a control surface, was reconfiguration reference input for the remaining control surfaces to preserve flight safety and return to base safely. In this flight test, Pilot was able to select three predetermined impairments-failures modes for right horizontal stabilator. During a failure, residual errors were generated due to the difference between aircraft mathematical model and aircraft by Fault Detection Isolation and Estimation (FDIE). Reconfiguration occurred for the remaining control surfaces [19].

NASA used MD-11 aircraft for PCA flight test. In this test, the electronic thrust command is generated by software to control aircraft for lateral and longitudinal under the full hydraulic power shut down. There is no throttle movement in the cockpit. For climbing and descending, software reduced power in engines, for heading change it created asymmetric thrust. In the final report, safe landing, level flight, maneuvers within 0.5 degree error, are accomplished [20].

NASA used Modified F-15 for IFCS flight test. During damage and failure, neural network and the improved controller is used to stabilize the aircraft [21].

The general scheme for Fault-Tolerant Control Systems is shown in Figure 1.9. Fault

Diagnosis and Detection (FDD) System has to detect the faults which occur in actuators, systems, and sensors. After diagnosis and detection, a signal is sent to the Reconfiguration Mechanism (RM) to reconfigure controllers in the system. In Figure 1.9,  $w$  is a process noise,  $v$  is a measurement noise,  $r(t)$  is a reference input,  $u(t)$  is an actuator input,  $y(t)$  is a system output.

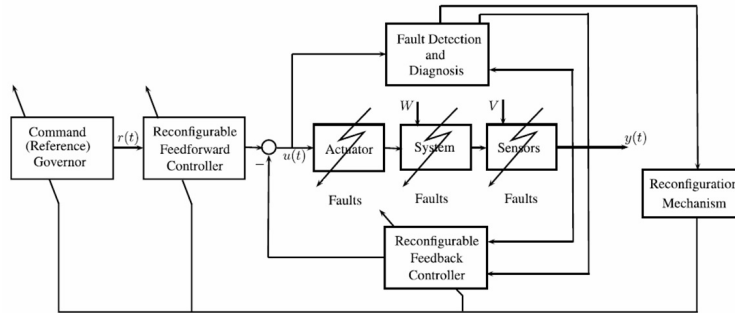


Figure 1.9: General structure for Fault-Tolerant Control System [8].

In [8], there is extensive information about Reconfigurable Fault-Tolerant Control Systems (FTCS). Generally, there are two types of fault-tolerant control [8]:

1. Passive Fault-Tolerant Control Systems (PFTCS)
2. Active Fault-Tolerant Control Systems (AFTCS)

### 1.5.1 Passive Fault-Tolerant Control Systems (PFTCS)

In Passive Fault-Tolerant Control Systems (PFTCS), the controller is designed to be robust for limited faults and failures. In other words, designing constant gain by taking account of some of the faults, for the controller, is robust. Furthermore, Passive Fault-Tolerant Control Systems (PFTCS) does not require online fault detection, diagnosis, isolation or controller reconfiguration, an adaptation which useful for computation. Also, it is not complex due to the application of classical control theory. On the other hand, if faults occur out of the stability region for controller compensation, the controller can not work properly. It only works properly for faults which have a minor effect on the system [5, 8].

### 1.5.2 Active Fault-Tolerant Control Systems (AFTCS)

In Active Fault-Tolerant Control Systems (AFTCS), the controller can be reconfigured. To reconfigure or adapt controller; fault detection, diagnosis, isolation is required. In other words, Fault Detection and Isolation (FDI) or Fault Detection and Diagnosis (FDD) has to be designed [5]. An FDD/FDI system monitors the health of the Aircraft [22]. After fault or failure occurs, FDD/FDI detects the problem and sends a signal to the Reconfiguration Mechanism (RM). After that, RM determines the best action for controller, guidance or navigation and sends configuration signal to controllers, guidance and navigational systems. The critical part for FDD and RM is the limited amount of time for both detection, isolation, and reconfiguration. Also, management of the redundancy, stability issues, robustness to all noises and taking account of uncertainties are very important parts to design FTCS [8].

For configuration, a precomputed control law (projection-based method) or a new control scheme on-line (on-line automatic control redesign methods) is used [8]. Also, the knowledge-based method can be used. In Figure 1.10, the types of passive and active FTC are depicted.

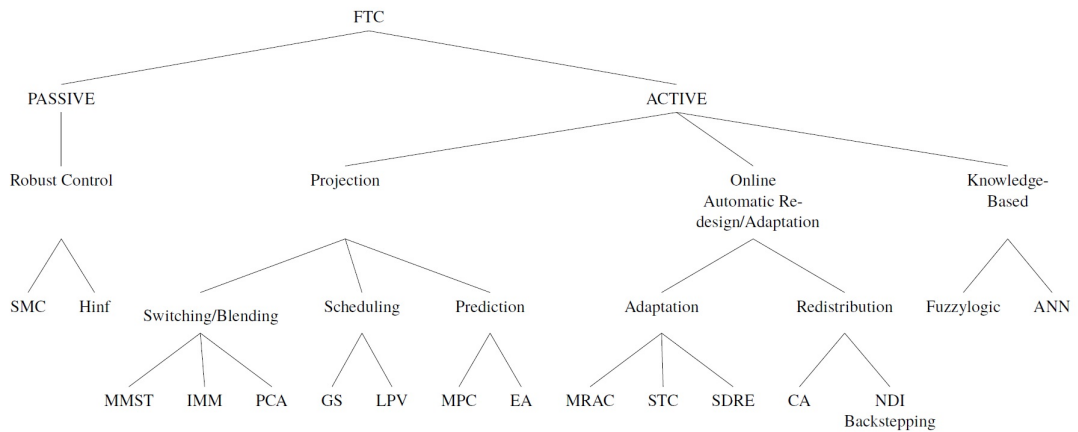


Figure 1.10: Classification of approaches to Fault-Tolerant Flight Control.

Controllers mentioned are to some degree adaptive. For example, an adaptive scheme can be used for Sliding Mode Control (SMC).

$H_\infty$  is robust when used for FTC. As in  $H_\infty$ , most robust control approaches do not require FDD/FDI. During the design process, the controller is tuned taking account

faults or failures in the event of emergency situations. To achieve robustness, instead of considering all faults, minimizing the effects of uncertainty and disturbances are targeted [11]. The application of  $H_\infty$  can be mixed with the Linear Parameter Varying (LPV) systems for aircraft flight control systems [23].

**Sliding Mode Control (SMC)** is a robust FTC (Fault-Tolerant Controller). Generally, SMC is robust against the system disturbances and uncertainties. The sliding surface is established to move states to the desired point. Sometimes adaptive feature can be added to overcome actuator rate and magnitude limitations. In [24] outer loop is designed with robust SMC. The inner loop is designed with an adaptive feature to overcome actuator limitations. As a result, during actuator partial loss, this adaptive feature can handle the situation despite some limitations for other faults and failures [5]. The Sliding Mode Control is used for Fault-Tolerant Control in [25], [26] and [27]. In addition to robustness against uncertainties and taking account actuator limitations, trajectory dynamics are lower order than the original model [25].

**Multiple Model Switching And Tuning (MMST)** is a projection, switching/blending FTC. Several parallel models are designed to represent faults and failures. Also, controllers are designed for each of them. During an emergency, FDD/FDI detects the fault/failure and select the related faulty model's controller to achieve stability [28]. In addition, Multiple Model fault-tolerant control can be classified as an adaptive [5].

**Interacting Multiple Models (IMM)** is a projection, switching/blending FTC. For IMM, every faulty situation has to be modelled, but different from MMST, faulty models have to be in a convex combination of a set of linear models. In other words, if the operating point changes, an estimation or control input is acquired by blending all linear models [11]. Due to the difficulty of achieving convex combination, Multiple Model Adaptive Estimation (MMAE) can be used. Also, as a controller, Model Predictive Control (MPC) [5], Linear Control Regulator (LQR) and Eigenstructure Assignment (EA) can be used with IMM [29].

**Propulsion Controlled Aircraft (PCA)** is a projection, switching/blending FTC. During hydraulic power emergencies like DHL Airbus A300B4-203F freighter hit by the surface-to-air missile, pilots managed to land aircraft with only thrust levers. In addition, other flight control emergencies due to a hydraulic leak, pilots manage

to control the aircraft to some degree. [17, 16, 13, 5]. Due to accidents related to flight controls, NASA Dryden Flight Research Center started a project about PCA. On April 21, 1993, F-15 is landed twice using only the PCA system [20]. PCA is an example of Multiple Model Switching And Tuning (MMST) approach except all flight controls are free floating [5].

**Gain Scheduling (GS)** is a projection, scheduling for FTC. In [30] Proportional-Integral-Derivative (PID) controllers are used. For different fault scenarios, different parameters are stored in the tables. After the FDD/FDI detects faults, predetermined PID values are switched by gain scheduling. Also, false identifications by FDD/FDI has to be taking account because gain scheduling is heavily dependent on FDD/FDI [31].

**Linear Parameter Varying (LPV)** is a projection, scheduling FTC. The LPV is basically a Linear Time-Invariant (LTI) system. However, the LPV model has a scheduling parameter which varies with the time to represent dynamics. LPV controllers without any adaptation, use time-varying parameters to improve the performance of the controller [32]. Also, about FTC, in [33], this scheduling parameter changes with the actuator fault degree to improve control law. However, FDD/FDI scheme is required. Besides, for fault-tolerant control, LPV can be classified as an adaptive [5]. In addition, it can be used with Receding Horizon Optimal Control (RHC) [34].

**Model Predictive Control (MPC)** is a projection, prediction FTC. Basically, MPC controller, solves optimal control problem which also includes constraints. It solves the problem with aircraft's predicted states to find optimal control [35]. The MPC controller is used commonly by systems in the process industry and the refinery industry which is relatively slow dynamics. As a result, due to frequency and computational characteristic, MPC controller is suitable for systems which have a slow dynamics [5]. However, in [36], EL AL Cargo Boeing 747-200F, flight number LY1862 [13] accident is studied and show that accident can be prevented by the MPC-based Fault-Tolerant Controller. After faults occur, FDD/FDI scheme updates the MPC controller.

**Eigenstructure Assignment (EA)** is a projection, prediction FTC. The main idea is relocating the eigenvalues and related eigenvectors by feedback controller to the desired value. The system's natural frequency and damping modes can be changed

by state or output feedback. Controllers which consist of EA can be reconfigured during faults or failures [37].

**Model Reference Adaptive Control (MRAC)** is an online automatic redesign/adaptation FTC. Adaptive means the controller is reconfigured. For the MRAC controller, a reference model is used [38]. Generally, there are two approaches to adaptation, namely direct and indirect adaptation. The direct adaptation is based on the error between the reference model and plant output. Conversely, indirect adaptation is based on the estimation model such that controller is updated indirectly [39] shown in Figure 1.11. Also, There are more examples in [40], [41], [42, 43].

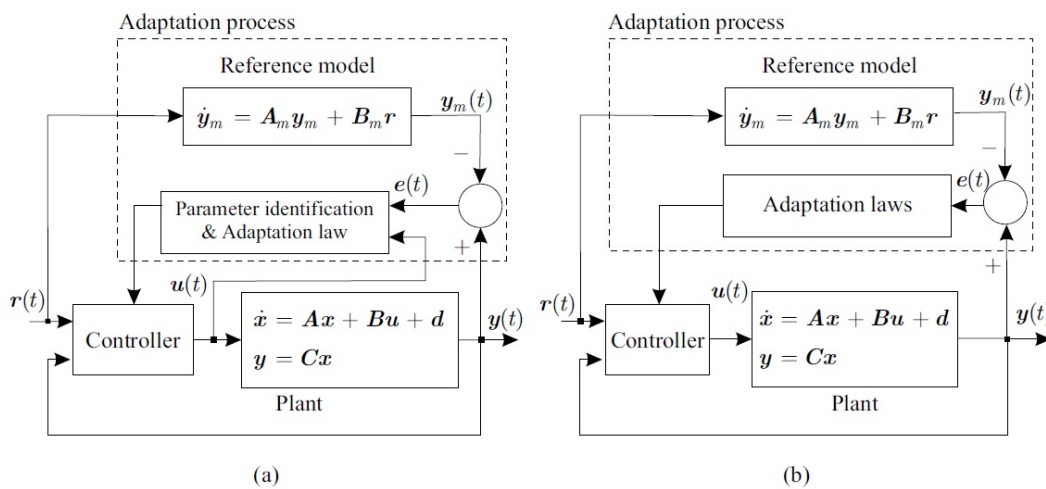


Figure 1.11: MRAC architecture: (a) indirect adaptive controller; and (b) direct adaptive controller [22].

**Self Tuning Control (STC)** is an online automatic redesign/adaptation, adaptation Fault-Tolerant Control (FTC) when used for FTC. The STC is an adaptive control that it uses parameter estimation of the plant outputs to update controller. In [44], STC is designed and used for actuator failures.

**State Dependent Riccati Equation (SDRE) Control** is a redesign/adaptation, adaptation Fault-Tolerant Control (FTC) when used for FTC. SDRE control, an optimal control which is updated online, is explained in Chapter 3. In [45, 46], optimal control is explained clearly and mathematically lucid. In [47], an overview is given about SDRE. In [48] a survey about SDRE, SDRE control is made and advantages and is-

sues of the SDRE are explained. The most prevalent issue is about global asymptotic stability. In [49], SDRE techniques for controllers, estimators, and compensators of nonlinear systems is explained mathematically. In [50], SDRE controller is used for ducted fan engine for thrust-vectoring aircraft; in [51], for control actuation system (CAS) of a guided missile; in [52], for flight control of Tilt duct UAV; in [53], for unmanned helicopter's agile maneuvering; in [54], with  $H_\infty$  to control agile missiles; in [55], with nonlinear feed-forward compensation technique to control unmanned helicopter; in [56] and [57], for guidance and control of the missile; in [58], for controlling Quadrotor UAV; in [59], for controlling relative position and formation of two spacecraft; in [60], for attitude control of a satellite; in [61], for a hydraulic actuator. In [62], SDRE is used for fault-tolerant control of Boeing 747 and NASA Generic Transport Model (GTM). By the way, drawbacks for SDRE control are slower real-time algorithms than conventional linear algorithms for flight control systems [57] and global asymptotic stability problem.

**Control Allocation (CA)** is a redesign/adaptation, redistribution FTC. Control Allocation takes calculated moments and forces from the controller which can be SMC, SDRE, PID etc. After that, through various methods, these moments and forces are converted into actuator inputs which can be described as a control effector (rudder, elevator, aileron, canard etc.). The basic controller allocation problem is easily formulated as  $B \times u = m_d$ . The desired moment is represented as  $m_d$  which is produced from the controller as stated. This equation can be different and solved with different methods which are explained in [63]. Also, in [64], CA problem formulation is described as a Direct Allocation Problem, Error Minimization Problem, Control Minimization Problem, and Mixed Optimization Problem. Three Simple Algorithm to solve CA problems are Redistributed Pseudo Inverse (PPI), Quadratic Programming (QP) and Fixed-Point Method (FPM) [64]. Also, in [65], control allocation is designed for fault-tolerant control.

**Nonlinear Dynamic Inversion (NDI)** is a redesign/adaptation, redistribution FTC. In addition, to compensate nonlinearity in the dynamics, there is no need to design the aerodynamic model structure for designing controller [66]. In [67] Adaptive Nonlinear Dynamic Inversion (ANDI) is used for Fault-Tolerant Control (FTC).

**An intelligent control system** is a control system that mimicking intelligent systems like humans, animals, etc. Intelligent behavior can be explained as an ability to learn (machine learning), plan, act, find a cause-result relation. By the way, one of the machine learning branches is Deep learning. Artificial Intelligence (AI) stores extensive data, it learns from there and behaves intelligently. In brief, intelligent control systems are the combination between Artificial Intelligence (AI) and the control system engineering [68]. Generally, instead of just using intelligent control for aircraft, lots of control techniques such as robust, optimal, linear, nonlinear controls are used together to adapt to different environment, damages, malfunctions, uncertainty. For example, about Intelligent Flight Control (IFC) program at the NASA Ames Research Center, Neural Flight and Propulsion Control System (INFPCS), which consists of daisy-chain control allocation technique, is used to compensate damage effects [69].

**Fuzzy Logic** is an intelligent FTC. Besides, Fuzzy logic can be regarded as an intelligent controller system [68]. First, fuzzy models are obtained to design fuzzy controllers. For fuzzy logic controllers, main parts are Fuzzy Sets, Fuzzy data or Membership Functions and Linguistic Variables. Steps are fuzzification, fuzzy interface process, and defuzzification [70]. In [71], for reconfiguration mechanism, the fuzzy controller is used for the fault-tolerant controller.

**Artificial Neural Network (ANN)** is one of the learning algorithms which classified as intelligent FTC. ANN or NN mimics human biological neural cell and its connections. ANN consists of input neurons, output neurons, interconnections, learning rules and finally weight which is used for to give importance which neuron effects more or less. In addition, there are input, output, and hidden layers which consist of neurons. About activation functions, there are a threshold, ramp, piecewise linear and sigmoid functions. Generally, architectural types of NN are Feedforward Neural Network (FNN) whose connections in the same or previous layer for neurons are disabled and Recursive Neural Network (RNN) whose stated connections are enabled [72]. Example for FNN is Multi-Layer Perceptron Neural Network which is the most known, for RNN is Hopfield Neural Network [73]. Six basic Learning rules for neural network are error-correction learning, memory-based learning, Hebbian learning, delta learning, competitive learning, and Boltzmann learning rule [74]. Some algorithms for neural network are Steepest Descent algorithm, Back-propagation algo-

rithm [72]. In [75], for aircraft controller, non-linear dynamic inversion (NDI) is used. However, after actuator failure or changes in aircraft dynamics, the neural network is used to compensate for inversion errors. Also, in [76], adaptive FTC is used and it is based on neural network model-following adaptive inversion control for surface damage. In [69], Level-2 Intelligent Flight Control System consists of Proportional-Integral (PI), Dynamic Inversion (DI), Neural Network (NN) and Control Allocation (CA) is used for controller. Neural network controller learns and behaves to remove errors by augmentation commands.

## 1.6 Literature Survey on the UAV Model

In this thesis, 169 kg UAV is used. For obtaining aerodynamic derivatives, inertia and other parameters; XFLR5, an open source program, is used. It is an analysis tool for airfoils, wings, and planes operating at low Reynolds numbers [77].

Further, open source program **Digital DATCOM** developed by US Air Force can be used for calculating aerodynamic derivatives with regard to Mach number, altitude, airspeed. It uses methods contained in the USAF Stability and Control Datcom (Data Compendium). However, the program is not used in this thesis but is an example and valuable tool for preliminary design operations [78]. The graphical user interface is not easy to cope with but can be learned from manual or other sources. In [79], a new light aircraft is designed in Digital DATCOM and the output file which contains aerodynamic derivatives are used by MATLAB/Simulink Digital DATCOM forces and moments block in Aerospace Blockset. Also, there are several Computational Fluid Dynamic (CFD) programs as open source software.

In this thesis, only control surfaces damage is simulated. It is assumed that aerodynamic derivatives are changing proportionally to the percentage of loss in structure.

Model of the aircraft, Airborne Subscale Transport Aircraft Research (AirSTAR) is designed for research about flight control laws in adverse flight conditions. In the research center, estimation of the aircraft's aerodynamic parameters was done by flight and wind tunnel tests. AirSTAR uses two test aircraft which are called GTM-T2 and S2. GTM is a % 5.5 dynamically scaled model of the commercial aircraft [80]. The

MATLAB/Simulink model of the GTM can be downloaded from the NASA website and it is an open source program. However, these models are not used in this thesis.

## 1.7 Contents of the Thesis

The following work is done in the context of this thesis:

1. Designing Model and obtaining Aerodynamic Derivatives from the XFLR5 Program.
2. Linearizing the Model by Simulink Control Design software and also by XFLR5 Program.
3. Constructing **The Model Block** in the MATLAB/Simulink environment.
4. Constructing **the Controller and the Autopilot** for Model in the MATLAB/Simulink environment.
5. Modelling **Atmospheric Environment** in the MATLAB/Simulink environment.
6. Constructing **faulty and damaged Model** in the MATLAB/Simulink environment.
7. Constructing **Fault Injection** to start the emergency situation in the MATLAB/Simulink environment.
8. Constructing **the Reconfiguration Mechanism** in the MATLAB/Simulink environment.
9. Constructing and updating **all simulation** again.

The UAV is designed in the XFLR5 which is an open-source program for obtaining aerodynamic derivatives. In the MATLAB/Simulink environment, by using tables, blocks shown in Figure 1.12, UAV model is simulated. For simulating and injecting of the faults, especially switch-case blocks are used. For the controller, Proportional-Integral-Derivative (PID), Linear Control Regulator (LQR), Linear Control Tracking (LQT) and State-Dependent Riccati Equation (SDRE) algorithms are used. In addition, SDRE and LQR/LQT controllers have reference commands which contain PID controllers. There are Avionics, Sensors, Navigation which are not modelled. To reconfigure the controller, there is a Reconfiguration Mechanism. Reconfiguration mechanism has a supervisor which is used for which reconfiguration is selected for a

specific identified fault or failure. These fault and failures are degradation and stuck of actuators, damage control surfaces, engine full shut down, controller problems.

In Chapter 1, passive and active FTC, types of fault and failures and finally algorithms for FTC are explained via a literature survey. In addition, flight controls for an aircraft, AIRBUS and BOEING philosophy are explained and related flight control accidents are given as an example in Appendix A.

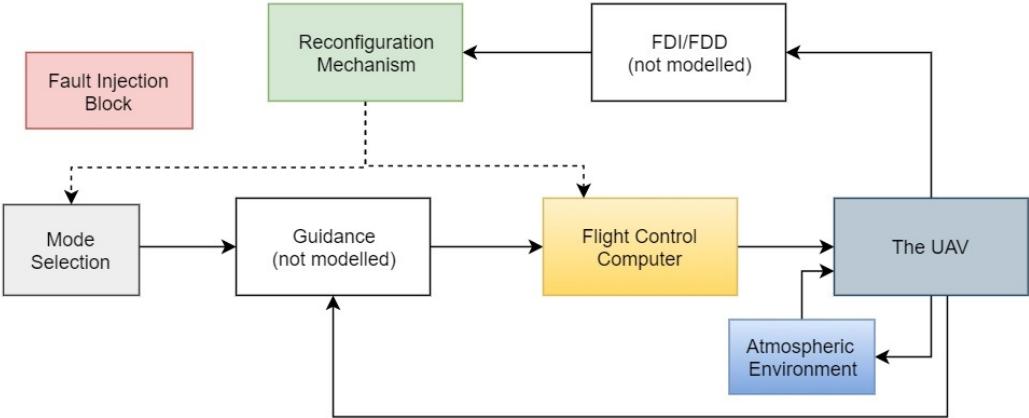


Figure 1.12: Blocks for the simulation.

In Chapter 2, reference frames, 6 degrees of freedom (DOF) equations, transformation matrices are explained. After that, specifications of the UAV used in this thesis and Pioneer UAV specifications are given for comparison. References, command filters and rate limiters in the mode selection (MS) block; reference commands and architecture in the flight control computer (FCC); atmospheric environment; aerodynamics, engine, and actuators in the UAV; reconfiguration mechanism; faulty and damaged aircraft and fault injection are explained. Especially, reconfiguration mechanism and FCC algorithm are explained in Chapter 4. Sensors, avionics, guidance, and FDI/FDD are not modelled in this thesis.

In Chapter 3, linearization is done by MATLAB/Simulink Linear Analysis Toolbox and XFLR5 program. Trim points are obtained and check with these programs. After that, longitudinal and lateral dynamics of a linear model is constructed.

In Chapter 4, first, linear controller-PID is explained. Second, a linear controller, LQR/LQT is explained. Besides, a detailed explanation is given about reference

commands which are connected with the SDRE or LQR/LQT algorithm controllers. Some cases are given and results are depicted with LQR/LQT algorithm for normal conditions. After that, nonlinear, SDRE algorithm is explained. Finally, detailed information is given for the reconfiguration mechanism and supervisor. Command filters and rate limiters which are connected to the reconfiguration mechanism are also explained in this chapter.

In Chapter 5, results for actuator stuck, degradation and for damage control surface are depicted. For aileron, elevator, rudder damage and degradation are studied at different levels. However, for the stuck case, a limited study is done.

In Chapter 6, results for other emergency situations are depicted. In emergency situations, engine shut down, controllability and observability problem for controller, turbulence and wind gust effects are explained.

In Chapter 7, conclusion is done and future work is explained.

## **1.8 Contribution of the Thesis**

During a fault/failure of actuators, damaged control surfaces and structures, linear algorithm controllers or autopilots can control the aircraft safely to some degree. However, if the failure, fault, damages are getting worse, a reconfigurable linear controller and non-linear controller like SDRE can control the aircraft safely. As stated in Section 1.3, one of the fault-tolerant technique to achieve dependability is reconfiguration. Reconfiguration is more suitable and easier than other techniques such as redundancy, diversity. For example, in redundancy for control surfaces more than one actuator has to be connected but for reconfiguration no need to assemble too much actuator to achieve dependability.

With regard to SDRE algorithm, by means of reconfiguration, not only  $A$  and  $B$  matrices about SDRE but also  $Q$  and  $R$  matrices can be reconfigured. It is design flexibility. As a result, controller behaves for a specific flight as an adaptive manner. Also, there is a reference commands in the flight control computer. In this block, command filters and PID controllers are available. As a result, during emergency

situations, FDI/FDD is assumed to be detected and located the fault/failure hypothetically and sends a signal to reconfiguration mechanism which contains supervisor as stated before. Another task of this reconfiguration mechanism is to change the values of command filters, limiters, and architecture of PID's. Especially, during actuator faults and control surface damages; limiting roll, pitch or yaw degree or rate, vertical speed or speed value and decreasing or increasing the movement of the actuators are crucial for survivability. In addition, in case of an engine failure, adjusting airspeed to glide speed and beginning to glide automatically is vital to make the best decision and decrease pilot's or operator's workload.

In this thesis, fault/failure scenarios are control surface damage; actuators degradation and stuck problems; controllability and observability problem about the controller; different levels of turbulence and wind gust; engine full shut down. Especially, during control surface damage and actuator faults, the saturation limits are changing, so least control surface movement must be ensured. During coordinated turn by aileron and rudder, if fault/failure occurs, controller reconfiguration has to be performed. During descent or climb, if fault/failure occurs, vertical speed has to be changed by altitude limiter. During control surface damage, actuator degradation and stuck,  $Q$  and  $R$  matrices of SDRE controller have to be reconfigured.

In summary, the main contribution of this thesis is using reconfigurable nonlinear, SDRE controller which can also be changed to a linear controller, LQR/LQT to prevent LOC-I. In addition, this reconfiguration is assisted by reconfiguration of rate limiters and command filters.



## CHAPTER 2

### DYNAMICS AND MATHEMATICAL MODELLING

#### 2.1 Reference Frames and Coordinate Systems

The reference frames are basically required for defining motion. The coordinate system can be called as a measurement device usually attached to a reference frame. In other words, it defines movement with respect to the reference frame. Reference Frames and coordinate Systems are given as [81]:

**Inertial Reference Frame or Coordinate system:** It is fixed with the distant stars and not rotating with the earth.  $X_I$ ,  $Y_I$  and  $Z_I$  are the representation for the axis.

**Earth-centered Reference Frame or Coordinate system:** This coordinate system is attached to the earth and rotates with the earth.  $Z_{ec}$  points to the north,  $X_{ec}$  and  $Y_{ec}$  are in the plane of the equator. The earth rotation is important. It is useful for satellites.

**Earth-fixed Reference Frame or Coordinate system:** This coordinate system is attached to the earth.  $X_E$  axis points to North pole,  $Y_E$  axis points to the east,  $Z_E$  axis points to the earth center. If the earth is assumed to be flat, vehicle carried and earth-fixed coordinate systems are parallel. The earth rotation is not important.

**Vehicle carried (NED-North East Down) Reference Frame or Coordinate system:** This coordinate system is attached to the aircraft.  $X_v$  axis points toward the north,  $Y_v$  axis points toward the east,  $Z_v$  axis points toward the local gravity vector. It is attached and moves but does not rotate with the aircraft. There are 90 degrees between  $X_v$  and  $Z_v$  axis because the earth is assumed as a perfect sphere.

**Body-fixed Reference Frame or Coordinate system:** This coordinate system is attached to the cg, fixed to the aircraft and rotate with the aircraft. The aircraft makes rolling in  $X_b$  axis, pitching in  $Y_b$  axis and yawing in  $Z_b$  axis. Forces, moments, velocity and rates are depicted in Figure 2.1.

**Air Trajectory (Wind) Reference Frame or Coordinate system:** This coordinate system is attached to the cg, not fixed and not rotate with the aircraft. The local velocity vector is on the opposite side of the trajectory.  $X_w$  axis points toward the trajectory,  $Z_w$  axis points to the symmetry of the aircraft and 90 degree difference with the  $X_w$  axis,  $Y_w$  axis points 90 degree right-hand side of the  $X_w$  axis. There are  $\alpha$  and  $\beta$  angles to define angle between  $X_b$  and  $X_w$ .

**Stability axis system :** This coordinate system is attached to the cg.  $X_s$  coincides with the local velocity vector. Difference from Air Trajectory (Wind) Reference Frame, only  $\alpha$  angle is used. In other words, there is a trimmed angle of attack which is between  $X_b$  and  $X_w$ .

Assumptions are given as:

1. The mass of the aircraft is constant.
2. The aircraft has a rigid body.
3. The earth is an inertial reference frame.
4. Sensors do not have errors.
5. The body of the UAV is not modelled.
6. Damages about control surfaces are symmetric.

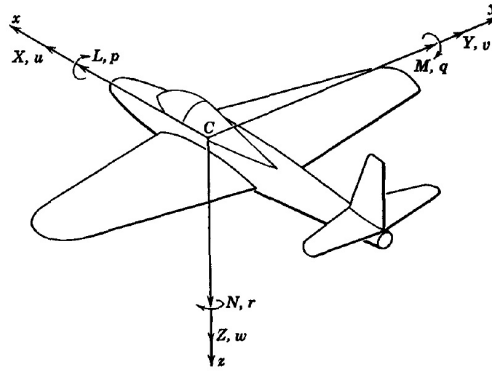


Figure 2.1: Body-fixed Reference Frame: Forces are X, Y, Z; moments are L, M, N; components of velocity are u, v, w; rates are p, q, r [81].

## 2.2 6-DOF Equations of Motion

In this section, stability derivatives are explained. These stability derivatives are used to obtain coefficients of forces and moments. After that, forces and the moments are calculated from these coefficients. Forces and moments have to be converted to the body axis. Finally, forces and moments which are in the body axis, enter 6-DOF equations of motion to find  $u$ ,  $v$ ,  $w$  and  $p$ ,  $q$ ,  $r$ .  $\alpha$  and  $\beta$  values are calculated.

Aerodynamic Stability Derivatives for this thesis are in the stability axis. In Section 2.4.1, stability derivatives of the UAV and Pioneer UAV are explained. After forces and moments calculation, a transformation is done from the stability axis coordinate system to body axis coordinate system. This transformation is done by the Aerodynamics Forces and Moments block in Simulink. For longitudinal and lateral axes, dimensionless stability derivatives are given in Table 2.1.

Coefficients of forces and moments [83] with respect to stability axis are given as:

Table 2.1: Dimensionless stability derivatives [82].

Normally (+)	$C_{D_0}$	Drag coefficient at AOA=0	Normally (-)	$C_{y\beta}$	Side force due to side slip
Normally (+)	$C_{L_0}$	Lift coefficient at AOA=0	Normally (-)	$C_{l\beta}$	Dihedral effect
Normally (+)	$C_{m_0}$	Pitch moment at AOA=0	Normally (+)	$C_{n\beta}$	Weathercock stability
Normally (+)	$C_{D\alpha}$	Drag curve slope	Normally (-)	$C_{yp}$	Side force due to roll rate
Normally (+)	$C_{L\alpha}$	Lift curve slope	Normally (-)	$C_{lp}$	Roll damping
Normally (-)	$C_{m\alpha}$	Pitch Moment due to AOA	Normally (-)	$C_{np}$	Adverse yaw
Normally (-)	$C_{m_q}$	Pitch damping	Normally (+)	$C_{y_r}$	Side force due to yaw rate
Normally (+)	$C_{L_q}$	Lift due to pitch rate	Normally (+)	$C_{l_r}$	Roll due to yaw rate
			Normally (-)	$C_{n_r}$	Yaw damping
Normally (+)	$C_{D_{\delta e}}$	Drag due to elevator	Normally (+)	$C_{y_{\delta r}}$	Side Force due to rudder
Normally (+)	$C_{L_{\delta e}}$	Lift due to elevator	Normally (+)	$C_{l_{\delta a}}$	Roll control power
Normally (-)	$C_{m_{\delta e}}$	Pitch control elevator	Normally (+)	$C_{n_{\delta a}}$	Aileron adverse yaw
			Normally (-)	$C_{l_{\delta r}}$	Roll due to rudder
			Normally (+)	$C_{n_{\delta r}}$	Yaw control power

$$C_D = C_{D_o} + C_{D_\alpha} \alpha + C_{D_q} q \frac{c}{2V} + C_{D_{\delta_e}} \delta_e + C_{D_{\delta_t}} \delta_t + C_{D_{\delta_{sb}}} \delta_{sb} \quad (2.1)$$

$$C_y = C_{y_o} + C_{y_\beta} \beta + C_{y_p} p \frac{b}{2V} + C_{y_{\delta_a}} \delta_a + C_{D_{\delta_r}} \delta_r \quad (2.2)$$

$$C_L = C_{L_o} + C_{L_\alpha} \alpha + C_{L_q} q \frac{c}{2V} + C_{L_{\delta_e}} \delta_e + C_{L_{\delta_t}} \delta_t \quad (2.3)$$

$$C_l = C_{l_o} + C_{l_\beta} \beta + C_{l_p} p \frac{b}{2V} + C_{l_r} r \frac{b}{2V} + C_{l_{\delta_a}} \delta_a + C_{l_{\delta_r}} \delta_r \quad (2.4)$$

$$C_m = C_{m_o} + C_{m_\alpha} \alpha + C_{m_q} q \frac{c}{2V} + C_{m_{\delta_e}} \delta_e + C_{m_{\delta_t}} \delta_t \quad (2.5)$$

$$C_n = C_{n_o} + C_{n_\beta} \beta + C_{n_p} p \frac{b}{2V} + C_{n_r} r \frac{b}{2V} + C_{n_{\delta_a}} \delta_a + C_{n_{\delta_r}} \delta_r \quad (2.6)$$

where  $C_D$  is the total airplane drag coefficient,  $C_y$  is the total airplane side-force coefficient,  $C_L$  is the total airplane lift coefficient,  $C_l$  is the total airplane aerodynamic rolling moment coefficient,  $C_m$  is the total airplane aerodynamic pitching moment coefficient,  $C_n$  is the total airplane aerodynamic yawing moment coefficient [82].

For the forces and moments notation, instead of

$$[X_s, Y, Z_s, L, M, N] \quad (2.7)$$

stability axis [84] can be given as:

$$[-D, Y, -L, \bar{L}, M, N] \quad (2.8)$$

Forces and Moments formula with respect to stability axis are given as:

$$\text{Drag : } \mathbf{-D} = -C_D \bar{q} S \quad (2.9)$$

$$\text{Side Force : } \mathbf{Y} = C_y \bar{q} S \quad (2.10)$$

$$\text{Lift : } \mathbf{-L} = -C_L \bar{q} S \quad (2.11)$$

$$\text{Roll Moment : } \bar{\mathbf{L}} = C_l \bar{q} S b \quad (2.12)$$

$$\text{Pitch Moment : } \mathbf{M} = C_m \bar{q} S c \quad (2.13)$$

$$\text{Yaw Moment : } \mathbf{N} = C_n \bar{q} S b \quad (2.14)$$

$\bar{q}$  : dynamics pressure

S : wing reference area

$b$  : wing span

$\bar{c}$  : wing mean geometric chord

We can explain forces and moments by from Equation (2.9) to Equation (2.14) which are in the stability axis shown in Figure 2.2.

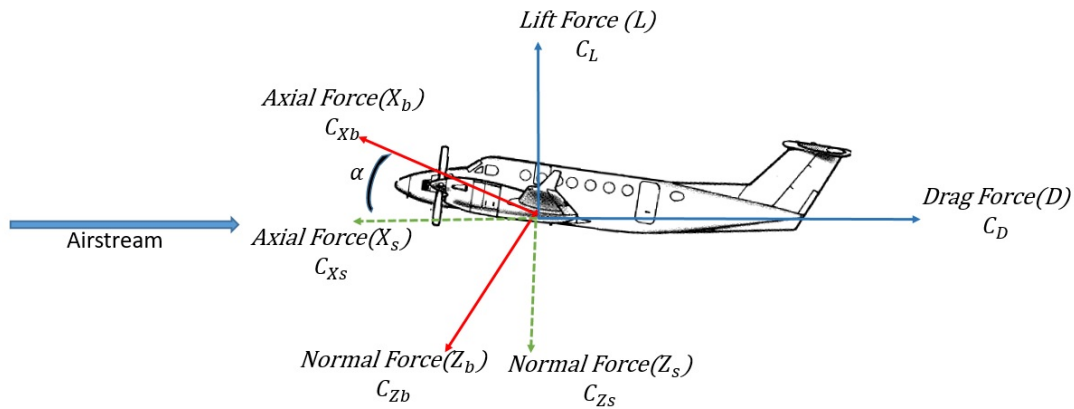


Figure 2.2: Forces in stability (  $X_s$ ,  $Z_s$  ) and body (  $X_b$ ,  $Z_b$  ) axis.

As a matrix form, the transformation from stability to body axis can be done by this equation:

$$\begin{bmatrix} X_b \\ Y_b \\ Z_b \end{bmatrix} = \begin{bmatrix} \cos \alpha & 0 & -\sin \alpha \\ 0 & 1 & 0 \\ \sin \alpha & 0 & \cos \alpha \end{bmatrix} \begin{bmatrix} -D \\ Y \\ -L \end{bmatrix} \quad (2.15)$$

$$\begin{bmatrix} \bar{L}_b \\ \mathbf{M}_b \\ \mathbf{N}_b \end{bmatrix} = \begin{bmatrix} \cos \alpha & 0 & -\sin \alpha \\ 0 & 1 & 0 \\ \sin \alpha & 0 & \cos \alpha \end{bmatrix} \begin{bmatrix} \bar{L} \\ \mathbf{M} \\ \mathbf{N} \end{bmatrix} \quad (2.16)$$

The transformation from stability to body axis also can be done by these equations [83]:

$$C_{X_b} = C_L \sin \alpha - C_D \cos \alpha \quad (2.17)$$

$$C_{Z_b} = -C_D \sin \alpha - C_L \cos \alpha \quad (2.18)$$

$$C_{Y_b} = C_Y \quad (2.19)$$

$$C_{m_b} = C_m \quad (2.20)$$

$$C_{l_b} = C_l \cos \alpha - C_n \sin \alpha \quad (2.21)$$

$$C_{n_b} = C_l \sin \alpha + C_n \cos \alpha \quad (2.22)$$

As stated before all coefficients which are obtained from XFLR5 program for this thesis for simulation. The difference between wind axis and the stability axis is about  $\beta$  value. The transformation from wind to body axis for forces can be done by this equation [84]:

$$\begin{bmatrix} X_b \\ Y_b \\ Z_b \end{bmatrix} = \begin{bmatrix} \cos \alpha \cos \beta & -\cos \alpha \sin \beta & -\sin \alpha \\ \sin \beta & \cos \beta & 0 \\ \sin \alpha \cos \beta & -\sin \alpha \sin \beta & \cos \alpha \end{bmatrix} \begin{bmatrix} -D \\ N \\ -L \end{bmatrix} \quad (2.23)$$

Finally, all forces and moments become in the body axis and can be used for 6 DOF equations. 6 degrees non-linear equations of motions are expressed by these equations [84]

$$\dot{\mathbf{u}} = \frac{X_b}{m} - wq + vr - g \sin \theta \quad (2.24)$$

$$\dot{\mathbf{v}} = \frac{Y_b}{m} - ru + pw + g \sin \phi \cos \theta \quad (2.25)$$

$$\dot{\mathbf{w}} = \frac{Z_b}{m} - pv + qu + g \cos \phi \cos \theta \quad (2.26)$$

$$\dot{\mathbf{p}} = I_1 L_b + I_2 N_b + I_3 qr + I_4 pq \quad (2.27)$$

$$\dot{\mathbf{q}} = \frac{M_b - I_7 pr - (p^2 - r^2)I_{xz}}{I_{yy}} \quad (2.28)$$

$$\dot{\mathbf{r}} = I_2 L_b + I_5 N_b - I_4 r q + I_6 p q \quad (2.29)$$

$$I_1 = \frac{I_{zz}}{I_8} \quad I_2 = \frac{I_{xz}}{I_8} \quad I_3 = \frac{(I_{yy} - I_{zz})I_{zz} - I_{xz}^2}{I_8} \quad I_4 = \frac{(I_{xx} - I_{yy} + I_{zz})I_{xz}}{I_8}$$

$$I_5 = \frac{I_{xx}}{I_8} \quad I_6 = \frac{(I_{xx} - I_{yy})I_{xz} + I_{xz}^2}{I_8} \quad I_7 = I_{xx} - I_{zz} \quad I_8 = I_{xx}I_{zz} - I_{xz}^2$$

In summary, the process for simulation can be shown in Figure 2.3.



Figure 2.3: Process for simulation.

Another and more convenient way to express moments and forces can be used which are in the body axis for 6 degrees of equations. These equations are used in SDRE to obtain SDC matrices and LQR/LQT controller which are explained at length in Chapter 4.

$$\mathbf{X}_b = m(X_u u + X_w w + X_q q + X_{\delta_e} \delta_e + X_{\delta_t} \delta_t) \quad (2.30)$$

$$\mathbf{Y}_b = m(Y_v v + Y_p p + Y_r r + Y_{\delta_a} \delta_a + Y_{\delta_r} \delta_r) \quad (2.31)$$

$$\mathbf{Z}_b = m(Z_u u + Z_w w + Z_q q + Z_{\delta_e} \delta_e) \quad (2.32)$$

$$\bar{\mathbf{L}}_b = I_{xx}(L_v v + L_p p + L_r r + L_{\delta_a} \delta_a + L_{\delta_r} \delta_r) \quad (2.33)$$

$$\mathbf{M}_b = I_{yy}(M_u u + M_w w + M_q q + M_{\delta_e} \delta_e) \quad (2.34)$$

$$\mathbf{N}_b = I_{zz}(N_v v + N_p p + N_r r + N_{\delta_a} \delta_a + N_{\delta_r} \delta_r) \quad (2.35)$$

### 2.3 Other Equations

Euler angles are expressed by these equations [84]:

$$\dot{\phi} = p + \tan \theta \sin \phi q + \tan \theta \cos \phi r \quad (2.36)$$

$$\dot{\theta} = q \cos \phi - r \sin \phi \quad (2.37)$$

$$\dot{\psi} = q \frac{\sin \phi}{\cos \theta} + r \frac{\cos \phi}{\cos \theta} \quad (2.38)$$

Euler angles can be expressed in matrix form:

$$\begin{bmatrix} \dot{\phi} \\ \dot{\theta} \\ \dot{\psi} \end{bmatrix} = \begin{bmatrix} 1 & \tan \theta \sin \theta & \tan \theta \cos \phi \\ 0 & \cos \phi & \sin \phi \\ 0 & \frac{\sin \phi}{\cos \theta} & \frac{\cos \phi}{\cos \theta} \end{bmatrix} \begin{bmatrix} p \\ q \\ r \end{bmatrix} \quad (2.39)$$

Altitude is expressed by this equation [84]:

$$\dot{h} = u \sin \theta - v \sin \phi \cos \theta - w \cos \phi \cos \theta \quad (2.40)$$

Angle of attack and side slip angle are expressed by these equations [84]:

$$\alpha = \tan^{-1} \frac{w}{u} \quad (2.41)$$

$$\beta = \tan^{-1} \frac{v}{\sqrt{u^2 + w^2}} \quad (2.42)$$

$$V = \sqrt{u^2 + v^2 + w^2} \quad (2.43)$$

$$u = V \cos \alpha \cos \beta \quad (2.44)$$

$$v = V \sin \beta \quad (2.45)$$

$$w = V \sin \alpha \cos \beta \quad (2.46)$$

Direction Cosine Matrix (DCM) is expressed by this equation [84]:

$$\begin{bmatrix} \cos \psi \cos \theta & \sin \psi \cos \theta & -\sin \theta \\ \cos \psi \sin \theta \sin \phi - \sin \psi \cos \phi & \sin \theta \sin \phi \sin \psi + \cos \psi \cos \phi & \cos \theta \sin \phi \\ \cos \psi \sin \theta \cos \phi + \sin \psi \sin \phi & \sin \theta \cos \phi \sin \psi - \cos \psi \sin \phi & \cos \theta \cos \phi \end{bmatrix} \quad (2.47)$$

## 2.4 The Aircraft Model

The general architecture of simulation is depicted in Figure 2.4. Fault injection is used for simulating faults and failures; MS is the interface between pilot and FCC; FCC is the controller which consist of SDRE, LQR and PID algorithms; Atmospheric Environment is used to generating atmospheric values, winds, turbulence; Reconfiguration Mechanism is used to reconfiguring FCC and MS for different emergency cases. In this thesis, FDI/FDD and Guidance are not modelled. Sensors and avionics are not modelled.

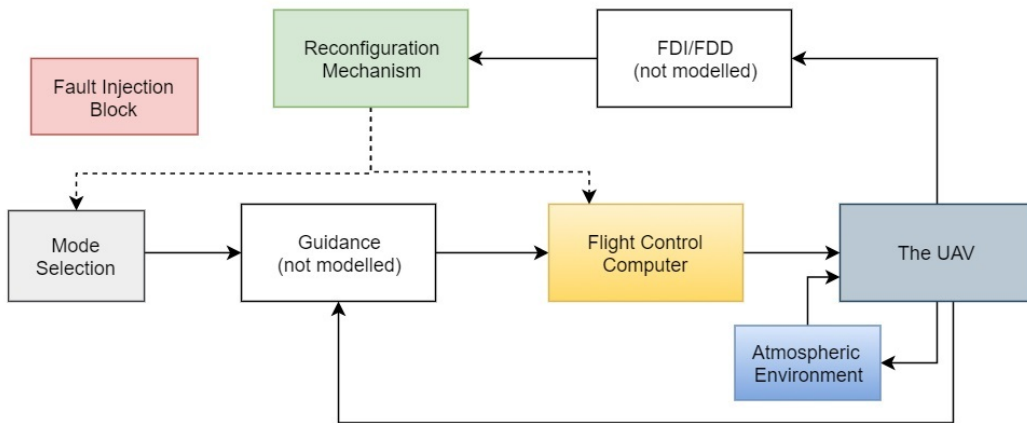


Figure 2.4: Simulation Model.

### 2.4.1 The UAV Model

This model shown in Figure 2.5 contains Aerodynamics, 6 DOF EOM, control surface actuators, engine actuator and parameter creator which is shown in Figure 2.6.

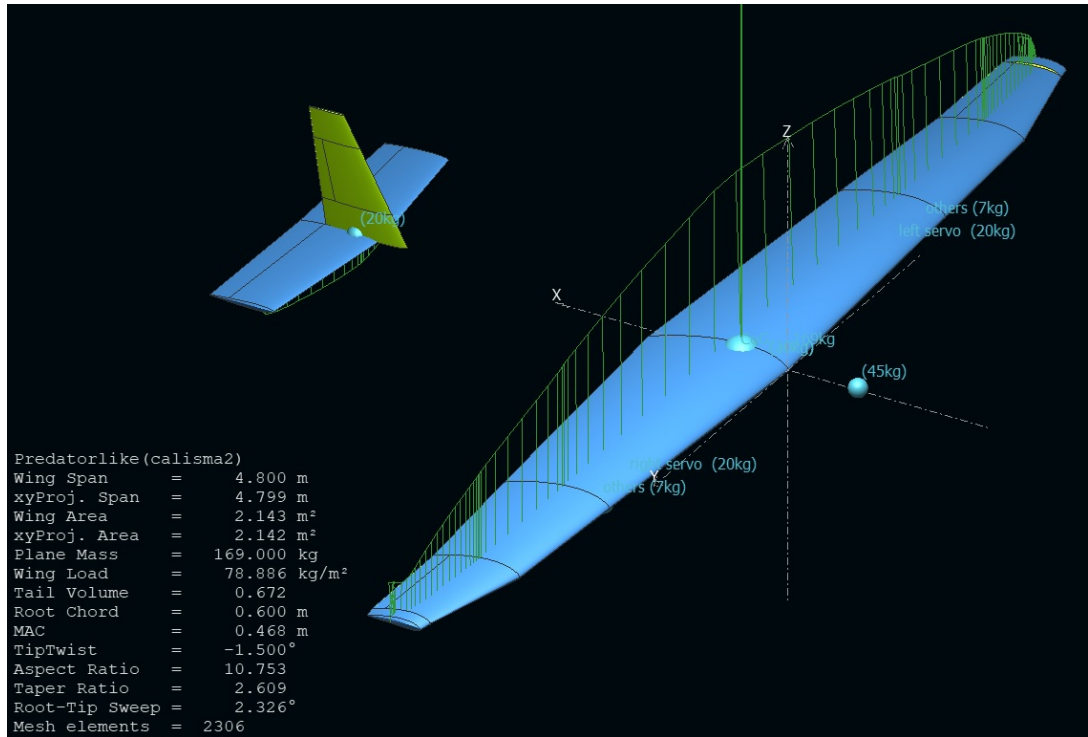


Figure 2.5: The UAV model in XFLR5.

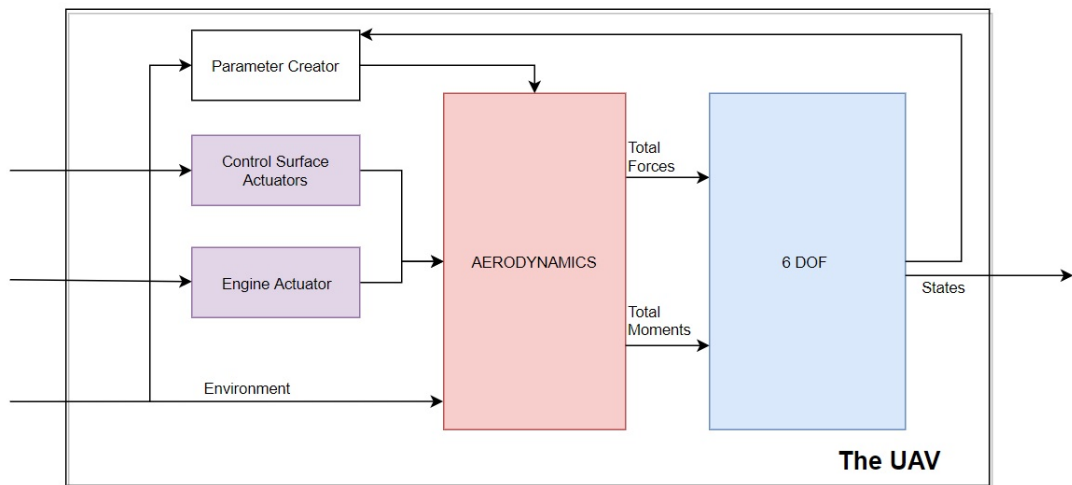


Figure 2.6: The UAV model in Simulink.

The aerodynamic block contains aerodynamic derivatives. Aerodynamic values split up to three block. These are Aerodynamic coefficients datum (they change with alpha and beta values), Aerodynamic body rate damping ( $p$ ,  $q$ ,  $r$  values), Aerodynamic coefficients of control surfaces ( $\delta_a$ ,  $\delta_e$ ,  $\delta_r$ ,  $\delta_{sb}$ ) which are shown in Figure 2.7. These

blocks contain stability axis derivatives. Stability derivatives of the UAV are shown in Table 2.2 and properties of the UAV are shown in Table 2.3. Control surface geometry is given in Table 2.4. Detailed properties are given for wing, horizontal and vertical stabilizer in Table 2.5.

Table 2.2: Stability derivatives of the UAV in the stability axis.

	$C_D$	$C_L$	$C_y$	$C_l$	$C_m$	$C_n$
$u$	0.03129	-0.00594	-	-	-	-
$\alpha$	0.1288	5.5776	-	-	-1.2005	-
$\beta$	-	-	-0.2006	-0.01534	-	0.065939
$p$	-	-	-0.0302	-0.5417	-	-0.0694
$q$	-	9.7010	-	-	-19.1029	-
$r$	-	-	0.1508	0.1197	-	-0.0462
$\delta_a$	-	-	-	0.1189	-	$-5.4293e - 04$
$\delta_e$	0.0446	0.5106	-	-	-1.7605	-
$\delta_r$	-	-	0.0571	0.0019	-	-0.0202
$\delta_{sb}$	0.030	-	-	-	-	-
	$C_{D_o}$	$C_{L_o}$	$C_{y_o}$	$C_{l_o}$	$C_{m_o}$	$C_{n_o}$
	0.0121	0.3515	0	0	0.0358	0

Stability derivatives, shown in Table 2.2 for the UAV are calculated by the open source program, **XFLR5**. This program is an analysis tool for airfoils for low Reynold numbers. XFLR is the previous version and developed by Mark Drela at MIT. The analysis methods are Lifting Line Theory (LLT), Vortex Lattice Method (VLM) and 3D Panel Method. For the UAV, VLM and Panel methods are used. Viscous drag is added during analysis but not included during control stability derivatives calculation due to the constraint of the program. The program calculates the inertia matrix, the center of gravity (Cg) and center of pressure (Cp). In [85], the conclusion about XFLR5 analysis for Body Freedom Flutter (BFF) aircraft is reasonable and agree with the physics of flight mechanics but XFLR5 can be used as a starting point and not an overall analysis tool for calculation or estimation of the aerodynamic derivatives. To understand limitation, assumption and technical details about the program, manual as

Table 2.3: Properties of the UAV

<b>Mass and Inertia</b>	<b>Definition</b>	<b>Value</b>	<b>Unit</b>
$I_{xx}$	Moment of inertia	60.340	$kg.m^2$
$I_{yy}$	Moment of inertia	66.920	$kg.m^2$
$I_{zz}$	Moment of inertia	126.900	$kg.m^2$
$I_{xy}$	Product of inertia	0	$kg.m^2$
$I_{xz}$	Product of inertia	-3.299	$kg.m^2$
$I_{yz}$	Product of inertia	0	$kg.m^2$
m	Mass	169	kg
<b>Wing and Ailerons</b>			
$\bar{c}$	Mean aerodynamic chord	0.4680	m
b	Wing reference span	4.7993	m
S	Wing reference area	2.1430	$m^2$
AW	Airfoil	NACA4415	
AD	Aileron Deflection	+40	degree
<b>Horizontal Stabilizer and Elevator</b>			
e	H. Stabilizer reference area	0.40	$m^2$
AH	Airfoil	NACA0009	
ED	Elevator Deflection	+40	degree
<b>Vertical Stabilizer and Rudder</b>			
f	Fin reference area	0.13	$m^2$
AV	Airfoil	NACA0009	
RD	Rudder Deflection	+40	degree
<b>Other values</b>			
wl	Wing load	78.886	$\frac{kg}{m^2}$
AR	Aspect ratio	10.793	-

aid has to be examined [77].

Table 2.4: Properties of the UAV control surface

<b>Control Surface</b>	<b>MAC</b>	<b>Span</b>	<b>Area</b>
Elevator	0.0615 <i>m</i>	1.30 <i>m</i>	0.08 <i>m</i> <sup>2</sup>
Aileron	0.0620 <i>m</i>	0.4690 <i>m</i>	0.0291 <i>m</i> <sup>2</sup>
Rudder	0.05 <i>m</i>	0.25 <i>m</i>	0.0125 <i>m</i> <sup>2</sup>

Table 2.5: Properties of the UAV wing, horizontal and vertical stabilizer.

	<b>Wing</b>	<b>H. Stabilizer</b>	<b>V. Stabilizer</b>
Wing span	4.80 <i>m</i>	1.30 <i>m</i>	1 <i>m</i>
Area	2.14 <i>m</i> <sup>2</sup>	0.40 <i>m</i> <sup>2</sup>	0.13 <i>m</i> <sup>2</sup>
Projected span	4.80 <i>m</i>	1.30 <i>m</i>	1 <i>m</i>
Projected area	2.14 <i>m</i> <sup>2</sup>	0.40 <i>m</i> <sup>2</sup>	0.13 <i>m</i> <sup>2</sup>
Mean Geo. Chord	0.45 <i>m</i>	0.31 <i>m</i>	0.25 <i>m</i>
Mean Aero. Chord	0.47 <i>m</i>	0.31 <i>m</i>	0.26 <i>m</i>
Aspect ratio	10.75	4.23	4
Taper ratio	2.61	1.24	2.33
Root to tip sweep	2.33 <i>degrees</i>	5.60 <i>degrees</i>	22.78 <i>degrees</i>

Stability derivatives which is shown in Table 2.2 for the UAV, are similar to Table 2.6 for Pioneer UAV. Also, the UAV's properties which are shown in Table 2.3, can be compared with Pioneer UAV shown in Table 2.6. The error with regard to aerodynamic derivatives between the UAV and Pioneer UAV is given in Appendix B.

Table 2.6: Stability derivatives of Pioneer UAV in the stability axis [86].

	$C_D$	$C_L$	$C_y$	$C_l$	$C_m$	$C_n$
$\alpha$	0.4300	4.7800	-	-	-2.1200	-
$\beta$	-	-	-0.819	-0.023	-	0.109
$p$	-	-	-	-0.450	-	-0.110
$q$	-	8.05	-	-	-36.6	-
$r$	-	-	0.1508	0.265	-	-0.200
$\delta_a$	-	-	-	0.161	-	-0.0200
$\delta_e$	0.0180	0.401	-	-	-1.76	-
$\delta_r$	-	-	0.191	-0.00229	-	-0.0917
	$C_{D_o}$	$C_{L_o}$	$C_{y_o}$	$C_{l_o}$	$C_{m_o}$	$C_{n_o}$
	0.060	0.385	0	0	0.194	0

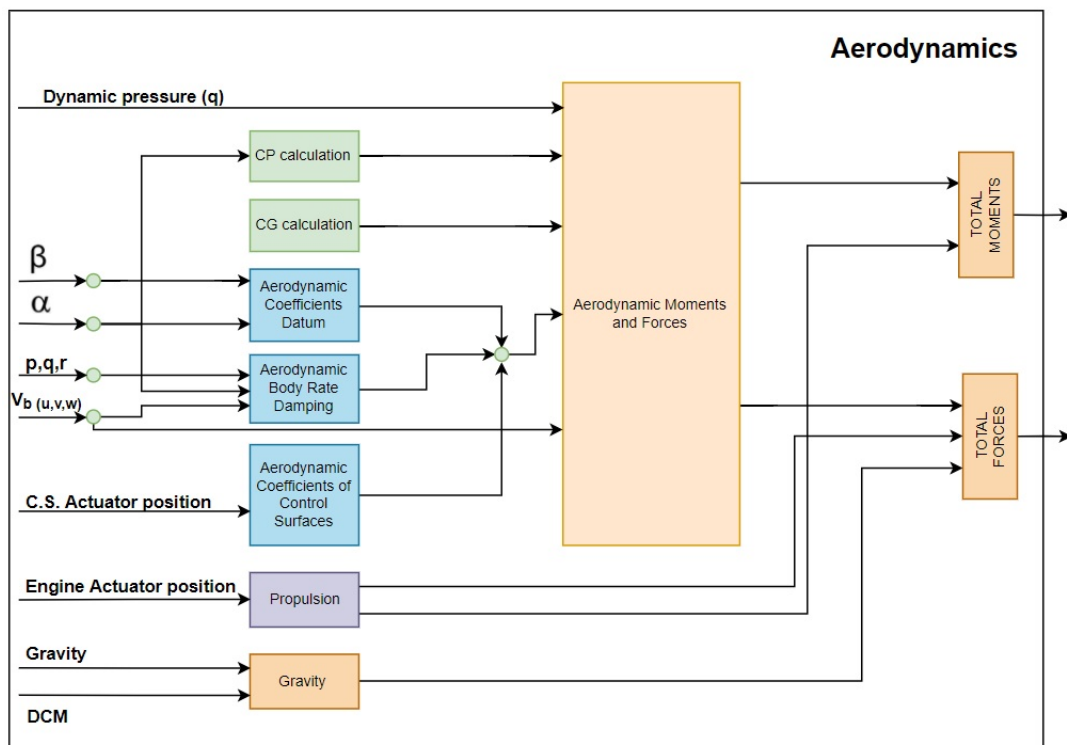


Figure 2.7: Aerodynamics block.

Table 2.7: Properties of Pioneer UAV [86].

<b>Mass and Inertia</b>	<b>Definition</b>	<b>Value</b>	<b>Unit</b>
$I_{xx}$	Moment of inertia	47.2258	$kg.m^2$
$I_{yy}$	Moment of inertia	90.9482	$kg.m^2$
$I_{zz}$	Moment of inertia	111.4753	$kg.m^2$
$I_{xy}$	Product of inertia	0	$kg.m^2$
$I_{xz}$	Product of inertia	-6.6462	$kg.m^2$
$I_{yz}$	Product of inertia	0	$kg.m^2$
m	Mass	200	kg
<b>Wing and Ailerons</b>			
$\bar{c}$	Mean aerodynamic chord	0.54864	m
b	Wing reference span	5.15	m
S	Wing reference area	2.8261	$m^2$
AW	Airfoil	NACA4415	
AD	Aileron Deflection	+20	degree
<b>Horizontal Stabilizer and Elevator</b>			
e	H. Stabilizer reference area	0.5639	$m^2$
AH	Airfoil	NACA0012	
ED	Elevator Deflection	+20	degree
<b>Vertical Stabilizer and Rudder</b>			
f	Fin reference area	0.2016	$m^2$
AV	Airfoil	NACA0012	
RD	Rudder Deflection	+20	degree
<b>Other values</b>			
wl	Wing load	-	$\frac{kg}{m^2}$
AR	Aspect ratio	9.36	-

After calculating stability derivatives, all of them are summed up and final values are calculated for  $C_D$  given in Equation (2.1),  $C_y$  given in Equation (2.2),  $C_L$  given in

Equation (2.3),  $C_l$  given in Equation (2.4),  $C_m$  given in Equation (2.5),  $C_n$  given in Equation (2.6). After that, these values are entered to Aerodynamic Forces and Moments block to calculate Drag given in Equation (2.9), Side Force given in Equation (2.10), Lift given in Equation (2.11), Pitch Moment given in Equation (2.13), Roll Moment given in Equation (2.12), Yaw Moment given in Equation (2.14). Also, center of pressure and center of gravity is calculated in the Aerodynamic Coefficients Datum which is shown in Figure 2.8. As seen in the figure, center of gravity is assumed to be constant value but center of pressure changes with the angle of attack and shown by interpolation table.

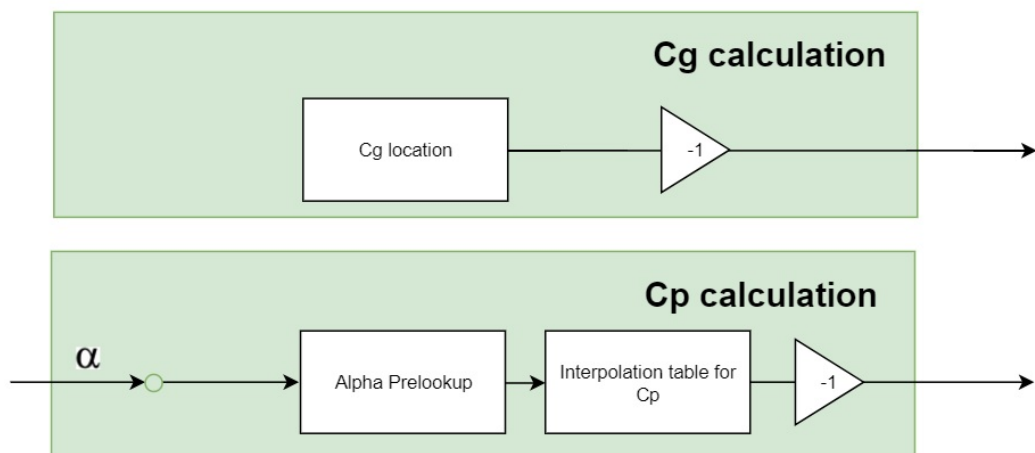


Figure 2.8: The Cg and Cp calculation in the Aerodynamic Coefficients Datum.

As seen in Figure 2.7, the input of the Aerodynamic Forces are in the stability axis. In other words, these stability derivatives have to be transformed to the body axis. By this block, first, with the input, forces and moments are calculated. After that, they are transformed from stability to body axis due to calculation used by the 6 DOF Block.

## 2.4.2 The Mode Selection (MS) block

### 2.4.2.1 Modes of an Autopilot

The Mode selection (MS) is used for creating a reference signal and it is an interface between pilot and FCC, which is shown in Figure 2.4. Normally, manned aircraft

autopilot modes for **roll axis** are heading (HD), lateral navigation (LNAV), localizer or VOR (LOC/ VOR); modes for **pitch axis** are altitude hold (ALT), altitude select and flight level change (ALT SEL/LVL CHG), altitude select and vertical speed (ALT SEL/ VS), vertical navigation (VNAV); mode for **yaw axis** is yaw damper (YD); mode for **air speed** is Indicated Airspeed (IAS) which is used for autothrottle or flight level change during climb; modes for **approach** are approach (APP), lateral navigation (LNAV), vertical navigation (VNAV). These autopilot modes can be used for UAVs.

In this thesis, not all modes are used for the autopilot. Excluded modes are lateral navigation (LNAV), vertical navigation (VNAV), localizer or VOR (LOC/ VOR) and all approach modes. In other words, there is not an autopilot mode for navigation. As a result, guidance is not modelled. The MS is shown in Figure 2.9. **The color of magenta means autopilot modes; orange means with controller and pilot, but without autopilot; yellow means reconfiguration, shown in Figure 2.9.** Also, the controller type can be selected by "1" as SDRE algorithm or "0" as LQR algorithm manually or by the reconfiguration mechanism.

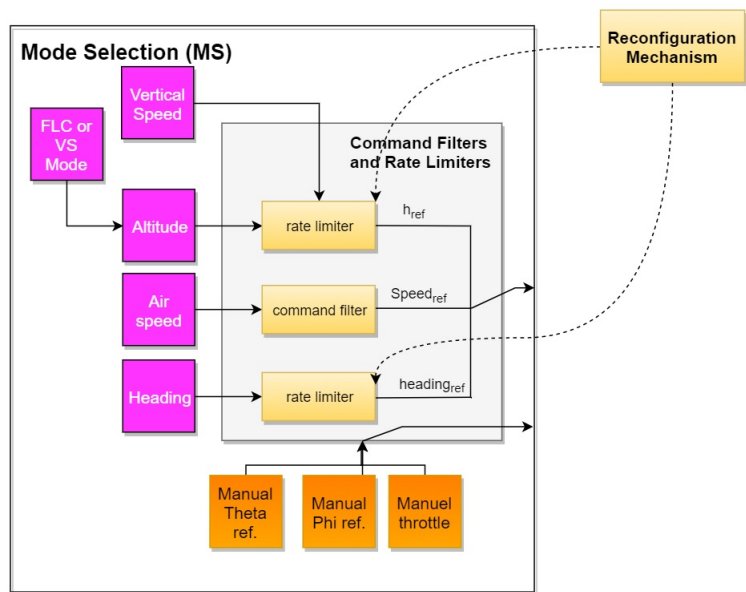


Figure 2.9: The Mode Selection of the UAV.

To make it clear, as an example, climbing with level change is explained. First, altitude is adjusted from 5000 ft. to 7000 ft. Secondly, IAS mode is selected to 50 kt.

and level change is selected. Finally, aircraft is climbing with a constant speed at 50 kt with climbing throttle setting. On the other hand, climbing with vertical speed is different from level change. First, altitude is selected from 5000 ft. to 7000 ft., then vertical speed is selected for example 0.5 which means 500 feet per minute, at that time speed, is selected to 50 kt. In other words, level change is about first aiming at holding speed whereas vertical speed is about first aiming to hold vertical speed. As a result, in this thesis, vertical speed mode is directly related to altitude rate limiter. However, flight level change is directly related to change the architecture of the reference command explained in Section 4.2.2.

Heading can be adjusted. After selected heading, rate limiter provides a standard turn.

#### 2.4.2.2 Command Filters and Rate Limiters

In the **MS**, there are command filter and rate limiters which are shown in Figure 2.9. For altitude change, rate limiter is used to provide desired vertical speed. Also, for heading change, rate limiter is used to provide desired turn rate. In addition, for airspeed change, a command filter is used to provide a desired command signal. On the other hand, manual control of  $\phi$ ,  $\theta$  and  $\delta_t$  can be selected which is shown in Figure 2.9. When it is selected, reference command is not needed and autopilot is disengaged. They are fed directly to SDRE or LQR/LQT controller part in the flight control computer (FCC) but after passing command filters shown in Figure 2.10.

In the **Reference command in the FCC**, there are also command filters for  $\theta_{ref}$ ,  $\phi_{ref}$ ,  $\delta_t$  shown in Figure 2.10. If the autopilot is not engage and manual  $\theta_{ref}$  and  $\phi_{ref}$  are used, no need to reference command block. As a result, signal is directly transmitted to SDRE or LQR controller. Besides, there is a saturation limiter for  $\phi_{ref}$ .

All these command filters, saturation limiter, and rate limiters can be reconfigurable.

The mathematical representation of a command filter is given in Equation (2.48). Rate limiter is used for limiting the first derivative of the signal. Basically, in Simulink, it

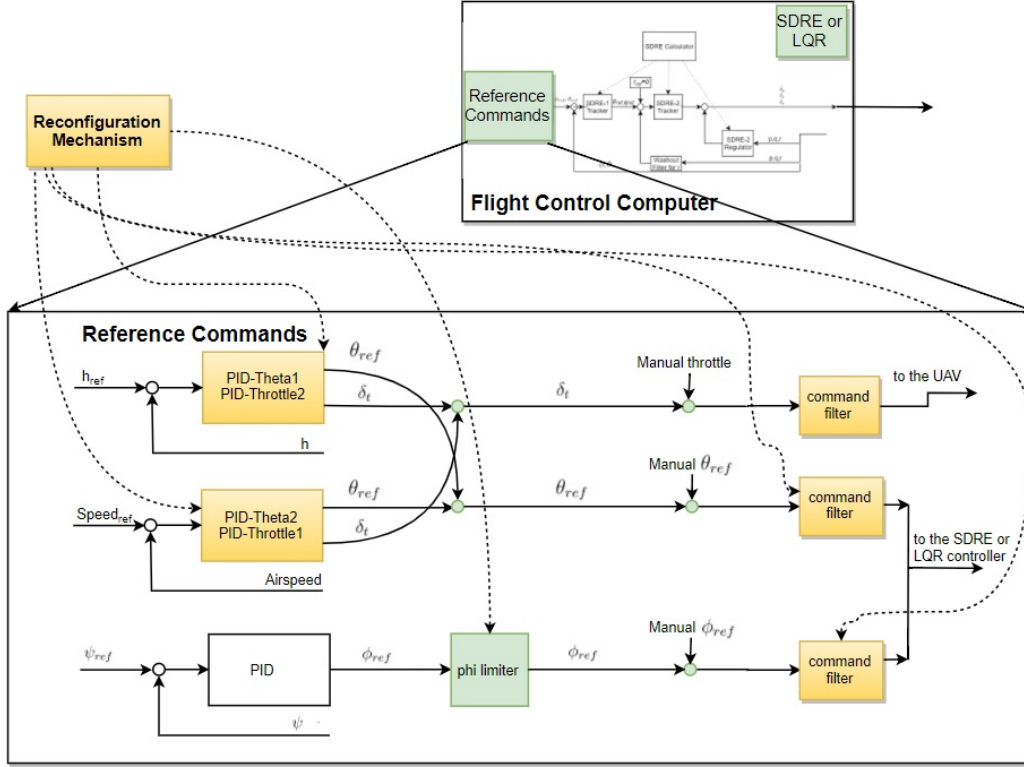


Figure 2.10: Command filters in the reference command in the FCC.

is calculated by a formula which is given in Equation (2.49).

$$H(s) = \frac{\tau}{s + \tau} \quad (2.48)$$

$$rate = \frac{u(i) - y(i - 1)}{t(i) - t(i - 1)} \quad (2.49)$$

$u(i)$  and  $t(i)$  are input and time, and  $y(i - 1)$  and  $t(i - 1)$  are the output and time at the previous step. If the rate is greater than  $R$  which is a rising slew rate parameter, the output is given in Equation (2.50). If the rate is less than  $F$  which is a falling slew rate parameter, the output is given in Equation (2.51).

$$y(i) = \Delta t.R + y(i-1) \quad (2.50)$$

$$y(i) = \Delta t.F + y(i-1) \quad (2.51)$$

### **2.4.3 Atmospheric Environment**

The atmospheric environment model, which is shown in Figure 2.4 is used for simulating atmospheric variations for the UAV model. This block contains the World Geodetic System (WGS84) Gravity Model, COESA Atmosphere Model, Wind Models. Wind models contain Wind Shear Model, Dryden Wind Turbulence Model, and Discrete Wind Gust Model. Respectively, gravity model is the mathematical model of geocentric equipotential ellipsoid of the WGS84. It is used for calculating the world's gravity which is different with respect to geodetic latitude, longitude, and altitude. The atmospheric environment model is the mathematical model of the 1976 Committee on Extension to the Standard Atmosphere (COESA) United States standard lower atmospheric values. It calculates the absolute temperature, pressure, density, and speed of sound with respect to altitude. The wind shear model is the mathematical model which represents the Military Specification MIL-F-8785C. The wind speed at 20 feet altitude and wind direction can be entered. It calculates the speed of the wind with respect to altitude and Direction Cosine Matrix (DCM). The Dryden Wind Turbulence Model is the mathematical model of the atmospheric turbulence which represents the Military Specification MIL-F-8785C and Military Handbook MIL-HDBK-1797. It uses filters for band-limited white noise. It calculates turbulence velocities and angular rates with respect altitude, aircraft speed and Direction Cosine Matrix (DCM).

### **2.4.4 Flight Control Computer**

The controller for autopilot or pilot is shown in Figure 2.4. In the controller, there is reference command for SDRE or LQR/LQT controller's gains which is shown in Figure 2.11. In the reference command, there are PID controllers, command filters and limiter. The controller architecture can be changed. The detailed information is given in Chapter 4 about controllers. Also, reference command block is explained in Section 4.2.2.

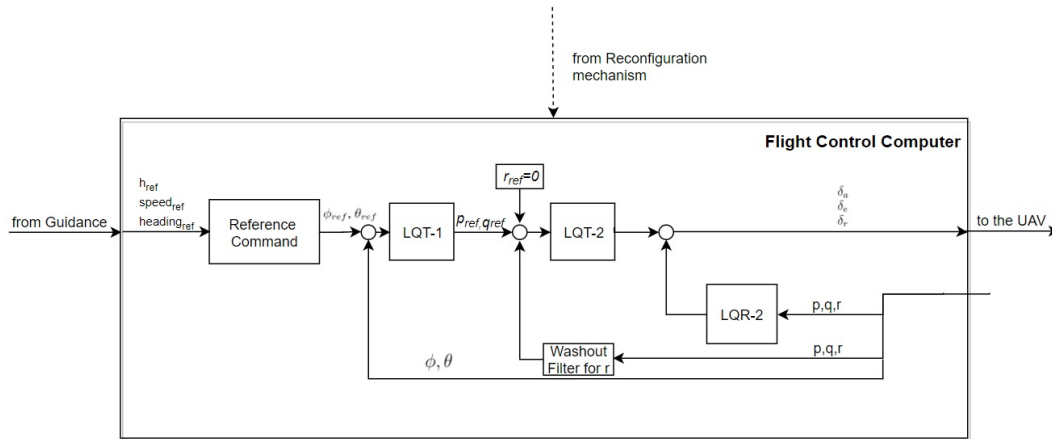


Figure 2.11: FCC and Reference command.

### 2.4.5 Actuators Model

Actuators model is in the UAV model which is shown in Figure 2.6. First, for control surface actuators, saturation blocks are used to limit control surface movement. Second, for engine actuators, also saturation block is used to simulate engine upper and lower limits. Degraded actuator models are explained with modelling faulty actuators in Section 2.5.2.1 and 2.5.2.2.

### 2.4.6 FDI/FDD

FDI/FDD is not modelled for this thesis. It is assumed that FDI/FDD finds the problem, problem location, level or stuck value. After that, it sends a signal to the supervisor in the reconfiguration mechanism.

### 2.4.7 Reconfiguration Mechanism

As stated in Section 1.3, one of the fault tolerant technique to achieve dependability, reconfiguration is used. As a result, reconfiguration mechanism is used for:

1. Reconfiguring **flight control computer (FCC)** by choosing or changing control algorithm,
2. Reconfiguring rate limiters and command filters both in the **MS** and **reference**

**command block in the FCC.**

3. Isolating some of the controls.

The supervisor is used for selecting precisely which mechanism is needed to be shown in Figure 4.30 for a fault or failure. For example, for full shutdown engine failure 6th reconfiguration mechanism has to be selected by the supervisor. For reconfiguration mechanism, detailed explanation is given in Chapter 4 because it is directly related to controllers.

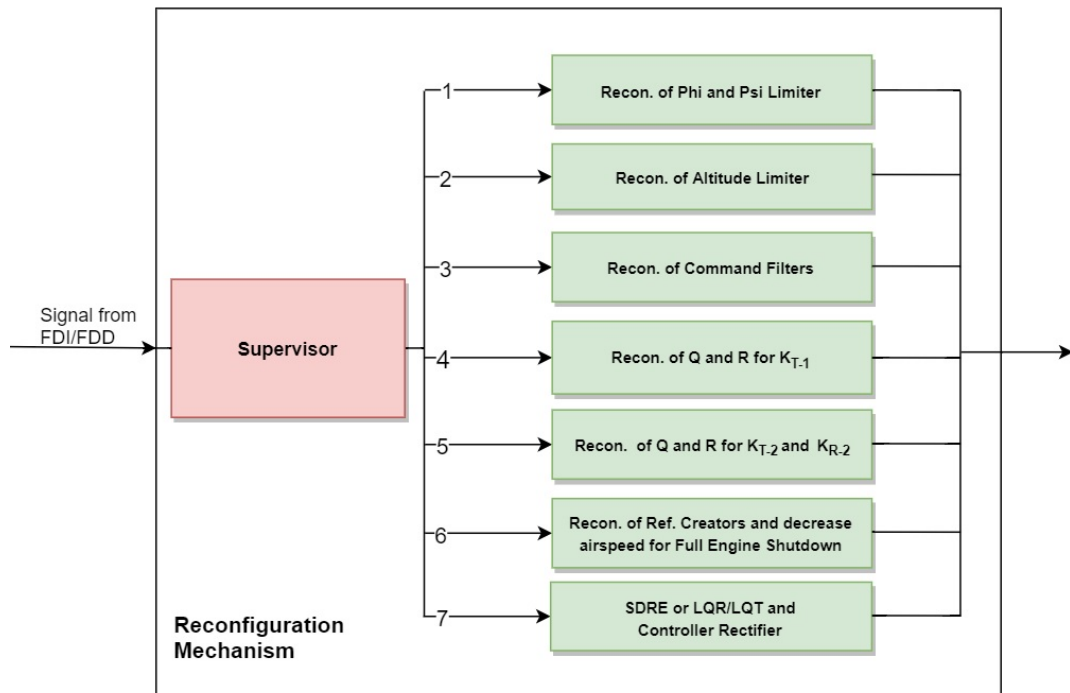


Figure 2.12: Inside the reconfiguration mechanism.

## 2.5 Faulty and Damaged Aircraft Model

Before damaged or faulty aircraft model, fault and damage injection is explained.

## 2.5.1 Fault Injection Block

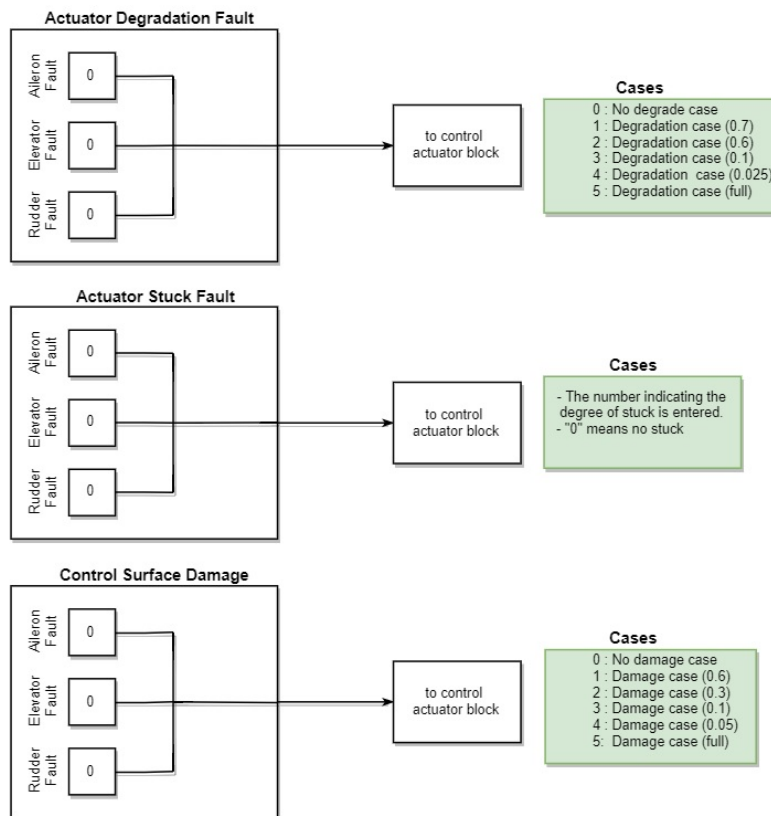


Figure 2.13: Inside The Fault injection (Control surfaces and actuators).

The Fault injection block is shown in Figure 2.4. **Actuator degradation faults** can be selected "0" which means no fault and signal is multiplied by 1; "1" which means 0.7 degradation; "2" which means 0.6 degradation; "3" which means 0.1 degradation; "4" which means 0.025 degradation; "5" which means full degradation for aileron, elevator and rudder actuator. In other words, after a signal is transmitted from the controller to actuators, it is multiplied by these numbers. Actuator degradation faults are depicted in Figure 2.13 and the process for degradation is depicted in Figure 2.16.

**Actuator stuck degree** can be selected from "0" means no stuck to any degree indicates stuck. Actuator stuck faults are depicted in Figure 2.13 and the process for degradation is depicted in Figure 2.16.

**Control surface damage** can be selected "0" which means no damage and the signal

is multiplied by 1; "1" which means 0.6 damage; "2" which means 0.3 damage; "3" which means 0.1 damage; "4" which means 0.05 damage; "5" which means full damage for aileron, elevator and rudder. Control surface damages are depicted in Figure 2.13 and the process for degradation is depicted in Figure 2.19.

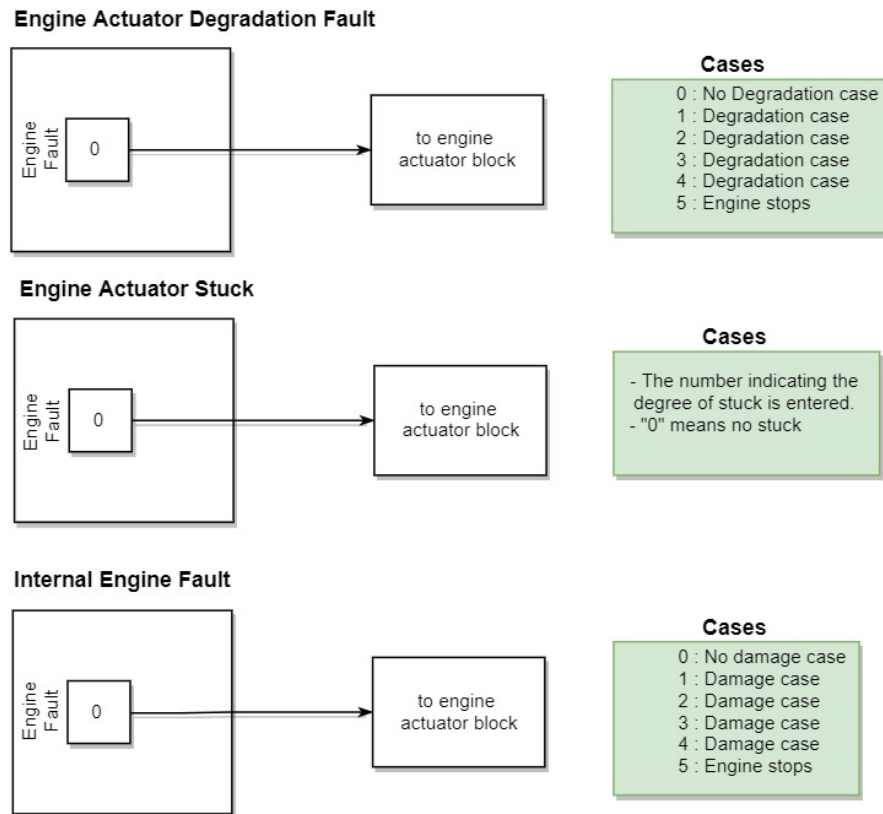


Figure 2.14: Inside The Fault injection (the engine and actuator).

**For engine actuator degradation** as in the control surface problem, can be selected from "0" means no degradation to "5" means engine full stop, depicted in Figure 2.14.

**Engine actuator stuck** can be selected other than "0" value , depicted in Figure 2.14.

**Engine internal problem** can be selected from "0" to "5", depicted in Figure 2.14.

**Controllability or observability problem** is selected individually, for SDRE controller, "0" can be selected which means the system is full controllable or observable, "1" can be selected which means the system is not controllable or not observable shown in Figure 2.15.

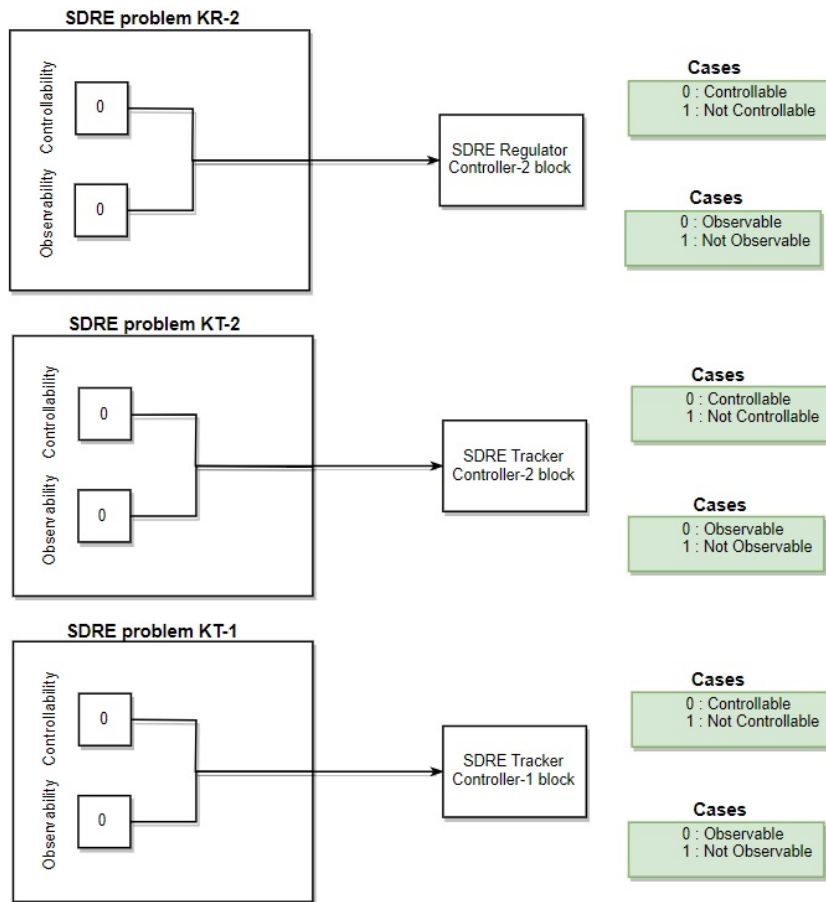


Figure 2.15: Inside The Fault injection (Flight control computer).

## 2.5.2 Damaged and Faulty UAV Model

### 2.5.2.1 Faulty Control Surface Actuator

The control surface actuator is shown in Figure 2.16. There are three pieces from this block, for aileron, elevator, and rudder.

The fault injection is explained. Now, how these faults and damages are simulated is explained. First, about degradation which can be selected from fault injection, the signal value which comes from the controller is multiplied by values which represent degraded performance. This process can be seen in Figure 2.16. Besides, aileron, elevator, and rudder degradation are simulated. With the help of the switch cases shown in Figure 2.17, degradation can be injected to actuators. In action blocks, values represent the degradation which is stated before, depicted in Figure 2.17. After

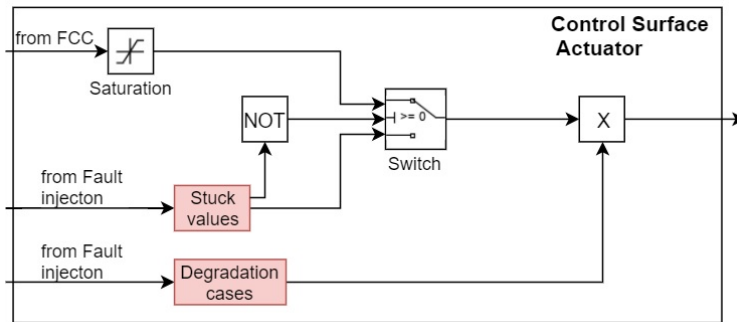


Figure 2.16: Inside control surface actuators.

that, the signal is transmitted from controller block to actuators block, the signal is multiplied by these values. Finally, the output of the actuators become degraded values.

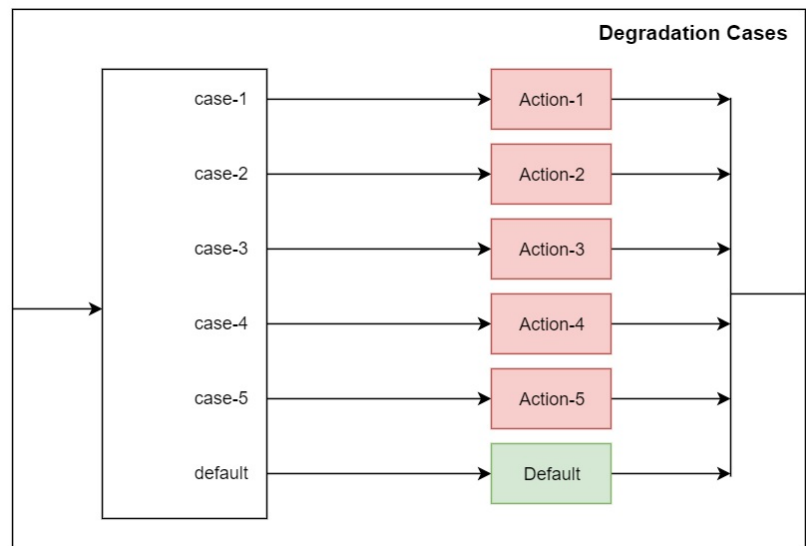


Figure 2.17: The actuator degraded cases.

Second, about stuck problem, the stuck values are selected from fault injection. These values enter to the logic block ("NOT") shown in Figure 2.16. Normally, an accurate signal is passed from the switch block. However, if the value of the stuck is different from zero, stuck value passes from the switch and remains.

### 2.5.2.2 Faulty Engine Actuator

Inside the engine actuator is shown in Figure 2.18.

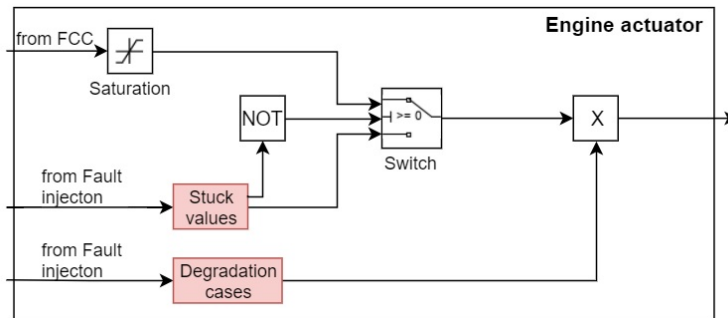


Figure 2.18: Inside the engine actuator.

About engine actuator degradation, the signal value for the engine which comes from the controller block is multiplied by selected values which can be selected from fault injection block. As shown in figure 2.17, the same switch case is used for degradation.

About engine actuator stuck problem, the stuck values are selected from fault injection block. These values enter to the logic block ("NOT") shown in Figure 2.18. If the value of the stuck is different from zero, stuck value passes from the switch and remain.

### 2.5.2.3 Damaged Control Surfaces

Due to physical damage to control surfaces, fuselage and lifting surfaces, estimating or identification of derivatives is a challenging task. Dynamics of the aircraft become highly uncertain and extraordinary aerodynamic results can be encountered [27]. Coupling occurs between pitching, yawing and rolling. For example, before,  $Cl_q$  is neglected. However, after wing damage occurs, this value increases significantly. Besides, symmetric assumptions about equations of motion, are not accurate due to the change of the body's center of mass [87].

Model of the aircraft, Airborne Subscale Transport Aircraft Research (AirSTAR) is designed for research about flight control laws in adverse flight conditions. In the re-

search center, estimation of the aircraft's aerodynamic parameters was done by flight and wind tunnel tests. AirSTAR uses two test aircraft which are called GTM-T2 and S2. GTM is a % 5.5 dynamically scaled model of the commercial aircraft [80]. The MATLAB/Simulink model of the GTM can be downloaded from the NASA website and it is an open source program.

In this thesis, only control surfaces damage is simulated. In this thesis, it is assumed that aerodynamic derivatives are changing proportionally to the percentage of loss in structure. In [88] and [89], despite the fact that further investigation is needed, change of the stability derivative is proportional to the percentage of loss in structure. In addition, as an assumption for the UAV, aerodynamic derivatives of the control surfaces decrease linearly and they are proportional to the damage; inertia and mass properties of the UAV are not changed.

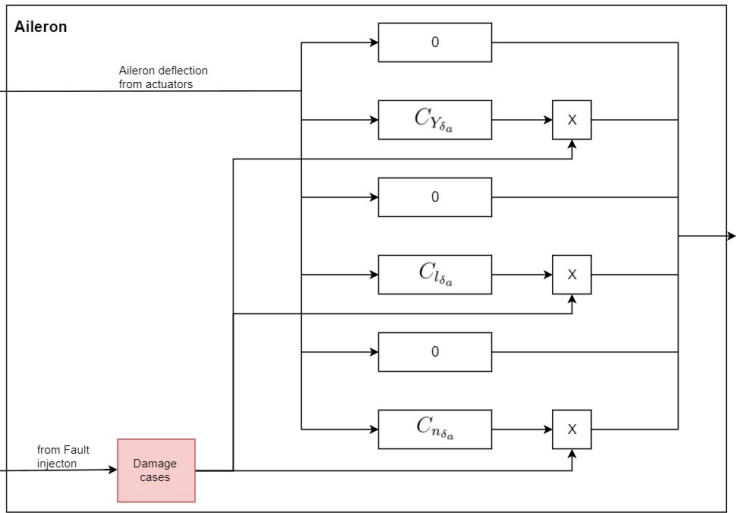


Figure 2.19: Inside Aerodynamics, Aerodynamic Coefficients of control surfaces, aileron block.

In Figure 2.19, there is a damage cases block which represents the percentage of the control surface damage, changing from "0" means no damage to "5" represents full damage. These values are explained in fault and failure injection. After the signal is passing, the deflection value is multiplied by the value to represent control surface damage. The same process is used for elevator and rudder.

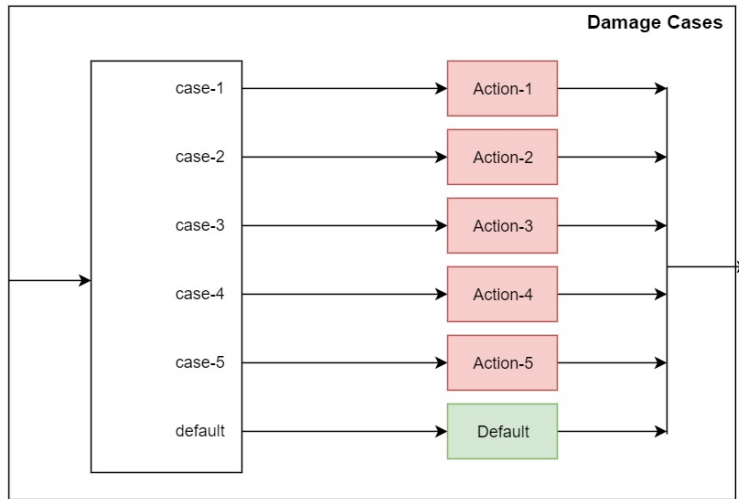


Figure 2.20: Aileron damage cases.

#### 2.5.2.4 Observability and Controllability Problem in the Controller

In the Controller, there are algebraic Riccati equation solvers which are used for calculating gains for SDRE controller stated in Section 4.3.2. During this process, observability and controllability are checked on-line. If the problem is injected by fault injection,  $B$  matrix is defected for controllability problem in Figure 2.21 and  $C$  matrix for observability problem. The mathematical background is explained in Section 4.3.1 and Section 4.3.2.

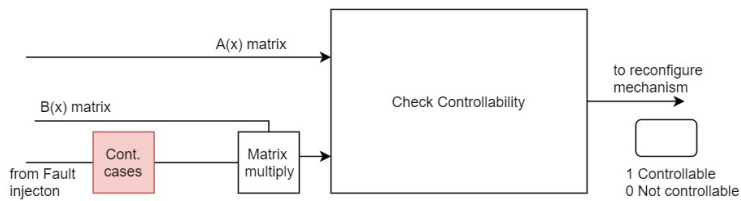


Figure 2.21: ARE calculator in the controller.

## CHAPTER 3

### LINEARIZATION AND LINEAR MODEL

#### 3.1 Trim and Linearization

Stability analysis for the trim point or equilibrium point is essential. Linear models are developed from trim points. In addition, designing and evaluating control systems can be done at the trim point [90]. Trim points can be steady state level flight, climbing, descending or constant turning. However, the most important and prolonged flight phase is the steady state level flight. For this thesis, the steady state is used. States are given as:

$$x^T = [u \quad v \quad w \quad p \quad q \quad r \quad \phi \quad \theta \quad \psi \quad x \quad y \quad h] \quad (3.1)$$

As an input; aileron, elevator, rudder and thrust are given respectively:

$$u^T = [\delta_a \quad \delta_e \quad \delta_r \quad \delta_t] \quad (3.2)$$

For trim analysis, state derivatives have to be zero:

$$\begin{aligned} \dot{u} = \dot{v} = \dot{w} = 0 \quad \text{or} \quad \dot{\alpha} = \dot{\beta} = 0 \\ \dot{p} = \dot{q} = \dot{r} = 0 \end{aligned} \quad (3.3)$$

Linearization is done by XFLR5 program. During linearization beta, roll angle, altitude, and temperature, viscous or inviscous analysis can be selected. For the UAV analysis, results are depicted in Table 3.1.

Linearization also is done by MATLAB/Simulink Linear Analysis Toolbox. For XFLR5, there is no different operating point for speed, because as stated before, it uses only  $C_{m_\alpha}$  graph. As a result, steady states are checked as  $u, v, w, p, q, r, \phi, \theta,$

Table 3.1: Trim values from XFLR5.

$V$	49.30914 $\frac{m}{s}$	<i>Density</i>	1.2162 $\frac{kg}{m^3}$
$\alpha$	1.73503 <i>deg.</i>	<i>Temperature</i>	14.3°C
$h$	100 <i>meter</i>		

$\psi$ ,  $y$  and  $z$  position.  $u$  is adjusted to 50 kt.,  $z$  position is adjusted to -100 meter. Also,  $x$  position is varying. For the UAV, level flight with a 50 kt. airspeed analysis results are depicted in Table 3.2.

Table 3.2: Trim values from MATLAB/Simulink Linear Analysis Toolbox.

<b>States</b>	<b>Values</b>	<b>Derivatives</b>	<b>States</b>	<b>Values</b>	<b>Derivatives</b>
$u$	50 $\frac{m}{s}$	-6.39e-13	$\phi$	1.28e-16 <i>rad</i>	-8.89e-21
$v$	2.22e-13 $\frac{m}{s}$	1.5e-19	$\theta$	0.0276 <i>rad</i>	1.58e-22
$w$	1.38 $\frac{m}{s}$	-5.25e-14	$\psi$	-4.44e-15 <i>rad</i>	-7.43e-21
$p$	-8.69e-21 $\frac{rad}{s}$	1.77e-18	$x$	-	-
$q$	1.58e-22 $\frac{rad}{s}$	1.83e-12	$y$	9.45e-19 <i>meter</i>	5.74e-19
$r$	-7.42e-21 $\frac{rad}{s}$	1.75e-19	$z$ or $-h$	-100m <i>meter</i>	-2.18e-14

From the Equation (2.41) and Table 3.2, angle of attack is found as 1.5814. The difference, from XFLR5 angle of attack, is the initial value of the elevator angle and the value of the  $u$ . For XFLR5,  $\delta_e = 0$  whereas for Matlab/simulink  $\delta_e = 0.2375$  degree. In Table 3.2, the values of  $v$ ,  $p$ ,  $q$ ,  $r$ ,  $\phi$ ,  $\psi$  and  $y$  are almost zero and derivatives mean difference from actual value and their values are too small which means conditions ensured successfully. Finally, comparison between XFLR5 and Matlab/Simulink is consistent.

## 3.2 Linear Model

### 3.2.1 General

After trimming model, the linear model is constructed. State space of the mathematical model of the linear system is given as:

$$\begin{aligned} \dot{x}(t) &= Ax(t) + Bu(t) \\ y(t) &= Cx(t) + Du(t) \end{aligned} \quad (3.4)$$

Nonlinear equations of motion are given from Equation (2.24) to Equation (2.29). These developed equations have to be linearized around trim or equilibrium point. One of the ways for linearization is small disturbance theory. In that theory, the motion of the aircraft is assumed to fly with small deviations from the equilibrium point. In other words, small perturbations are used to developed linearized equations [81]. For the UAV, in this thesis,  $M_{\dot{w}}$  value is not used for the linear model. Besides, for the linear model  $\psi, x, y, h$  states are not taken into account for stability analysis.

The longitudinal equation of motion is linearized and the matrix representation is given in Equation (3.5) and Equation (3.6) [91]. Normally, all states are denoted with  $\Delta$  in the state space matrix.

$$\begin{bmatrix} \dot{u} \\ \dot{w} \\ \dot{q} \\ \dot{\theta} \end{bmatrix} = \begin{bmatrix} X_u & X_w & 0 & -g \\ Z_u & Z_w & u_0 & 0 \\ M_u + M_{\dot{w}} Z_u & M_w + M_{\dot{w}} Z_w & M_q + M_{\dot{w}} u_0 & 0 \\ 0 & 0 & 1 & 0 \end{bmatrix} \begin{bmatrix} u \\ w \\ q \\ \theta \end{bmatrix} + \quad (3.5)$$

$$\begin{bmatrix} X_{\delta_e} & X_{\delta_t} \\ Z_{\delta_e} & Z_{\delta_t} \\ M_{\delta_e} + M_{\dot{w}} Z_{\delta_e} & M_{\delta_t} + M_{\dot{w}} Z_{\delta_t} \\ 0 & 0 \end{bmatrix} \begin{bmatrix} \delta_e \\ \delta_t \end{bmatrix} \quad (3.6)$$

The lateral equation of motion is linearized and the matrix representation is given in

Equation (3.7) and Equation (3.8) [91]. Normally all states are denoted with  $\Delta$  in the state space matrix.

$$\begin{bmatrix} \dot{v} \\ \dot{p} \\ \dot{r} \\ \dot{\phi} \end{bmatrix} = \begin{bmatrix} Y_v & Y_p & -u_0 + Y_r & g \cos \theta \\ L_v^* + \frac{I_{xz}}{I_{xx}} N_v^* & L_p^* + \frac{I_{xz}}{I_{xx}} N_p^* & L_r^* + \frac{I_{xz}}{I_{xx}} N_r^* & 0 \\ N_v^* + \frac{I_{xz}}{I_{zz}} L_v^* & N_p^* + \frac{I_{xz}}{I_{zz}} L_p^* & N_r^* + \frac{I_{xz}}{I_{zz}} L_r^* & 0 \\ 0 & 1 & 0 & 0 \end{bmatrix} \begin{bmatrix} v \\ p \\ r \\ \phi \end{bmatrix} + \quad (3.7)$$

$$\begin{bmatrix} 0 & Y_{\delta_r} \\ L_{\delta_a}^* + \frac{I_{xz}}{I_{xx}} N_{\delta_a}^* & L_{\delta_r}^* + \frac{I_{xz}}{I_{xx}} N_{\delta_r}^* \\ N_{\delta_a}^* + \frac{I_{xz}}{I_{zz}} L_{\delta_a}^* & N_{\delta_r}^* + \frac{I_{xz}}{I_{zz}} L_{\delta_r}^* \\ 0 & 0 \end{bmatrix} \begin{bmatrix} \delta_a \\ \delta_r \end{bmatrix} \quad (3.8)$$

Starred derivatives are given in Equation (3.9).

$$L_v^* = \frac{L_v}{1 - (I_{xz}^2 / (I_{xx} I_{zz}))} \quad N_v^* = \frac{N_v}{1 - (I_{xz}^2 / (I_{xx} I_{zz}))} \quad etc. \quad (3.9)$$

In addition, in Equation (3.5), instead of  $w$ ,  $\alpha$  can be used and approximated as a state in Equation (3.10).

$$\Delta \alpha = \tan^{-1} \frac{\Delta w}{u_0} = \frac{\Delta w}{u_0} \quad (3.10)$$

As a result,  $Z_\alpha = u_0 Z_w$  and  $M_\alpha = u_0 M_w$  can be used. Derivatives formulas for longitudinal motion are given in Table 3.3.

Table 3.3: Longitudinal stability derivatives formula [91, 82].

	$\alpha$	$u$	$w$	$q$	$\delta_e$
$X$	$\frac{-(C_{D\alpha} - C_{L0})QS}{m}$	$\frac{-(C_{Du} + 2C_{D0})QS}{mu_0}$	$\frac{-(C_{D\alpha} - C_{L0})QS}{mu_0}$	-	$\frac{-C_{D\delta_e} QS}{m}$
$Z$	$\frac{-(C_{Lu} + 2C_{L0})QS}{m}$	$\frac{-(C_{Lu} + 2C_{L0})QS}{mu_0}$	$\frac{-(C_{L\alpha} + C_{D0})QS}{mu_0}$	$\frac{-C_{Lq} QS \bar{c}}{m2u_0}$	$\frac{-C_{L\delta_e} QS}{m}$
$M$	$\frac{C_{M\alpha} QS \bar{c}}{I_{yy}}$	$\frac{C_{Mu} QS \bar{c}}{I_{yy} u_0}$	$\frac{C_{M\alpha} QS \bar{c}}{I_{yy} u_0}$	$\frac{C_{mq} QS \bar{c}^2}{I_{yy} 2u_0}$	$\frac{C_{M\delta_e} QS \bar{c}}{I_{yy}}$

In addition, in Equation (3.7), instead of  $v$ ,  $\beta$  can be used and approximated as a state in Equation (3.11).

$$\Delta\beta = \tan^{-1} \frac{\Delta v}{u_0} = \frac{\Delta v}{u_0} \quad (3.11)$$

As a result,  $Y_\beta = u_0 Y_v$ ,  $L_\beta = u_0 L_v$ ,  $N_\beta = u_0 N_v$  can be used. Derivatives formulas for lateral motion are given in Table 3.4.

Table 3.4: Lateral stability derivatives formula [91, 82].

	$\beta$	$v$	$p$	$r$	$\delta_a$	$\delta_r$
$Y$	$\frac{(C_{y\beta})QS}{m}$	$\frac{(C_{y\beta})QS}{mu_0}$	$\frac{(C_{yp})Q Sb}{2mu_0}$	$\frac{(C_{yr})Q Sb}{2mu_0}$	$\frac{(C_{y\delta_a})QS}{m}$	$\frac{(C_{y\delta_r})Q Sb}{2mu_0}$
$L$	$\frac{(C_{l\beta})Q Sb}{I_{xx}}$	$\frac{(C_{l\beta})Q Sb}{I_{xx}u_0}$	$\frac{(C_{lp})Q Sb^2}{2I_{xx}u_0}$	$\frac{(C_{lr})Q Sb^2}{2I_{xx}u_0}$	$\frac{(C_{l\delta_a})Q Sb}{I_{xx}}$	$\frac{(C_{l\delta_r})Q Sb}{I_{xx}}$
$N$	$\frac{(C_{n\beta})Q Sb}{I_{zz}}$	$\frac{(C_{l\beta})Q Sb}{I_{zz}u_0}$	$\frac{(C_{np})Q Sb^2}{2I_{zz}u_0}$	$\frac{(C_{nr})Q Sb^2}{2I_{zz}u_0}$	$\frac{(C_{n\delta_a})Q Sb}{I_{zz}}$	$\frac{(C_{n\delta_r})Q Sb}{I_{zz}}$

### 3.2.2 Longitudinal Dynamics

For longitudinal motion of the UAV,  $A$  and  $B$  matrices are given in Equation (3.12).

$$\begin{bmatrix} \dot{u} \\ \dot{w} \\ \dot{q} \\ \dot{\theta} \end{bmatrix} = \begin{bmatrix} -0.019 & 0.084 & 0 & -9.810 \\ -0.254 & -1.986 & 49.986 & 0 \\ -0.000 & -0.501 & -1.867 & 0 \\ 0 & 0 & 1.000 & 0 \end{bmatrix} \begin{bmatrix} u \\ w \\ q \\ \theta \end{bmatrix} + \begin{bmatrix} -0.787 & 1 \\ -9.013 & 0 \\ -36.766 & 0 \\ 0 & 0 \end{bmatrix} \begin{bmatrix} \delta_e \\ \delta_t \end{bmatrix} \quad (3.12)$$

Stability characteristic of the UAV can be examined best from eigenvalues of the  $A$  matrix.  $A$  matrix can be described as internal dynamics without control forces. Eigenvalues are found by  $0 = |A - \lambda I|$  which  $I$  is an identity and  $A$  is a 4 by 4 matrix. As a result, characteristic equation is a fourth-degree polynomial given in Equation (3.13) [92].

$$\lambda^4 + a_1\lambda^3 + a_2\lambda^2 + a_3\lambda + a_4 = 0 \quad (3.13)$$

If all eigenvalues of the  $A$  matrix are negative real parts, the system is stable. The natural frequency is denoted as  $\omega_n$  and damping ratio is denoted as  $\zeta$ . Natural frequency and damping ratio are found from eigenvalues but also by short period and phugoid approximation which is explained in [91] clearly.

Eigenvalues of the longitudinal  $A$  matrix is given in Equation (3.14).

$$\lambda_{1,2} = -0.0077 \pm 0.2082i \quad \lambda_{3,4} = -1.9291 \pm 5.0038i \quad (3.14)$$

Modes of the longitudinal motion are given in Table 3.5.

Table 3.5: Longitudinal Modes.

<b>Modes</b>	<b>Roots</b>	<b>Natural Frequency</b>	<b>Damping Ratio</b>
<i>PhugoidMode</i>	$\lambda_{1,2} = -0.0077 \pm 0.2082i$	0.2083	0.0370
<i>ShortMode</i>	$\lambda_{3,4} = -1.9291 \pm 5.0038i$	5.3628	0.3597

### 3.2.3 Lateral Dynamics

For lateral motion of the UAV,  $A$  and  $B$  matrices are given in Equation (3.15).

$$\begin{bmatrix} \dot{v} \\ \dot{p} \\ \dot{r} \\ \dot{\phi} \end{bmatrix} = \begin{bmatrix} -0.071 & -0.024 & -49.858 & 9.807 \\ -0.087 & -6.264 & 1.380 & 0 \\ 0.151 & -0.213 & -0.286 & 0 \\ 0 & 1.000 & 0 & 0 \end{bmatrix} \begin{bmatrix} v \\ p \\ r \\ \phi \end{bmatrix} + \begin{bmatrix} 0 & 0.128 \\ 28.279 & 0.579 \\ -0.796 & -2.299 \\ 0 & 0 \end{bmatrix} \begin{bmatrix} \delta_a \\ \delta_r \end{bmatrix} \quad (3.15)$$

Characteristic equation for  $A$  matrix of lateral motion is the same as in Equation (3.13) due to 4 states. However, sometimes 5th state,  $\psi$  can be included. Eigenvalues of the lateral  $A$  matrix is given in Equation (3.16).

$$\lambda_1 = -6.2702 + 0i \quad \lambda_{2,3} = -0.1940 \pm 2.8038i \quad \lambda_4 = 0.0364 + 0i \quad (3.16)$$

Modes of the lateral motion are given in Table 3.6.

Table 3.6: Lateral Modes.

<b>Modes</b>	<b>Roots</b>	<b>Natural Frequency</b>	<b>Damping Ratio</b>
<i>RollMode</i>	$\lambda_1 = -6.2702 + 0i$	6.2702	1
<i>DutchRollMode</i>	$\lambda_{2,3} = -0.1940 \pm 2.8038i$	2.8105	0.0690
<i>SpiralMode</i>	$\lambda_4 = 0.0364 + 0i$	-	-

### 3.2.4 Linear Model in MATLAB/Simulink

Linear model is represented by state space model block. Inputs of the model are respectively  $\delta_a, \delta_e, \delta_r, \delta_t$  and their initial condition given in Equation (3.20). There are  $u, v, w, p, q, r, \phi, \theta, \psi$ , and  $h$  states and their initial conditions are given in Equation (3.19). There are also  $\psi$  and  $h$  states which is not linearized before and nonlinear version is given respectively in Equation (2.38) and Equation (2.40). Linear version is given in Equation (3.17) and Equation (3.18).

$$\psi = r \quad (3.17)$$

$$h = -w + u_0\theta \quad (3.18)$$

$$x_0 = \begin{bmatrix} 50 & 0 & 1.4 & 0 & 0 & 0 & 0 & 0.03 & 0 & 100 \end{bmatrix} \quad (3.19)$$

$$u_0 = \begin{bmatrix} 0 & 0.0044 & 0 & 51 \end{bmatrix} \quad (3.20)$$



## CHAPTER 4

### LINEAR AND NONLINEAR CONTROLLERS AND RECONFIGURATION

In this chapter, linear and nonlinear controllers and autopilots are described. The reconfiguration mechanism is explained. Normally, for controllers, there are two loops. One of them is for position or guidance controller which is in the model of guidance but not modelled for this thesis and another one is for attitude and speed controller which is modelled and called Flight Control Computer (SDRE/LQR/LQT+PID) which is shown in Figure 2.4.

#### 4.1 Linear Controller-PID

Generally, PID controllers are extensively used in not only the whole control industry but also in the aviation industry. In this thesis, PID controller is used as a starting point for constructing other controllers. It is not used in an emergency case.

For linear controllers, classical controller, PID is designed. There are heading controller for the autopilot or only roll controller can be adjusted; altitude controller for the autopilot or only pitch controller can be adjusted; yaw rate controller; speed controller for the autopilot shown in Figure 4.1. Roll and pitch controller can be selected differently from autopilot modes. For example, sometimes, for remote controller,  $\theta$  and  $\phi$  controllers are required [93]. Besides, selected  $\theta_{ref.}$  and  $\phi_{ref.}$  are very helpful for tuning PID controllers. However, for the autopilot; speed, heading, altitude, and yaw rate controllers are required. As stated before, only attitude modes are designed, navigational modes which LNAV, ILS etc. are not designed.

For all PID controller values, first, tuning is done by manually and then with the help

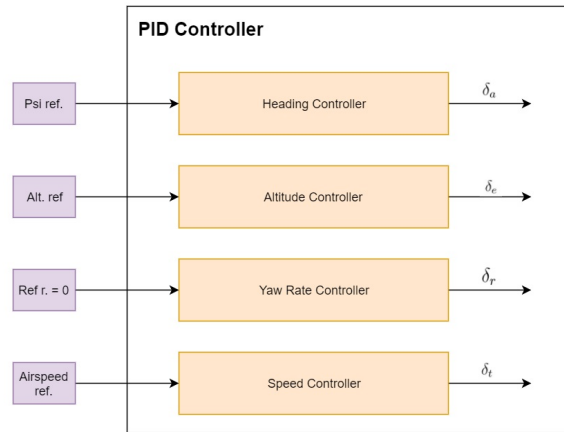


Figure 4.1: PID controller for Autopilot.

of the Matlab/Simulink PID tuner to achieve the desired response. During tuning, MATLAB/Simulink linearizes the system and then it determines system's input and output. Starting from good values make the work simple. Step reference tracking performance plot can be tracked during tuning shown in Figure 4.2, so that the best performance and robustness can be achieved.

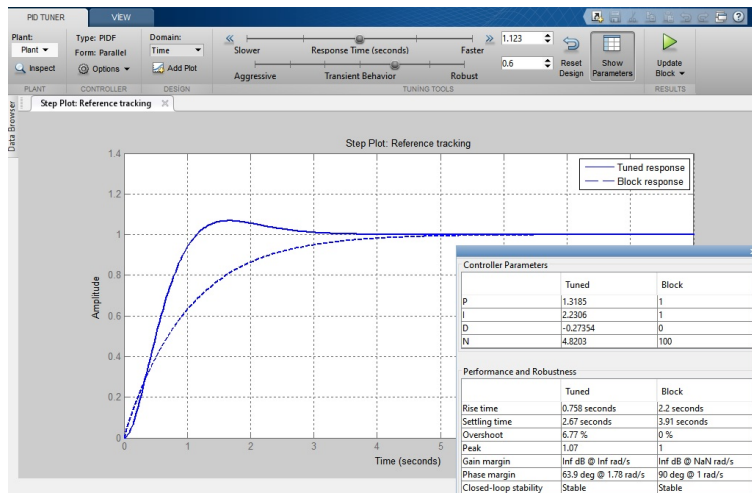


Figure 4.2: PID Tuner in MATLAB/Simulink.

The system responses, after (tuned response) and before (block response) tuning are shown at the same time. In addition, rise, settling, overshoot, peak time; phase, gain margin and whether the system stable or not after tuning, are depicted simultaneously.

### 4.1.1 Heading or Roll Controller

For the directional or heading controller, three loops are used. PID Controller-1, 2, 3 are used for tracking, 4 is used for the regulator. The first loop is about controlling  $\psi$ . An error is generated between  $\psi_{ref}$  which is transmitted from Mode Selection (MS) explained in Section 2.4.2 and  $\psi_{sensor}$  which is transmitted from sensors. This error is multiplied by PID Controller-1. After that, rate limiter is used for limiting roll rate to 20 degrees. The signal become a  $\phi_{ref}$ . A new error is generated between  $\phi_{ref}$  and  $\phi_{sensor}$ . This error is multiplied by PID Controller-2 and become  $p_{ref}$ . Similarly, an error is generated between  $p_{ref}$  and  $p_{sensor}$  and it is multiplied by PID Controller-3. Finally, signal become  $\delta_a$  value. By the way, PID Controller-4 is used for Stability Augmentation System (SAS). After  $p_{sensor}$  is multiplied by PID Controller-4, it is similarly become  $\delta_a$  value shown in Figure 4.3. As stated before, the manual switch is used to send  $\phi_{ref}$  value manually.

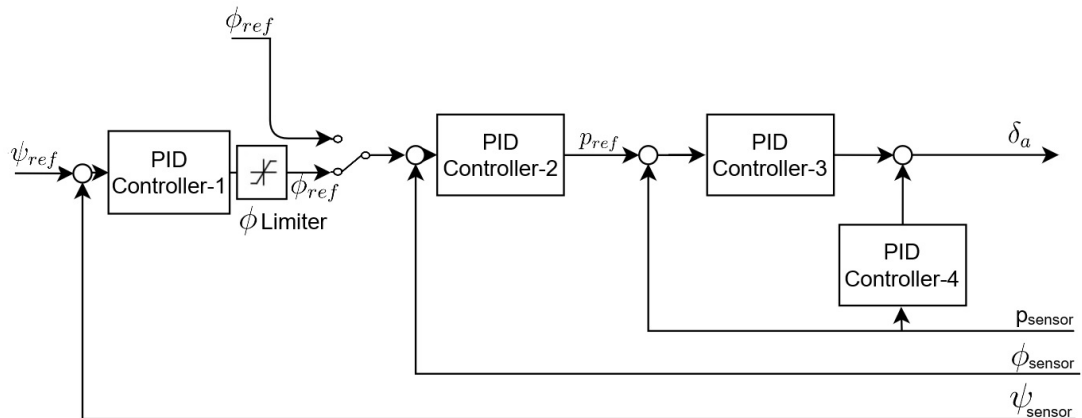


Figure 4.3: Heading Controller.

### 4.1.2 Altitude or Pitch Controller

Similarly, for altitude controller, three loops are used. PID Controller-1, 2, 3 are used for tracking, 4 is used for the regulator. The altitude reference signal is generated from Mode Selection (MS). An error is generated between sensor altitude ( $h_{sensed}$ ) and reference altitude ( $h_{ref}$ ) and it is multiplied by PID Controller-1. The value becomes  $\theta_{ref}$ . The process is the same as heading controller for PID Controller-2, 3,

4. As stated before, the manual switch is used to send  $\theta_{ref}$  value manually shown in Fig. 4.4.

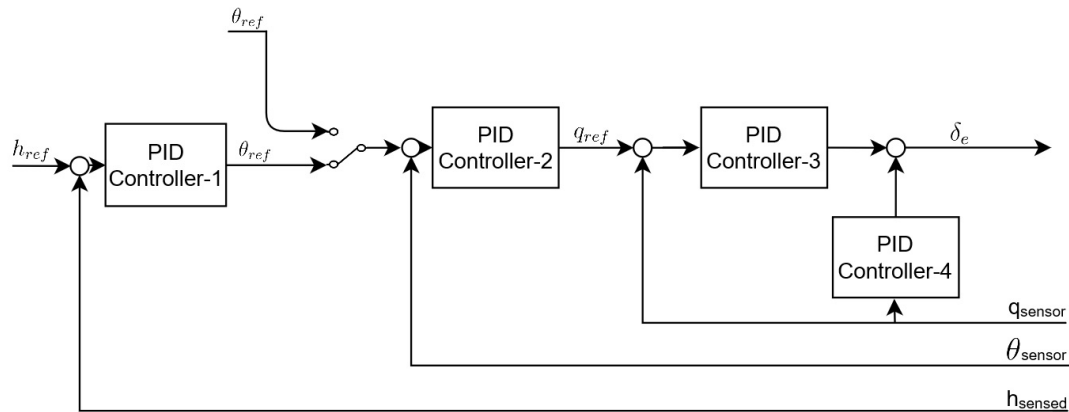


Figure 4.4: Altitude or Pitch Controller.

### 4.1.3 Yaw Rate Controller

Yaw rate or yaw damper is used for reducing dutch roll. Normally, for some general aviation (GA) aircraft, nearly all airline aircraft and fighter aircraft, have to have a yaw dampers to achieve handling qualities for the dutch roll. For example in [82], one of the fighter aircraft has an unstable dutch roll root. As a result, to achieve flying qualities yaw damper is used to make dutch roll root stable. Yaw rate or yaw dampers are used to minimize  $\beta$  value during a coordinated turn.

As a reference,  $r_{ref}$  is zero to make lateral acceleration zero during straight flight. However, during heading change, it does not work well and struggles with the pilot command due to zero value. Therefore, to solve this problem during heading change, the washout filter is used to make a small delay. There are two ways for developing washout filter [82]:

1. Use computed yaw rate as a reference input.

$$r_{ref} = \dot{\psi} \cos \theta \cos \phi \quad (4.1)$$

2. Use zero as a reference input given in Equation (4.2) but with washout filter

given in Equation (4.3).

$$r_{ref} = 0 \quad (4.2)$$

$$K_{washout} = \frac{\tau s}{\tau s + 1} \quad (4.3)$$

In this thesis, the second way, the washout filter is chosen. If the value of the  $\tau$  is too small, it will not perform properly. Otherwise, it will struggle with the pilot command. As a result, the value  $\tau$  is chosen as 1, shown in Figure 4.5.

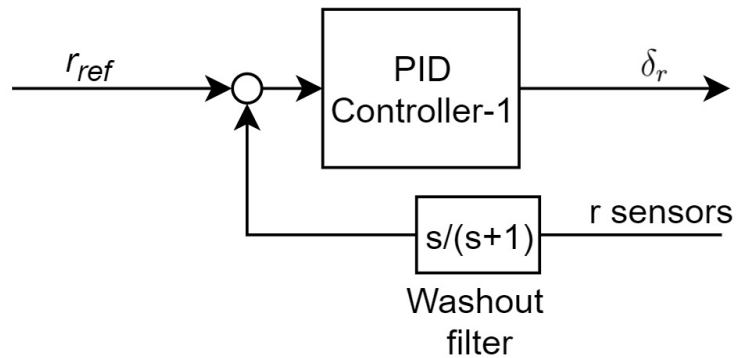


Figure 4.5: Yaw Rate Controller

#### 4.1.4 Speed Controller

Reference speed signal is generated from Mode Selection (MS). An error is generated between  $speed_{sensor}$  and  $speed_{ref}$ . After that, the value is multiplied by PID Controller-1 shown in Figure 4.6. Finally, signal is transmitted to the engine actuator as  $\delta_t$ .

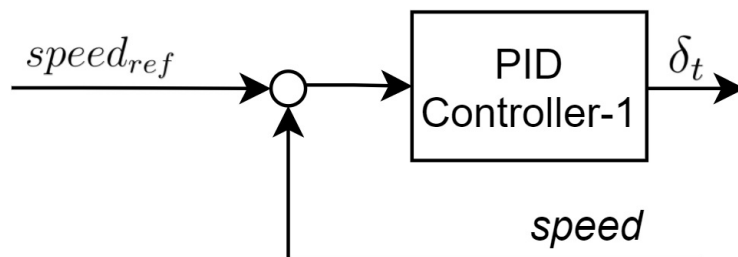


Figure 4.6: Speed Controller.

Table 4.1: All PID values for controllers.

Heading Controller	Proportional	Integral	Derivative	Filter
PID-1	2.3203	0.0090	-0.4952	4.6854
PID-2	22.3581	0	0	1
PID-3	0.0742	0	0	1
PID-4 (SAS)	0.1735	0	0	1
Altitude Controller	Proportional	Integral	Derivative	Filter
PID-1	0.0542	0.0013	0.0276	7.7338
PID-2	22.3607	0	0	1
PID-3	-0.7053	0	0	1
PID-4 (SAS)	-0.6580	0	0	1
Yaw Rate Controller	Proportional	Integral	Derivative	Filter
PID-1	-0.07	-2	-0.14	1
Speed Controller	Proportional	Integral	Derivative	Filter
PID-1	254.0610	3.0407	-87.857	2.8917

## 4.2 Linear Controller-LQR and LQT

### 4.2.1 Mathematical Background for LQR and LQT

Linear Quadratic Regulator (LQR) and Linear Quadratic Tracking (LQT) are an optimal control, modern control technique. The background is explained in Section 4.3.

### 4.2.2 Reference Command

First, for LQR and LQT controllers;  $\phi_{ref}$  and  $\theta_{ref}$  have to be generated. Therefore, reference command, shown in Figure 4.7, is used which is developed in the controller block shown in Figure 2.4. Before LQR and LQT controllers, reference command is explained shown in Figure 4.8. In SDRE controller, the same reference command is used.

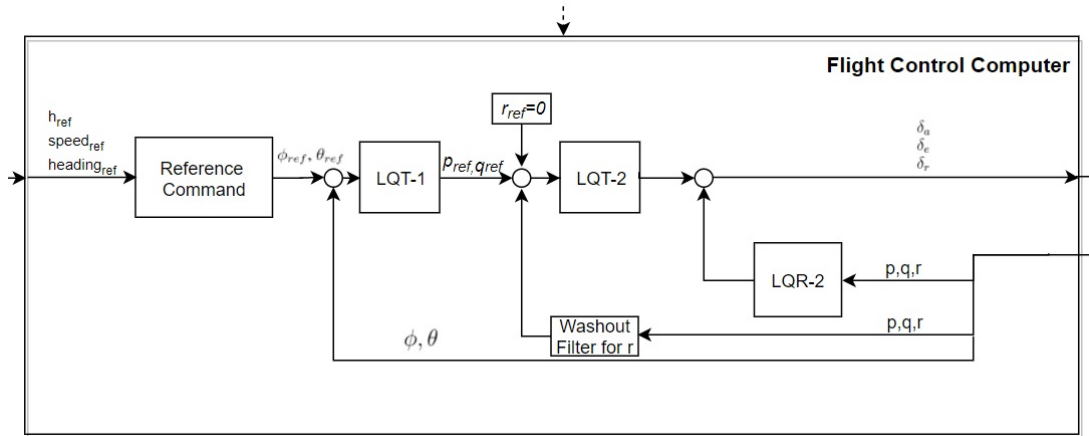


Figure 4.7: LQR and LQT Controller.

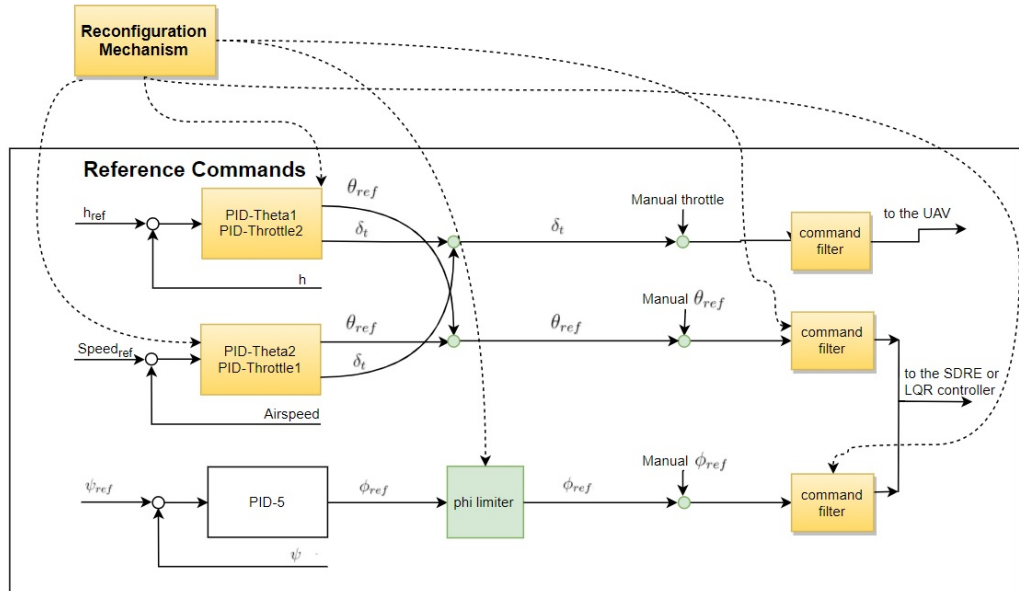


Figure 4.8: Inside the reference command.

There are two different longitudinal architecture for  $\theta_{ref}$  and  $\delta_t$  shown in Figure 4.8. The first one is shown in Figure 4.9,  $\theta_{ref}$  is generated from reference altitude and  $\delta_t$  is generated from reference speed. If the UAV begins making small altitude deviations due to turbulence, the first reaction is changing the  $\theta_{ref}$  by PID controller. In addition, if the airspeed of the UAV decreases, the auto throttle's first reaction is increasing  $\delta_t$ . Normally, during level flight, climbing with vertical speed with autopilot or manual flight with auto throttle, this architecture is useful. In summary,  $altitude_{ref}$  affects  $\theta_{ref}$ , and  $speed_{ref}$  affects  $\delta_t$ .

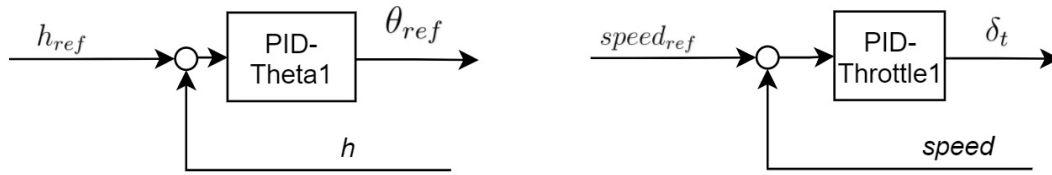


Figure 4.9:  $\theta_{ref}$  and  $\delta_t$  Controller-1.

However, in Figure 4.10,  $\theta_{ref}$  is generated from reference speed and  $\delta_t$  is created from reference altitude. During climbing with flight level change, the speed is important in lieu of vertical speed. For example, if reference speed is 50 kt and reference altitude is more than level flight value, with this architecture shown in Figure 4.10, the UAV begins to climb with a constant speed regardless of vertical speed and it uses maximum throttle setting for climbing. Normally, when the altitude is reached, the architecture is changed to  $\theta_{ref}$  and  $\delta_t$  Controller-1. Besides, FLC is not used for descending. In this thesis, these rules are not taken into account.

To make it clear, if there is no autothrottle for the aircraft such as Cessna 182T or Beechcraft 350, pilot adjusts the throttle manually. For example, a pilot decides to climb to the new altitude with the flight level change mode at a constant speed. If the throttle is not increased, the aircraft can not begin to climb, due to the effect of the reference speed to the  $\theta_{ref}$ .

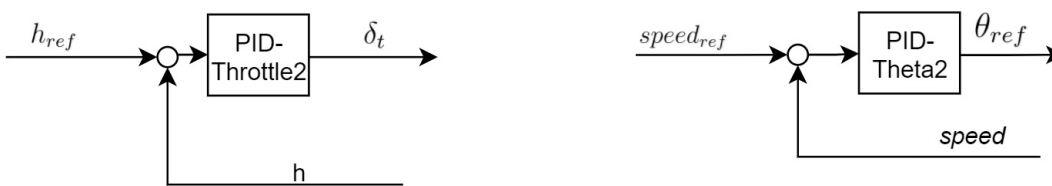


Figure 4.10:  $\theta_{ref}$  and  $\delta_t$  Controller-2.

For the lateral controller,  $\phi_{ref}$  has to be generated by the reference command shown in Figure 4.11. In addition, there are  $\phi_{ref}$  limiter to limit roll angle to 20 degrees and  $\phi_{ref}$  command filter to slow down the signal.

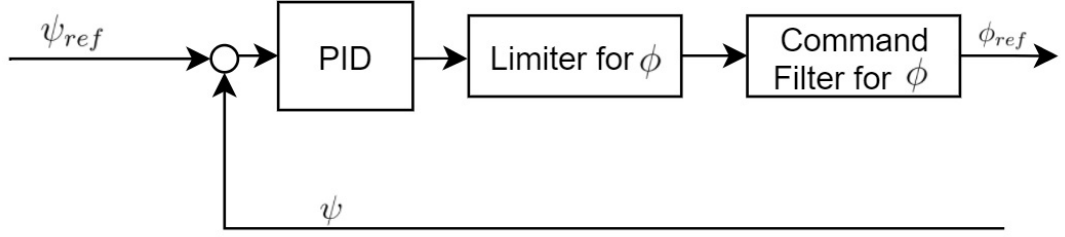


Figure 4.11:  $\psi_{ref}$  Controller.

### 4.2.3 LQR and LQT Controllers

After reference command,  $\phi_{ref}$  and  $\theta_{ref}$  is transmitted to the LQR and LQT controllers shown in Figure 4.7. Both of them are in the same block called flight control computer (FCC).

For LQT-1 gain,  $A_{lqt-1}$ ,  $B_{lqt-1}$ ,  $C_{lqt-1}$ ; for LQR/T-2 gains,  $A_{lqt/r-2}$ ,  $B_{lqt/r-2}$ ,  $C_{lqt/r-2}$  have to be calculated. States are only  $p$ ,  $q$ ,  $r$  and  $A_{lqt/r-2}$ ,  $B_{lqr/r-2}$  matrices are given in Equation (4.4). All  $C$  matrices are 3 by 3 identity matrices.

$$\begin{bmatrix} \dot{p} \\ \dot{q} \\ \dot{r} \end{bmatrix} = \begin{bmatrix} -6.26 & 0 & 1.38 \\ 0 & -1.87 & 0 \\ -0.21 & 0 & -0.29 \end{bmatrix} \begin{bmatrix} p \\ q \\ r \end{bmatrix} + \begin{bmatrix} 28.27 & 0 & 0.58 \\ 0 & -36.77 & 0 \\ -0.79 & 0 & -2.30 \end{bmatrix} \begin{bmatrix} \delta_a \\ \delta_e \\ \delta_r \end{bmatrix} \quad (4.4)$$

As regards  $A_{lqt-1}$  and  $B_{lqt-1}$ , Equation (4.5) is used.

$$\begin{bmatrix} \dot{\phi} \\ \dot{\theta} \\ \dot{\psi} \end{bmatrix} = \begin{bmatrix} 0 & 0 & 0 \\ 0 & 0 & 0 \\ 0 & 0 & 0 \end{bmatrix} \begin{bmatrix} \phi \\ \theta \\ \psi \end{bmatrix} + \begin{bmatrix} 1 & 0 & 0 \\ 0 & 1 & 0 \\ 0 & 0 & 1 \end{bmatrix} \begin{bmatrix} p \\ q \\ r \end{bmatrix} \quad (4.5)$$

For LQT-1,  $Q_1$  and  $R_1$  are given in Equation (4.6); for LQT-2 and LQR-2,  $Q_2$  and  $R_2$  are given in Equation (4.7).

$$Q_1 = \text{diag}[50, 50, 50] \quad R_1 = \text{diag}[0.1, 0.1, 0.1] \quad (4.6)$$

$$Q_2 = \text{diag}[5, 5, 2] \quad R_2 = \text{diag}[50, 10, 10] \quad (4.7)$$

#### 4.2.4 Results for LQR and LQT Controller

**In the first example**, the UAV begins climbing from 100 meters to 200 meters at the 3rd second with vertical speed shown in Figure 4.12. About vertical speed, the UAV is climbing 8 ft. in 1 second shown in Figure 4.12 and it equals to 480 ft. in 60 seconds. In other words, in this case, pilot adjusts vertical speed approximately to 0.5 which means 500 ft./minute. In Figure 4.13, control surfaces deflection is depicted. In Figure 4.14, throttle command is depicted.

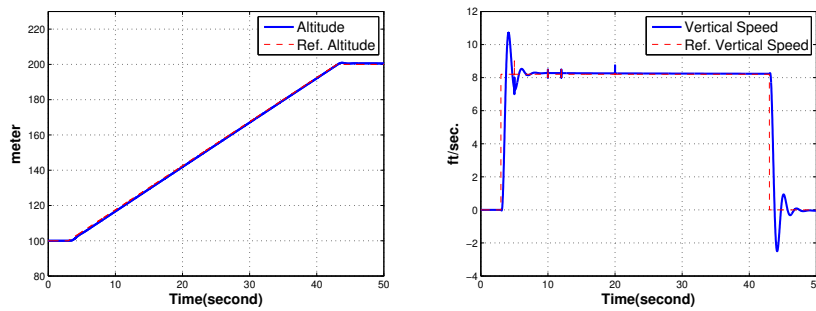


Figure 4.12: Altitude and vertical speed during climbing.

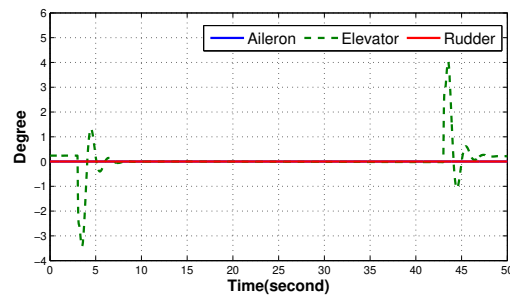


Figure 4.13: Control surface deflection during altitude change.

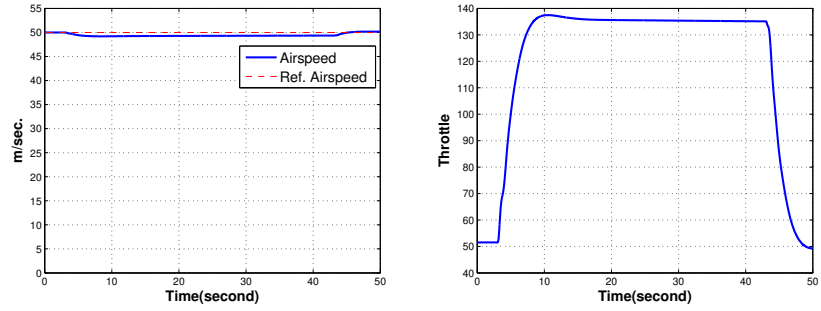


Figure 4.14: Air speed and throttle command during climbing.

**In the second example**, the UAV begins heading change from 360 degrees to 90 degrees at the 2th second shown in Figure 4.15 and Figure 4.16. Altitude and airspeed responses are depicted in Figure 4.17. Control surface deflection is depicted in Figure 4.18.

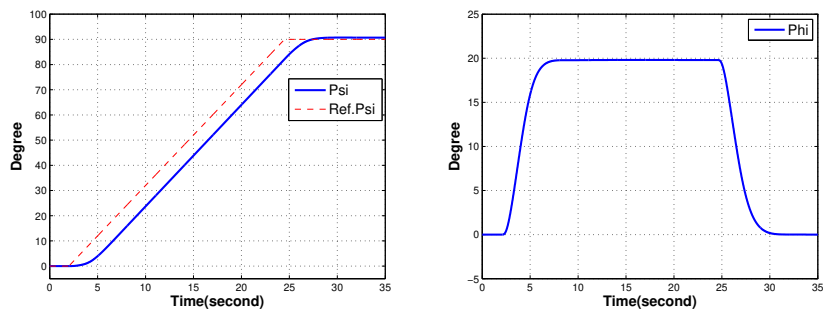


Figure 4.15: Heading ( $\psi$ ) and roll angle ( $\phi$ ) responses during heading change.

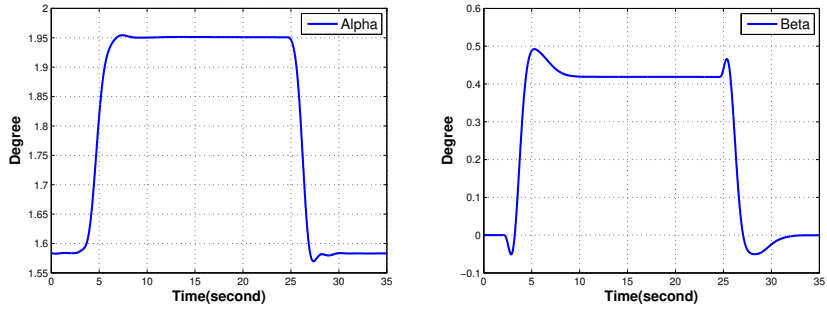


Figure 4.16: Alpha and beta angle responses during heading change.

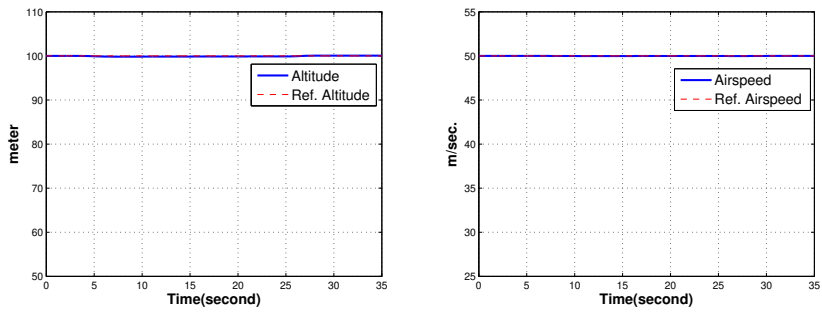


Figure 4.17: Altitude and Airspeed responses during heading change.

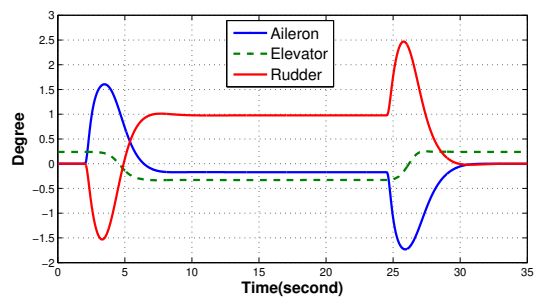


Figure 4.18: Control surface deflection during heading change.

**In the third example**, the UAV begins changing speed from 50 kt. to 45 kt at the 3rd second and from 45 kt. to 55 kt at the 20th second shown in Figure 4.19. Altitude and

airspeed responses are depicted in Figure 4.20. Control surface deflection is depicted in Figure 4.21.

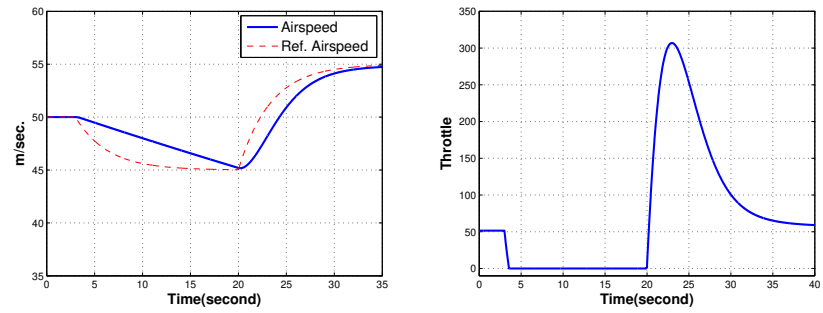


Figure 4.19: Airspeed and throttle responses during airspeed change.

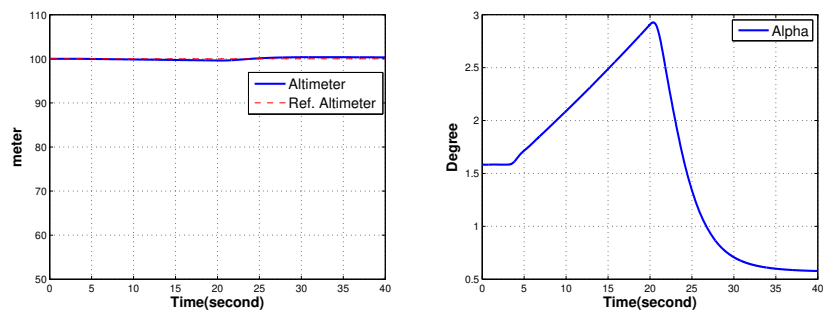


Figure 4.20: Altitude and alpha angle responses during airspeed change.

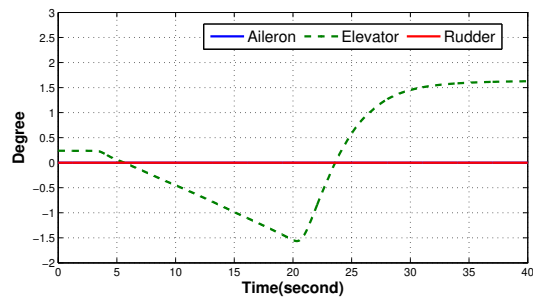


Figure 4.21: Control surface deflection during airspeed change.

**In the fourth example**, the UAV begins heading change from 360 degrees to 90 degrees and climbing from 100 meters to 150 meters at the 2nd second. In addition, it begins changing speed from 50 kt. to 40 kt. at the 10th second. All responses are depicted in Figure 4.22, Figure 4.23, Figure 4.24 and Figure 4.25.

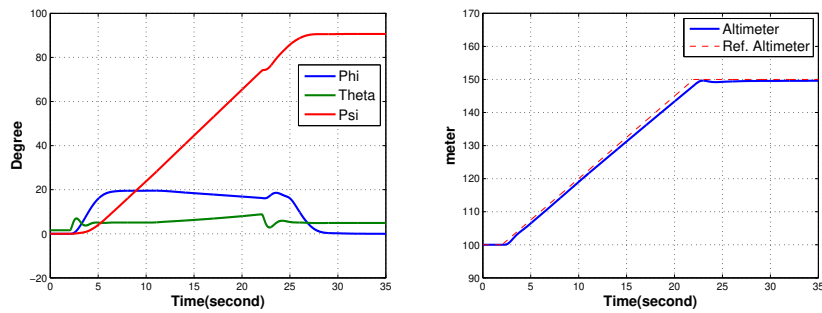


Figure 4.22: Euler angles and altitude responses during airspeed, altitude and heading change.

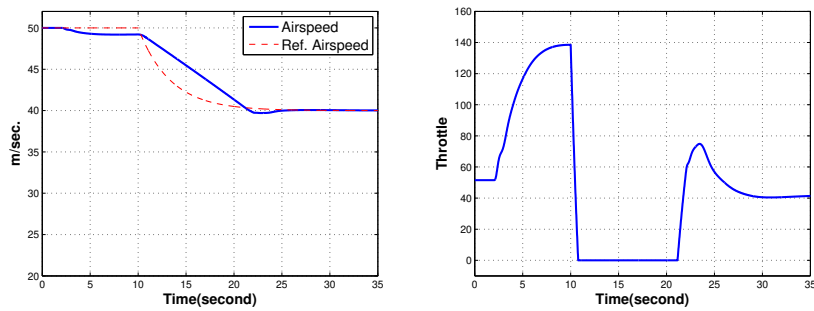


Figure 4.23: Airspeed and throttle command responses during airspeed, altitude and heading change.

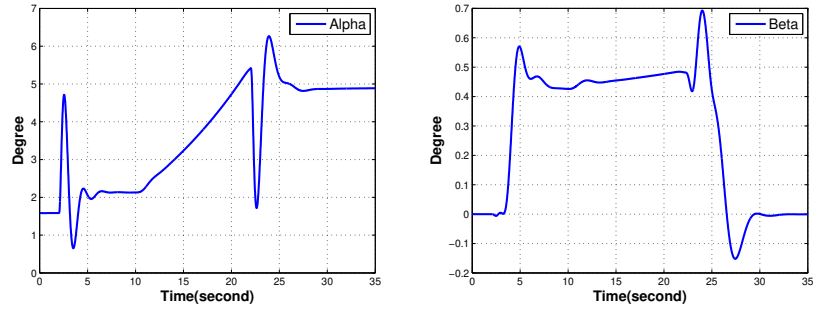


Figure 4.24: Alpha and beta angle responses during airspeed, altitude and heading change.

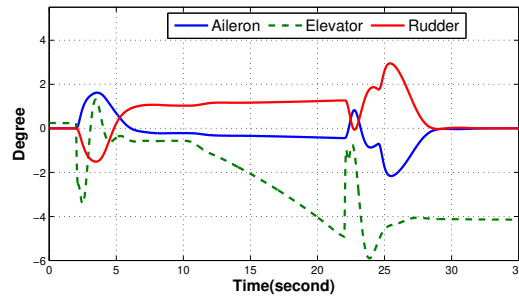


Figure 4.25: Control surface deflection during airspeed, altitude and heading change.

### 4.3 Non-linear Controller-SDRE

#### 4.3.1 Mathematical Background for SDRE

State-Dependent Riccati Equation (SDRE) method is a nonlinear control algorithm. The non-linear system can be expressed as:

$$\begin{aligned} \dot{x}(t) &= f(x) + B(x)u \quad x(0) = x_0 \\ y(t) &= Cx(t) \end{aligned} \quad (4.8)$$

Nonlinear term,  $f(x)$  is transformed to  $A(x)x$ .  $A(x)$  consists of states and is updated by states. As a result,  $A(x)$  is constantly changing. Theoretically, there are infinite  $A(x)$

matrix developed. This process is called extended linearization, apparent linearization or SDC parameterization [48]. The equation becomes as:

$$\begin{aligned}\dot{x}(t) &= A(x)x(t) + B(x)u(t) + f(t) \\ y(t) &= Cx(t)\end{aligned}\tag{4.9}$$

$A(x)$  is not unique. Some of the assumptions have to be made: the system is affine in the input, nonlinear in the state, autonomous, full state observable. Also,  $f(t)$  is a nonlinear term which can not be included in the  $A(x)$  matrix. At each instant time, the matrix  $A(x)$  is linear, so that the solution of the problem can be found by the linear quadratic optimal problem. One of the best-known performance index, quadratic performance index function or cost functional is given as respectively for regulator and tracking for infinite time and one of the main objectives is minimizing these cost functions:

$$J_R = \frac{1}{2} \int_0^{\infty} [x^T(t)Qx(t) + u^T(t)Ru(t)]dt\tag{4.10}$$

$$J_T = \frac{1}{2} \int_0^{\infty} [e^T(t)Qe(t) + u^T(t)Ru(t)]dt\tag{4.11}$$

$\mathbf{x}(t)$  is nth order state vector;  $\mathbf{Q}$  is nxn order positive and symmetric semidefinite matrix ( $Q \geq 0$ );  $\mathbf{R}$  is mxm order positive and symmetric definite matrix ( $R > 0$ );  $\mathbf{e}$  is an error between measured and reference state.  $Q$  and  $R$  are weight matrices and they can be expressed in the form of a function of states which means it becomes state dependent weight matrices and they represented by  $\mathbf{Q}(\mathbf{x})$  and  $\mathbf{R}(\mathbf{x})$ . Weight Matrices are heuristically tuned with the result of the simulation. In this thesis,  $Q$  and  $R$  matrices are functions of reconfigurable mechanism signal and represented as  $Q(a)$  and  $R(a)$ .

Algebraic Riccati Equation for SDRE is given as respectively for regulator and tracking:

$$PA(x) + A^T(x)P + Q - PBR^{-1}B^T P = 0\tag{4.12}$$

$$PA(x) + A^T(x)P + C^TQC - PBR^{-1}B^T P = 0\tag{4.13}$$

As regards solving method for ARE, there are iterative and direct methods which are shown in Figure 4.26. Also, there are doubling, information filter, square root,

and Chandrasekhar algorithms [57]. Direct methods are faster computational time for real-time applications than iterative methods. However, during computation, more storage is required. Sometimes direct solutions can be used as a backup when the iterative solution is used [94]. With respect to the iterative method, the starting solution has to be known and if the chosen value is valid, then the final solution is sufficient. In addition, if the  $A$ ,  $B$ ,  $Q$  and  $R$  matrices are ill-conditioned which means large deviations in the solution, not due to the computational method, the iterative method works well. For this thesis, one of the direct method, the eigenvalue, and the eigenvector method is used.

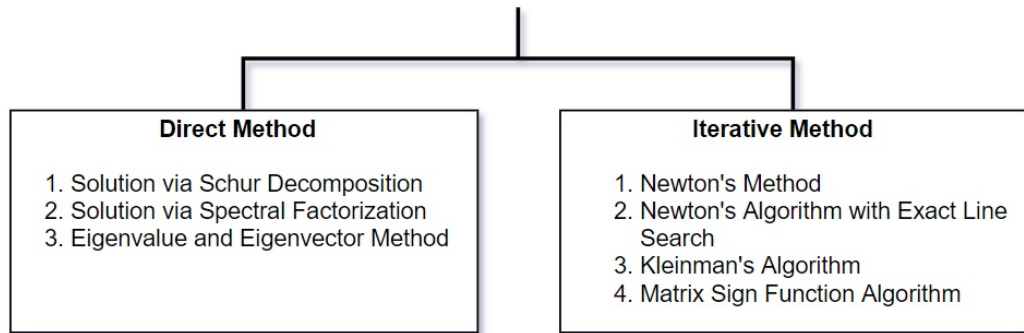


Figure 4.26: Mathematical methods for solving ARE.

After finding  $P$  from the algebraic equation, the control law is calculated. In the control law, tracking gain is represented as  $K_T$  and regulator gain is represented as  $K_R$ . The control law is given as [45]:

$$u(t) = -K_R x(t) + K_T z(t) \quad (4.14)$$

$$K_R = R^{-1} B^T P \quad (4.15)$$

$$K_T = R^{-1} B^T (P E - A^T)^{-1} W \quad (4.16)$$

$$E = B R^{-1} B^T \quad (4.17)$$

$$W = C^T Q \quad (4.18)$$

For SDRE,  $K$  is always vary due to  $P$ ,  $A(x)$  and  $B(x)$  matrices, so that  $K$  can be a function of  $P$ ,  $A(x)$  and  $B(x)$ . The mathematical representation of gains can be given as  $K_{R/T}(P, A(x), B(x))$ .

### 4.3.2 SDRE Controllers in the Flight Control Computer

Diversity is the one of the fault tolerant technique to achieve dependability which is stated in Section C.2.2. In the controller, there are two algorithms. One them is LQR/LQT algorithm which is explained, another one is the SDRE algorithm. As a result, diversity is ensured.

SDRE controller architecture is depicted in Figure 4.27. The architecture of the SDRE controller is the same as the LQR/LQT controller shown in Figure 4.7 except updated gains. There are three gain matrices,  $K_{T-1}$  (3 by 3 SDRE Tracker-1 matrix),  $K_{T-2}$  (3 by 3 SDRE Tracker-2 matrix) and  $K_{R-2}$  (3 by 3 SDRE Regulator-2 matrix) as a SAS. Even though,  $K_{T-1}$  is a 3 by 3 matrix, only upper 2 by 2 part is used. These gains are updated synchronously with the simulation.

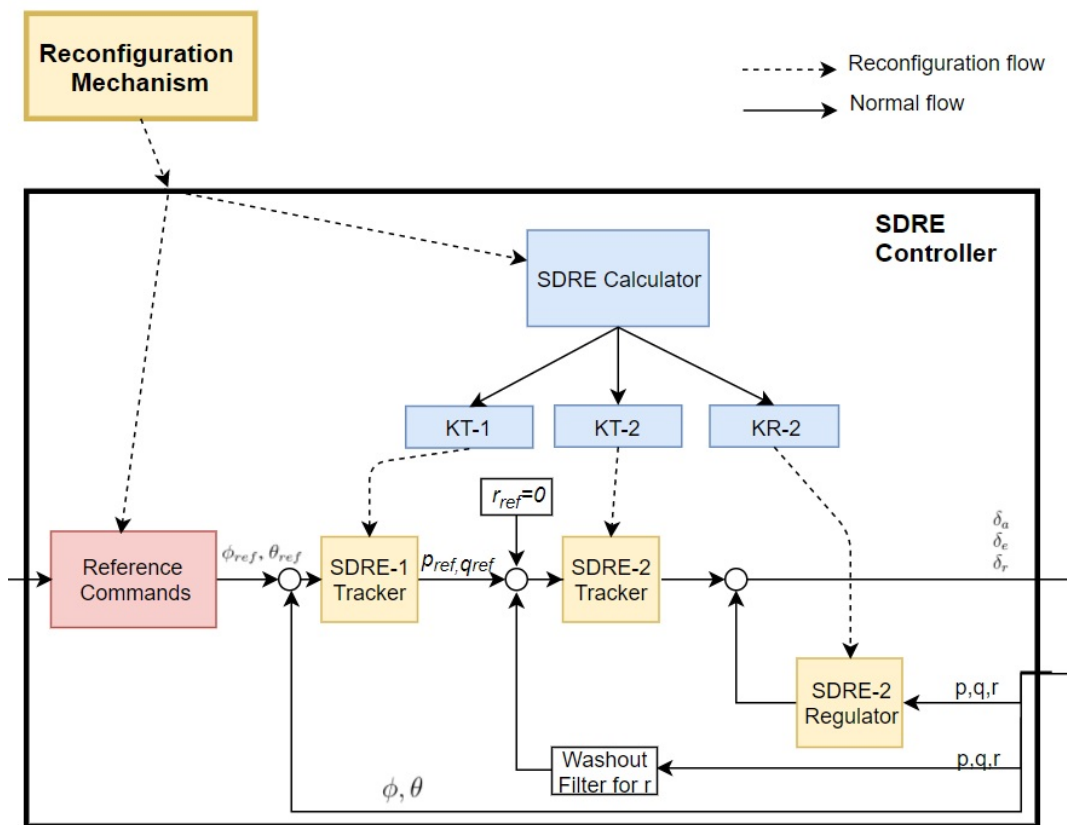


Figure 4.27: SDRE Controller.

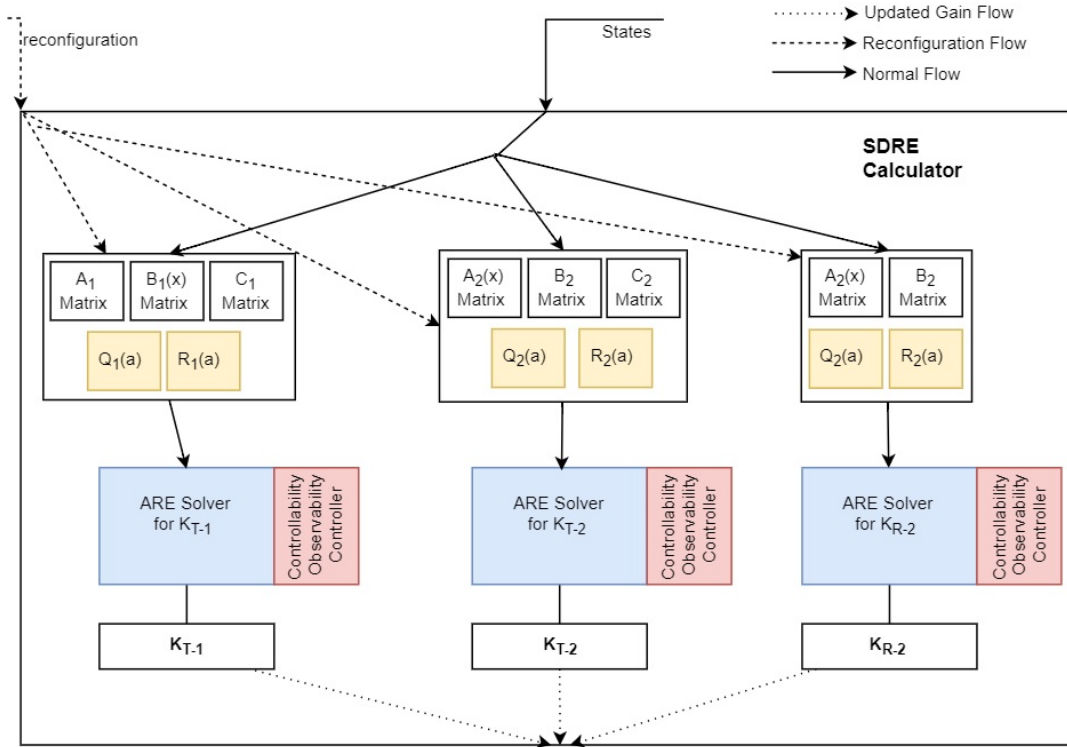


Figure 4.28: SDRE Calculator in the controller.

The SDRE Calculator is shown in Figure 4.28. Before Algebraic Riccati equation solver, extended linearized SDC matrices have to be developed. Therefore, nonlinear like  $B_1(x)$  SDC matrix and  $A_1$  for calculating  $K_{T-1}$ , are taken from Equation (4.21), (4.22), (4.23). In Equation (4.19), states vector and in Equation (4.20), inputs vector are given for the outer loop.

$$x_1 = \begin{bmatrix} \phi & \theta & \psi \end{bmatrix}^T \quad (4.19)$$

$$u_1 = \begin{bmatrix} p & q & r \end{bmatrix}^T \quad (4.20)$$

$$\begin{bmatrix} \dot{\phi} \\ \dot{\theta} \\ \dot{\psi} \end{bmatrix} = \begin{bmatrix} 0 & 0 & 0 \\ 0 & 0 & 0 \\ 0 & 0 & 0 \end{bmatrix} \begin{bmatrix} \phi \\ \theta \\ \psi \end{bmatrix} + \quad (4.21)$$

$$\begin{bmatrix} 1 & \tan \theta \sin \phi & \tan \theta \cos \phi \\ 0 & \cos \phi & -\sin \phi \\ 0 & \frac{\sin \phi}{\cos \theta} & \frac{\cos \phi}{\cos \theta} \end{bmatrix} \begin{bmatrix} p \\ q \\ r \end{bmatrix} \quad (4.22)$$

$$C_1 = I_{3 \times 3} \quad (4.23)$$

Nonlinear like  $A_2(x)$  SDC matrix,  $B_2$  and  $C_2$  matrices for calculating  $K_{T-2}$  and  $K_{R-2}$  are taken from Equation (4.26), (4.28), (4.29). Only  $p, q, r$  states are taken for  $A_2(x)$ . In Equation (4.24), states vector and in Equation (4.25), inputs vector are given for the inner loop.

$$x_2 = \begin{bmatrix} p & q & r \end{bmatrix}^T \quad (4.24)$$

$$u_2 = \begin{bmatrix} \delta_a & \delta_e & \delta_r \end{bmatrix}^T \quad (4.25)$$

$$\begin{bmatrix} \dot{u} \\ \dot{v} \\ \dot{w} \\ \dot{p} \\ \dot{q} \\ \dot{r} \\ \dot{\phi} \\ \dot{\theta} \\ \dot{\psi} \\ \dot{h} \end{bmatrix} = \begin{bmatrix} X_u & 0 & X_w & 0 & X_q - w & 0 & 0 & 0 & 0 \\ 0 & Y_v & 0 & Y_p + w & 0 & Y_r - u & 0 & 0 & 0 \\ Z_u & 0 & Z_w & -v & Z_q + u & 0 & 0 & 0 & 0 \\ 0 & I_1 I_{xx} L_v + I_2 I_{zz} N_v & 0 & I_1 I_{xx} L_p + I_2 I_{zz} N_p + I_4 q & 0 & I_1 I_{xx} L_r + I_2 I_{zz} N_r + I_3 q & 0 & 0 & 0 \\ M_u & 0 & M_w & -\frac{I_{xz}}{I_{yy}} p - \frac{I_{\tau}}{I_{yy}} r & M_q & \frac{I_{xz}}{I_{yy}} r & 0 & 0 & 0 \\ 0 & I_2 I_{xx} L_v + I_5 I_{zz} N_v & 0 & I_2 I_{xx} L_p + I_5 I_{zz} N_p + I_6 q & 0 & I_2 I_{xx} L_r + I_5 I_{zz} N_r - I_4 q & 0 & 0 & 0 \\ 0 & 0 & 0 & 1 & \tan \theta \sin \phi & \tan \theta \cos \phi & 0 & 0 & 0 \\ 0 & 0 & 0 & 0 & \cos \phi & -\sin \phi & 0 & 0 & 0 \\ 0 & 0 & 0 & 0 & \frac{\sin \phi}{\cos \theta} & \frac{\cos \phi}{\cos \theta} & 0 & 0 & 0 \\ \sin \theta & -\sin \phi \cos \theta & \cos \phi \cos \theta & 0 & 0 & 0 & 0 & 0 & 0 \end{bmatrix} + \begin{bmatrix} u \\ v \\ w \\ p \\ q \\ r \\ \phi \\ \theta \\ \psi \\ h \end{bmatrix} \quad (4.26)$$

$$\begin{aligned}
I_{num} &= I_{xx} I_{zz} - I_{xz}^2 & I_1 &= \frac{I_{zz}}{I_{num}} & I_2 &= \frac{I_{xz}}{I_{num}} & I_3 &= \frac{(I_{yy} - I_{zz}) I_{zz} - I_{xz}^2}{I_{num}} & I_4 &= \frac{(I_{xx} - I_{yy} + I_{zz}) I_{xz}}{I_{num}} & I_5 &= \frac{I_{xx}}{I_{num}} \\
I_6 &= \frac{(I_{xx} - I_{yy}) I_{xx} - I_{xz}^2}{I_{num}} & I_7 &= I_{xx} - I_{zz}
\end{aligned} \quad (4.27)$$

$$\begin{bmatrix}
0 & X_{\delta_e} & 0 & X_{\delta_t} \\
Y_{\delta_a} & 0 & Y_{\delta_r} & 0 \\
0 & Z_{\delta_e} & 0 & 0 \\
I_1 I_{xx} L_{\delta_a} + I_2 I_{zz} N_{\delta_a} & 0 & I_1 I_{xx} L_{\delta_r} + I_2 I_{zz} N_{\delta_r} & 0 \\
0 & M_{\delta_e} & 0 & 0 \\
I_2 I_{xx} L_{\delta_a} + I_5 I_{zz} N_{\delta_a} & 0 & I_2 I_{xx} L_{\delta_r} + I_5 I_{zz} N_{\delta_r} & 0 \\
0 & 0 & 0 & 0 \\
0 & 0 & 0 & 0 \\
0 & 0 & 0 & 0 \\
0 & 0 & 0 & 0
\end{bmatrix}
\begin{bmatrix}
\delta_a \\
\delta_e \\
\delta_r \\
\delta_t
\end{bmatrix}
+
\begin{bmatrix}
-g \sin \theta \\
g \cos \theta \sin \phi \\
g \cos \theta \cos \phi \\
0 \\
0 \\
0 \\
0 \\
0 \\
0 \\
0
\end{bmatrix}
\quad (4.28)$$

$$C_2 = I_{3 \times 3} \quad (4.29)$$

After  $A_1$  and  $A_2(x)$ ,  $B_1(x)$  and  $B_2$ ,  $C_1$  and  $C_2$  matrices are developed and state feed from sensors, these matrices are transmitted to Algebraic Riccati Equation solver shown in Figure 4.28. ARE solver in Simulink, contains Matlab function which is used for writing Matlab function for Simulink model. For this thesis, one of the direct methods for solving Algebraic Riccati Equation, eigenvalue and eigenvector method is used.

Also, during simulation, controllability, and observability are checked by Matlab function block simultaneously.

Choosing weighing matrices are very important part for SDRE controller.  $Q$  is for states,  $R$  is for controls. If problems such as fault and failure conditions, do not occur, for  $K_{T-1}$ ,  $Q_1$  and  $R_1$  are used shown in Equation (4.30) and Equation (4.31), for  $K_{T-2}$  and  $K_{R-2}$ ,  $Q_2$  and  $R_2$  are used shown in Equation (4.32) and Equation (4.33). However, during damage, degrade or stuck problem, different values of  $Q$  and  $R$  matrices are sent from reconfiguration mechanism which is explained in Section 4.3.3.

$$Q_1 = \text{diag}[50, 50, 50] \quad (4.30)$$

$$R_1 = \text{diag}[0.1, 0.1, 0.1] \quad (4.31)$$

$$Q_2 = \text{diag}[5, 5, 2] \quad (4.32)$$

$$R_2 = \text{diag}[50, 10, 10] \quad (4.33)$$

Controllability and observability are checked simultaneously during simulation shown in Figure 4.28. Therefore, for controllability shown in Figure 4.29, these equations are used:

$$C_{tracker1} = [B_1 \quad A_1 B_1 \quad A_1^2 B_1] \quad (4.34)$$

$$C_{tracker2} = [B_2 \quad A_2 B_2 \quad A_2^2 B_2] \quad (4.35)$$

$$C_{regulator2} = [B_2 \quad A_2 B_2 \quad A_2^2 B_2] \quad (4.36)$$

If the rank of the  $C_{tracker1}$ ,  $C_{tracker2}$ ,  $C_{regulator2}$  individually, equals to 3, the system is controllable. For observability, these equations are used:

$$O_{tracker1} = [C_1 \quad C_1 A_1 \quad C_1 A_1^2]^T \quad (4.37)$$

$$O_{tracker2} = [C_2 \quad C_2 A_2 \quad C_2 A_2^2]^T \quad (4.38)$$

$$O_{regulator2} = [C_2 \quad C_2 A_2 \quad C_2 A_2^2]^T \quad (4.39)$$

If the rank of the  $O_{tracker1}$ ,  $O_{tracker2}$ ,  $O_{regulator2}$  individually, equals to 3, the system is observable.

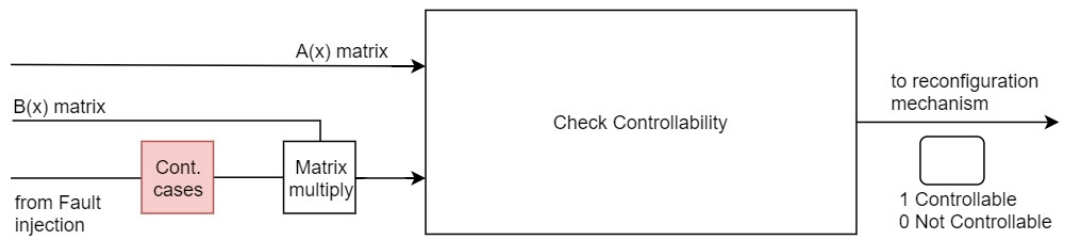


Figure 4.29: Controllability controller in SDRE calculator.

### 4.3.3 Reconfiguration Mechanism for SDRE

Reconfiguration mechanism (RM) is used for reconfiguring rate limiters in the Mode Selection (MS); reference command, command filters and limiter in the FCC; controller algorithm in the FCC, depicted in Figure 4.36. RM consists of seven mechanisms, depicted in Figure 4.30.

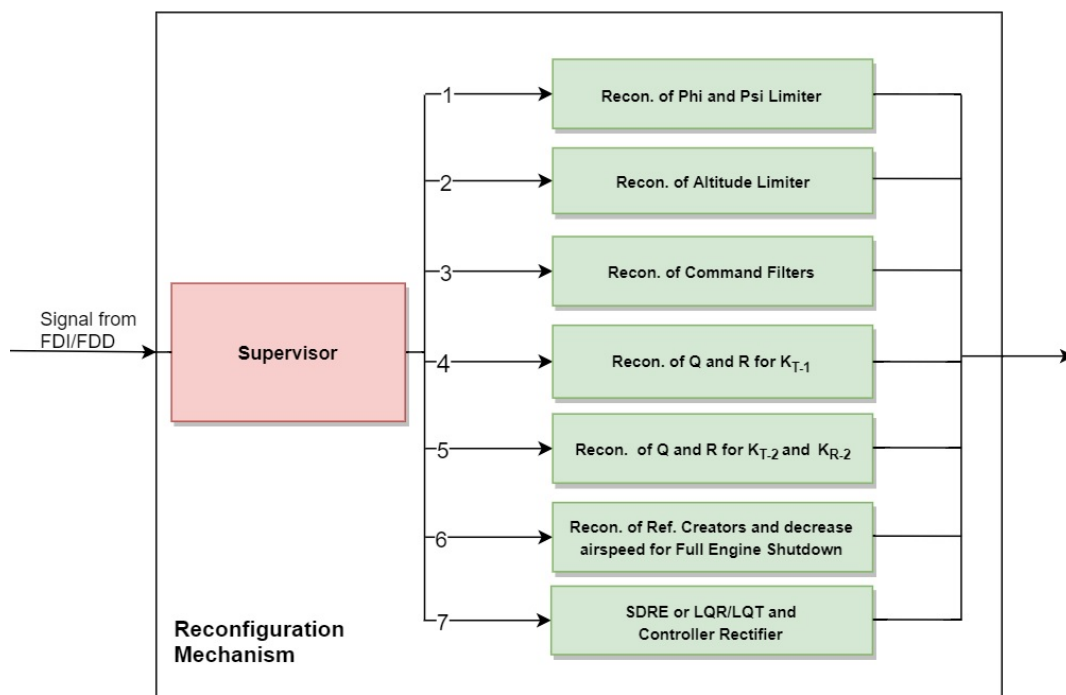


Figure 4.30: Reconfiguration Mechanism.

1. Reconfiguration of  $\phi$  (limiter) and  $\psi$  (rate limiter) limiter,
2. Reconfiguration of altitude (rate) limiter,
3. Reconfiguration of  $\phi$  and  $\theta$  command filters,
4. Reconfiguration of  $Q_1$  and  $R_1$  for  $K_{T-1}$ ,
5. Reconfiguration of  $Q_2$  and  $R_2$  for  $K_{T-2}$  and  $K_{R-2}$ ,
6. Reconfiguration of reference commands architecture and decrease airspeed for full engine shut down,
7. SDRE or LQR/LQT, and control derivative rectifier.

#### 4.3.3.1 Reconfiguration of $\phi$ and $\psi$ limiter

In the Mode Selection (MS) block, there is  $\psi$  rate limiter depicted in Figure 4.36. Normally, during flight, the value of rate limiter rising slew rate is 4 and falling slew rate is -4. This provides standard turn rate during heading change. Rate limiter is used for limiting the first derivative of the signal. The value of 4 and -4 slew rate approximately equal to 4 deg./second. During reconfiguration, this value can be 2 or 1, depending on the emergency. In the reference command in FCC, there is a  $\phi$  limiter. In the limiter, saturation block is used to limit  $\phi$  to a value of 20 degrees and -20 degrees. During an emergency, this value is changed to 14 degrees or 10 degrees, depending on the problem.

#### 4.3.3.2 Reconfiguration of altitude limiter

In the Mode Selection (MS) block, there are altitude rate limiters depicted in Figure 4.36. The mathematical background is the same as  $\psi$  rate limiter but different in use. Normally, a pilot can adjust the vertical speed from MS, like 0.5, 1, 1.5 and 2 vario. As stated before, for example, 0.5 means 500 ft./second. With the help of the switch case block, if there is an emergency situation, this reconfiguration mechanism decreases vario to 0.5 during a climb, even though the pilot adjusts any vario. Especially, it is very useful to prevent elevator actuator saturation during elevator damage case.

#### 4.3.3.3 Reconfiguration of $\phi$ and $\theta$ command filters

The architecture and reconfiguration structure is developed for command filters, depicted in Figure 4.36. There are command filters which consist of transfer functions, for airspeed in the Mode Selection (MS);  $\phi$ ,  $\theta$  and throttle in the reference command in FCC. For reconfiguration, switch case block is only used for  $\phi$  and  $\theta$  command filters. Different transfer functions are used for different cases. However, stated in Chapter 5, this mechanism is not used in any emergency case in this thesis. The purpose of the development of this mechanism is for further studies.

#### 4.3.3.4 Reconfiguration of $Q_1$ and $R_1$ for $K_{T-1}$

The architecture and reconfiguration structure is developed for  $K_{T-1}$ . However, stated in Chapter 5, this mechanism is not used in any emergency case in this thesis because reconfiguration of  $Q_2$  and  $R_2$  for  $K_{T-2}$  and  $K_{R-2}$  is more effective and useful. The purpose of the development of this mechanism is for further studies.

#### 4.3.3.5 Reconfiguration of $Q_2$ and $R_2$ for $K_{T-2}$ and $K_{R-2}$

Normally, the values of the  $Q_2(a)$  and  $R_2(a)$  are given as:

$$Q_2 = \text{diag}[5, 5, 2] \quad (4.40)$$

$$R_2 = \text{diag}[50, 10, 10] \quad (4.41)$$

During normal flight, these values are good for safety. However, if an emergency occurs, they are not only useless but also cause of the LOC-I, depicted in Chapter 5. As a result, these values have to be changed by the reconfiguration mechanism. Therefore, interpolation tables are used for  $Q_2(a)$  and  $R_2(a)$ . With regard to  $R_2(a)$ , these tables consist of 0.01 , 0.1, 50, 1250, 2050 for aileron (50 is the normal value); 0.1, 1, 10, 30, 110 for elevator (10 is the normal value); 0.0001, 0.001, 10, 130, 210 for rudder (10 is the normal value) depicted in Figure 4.31. In this thesis, there is no need for a reconfiguration of  $Q_2(a)$  matrix but it can be used for further studies. During an emergency, these values are sent to ARE calculator in the FCC depending on the problem and decided by the supervisor. Supervisor sent -2, -1, 0, 1 or 2 for slowing or increasing the controller response. Also, for example, 1.2 can be adjusted. Positive values represent the slower movement of the control surface, while the negative values are the opposite.

A rule for all aircraft during flying in a turbulence condition, especially severe ones, pilots do not chase the altitude and heading precisely. Applying too much and abrupt control could cause structural damage due to excessive G-force. In addition, turns have to be slow and beware of large bank angle is crucial [95]. Normally, for a pilot, it requires more workload in the cockpit or in the ground control unit for the UAV. However, if the controller can be reconfigured and make the control surfaces

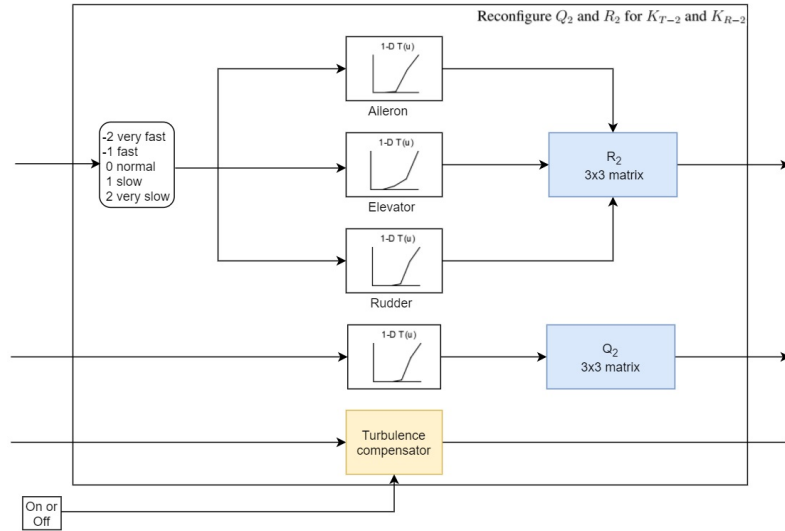


Figure 4.31: Reconfiguration of  $Q_2$  and  $R_2$  for  $K_{T-2}$  and  $K_{R-2}$

movement slower than before, aircraft will descent or climb a little but a golden rule can be achieved. This can be done by reconfiguration of Q and R matrices of SDRE controller. For the reconfiguration mechanism, turbulence can be divided into five groups, given as:

1. Light
2. Light to Moderate
3. Moderate
4. Moderate to Severe
5. Severe

Therefore, different  $R_2$  values are used for each control surface. Besides, reconfiguration varies with the altitude. As a result, 2D interpolation tables are used for  $Q_2(a)$  and  $R_2(a)$  depicted in Figure 4.32. If the UAV is flying in the previously determined altitude range which consists of 0-2000 meters, 2000-3000 meters, 3000-5000 meters, the reconfiguration is done according to it. Therefore, pre-lookup tables are used. Also, these values can be changed with respect to turbulence magnitude which consists of five severity stated before. As a result, it is said that supervisor sends five values for turbulence severity and three values for altitude range. In this thesis, there is no need for a reconfiguration of  $Q_2(a)$  matrix but it can be used for further studies.

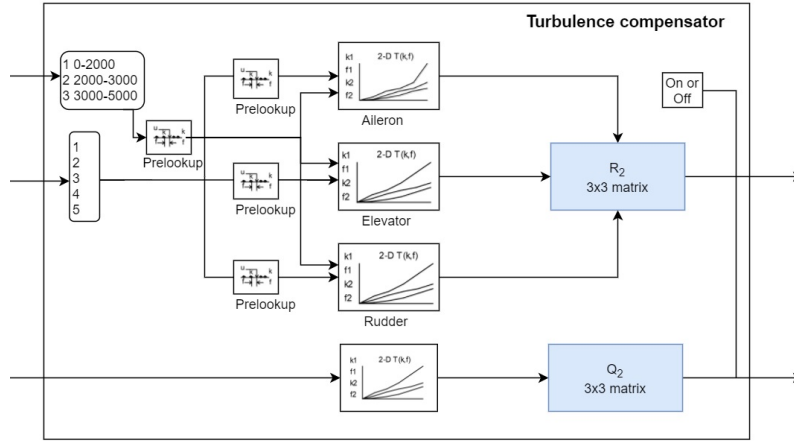


Figure 4.32: Turbulence part of the reconfiguration of  $Q_2$  and  $R_2$  for  $K_{T-2}$  and  $K_{R-2}$

#### 4.3.3.6 Reconfiguration of Reference Commands Architecture and Decreasing Airspeed for Full Engine Shut Down

All engine full shut down emergencies during flight, is really challenging task for pilots because consequences can be fatal. The procedure, nearly the same from the large to small aircraft, is to fly the aircraft first and then glide with the aircraft best glide speed. If the autopilot does this task, a pilot can search the best emergency landing airport or terrain.

During full engine shut down, there is no thrust force. As a result, if pilot or autopilot maintains altitude, airspeed decreases to a dangerously low value and the result can be a stall. To prevent this, as stated above, aircraft have to descend with a glide speed and this speed is lower than level flight speed. Besides, flying with this speed, minimum drag is created to ensure maximum distance. To ensure constant speed,  $\theta_{ref}$  and  $\delta_t$  Controller-2 depicted in Figure 4.10, has to be used in the reference command. This controller adjusts airspeed with changing  $\theta_{ref}$  and sends to the SDRE or LQR/LQT controller. As a result, airspeed can be fixed by the movement of the elevator during the glide.

For the UAV, level flight speed is 50 m./second and it is assumed that minimum glide speed is 35 m./second. As a result, this reconfiguration mechanism sends a command to the controller to decrease airspeed to 35 m./second. After that, whatever flight maneuver the UAV made (climbing with vertical speed or normal level flight), the

reference command architecture change to a  $\theta_{ref}$  and  $\delta_t$  Controller-2. Besides, by this mechanism throttle command is isolated from the FCC.

**4.3.3.7 SDRE or LQR/LQT, and control derivative rectifier**

Controllability and observability are checked simultaneously during simulation as stated in Section 4.3.2. Controllability or observability controllers, depicted in Figure 4.29 and in Figure 4.33 in SDRE calculator for all gains, check controllability or observability and if the calculation result is uncontrollable or unobservable for any gains, 0 is sent to this mechanism depicted in Figure 4.34. As a result, it changes from SDRE to LQR/LQT.

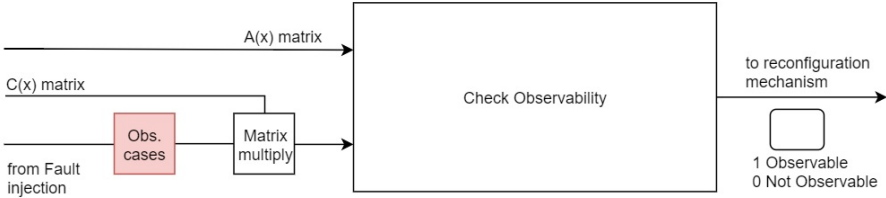


Figure 4.33: Observability controller in SDRE calculator.

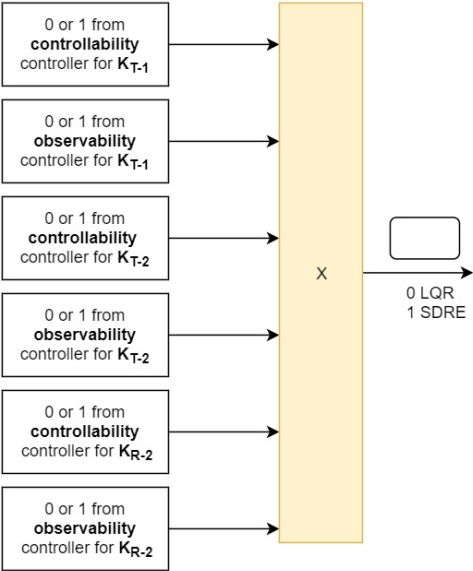


Figure 4.34: SDRE or LQR/LQT mechanism.

Also, another mechanism, control derivative rectifier, depicted in Figure 4.35 is in

this block. This mechanism sends a signal to ARE calculator. With respect to damage case, control derivatives in the  $B$  matrix in ARE calculator are multiplied with the percentage damage. For example, there is a 2nd damage case for aileron. The multiplied value of the damage of the aileron equals to 0.3. As a result, this mechanism sends 0.3 to ARE calculator to multiply aileron control derivative. Finally, ARE calculator solves ARE with new control derivatives.

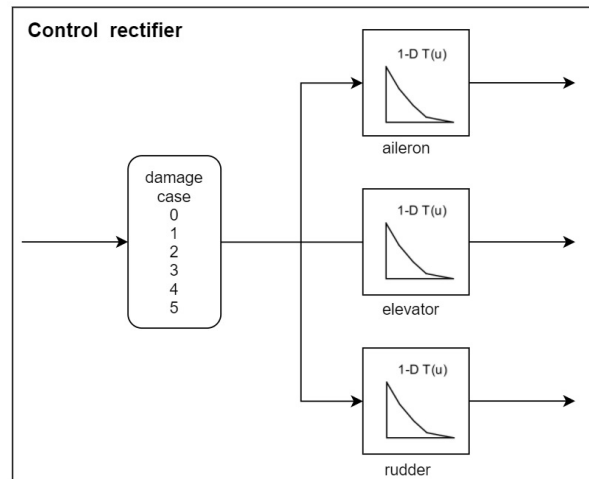


Figure 4.35: Control derivative rectifier.

#### 4.3.3.8 FTC Supervisor

The supervisor is a decision maker for a different emergency situation. It is assumed that FDI/FDD finds the problem, problem location, level or stuck value. After that, it sends a signal to the supervisor in the reconfiguration mechanism shown in Figure 4.37. This signal is about fault type (problem) which consists damage, degradation, stuck; fault location (problem location) which consists of aileron, elevator, rudder, engine, FCC; severity (level or stuck value), the level of the damage or degradation, the value of the stuck. As a result, reconfiguration and reconfiguration degree are chosen by the supervisor which consists of seven mechanisms as stated and shown in Table 4.2. In Section 5 and Section 6, the solution path for faults and failures are depicted with figures.

For example, FDI/FDD detects the 3rd level damage at the aileron. After that, it is

assumed that it sends this signal to the reconfiguration mechanism shown in Figure 4.37. Supervisor in the reconfiguration mechanism makes a decision by its logic which is shown in Table 4.2. In this logic table, reconfiguration for 3rd level aileron damage is done by activating 1, 5 and 7th mechanism. In the 1st mechanism,  $\psi$  rate limiter slew rate changes to 2 deg./sec. and  $\phi$  limiter change to 14 degrees. In the 5th mechanism, to increase the movement of the aileron 1 faster,  $R_2$  matrix aileron value changes from 50 to 0.1 and sent to the SDRE calculator in the FCC. As a result, SDRE controller is reconfigured. Besides, in the 7th mechanism, new aileron control derivative value is sent to  $B_2$  matrix in the SDRE calculator in the FCC.

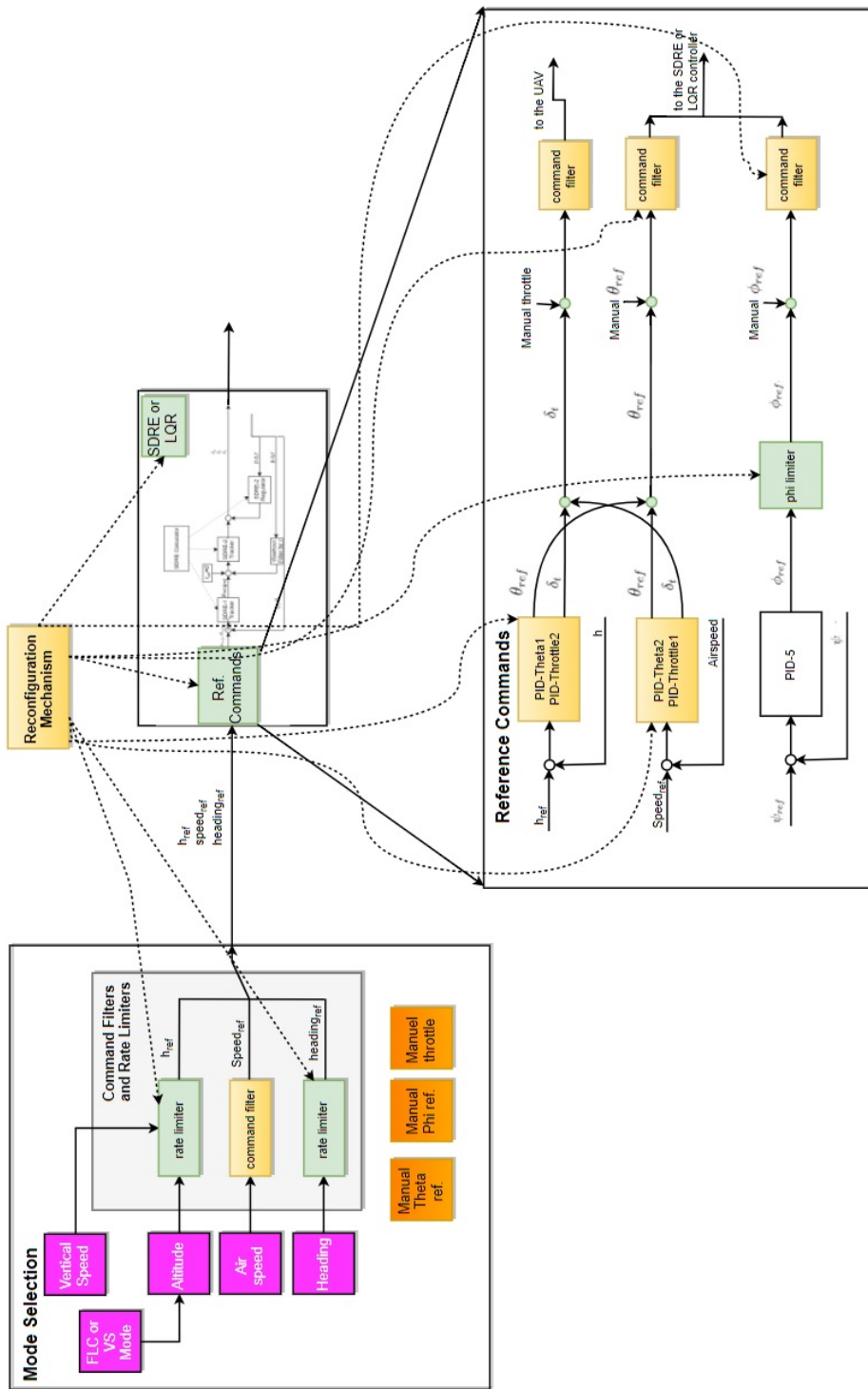


Figure 4.36: Reconfiguration Mechanism with SDRE controller, command filters and rate limiters.

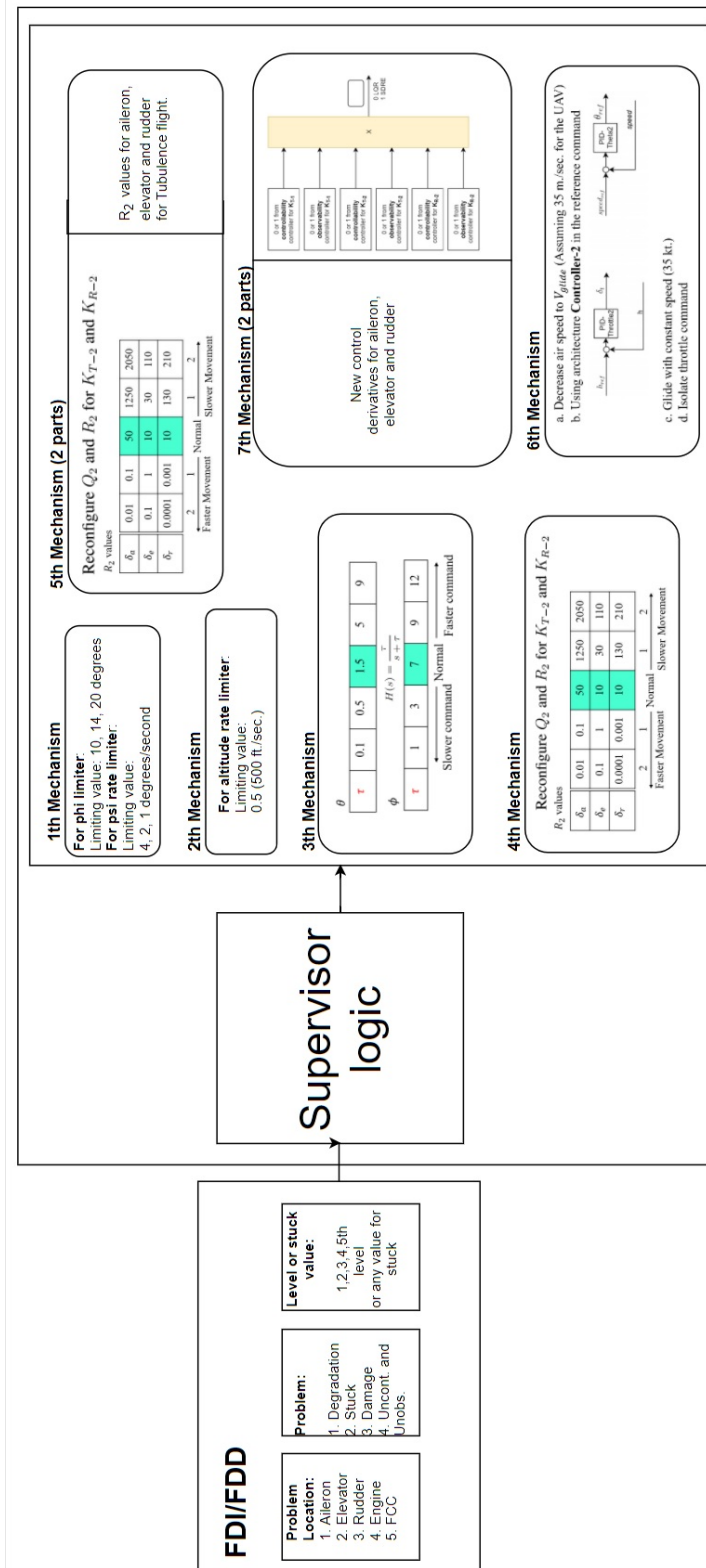


Figure 4.37: Summary for reconfiguration strategies.

Location	Problem	Problem Level	Reconfiguration Mechanism	Reconfiguration Degree
Aileron	Degradation	3th level	5th	For Aileron 0.05 faster, For rudder 2.5 slower
		4th level	5th	For Aileron 0.5 faster, For rudder 4 slower
Elevator	Degradation	3th level	2th	Decrease vario to 0.5 (500 ft./sec.)
			5th	For Elevator 2 slower
		4th level	5th	For Elevator 3 slower
Rudder	Degradation	3th level	5th	For Rudder 0.5 faster, For aileron 0.5 slower
		4th level	5th	For Rudder 0.5 faster, For aileron 1 slower
Aileron	Stuck	0.5 degrees	1th	Psi rate limiter to 1 deg./sec., Phi limiter to 14 degrees
			5th	For Rudder 3 faster
Elevator	Stuck	-	-	-
Rudder	Stuck	20 degrees	1th	Psi rate limiter to 2 deg./sec., Phi limiter to 14 degrees
			5th	For aileron 1 slower
		40 degrees	1th	Psi rate limiter to 2 deg./sec., Phi limiter to 14 degrees
			5th	For aileron 1 slower
Aileron	Damage	3th level	1th	Psi rate limiter to 2 deg./sec., Phi limiter to 14 degrees
			5th	For aileron 1 faster
			7th	New derivatives for aileron control in B2(x) martrix
		4th level	1th	Psi rate limiter to 2 deg./sec., Phi limiter to 14 degrees
			5th	For aileron 1 faster
			7th	New derivatives for aileron control in B2(x) martrix
Elevator	Damage	3th level	2th	Decrease vario to 0.5 (500 ft./sec.)
			5th	For elevator 1 slower
			7th	New derivatives for elevator control in B2(x) martrix
		4th level	2th	Decrease vario to 0.5 (500 ft./sec.)
			5th	For elevator 1 slower
			7th	New derivatives for elevator control in B(x) martrix
Rudder	Damage	3th level	1th	Psi rate limiter to 2 deg./sec., Phi limiter to 14 degrees
			5th	For aileron 1 slower, For rudder 0.3 faster
			7th	New derivatives for rudder control in B(x) martrix
		4th level	1th	Psi rate limiter to 2 deg./sec., Phi limiter to 14 degrees
			5th	For aileron 1 slower, For rudder 0.5 faster
			7th	New derivatives for rudder control in B(x) martrix

Table 4.2: Supervisor logic.

## CHAPTER 5

### RESULTS FOR ACTUATOR STUCK, DEGRADATION AND FOR DAMAGED CONTROL SURFACE

#### 5.1 Emergency Case-1 Control Surface Actuator Degradation

As stated in Section 1.4.3, faults/failures can be multiplicative in terms of way. Besides, as stated in Section 1.4.2, faults/failures can be abrupt in terms of time. Besides, all failures/faults are abrupt. As a general rule, the controller is reconfigured by the supervisor in the reconfiguration mechanism.

##### 5.1.1 Aileron Degradation

###### 5.1.1.1 The 3rd Level Degradation Without Reconfiguration

The 3rd level (0.1) aileron degradation at the 25th second and 40 degree heading change at the 20th second without reconfiguration:

At the beginning, the UAV decreases speed from 50 to 45 kt. After, it makes a 40 degree heading change. First, there is not any safety problem with respect to altitude, airspeed,  $\alpha$  which is shown in Figure 5.1 and Figure 5.2. The UAV make a 40 degree heading change safely with an approximately 16 degree bank angle. However, after heading change is completed, the UAV is not stabilized in the lateral and oscillations about  $\phi$  are growing steadily shown in Figure 5.3 and this results in LOC-I. These oscillations are caused due to rudder movement shown in Figure 5.4. As a result, aileron movement has to be accelerated and rudder movement has to be decelerated.

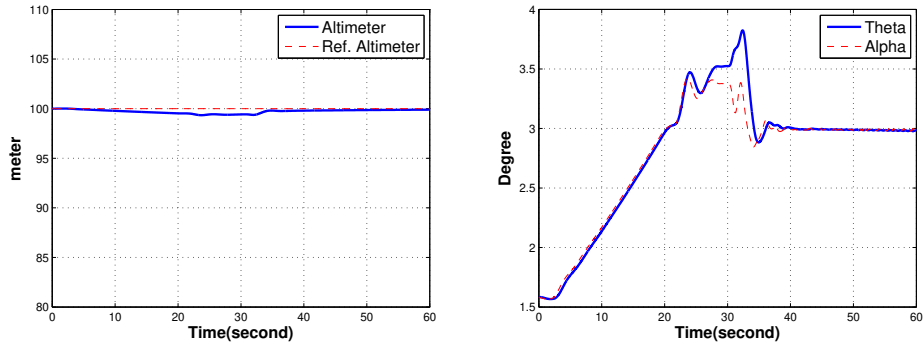


Figure 5.1: Altimeter and  $\theta$ ,  $\alpha$  responses without reconfiguration.

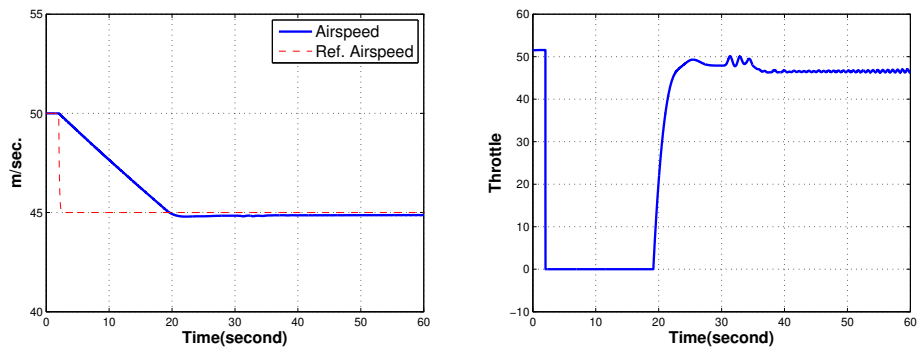


Figure 5.2: Airspeed and throttle responses without reconfiguration.

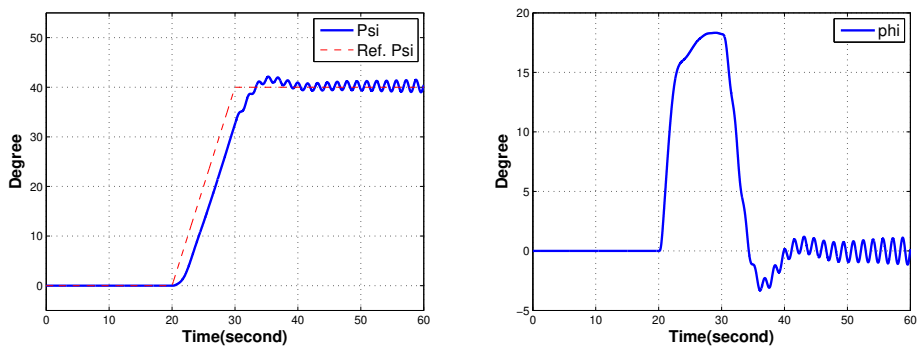


Figure 5.3:  $\psi$  and  $\phi$  responses without reconfiguration.

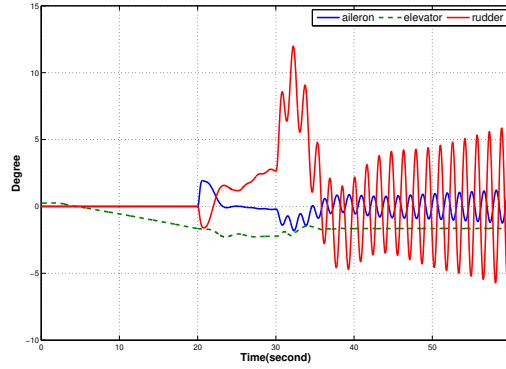


Figure 5.4: Actuator responses without reconfiguration.

### 5.1.1.2 The 3rd Level Degradation With Reconfiguration

The 3rd level (0.1) aileron degradation at the 25th second and 40 degree heading change at the 20th second with reconfiguration: The path for the solution is shown in Table 5.1.

Table 5.1: The solution for aileron degradation at the 3rd level.

Problem location	Aileron
Problem	3rd level degradation
Which Reconfiguration Mech. Block	5
What Reconfiguration Degree	aileron 0.05 faster
	rudder 2.5 slower

Reconfiguration mechanism-5 (Recon.  $Q$  and  $R$  for  $K_{T-2}$  and  $K_{R-2}$ ) is activated by Supervisor to change  $Q$  and  $R$  matrices to a different value to change control surface movement. There is no safety problem with respect to altitude, airspeed,  $\alpha$  which are shown in Figure 5.5 and Figure 5.6. The UAV makes a 40 degree heading change safely with an approximately 16 degree bank angle shown in Figure 5.7. Besides, rudder and aileron oscillations are prevented shown in Figure 5.8. As a result, with the reconfiguration, LOC-I is prevented.

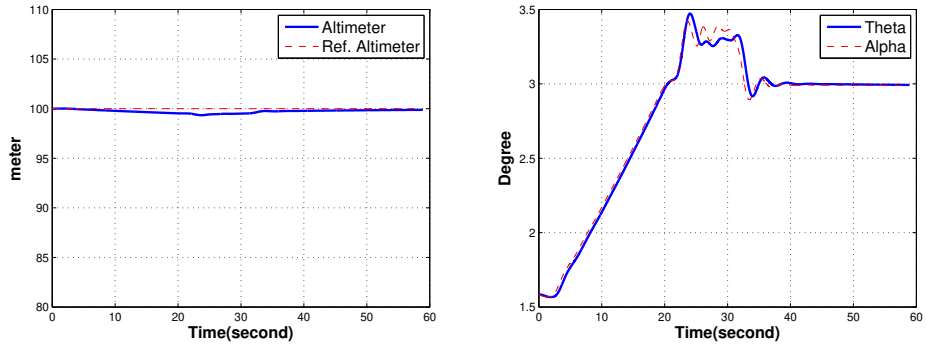


Figure 5.5: Altimeter and  $\theta$ ,  $\alpha$  responses with reconfiguration.

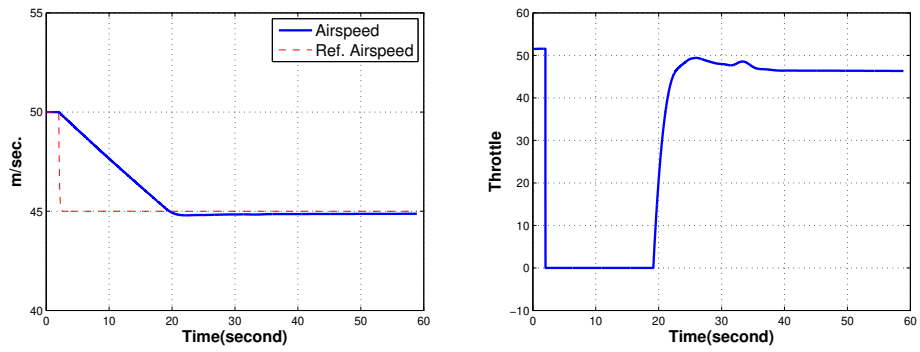


Figure 5.6: Airspeed and throttle responses and with reconfiguration.

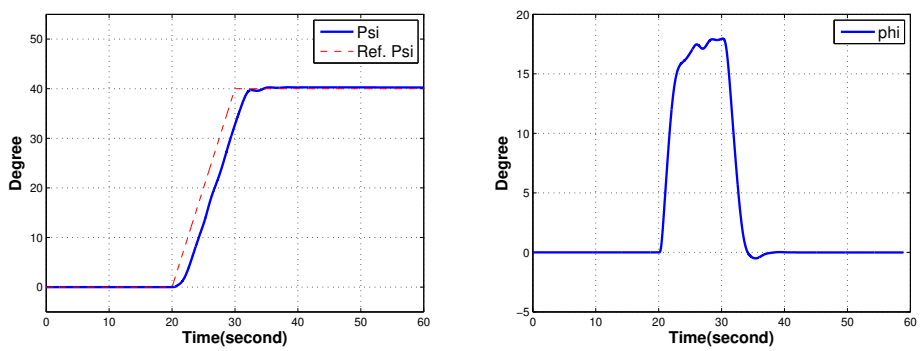


Figure 5.7:  $\psi$  and  $\phi$  responses with reconfiguration.

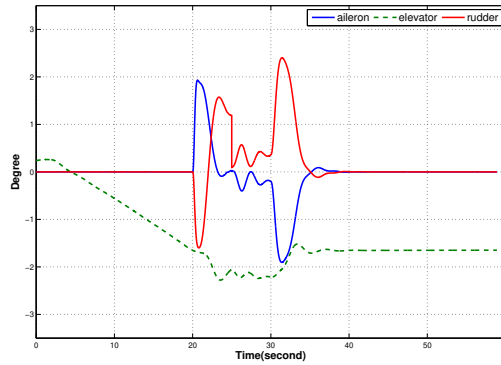


Figure 5.8: Actuator responses with reconfiguration.

### 5.1.1.3 The 4th Level Degradation Without Reconfiguration

The 4th level (0.025) aileron degradation at the 25th second and 40 degree heading change at the 20th second without reconfiguration:

There is a safety problem with respect to altitude and  $\alpha$  which are shown in Figure 5.9. Besides, the UAV's airspeed oscillates too much and is going to decrease to the stall speed shown in Figure 5.10. The UAV makes a 40 degree heading change safely with an approximately 16 degree bank angle. However, after heading change is completed, the UAV is not stabilized in the lateral and oscillations about  $\phi$  are growing extremely shown in Figure 5.11. Besides, rudder oscillation is too much shown in Figure 5.12. This situation results in LOC-I.

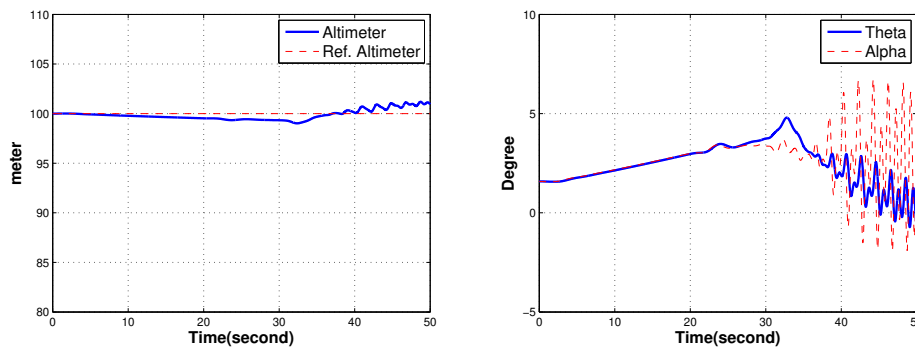


Figure 5.9: Altimeter and  $\theta$ ,  $\alpha$  responses without reconfiguration.

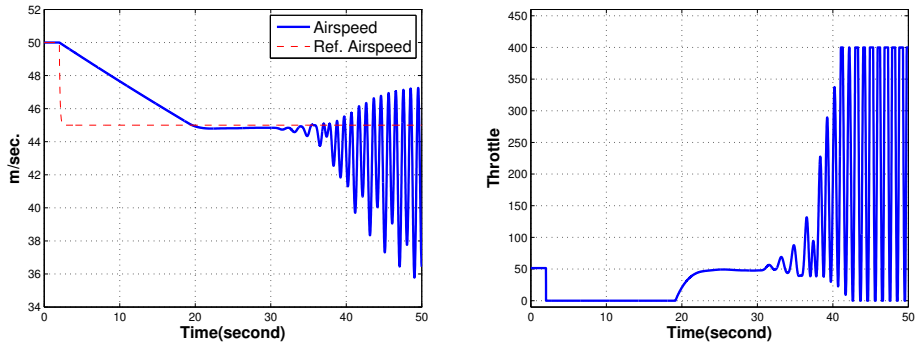


Figure 5.10: Airspeed and throttle responses without reconfiguration.

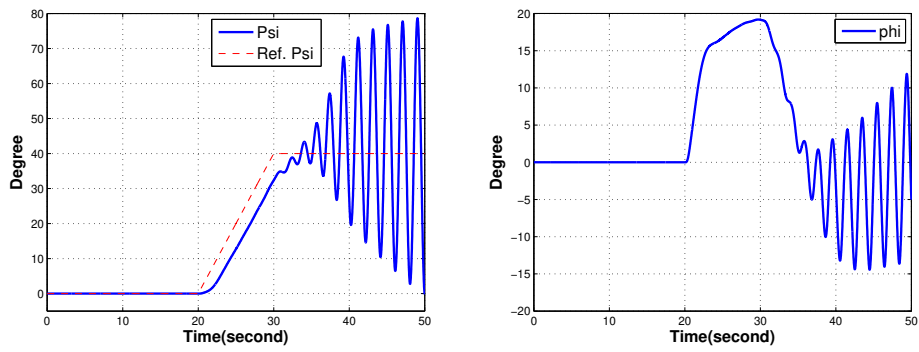


Figure 5.11:  $\psi$  and  $\phi$  responses without reconfiguration.

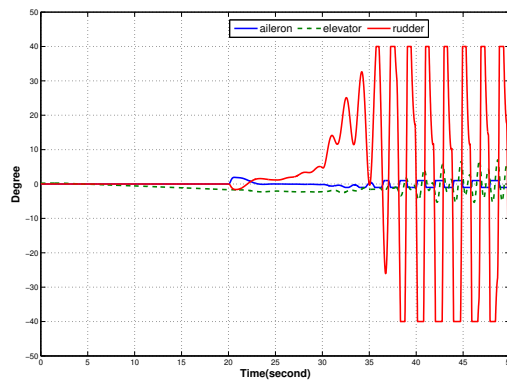


Figure 5.12: Actuator responses without reconfiguration.

#### 5.1.1.4 The 4th Level Degradation With Reconfiguration

The 4th level (0.025) aileron degradation at the 25th second and 40 degree heading change at the 20th second with reconfiguration: The path for the solution is shown in Table 5.2.

Table 5.2: The solution for aileron degradation at the 4th level.

Problem location	Aileron
Problem	4th level degradation
Which Reconfiguration Mech. Block	5
What Reconfiguration Degree	aileron 0.5 faster
	rudder 4 slower

Reconfiguration mechanism-5 (Recon.  $Q$  and  $R$  for  $K_{T-2}$  and  $K_{R-2}$ ) are activated by Supervisor to change  $Q$  and  $R$  matrices to a different value to change control surface movement. There is no safety problem with respect to altitude, airspeed,  $\alpha$  which are shown in Figure 5.13 and Figure 5.14. The UAV makes a 40 degree heading change safely with an approximately 16 degree bank angle shown in Figure 5.15. Besides, rudder and aileron oscillations are prevented shown in Figure 5.16. Only, there is an overshoot about  $\psi$  and  $\phi$  due to ineffective 1 degree aileron command because of degrade. However, this problem does not lead to instability. As a result, with the reconfiguration, LOC-I is prevented.

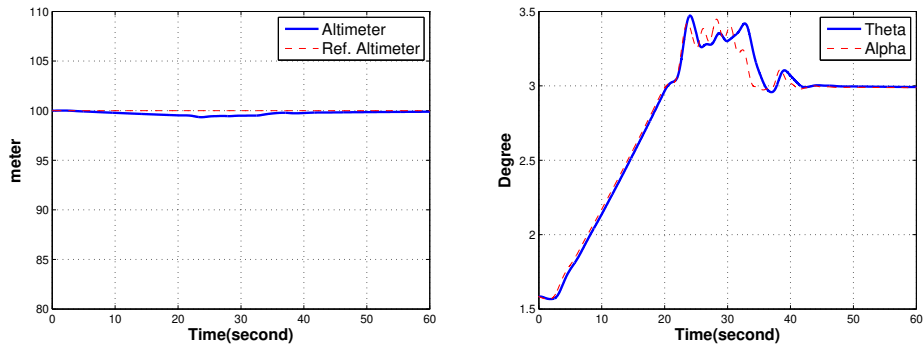


Figure 5.13: Altimeter and  $\theta$ ,  $\alpha$  responses with reconfiguration.

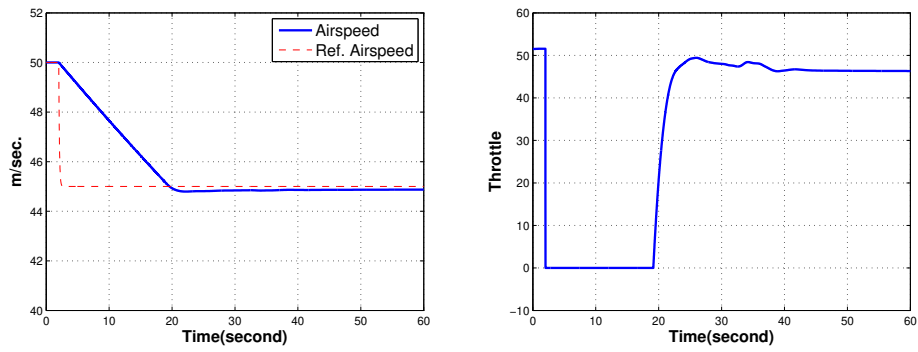


Figure 5.14: Airspeed and throttle responses with reconfiguration.

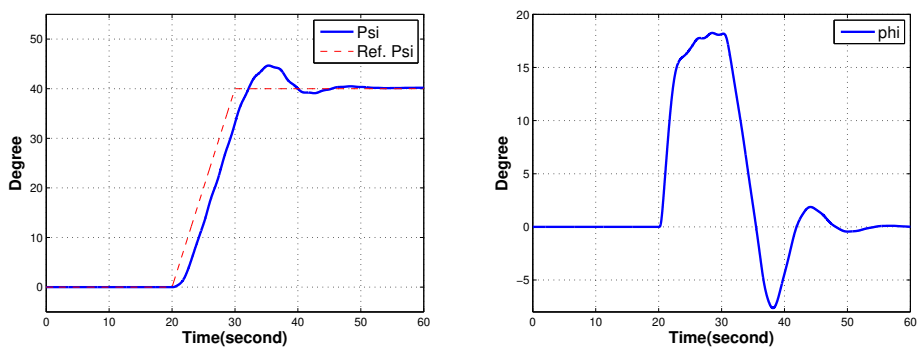


Figure 5.15:  $\psi$  and  $\phi$  responses with reconfiguration.

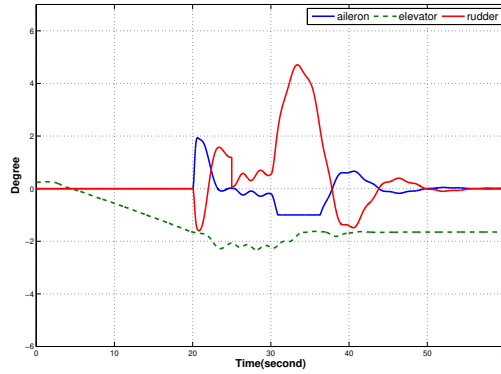


Figure 5.16: Actuator responses with reconfiguration.

## 5.1.2 Elevator Degradation

### 5.1.2.1 The 3rd Level Degradation Without Reconfiguration

The 3rd level (0.1) elevator degradation at the 3rd second and 50 meter altitude change at the 4th second without reconfiguration:

The UAV climbs to a 150 meters with 1 vario vertical speed, depicted in Figure 5.17. Airspeed and throttle responses are shown in Figure 5.18. There is no heading change shown in Figure 5.19. Besides, elevator saturates shown in Figure 5.20. As a result, reconfiguration is needed to prevent saturation.

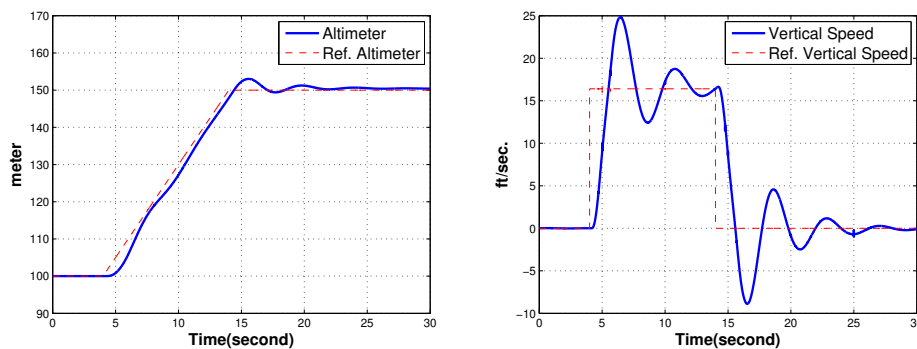


Figure 5.17: Altimeter and vertical speed responses without reconfiguration.

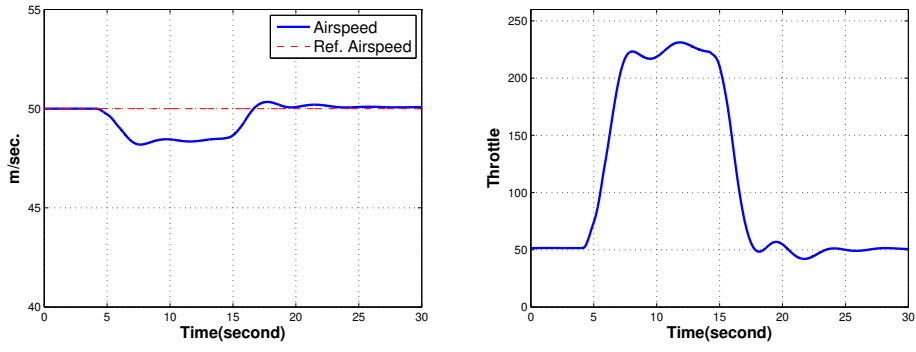


Figure 5.18: Airspeed and throttle responses without reconfiguration.

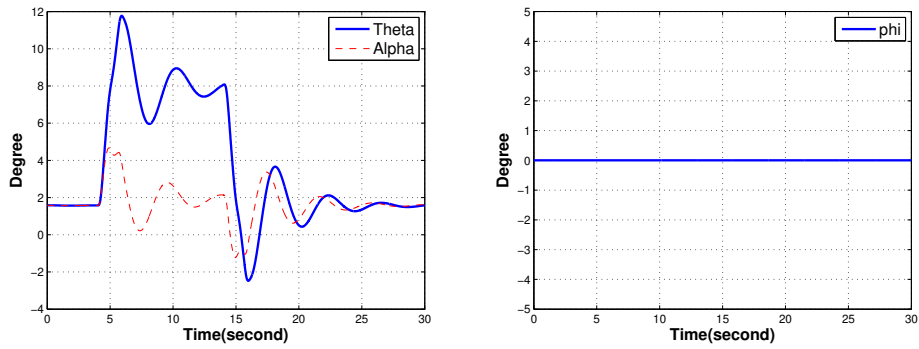


Figure 5.19:  $\theta$ ,  $\alpha$  and  $\phi$  responses without reconfiguration.

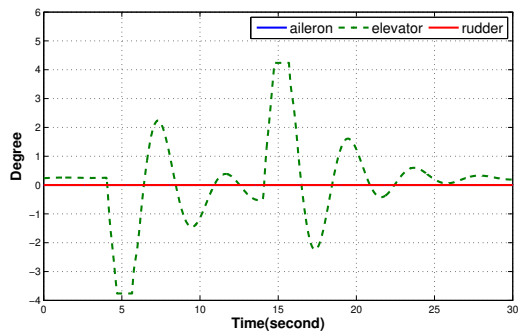


Figure 5.20: Actuator responses without reconfiguration.

**5.1.2.2 The 3rd Level Degradation With Reconfiguration**

The 3rd level (0.1) elevator degradation at the 3rd second and 50 meter altitude change at the 4th second with reconfiguration: The path for the solution is shown in Table 5.3.

Table 5.3: The solution for elevator degradation at the 3rd level.

Problem location	Elevator
Problem	3rd level degradation
Which Reconfiguration Mech. Block	2 and 5
What Reconfiguration Degree	2 slower

The UAV climbs to a 150 meters with 1 vario vertical speed but after the 3rd level elevator degradation, supervisor decreases vertical speed to 0.5 vario with activating reconfiguration mechanism-2, depicted in Figure 5.21. Besides, reconfiguration mechanism-5 (Recon.  $Q$  and  $R$  for  $K_{T-2}$  and  $K_{R-2}$ ) are activated by Supervisor to change  $Q$  and  $R$  matrices to a different value to change control surface movement. Airspeed and throttle responses are shown in Figure 5.22. There is no heading change shown in Figure 5.23. Besides, elevator does not saturate shown in Figure 5.24. As a result, saturation is prevented.

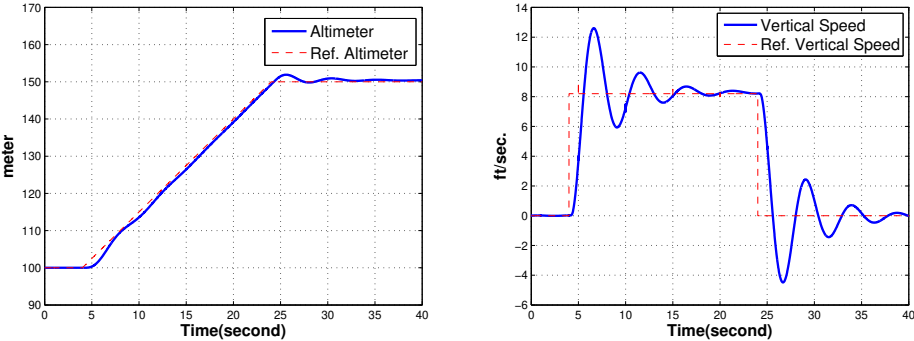


Figure 5.21: Altimeter and vertical speed responses with reconfiguration.

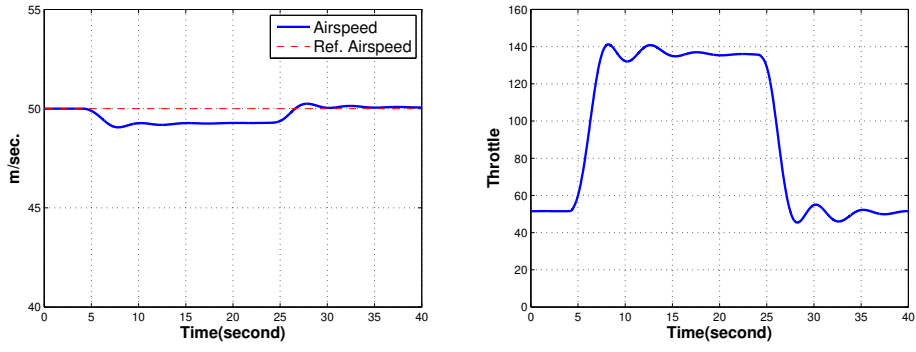


Figure 5.22: Airspeed and throttle responses with reconfiguration.

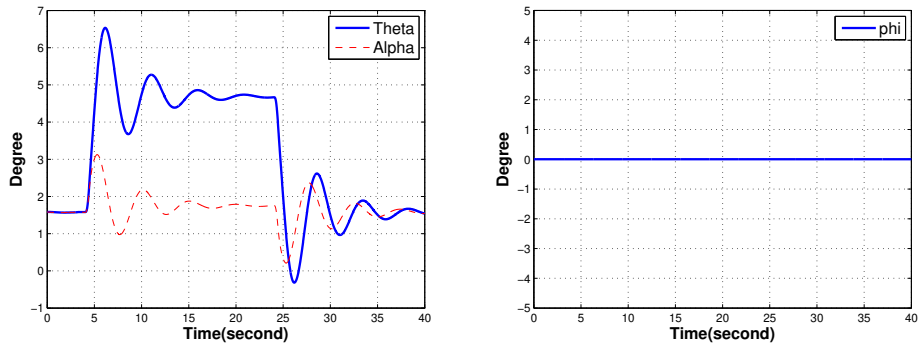


Figure 5.23:  $\theta$ ,  $\alpha$  and  $\phi$  responses with reconfiguration.

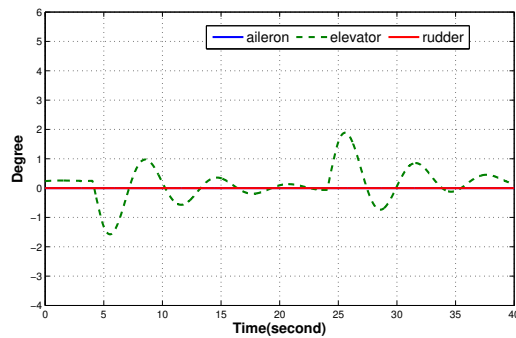


Figure 5.24: Actuator responses with reconfiguration.

### 5.1.3 Rudder Degradation

#### 5.1.3.1 The 3rd Level Degradation Without Reconfiguration

The 3rd level (0.1) rudder degradation at the 3rd second and 40 degree heading change at the 4th second without reconfiguration:

The UAV makes a 40 degree heading change. First, there is not any safety problem with respect to altitude, airspeed,  $\alpha$  which is shown in Figure 5.25 and Figure 5.26. The UAV makes a 40 degree heading change safely with an approximately 16 degree bank angle. However, after heading change is completed, the UAV is not stabilized in the lateral and oscillations about  $\phi$  are growing steadily shown in Figure 5.27 and this causes in LOC-I. These oscillations are resulted from aileron movement shown in Figure 5.28. As a result, aileron movement has to be decelerated and rudder movement has to be accelerated.

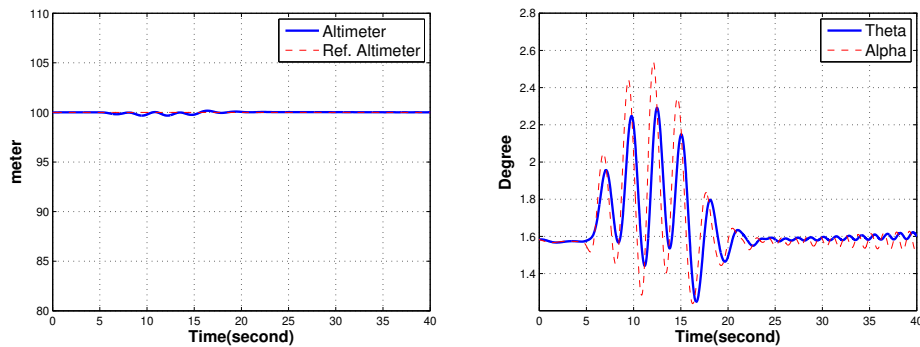


Figure 5.25: Altimeter and  $\theta$ ,  $\alpha$  responses without reconfiguration.

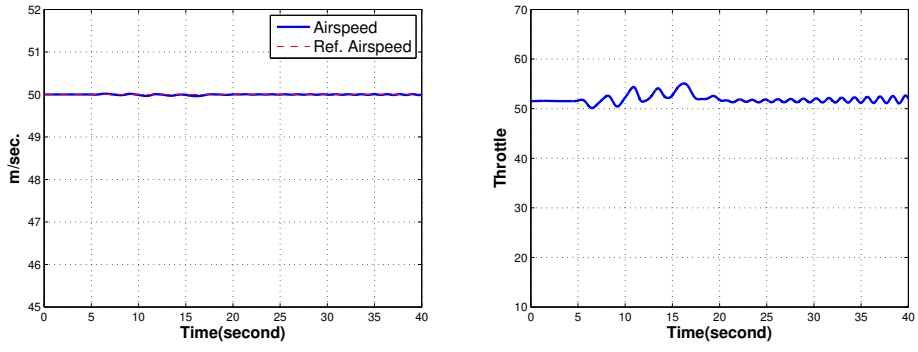


Figure 5.26: Airspeed and throttle responses without reconfiguration.

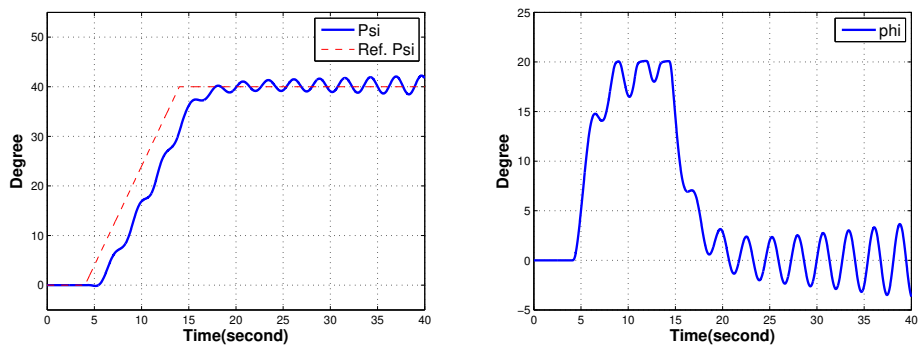


Figure 5.27:  $\psi$  and  $\phi$  responses without reconfiguration.

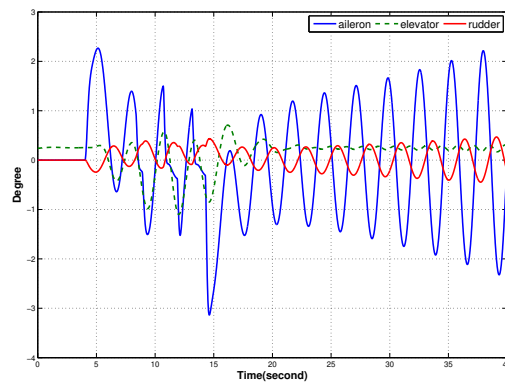


Figure 5.28: Actuator responses without reconfiguration.

### 5.1.3.2 The 3rd Level Degradation With Reconfiguration

The 3rd level (0.1) rudder degradation at the 3rd second and 40 degree heading change at the 4th second with reconfiguration: The path for the solution is shown in Table 5.4.

Table 5.4: The solution for rudder degradation at the 3rd level.

Problem location	Rudder
Problem	3rd level degradation
Which Reconfiguration Mech. Block	5
What Reconfiguration Degree	rudder 0.5 faster
	aileron 0.5 slower

Reconfiguration mechanism-5 (Recon.  $Q$  and  $R$  for  $K_{T-2}$  and  $K_{R-2}$ ) is activated by Supervisor to change  $Q$  and  $R$  matrices to a different value to change control surface movement. There is no safety problem with respect to altitude, airspeed and  $\alpha$  which are shown in Figure 5.5 and Figure 5.6. The UAV makes a 40 degree heading change safely with an approximately 20 degree bank angle shown in Figure 5.7. Besides, rudder and aileron oscillations are prevented shown in Figure 5.8. As a result, with the reconfiguration, LOC-I is prevented.

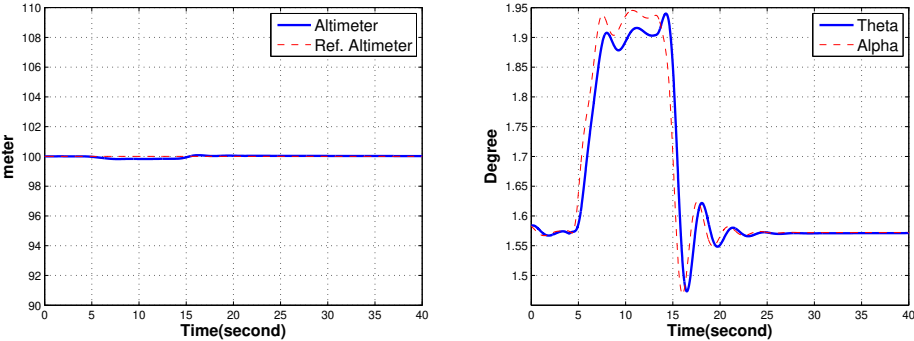


Figure 5.29: Altimeter and  $\theta$ ,  $\alpha$  responses with reconfiguration.

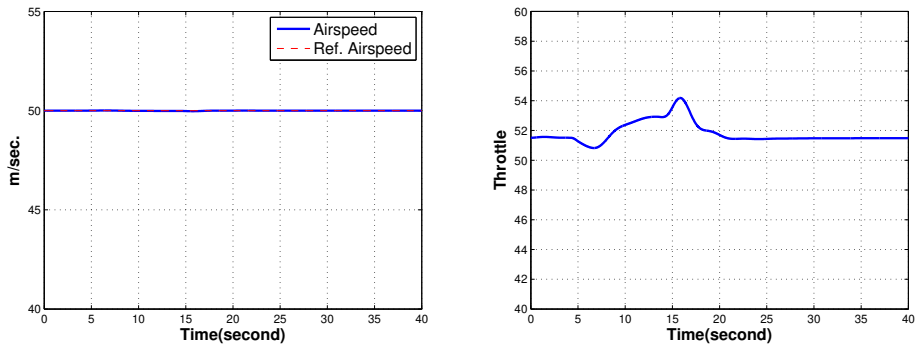


Figure 5.30: Airspeed and throttle responses with reconfiguration.

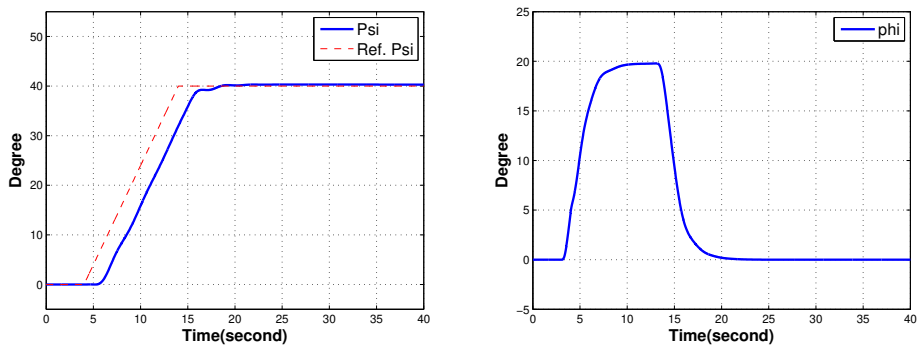


Figure 5.31:  $\psi$  and  $\phi$  responses with reconfiguration.

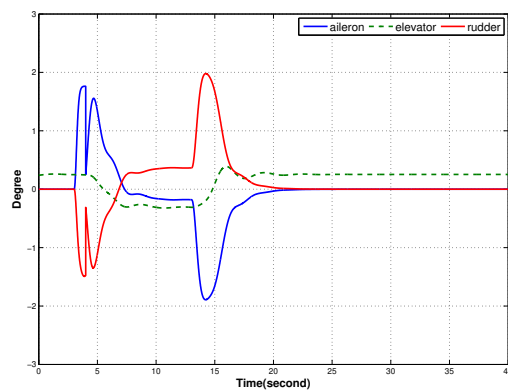


Figure 5.32: Actuator responses with reconfiguration.

### 5.1.3.3 The 4th Level Degradation Without Reconfiguration

The 4th level (0.025) rudder degradation at the 3rd second and 40 degree heading change at the 4th second without reconfiguration:

There is a safety problem with respect to altitude and  $\alpha$  which are shown in Figure 5.33. Besides, the UAV's airspeed oscillates shown in Figure 5.34. The UAV makes a 40 degree heading change safely with a approximately 20 degree bank angle. However, after heading change is completed, the UAV is not stabilized in the lateral and oscillations about  $\phi$  are growing extremely shown in Figure 5.35. Besides, aileron oscillation is too much shown in Figure 5.36. This situation results in LOC-I.

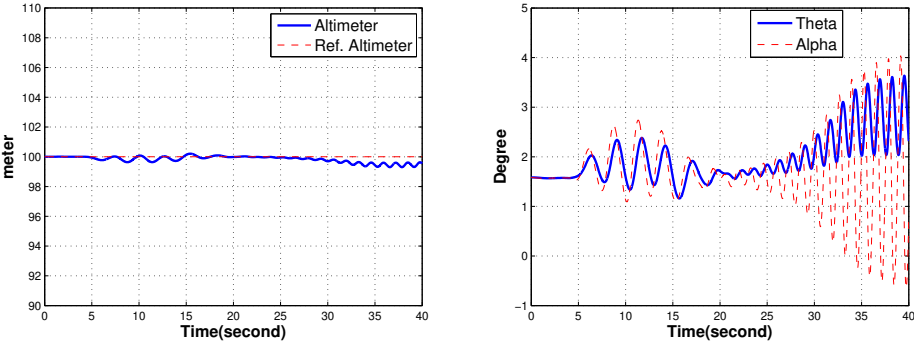


Figure 5.33: Altimeter and  $\theta$ ,  $\alpha$  responses without reconfiguration.

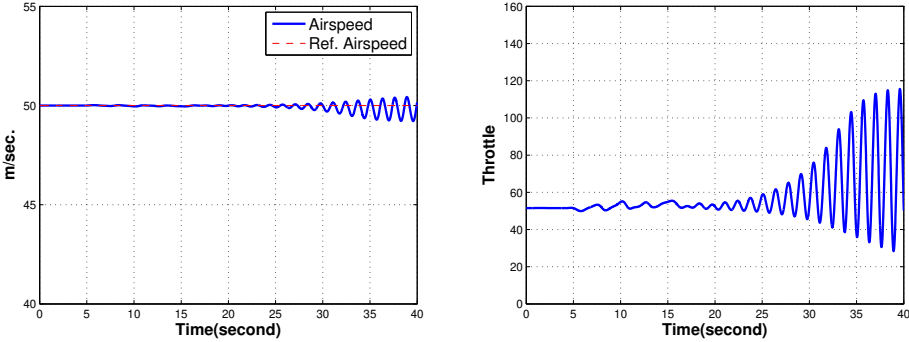


Figure 5.34: Airspeed and throttle responses without reconfiguration.

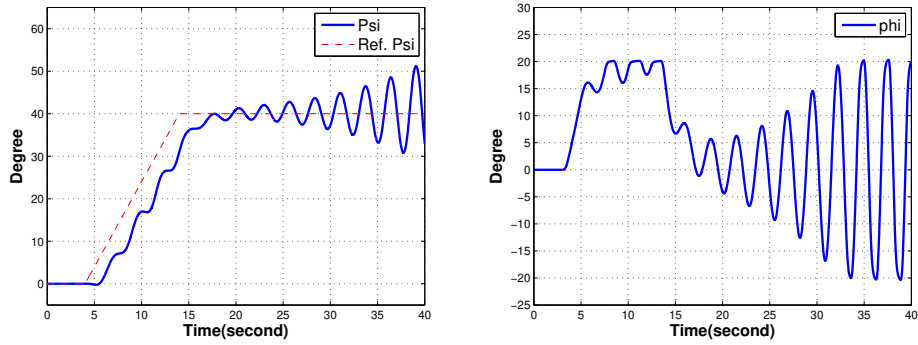


Figure 5.35:  $\psi$  and  $\phi$  responses without reconfiguration.

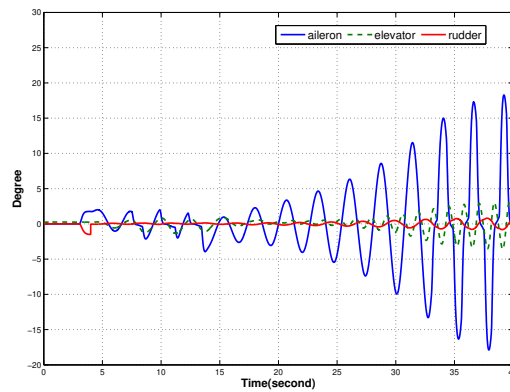


Figure 5.36: Actuator responses without reconfiguration.

#### 5.1.3.4 The 4th Level Degradation With Reconfiguration

The 4th level (0.025) rudder degradation at the 3rd second and 40 degree heading change at the 4th second with reconfiguration: The path for the solution is shown in Table 5.5.

Reconfiguration mechanism-5 (Recon.  $Q$  and  $R$  for  $K_{T2}$  and  $K_{R2}$ ) is activated by Supervisor to change  $Q$  and  $R$  matrices to a different value to change control surface movement. There is no safety problem with respect to altitude, airspeed,  $\alpha$  which are shown in Figure 5.37 and Figure 5.38. The UAV makes a 40 degree heading change

Table 5.5: The solution for rudder degradation at the 4th level.

Problem location	Rudder
Problem	4th level degradation
Which Reconfiguration Mech. Block	5
What Reconfiguration Degree	rudder 0.5 faster aileron 1 slower

safely with an approximately 20 degree bank angle shown in Figure 5.39. Besides, rudder and aileron oscillations are prevented shown in Figure 5.40. As a result, with the reconfiguration, LOC-I is prevented.

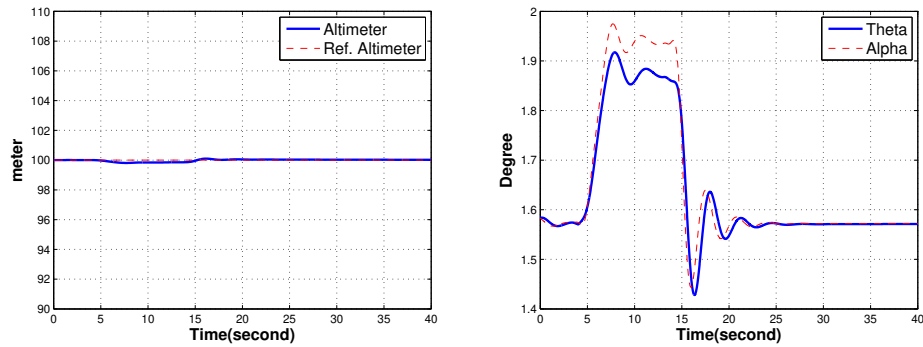


Figure 5.37: Altimeter and  $\theta$ ,  $\alpha$  responses with reconfiguration.

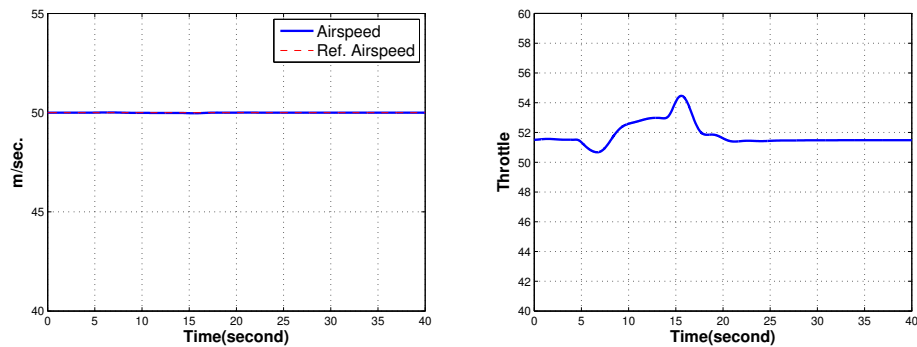


Figure 5.38: Airspeed and throttle responses with reconfiguration.

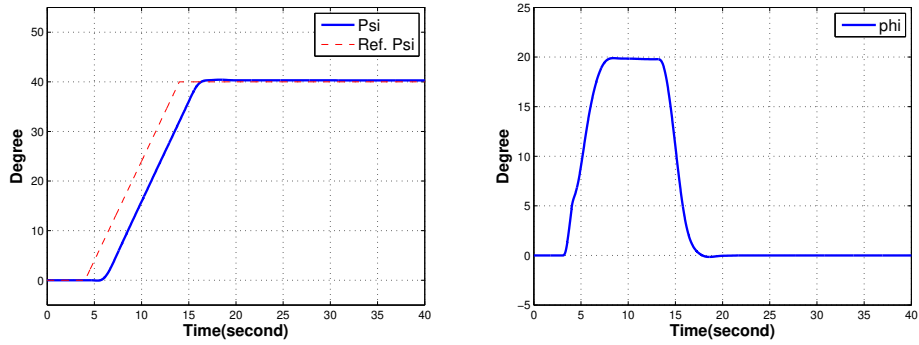


Figure 5.39:  $\psi$  and  $\phi$  responses with reconfiguration.

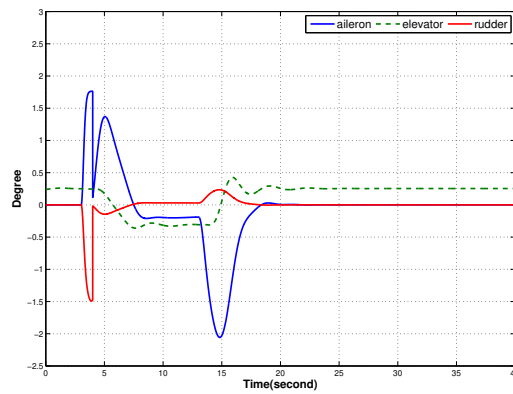


Figure 5.40: Actuator responses with reconfiguration.

## 5.2 Emergency Case-2 Control Surface Actuator Stuck

Actuator stuck is the most dangerous and challenging task for safety in aviation as stated in the Appendix A.4.

### 5.2.1 Aileron Stuck

This case is very dangerous for single engine aircraft or UAVs, because especially for large aileron yaw moment can not be compensated by the rudder yaw moment. Es-

pecially, for accidents which are stated in Appendix A.4, yawing moment is balanced by asymmetric thrust for multi engine aircraft easily.

### 5.2.1.1 0.5 Degree Stuck Without Reconfiguration

0.5 degree aileron stuck at the 3rd second without reconfiguration: If there is not any reconfiguration, there is a LOC-I problem. Altitude, airspeed,  $\alpha$ ,  $\theta$ , shown in Figure 5.41 and Figure 5.42, oscillate too much. Besides, oscillation in the lateral with regard to  $\psi$  and  $\phi$ , gradually grow due to especially rudder movement shown in Figure 5.43. The UAV's control surface actuators and saturation of the rudder are shown in Figure 5.44. As a result, reconfiguration is required.

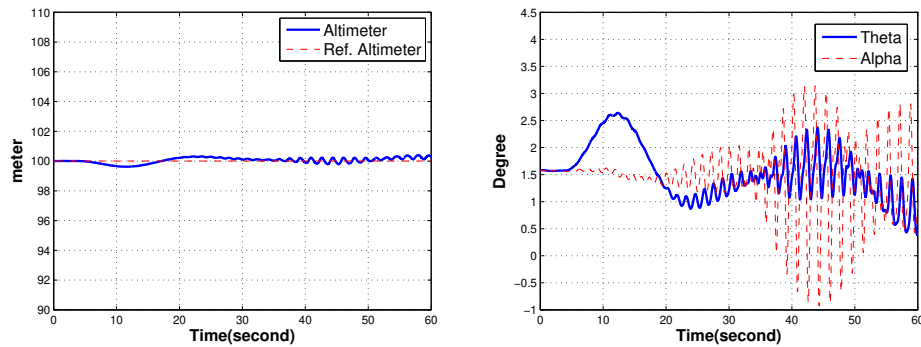


Figure 5.41: Altimeter and  $\theta$ ,  $\alpha$  responses without reconfiguration.

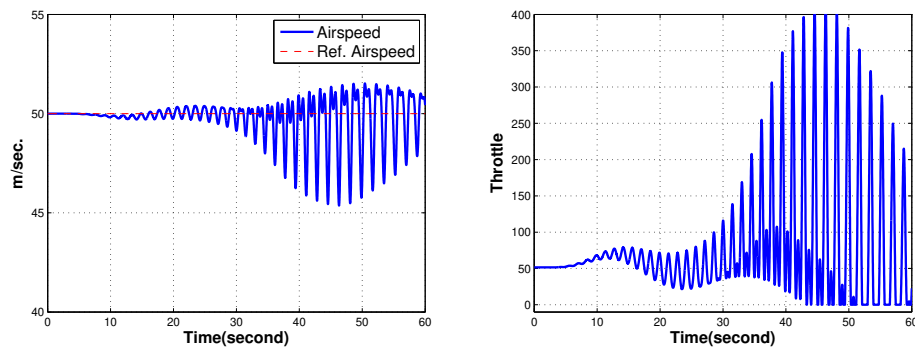


Figure 5.42: Airspeed and throttle responses without reconfiguration.

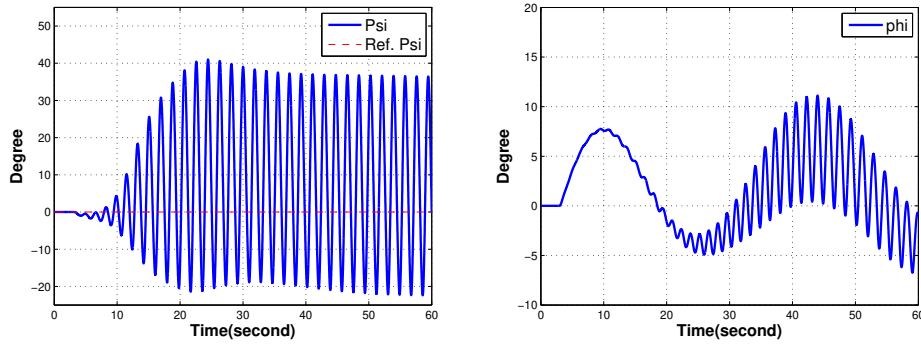


Figure 5.43:  $\psi$  and  $\phi$  responses without reconfiguration.

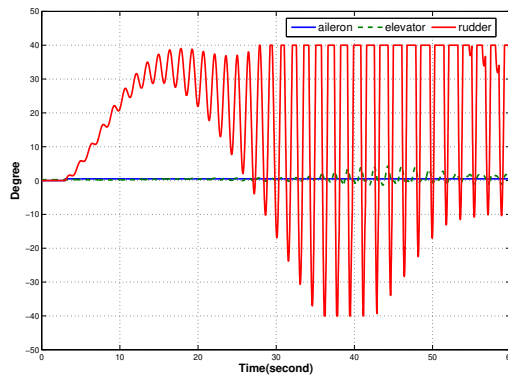


Figure 5.44: Actuator responses without reconfiguration.

### 5.2.1.2 0.5 Degree Stuck With Reconfiguration

0.5 degree aileron stuck at the 3rd second with reconfiguration: The path for the solution is shown in Table 5.6.

Reconfiguration mechanism-1 (Recon. Phi and psi limiter) is activated by Supervisor to change  $\psi$  rate limiter slew rate from 4 to 1 and phi saturation limit from 20 degrees to 14 degrees to make a smooth turns. However, during recovery  $\phi$  is not limited as stated before. Also, reconfiguration mechanism-5 (Recon.  $Q$  and  $R$  for  $K_{T-2}$  and  $K_{R-2}$ ) are activated by Supervisor to change  $Q$  and  $R$  matrices to a smaller value to accelerate control surface movement. There is no safety problem with respect to

Table 5.6: The solution for aileron stuck at 0.5 degree.

Problem location	Aileron
Problem	0.5 degree stuck
Which Reconfiguration Mech. Block	1 and 5
What Reconfiguration Degree	3 Faster

altitude, airspeed,  $\alpha$  which are shown in Figure 5.45 and Figure 5.46. The UAV makes a level flight safely in Figure 5.47. Besides, aileron stuck is shown in Figure 5.48.

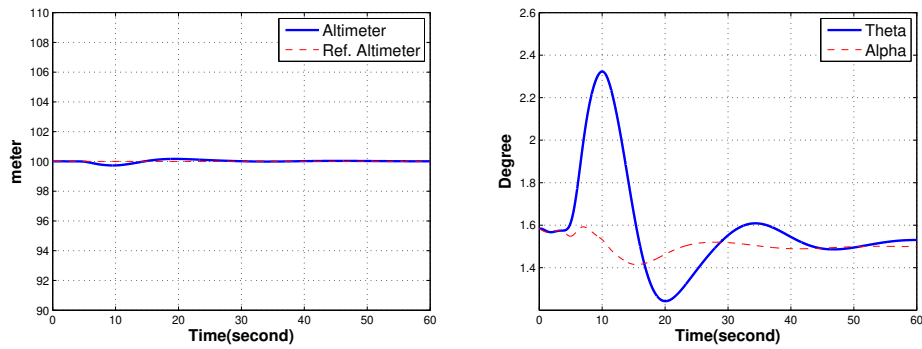


Figure 5.45: Altimeter and  $\theta$ ,  $\alpha$  responses with reconfiguration.

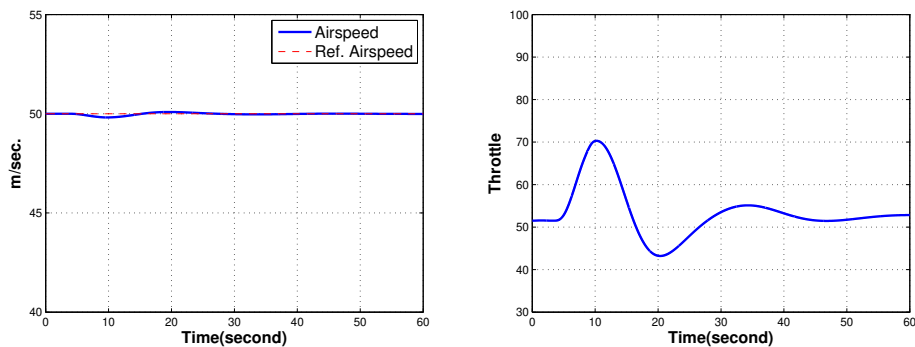


Figure 5.46: Airspeed and throttle responses with reconfiguration.

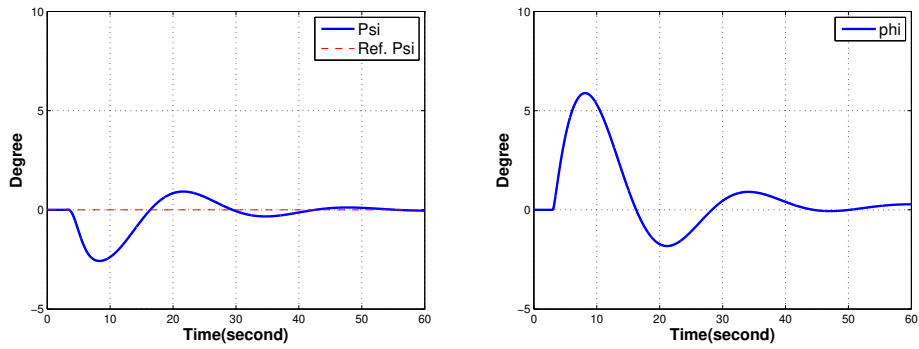


Figure 5.47:  $\psi$  and  $\phi$  responses with reconfiguration.

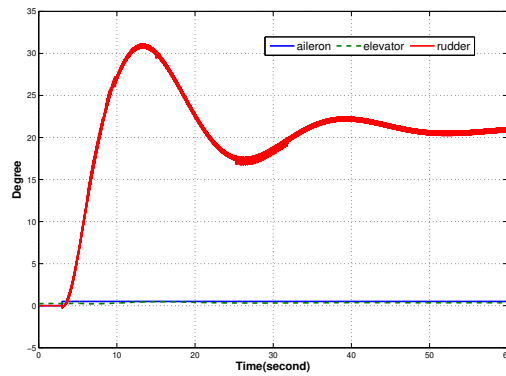


Figure 5.48: Actuator responses with reconfiguration.

### 5.2.2 Elevator Stuck

This case is very dangerous and different approach is required to cope with. For stuck problem about elevator, throttle command has to control altitude. As stated in Section A.4, pilots can control the aircraft with only thrust levers or throttle. Besides, for multi engine aircraft, bank angle can be controlled by asymmetric thrust. As a result this problem can be solved with Propulsion Controlled Aircraft (PCA) application.

### 5.2.3 Rudder Stuck

#### 5.2.3.1 20 Degree Stuck Without Reconfiguration

20 degree rudder stuck at the 3rd second without reconfiguration: If there is not any reconfiguration, there is a LOC-I problem. Altitude, airspeed,  $\alpha$ ,  $\theta$ ,  $\psi$  and  $\phi$  responses are shown in Figure 5.49, Figure 5.50 and Figure 5.51. The UAV's aileron and elevator actuators are going to saturate which are shown in Figure 5.52. As a result, fast response of the controllers sometimes ends up in a deadly manner so reconfiguration is vital and obligatory.

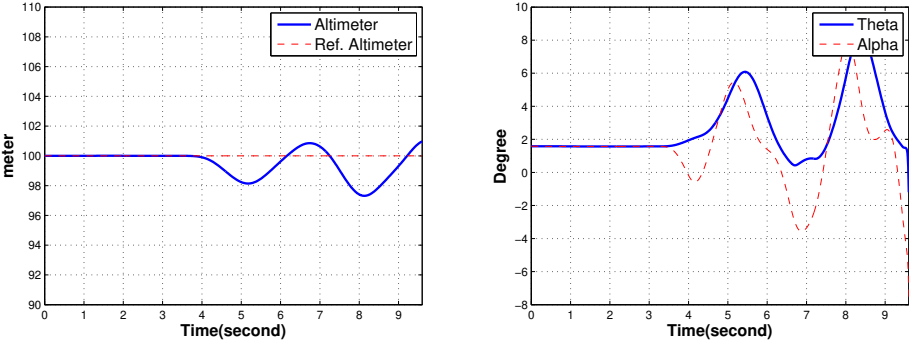


Figure 5.49: Altimeter and  $\theta$ ,  $\alpha$  responses without reconfiguration.

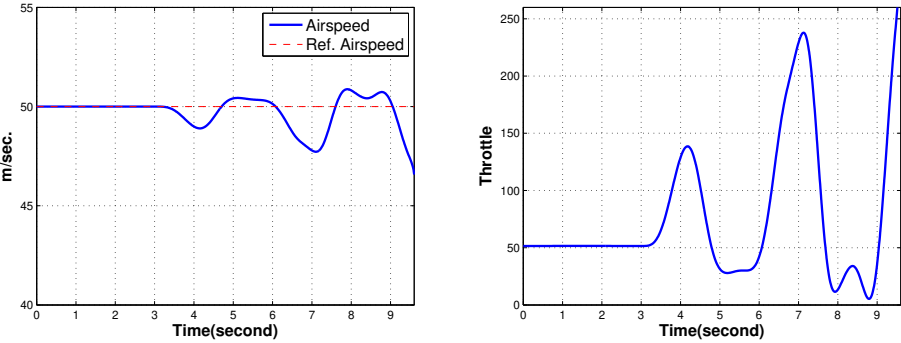


Figure 5.50: Airspeed and throttle responses without reconfiguration.

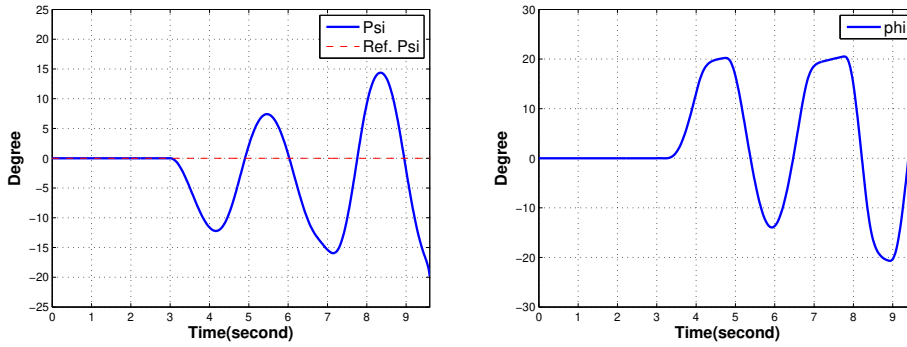


Figure 5.51:  $\psi$  and  $\phi$  responses without reconfiguration.

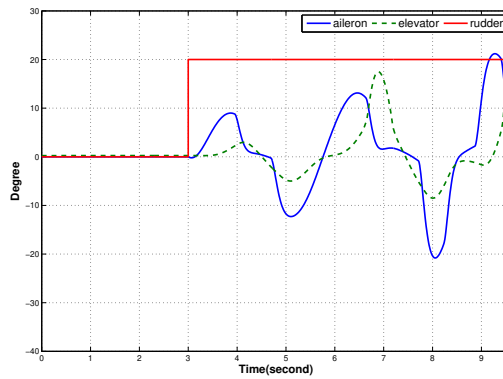


Figure 5.52: Actuator responses without reconfiguration.

### 5.2.3.2 20 Degree Stuck With Reconfiguration

20 degree rudder stuck at the 3rd second and 40 degree heading change at the 20th second with reconfiguration: The path for the solution is shown in Table 5.7.

Reconfiguration mechanism-1 (Recon. Phi and psi limiter) is activated by Supervisor to change  $\psi$  rate limiter slew rate from 4 to 2 and phi saturation limit from 20 degrees to 14 degrees to make a smooth turns. However, it can be dangerous during recovery to limit  $\phi$  because during emergency, sometimes deep maneuvers are required. As a result, during recovery  $\phi$  is not limited. Also, reconfiguration mechanism-5 (Recon.  $Q$  and  $R$  for  $K_{T-2}$  and  $K_{R-2}$ ) are activated by Supervisor to change  $Q$  and  $R$  matrices

Table 5.7: The solution for rudder stuck at 20 degrees.

Problem location	Rudder
Problem	20 degree stuck
Which Reconfiguration Mech. Block	1 and 5
What Reconfiguration Degree	1 slower

to a higher value to slowing down control surface movement. There is no safety problem with respect to altitude, airspeed,  $\alpha$  shown in Figure 5.53 and Figure 5.54. The UAV makes a 60 degree heading change safely with an approximately 11 degree bank angle shown in Figure 5.55. Besides, rudder stuck is shown in Figure 5.56.

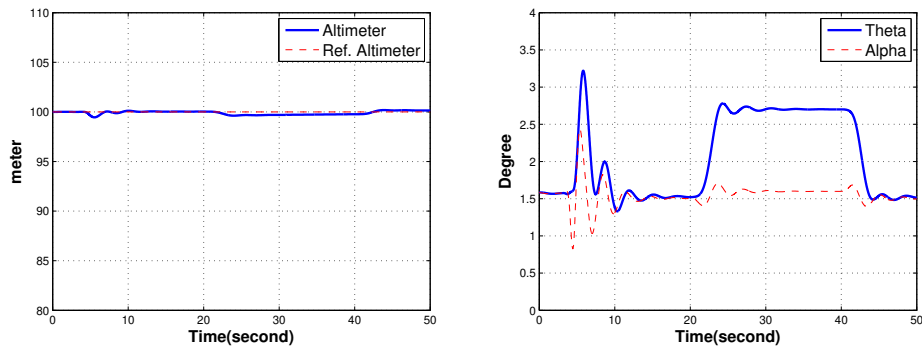


Figure 5.53: Altimeter and  $\theta$ ,  $\alpha$  responses with reconfiguration.

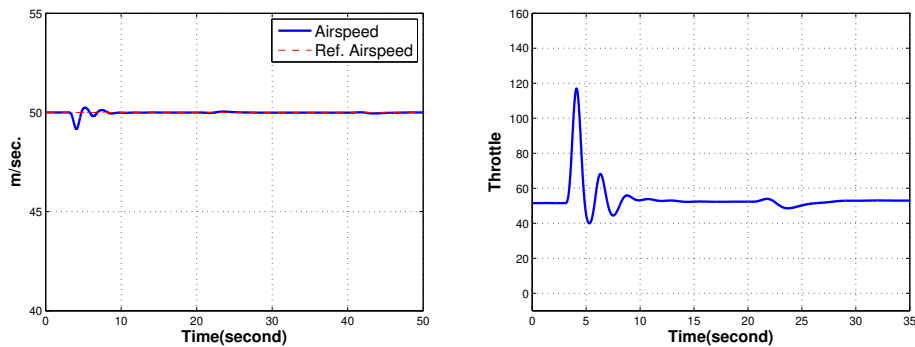


Figure 5.54: Airspeed and throttle responses with reconfiguration.

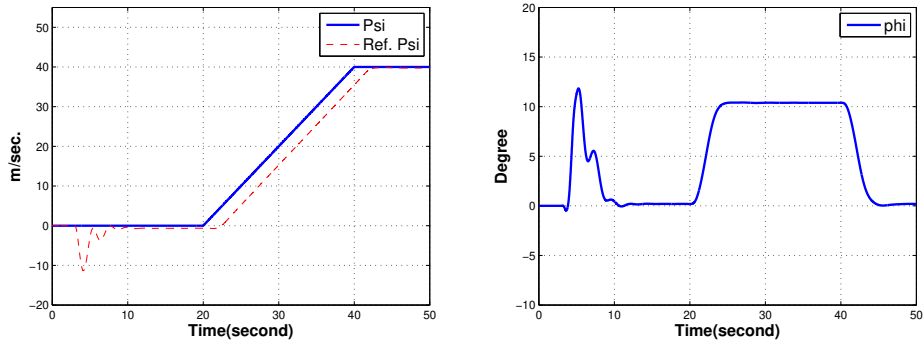


Figure 5.55:  $\psi$  and  $\phi$  responses with reconfiguration.

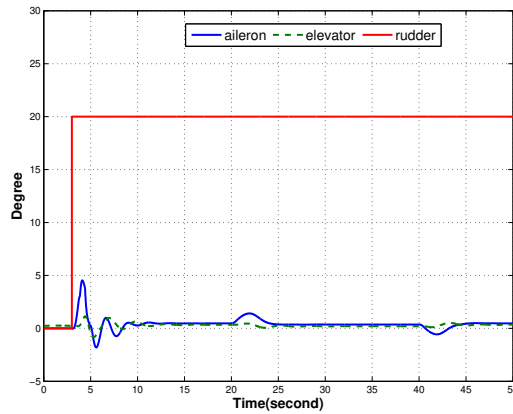


Figure 5.56: Actuator responses with reconfiguration.

### 5.2.3.3 40 Degree Stuck With Reconfiguration

40 degree rudder stuck at the 3rd second and 40 degree heading change at the 20th second: The path for the solution is shown in Table 5.8.

Reconfiguration mechanism-1 (Recon. Phi and psi limiter) is activated by Supervisor to change  $\psi$  rate limiter from 4 to 2 and phi saturation limit from 20 degrees to 14 degrees to make a smooth turns. However, during recovery  $\phi$  is not limited. Also, reconfiguration mechanism-5 (Recon.  $Q$  and  $R$  for  $K_{T-2}$  and  $K_{R-2}$ ) is activated by Supervisor to change  $Q$  and  $R$  matrices to a higher value to slowing down control

Table 5.8: The solution for rudder stuck at 40 degrees.

Problem location	Rudder
Problem	40 degree stuck
Which Reconfiguration Mech. Block	1 and 5
What Reconfiguration Degree	1 slower

surface movement. There is no safety problem with respect to altitude, airspeed,  $\alpha$  which are shown in Figure 5.57 and Figure 5.58. The UAV makes a 40 degrees heading change safely with an approximately 5 degrees bank angle shown in Figure 5.59. Besides, rudder stuck is shown in Figure 5.60.

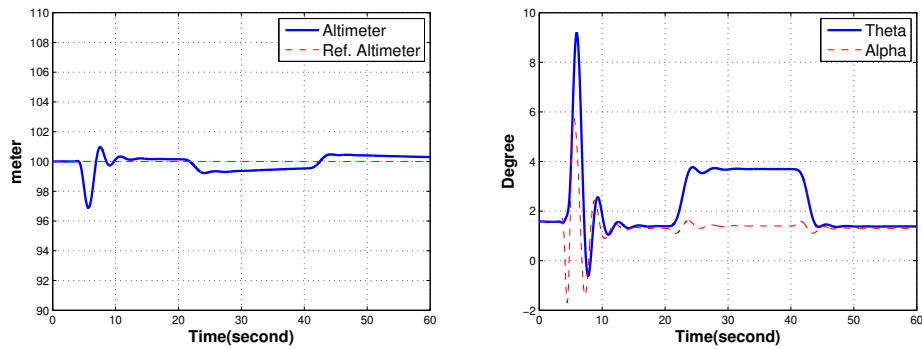


Figure 5.57: Altimeter and  $\theta$ ,  $\alpha$  responses with reconfiguration.

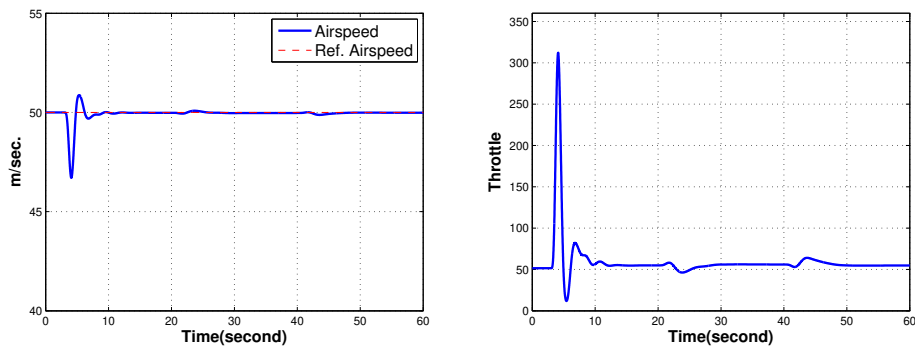


Figure 5.58: Airspeed and throttle responses with reconfiguration.

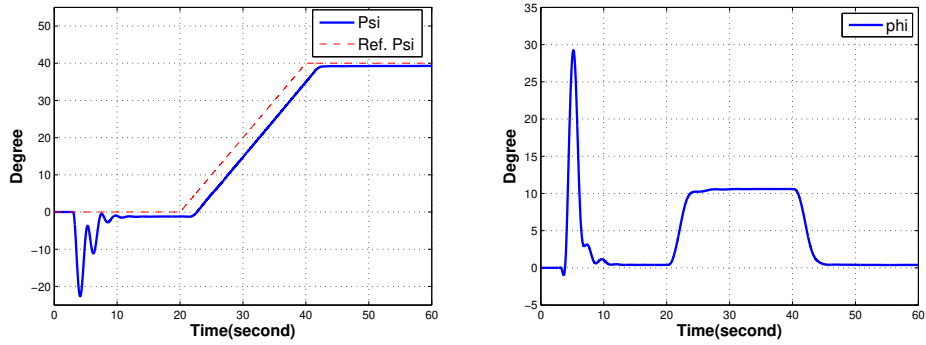


Figure 5.59:  $\psi$  and  $\phi$  responses with reconfiguration.

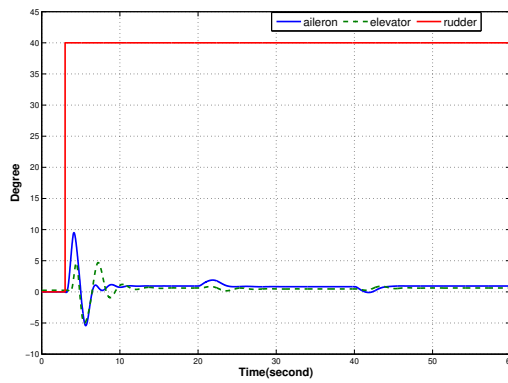


Figure 5.60: Actuator responses with reconfiguration.

### 5.3 Emergency Case-3 Control Surface Damage

#### 5.3.1 Aileron Damage

##### 5.3.1.1 The 3rd Level Damage Without Reconfiguration

The 3rd level (control surface) aileron damage at the 4th second and 60 degree heading change at the 3rd second without reconfiguration: Without reconfiguration, the UAV can maintain altitude with a small  $\alpha$  oscillation, shown in Figure 5.61. Besides, airspeed and throttle values are very well shown in Figure 5.62. During heading

change,  $\psi$  and  $\phi$  are overshoot a little, shown in Figure 5.63. Rudder and aileron oscillations are shown in Figure 5.64. As a result, for the best performance of the control surface, reconfiguration can be done.

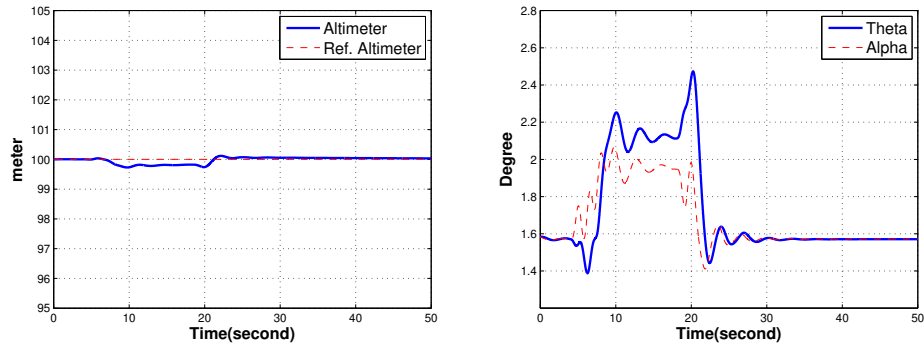


Figure 5.61: Altimeter and  $\theta$ ,  $\alpha$  responses without reconfiguration.

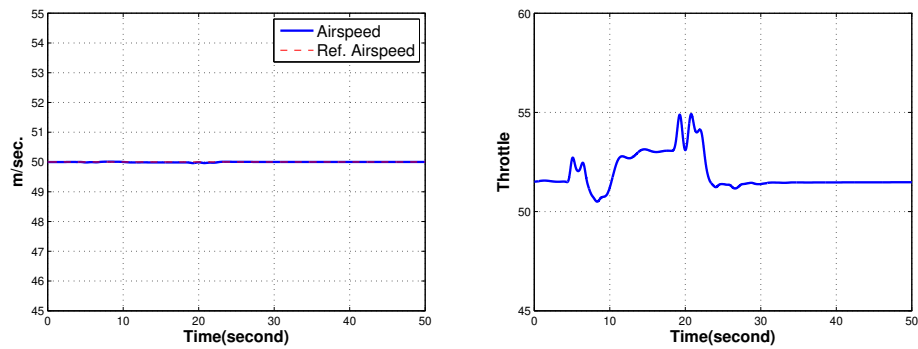


Figure 5.62: Airspeed and throttle responses without reconfiguration.

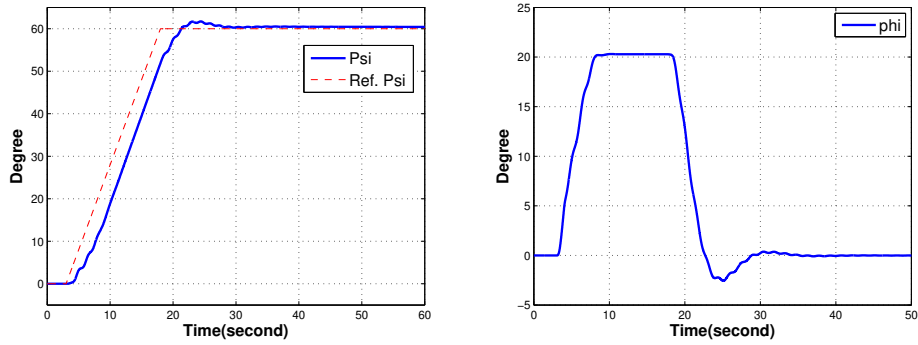


Figure 5.63:  $\psi$  and  $\phi$  responses without reconfiguration.

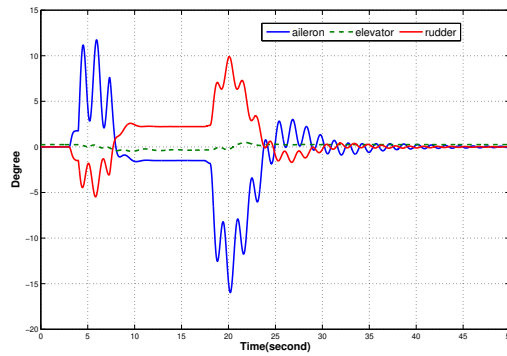


Figure 5.64: Actuator responses without reconfiguration.

### 5.3.1.2 The 3rd Level Damage With Reconfiguration

The 3rd level (control surface) aileron damage at the 4th second and 60 degree heading change at the 3rd second with reconfiguration: The path for the solution is shown in Table 5.9.

Altitude,  $\theta$ ,  $\alpha$  responses are reliable shown in Figure 5.65. Besides, airspeed and throttle responses are at desired value, shown in Figure 5.66.  $\psi$  rate limiter slew rate is reconfigured from 4 to 2 and  $\phi$  saturation limiter from 20 to 14 degrees shown in Figure 5.67. Also, this helps to prevent potential aileron actuator saturation and oscillation because more deflection is required to reach desired attitude by damaged

Table 5.9: The solution for aileron damage at the 3rd level.

Problem location	Aileron
Problem	3rd level damage
Which Reconfiguration Mech. Block	1, 5 and 7
What Reconfiguration Degree	1 Faster

control surface. As a result, smooth aileron command can be created by reconfiguration, shown in Figure 5.68.

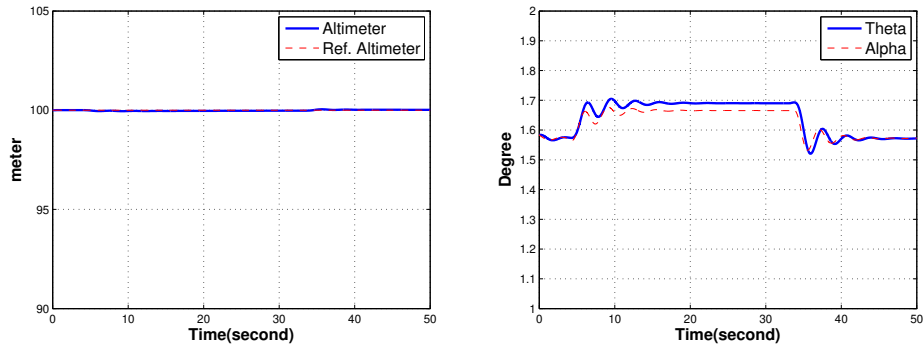


Figure 5.65: Altimeter and  $\theta$ ,  $\alpha$  responses with reconfiguration.

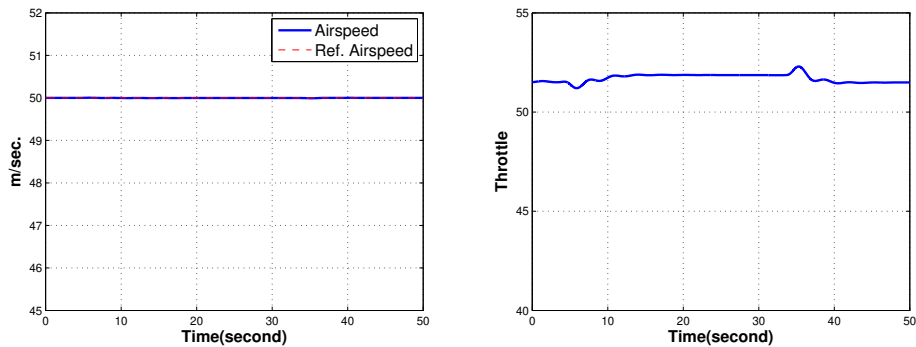


Figure 5.66: Airspeed and throttle responses with reconfiguration.

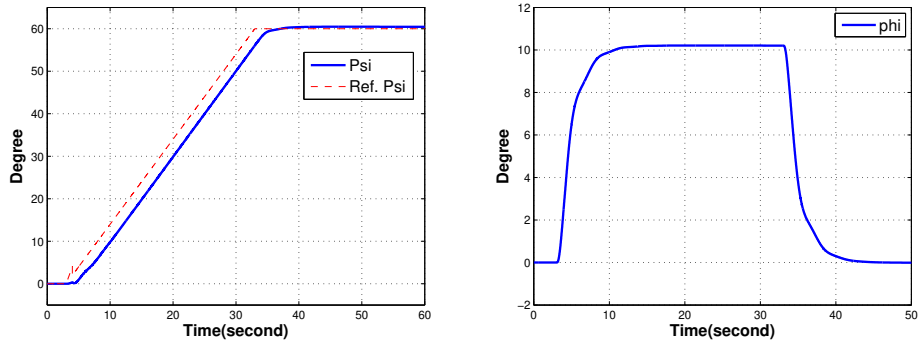


Figure 5.67:  $\psi$  and  $\phi$  responses with reconfiguration.

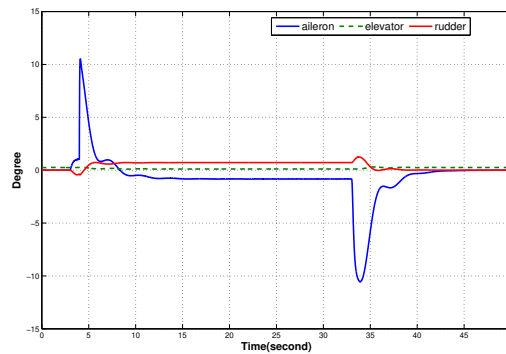


Figure 5.68: Actuator responses with reconfiguration.

### 5.3.1.3 The 4th level Damage Without Reconfiguration

The 4th level (control surface) aileron damage at the 4th second and 60 degree heading change at the 3rd second without reconfiguration: Without reconfiguration, the UAV can maintain altitude with an  $\alpha$  oscillation, shown in Figure 5.69. Besides, air-speed and throttle oscillate and sometimes airspeed decreases, shown in Figure 5.70. After heading change is completed,  $\psi$  and  $\phi$  oscillations continue and  $\phi$  can not be stabilized, shown in Figure 5.71. Rudder and aileron saturate and oscillate, shown in Figure 5.72. As a result, reconfiguration is required for safe flight.

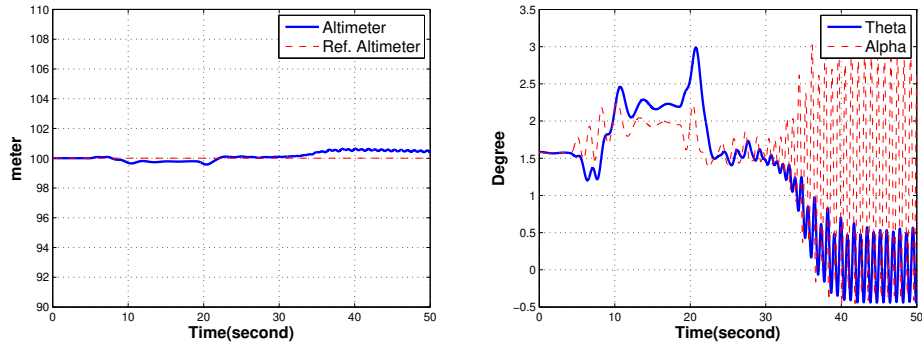


Figure 5.69: Altimeter and  $\theta$ ,  $\alpha$  responses without reconfiguration.

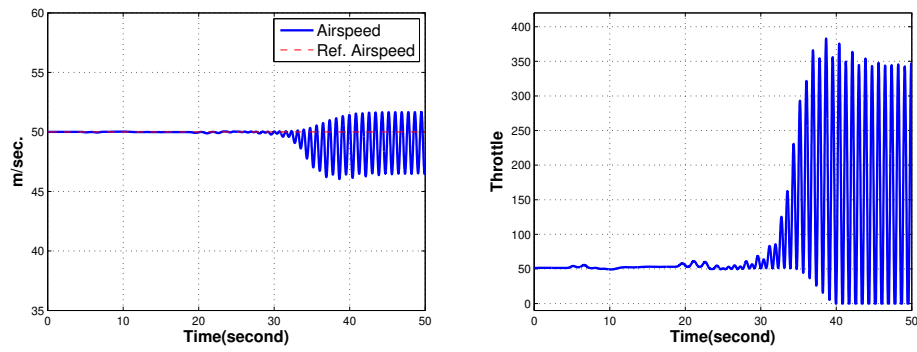


Figure 5.70: Airspeed and throttle responses without reconfiguration.

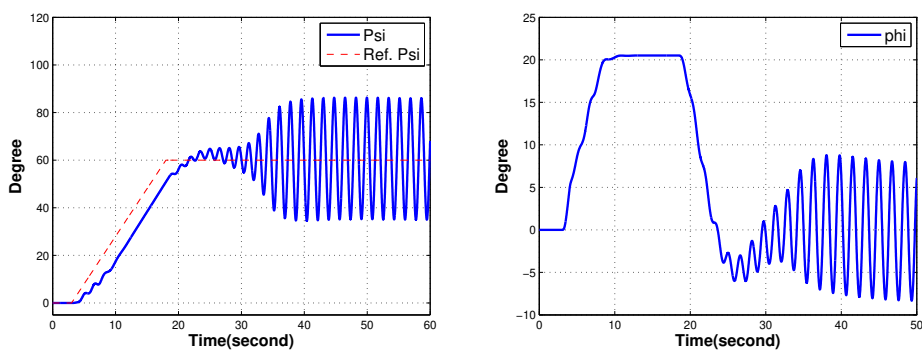


Figure 5.71:  $\psi$  and  $\phi$  responses without reconfiguration.

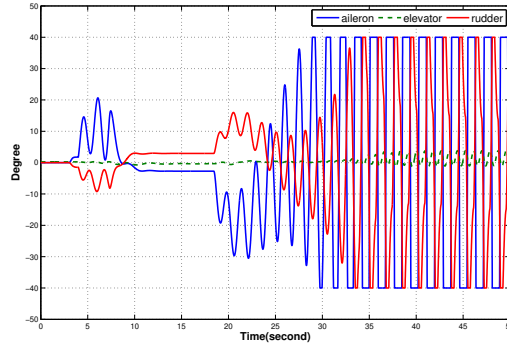


Figure 5.72: Actuator responses without reconfiguration.

#### 5.3.1.4 The 4th level Damage With Reconfiguration

The 4th level aileron damage at the 4th second and 60 degree heading change at the 3rd second with reconfiguration: The path for the solution is shown in Table 5.10.

Table 5.10: The solution for aileron damage at the 4th level.

Problem location	Aileron
Problem	4th level damage
Which Reconfiguration Mech. Block	1, 5 and 7
What Reconfiguration Degree	1 Faster

Altitude,  $\theta$ ,  $\alpha$  responses are reliable shown in Figure 5.73. Besides, airspeed and throttle responses are at desired value shown in Figure 5.74.  $\psi$  rate limiter slew rate is reconfigured from 4 to 2 and  $\phi$  saturation limiter from 20 to 14 degrees, shown in Figure 5.75. Also, this helps to prevent aileron actuator saturation, shown in Figure 5.76, because more deflection is required to reach desired attitude by damaged control surface.

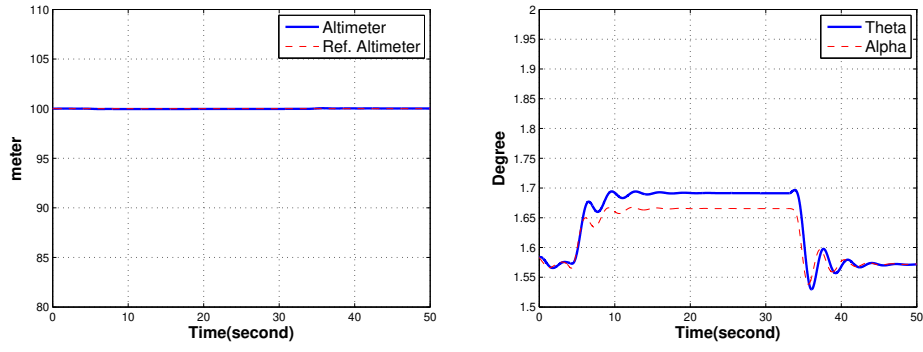


Figure 5.73: Altimeter and  $\theta$ ,  $\alpha$  responses with reconfiguration.

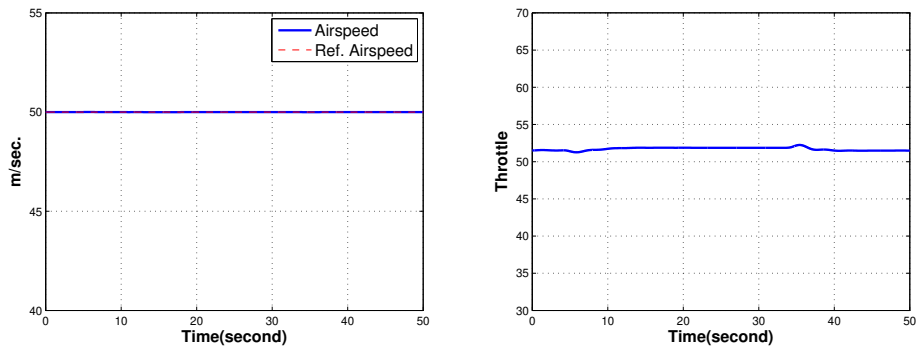


Figure 5.74: Airspeed and throttle responses with reconfiguration.

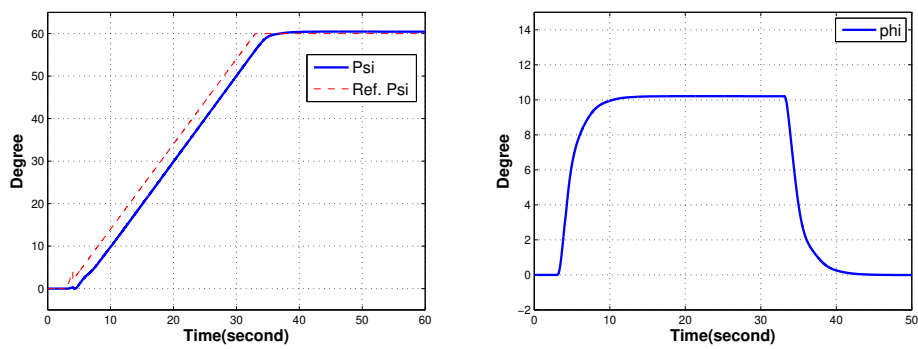


Figure 5.75:  $\psi$  and  $\phi$  responses with reconfiguration.

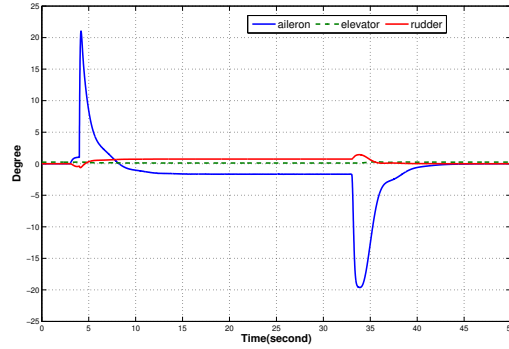


Figure 5.76: Actuator responses with reconfiguration.

## 5.3.2 Elevator Damage

### 5.3.2.1 The 3rd Level Damage Without Reconfiguration

The 3rd level elevator damage at the 4th second and altitude change from 100 to 150 meters with 1 vario (1000 ft./min.) at the 3rd second without reconfiguration:

Without reconfiguration, the UAV can maintain and change altitude safely, shown in Figure 5.77. Besides, airspeed and throttle values are very well shown in Figure 5.78. There is not any change for  $\psi$  and  $\phi$  responses, shown in Figure 5.79. Elevator does not saturate, shown in Figure 5.80. As a result, for the best performance and decreasing elevator movement to a lower degree, reconfiguration can be made.

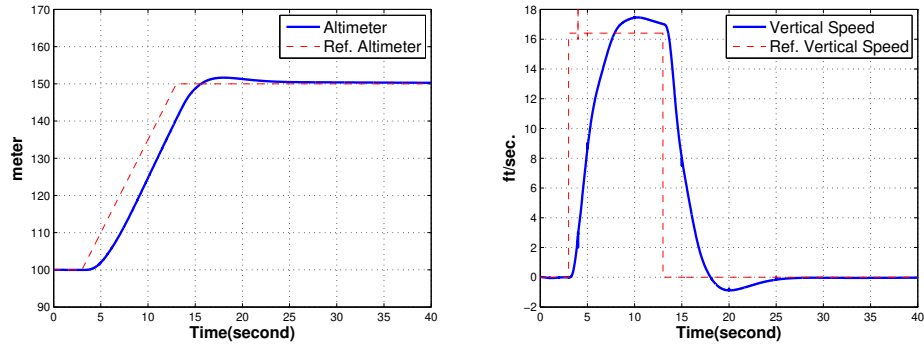


Figure 5.77: Altimeter and vertical speed responses without reconfiguration.

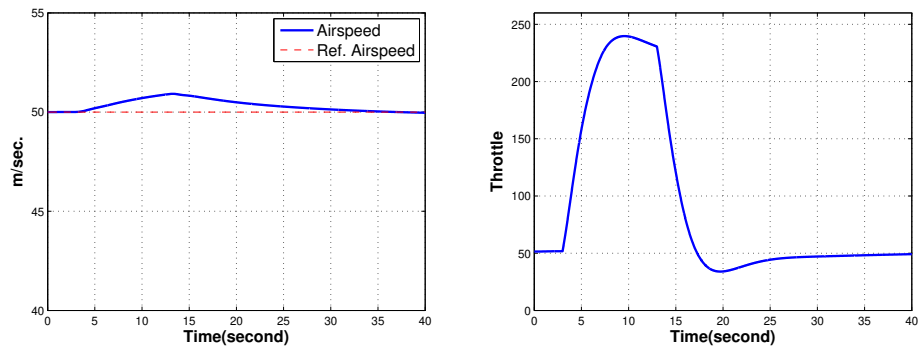


Figure 5.78: Airspeed and throttle responses without reconfiguration.

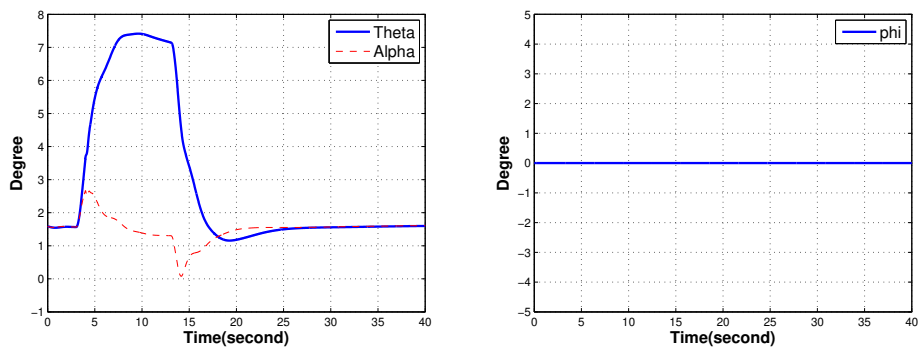


Figure 5.79:  $\theta$ ,  $\alpha$  and  $\Phi$  responses without reconfiguration.

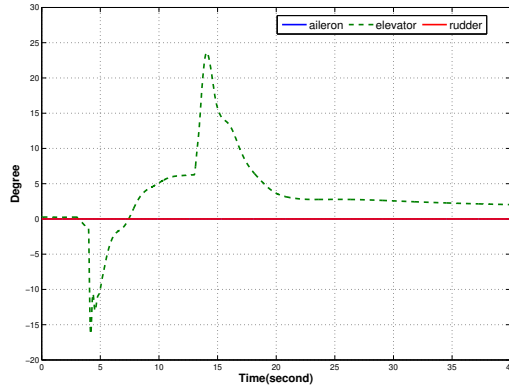


Figure 5.80: Actuator responses without reconfiguration.

### 5.3.2.2 The 3rd Level Damage With Reconfiguration

The 3rd level elevator damage at the 4th second and altitude change from 100 to 150 meters at the 3rd second with reconfiguration: The path for the solution is shown in Table 5.11.

Table 5.11: The solution for elevator damage at the 3rd level.

Problem location	Elevator
Problem	3rd level damage
Which Reconfiguration Mech. Block	2, 5 and 7
What Reconfiguration Degree	1 Slower

First, for level change, vario is limited to 1 (1000 ft./min.). However, after by reconfiguration block-2, vario is limited to 0.5 (500 ft./min.). Besides, elevator movement is decreased by reconfiguration block-5. The UAV can maintain and change altitude safely, shown in Figure 5.77. Besides, airspeed and throttle values are very well, shown in Figure 5.78. There is not any change for  $\psi$  and  $\phi$  responses, shown in Figure 5.79. Elevator actuator degree is at an approximately 13 degrees, shown in Figure 5.80.

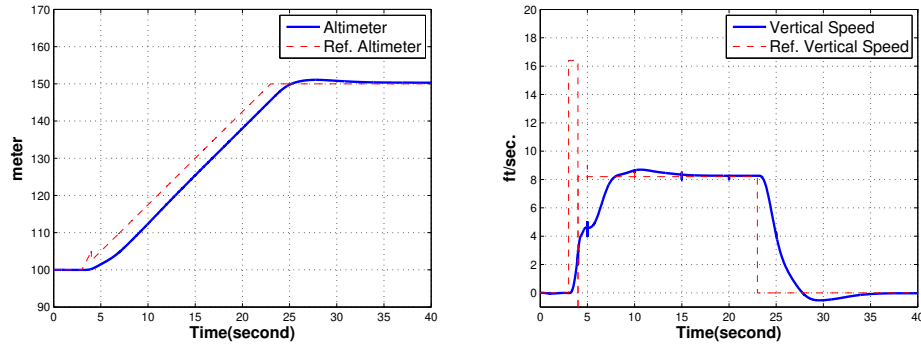


Figure 5.81: Altimeter and vertical speed responses with reconfiguration.

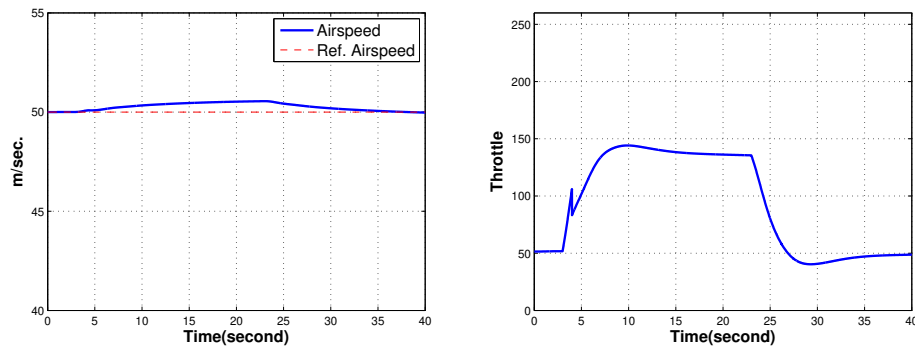


Figure 5.82: Airspeed and throttle responses with reconfiguration.

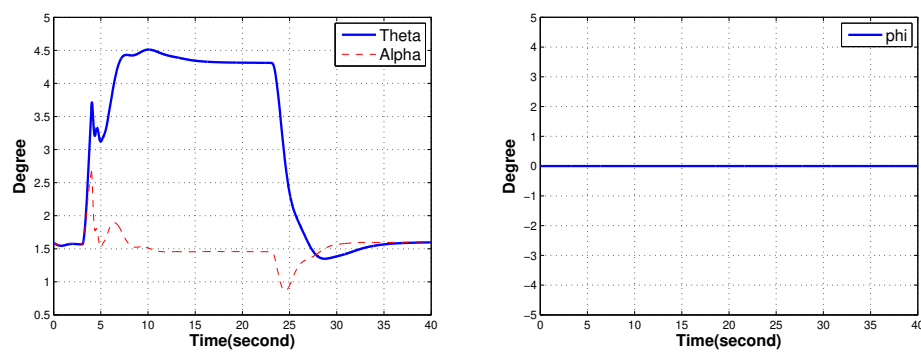


Figure 5.83:  $\theta$ ,  $\alpha$  and  $\phi$  responses with reconfiguration.

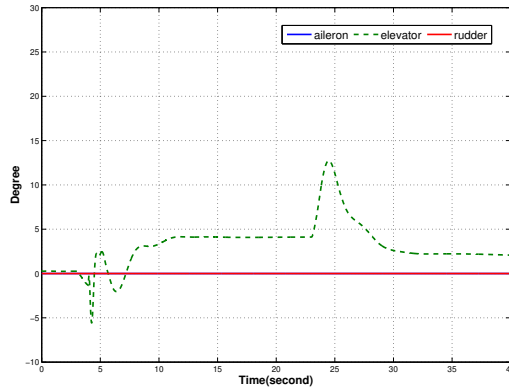


Figure 5.84: Actuator responses with reconfiguration.

### 5.3.2.3 The 4th Level Damage Without Reconfiguration

The 4th level elevator damage at the 4th second and altitude change from 100 to 150 meters with flight level change at the 3rd second without reconfiguration:

Without reconfiguration, the UAV can change altitude with a little deviation from reference altitude shown in Figure 5.85. Besides, airspeed increases a little, shown in Figure 5.86. During altitude change  $\theta$  and  $\alpha$  and no change in  $\phi$  are shown in Figure 5.87. Despite throttle command, elevator saturates due to large damage, shown in Figure 5.88. As a result, without reconfiguration, it is dangerous for an elevator actuator.

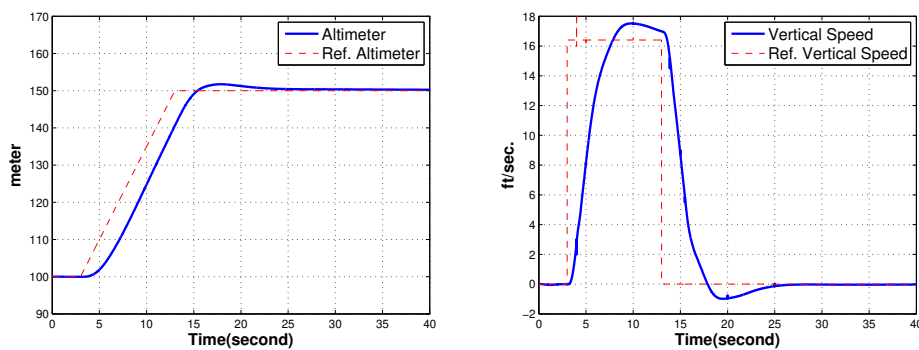


Figure 5.85: Altimeter and vertical speed responses without reconfiguration.

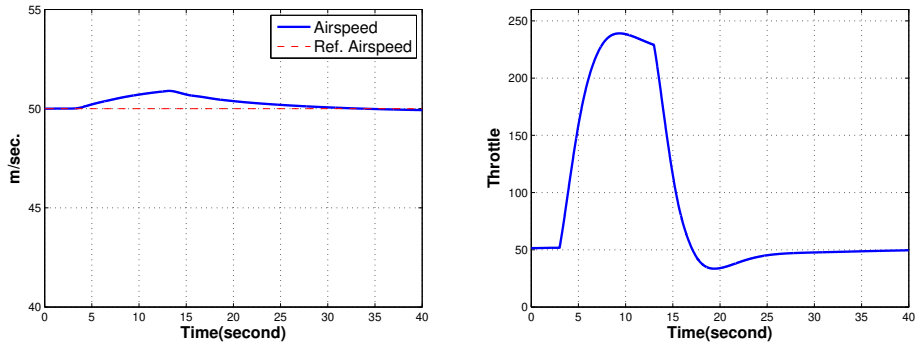


Figure 5.86: Airspeed and throttle responses without reconfiguration.

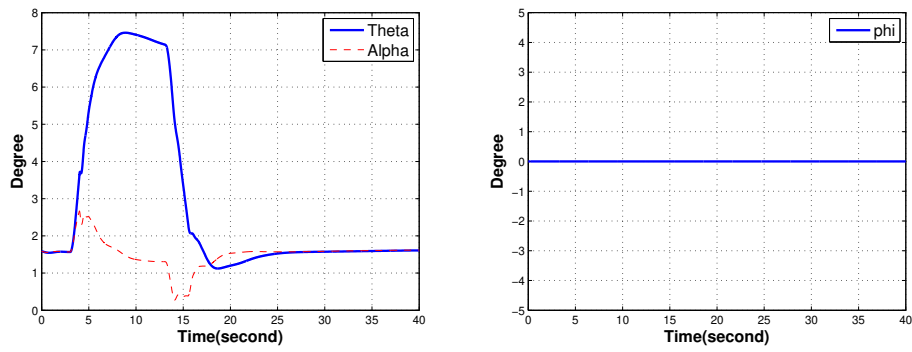


Figure 5.87:  $\theta$ ,  $\alpha$  and  $\phi$  responses without reconfiguration.

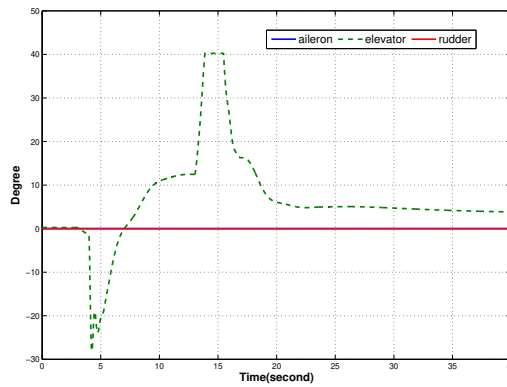


Figure 5.88: Actuator responses without reconfiguration.

### 5.3.2.4 The 4th Level Damage With Reconfiguration

The 4th level elevator damage at the 4th second and altitude change from 100 to 150 meters with flight level change at the 3rd second with reconfiguration: The path for the solution is shown in Table 5.12.

Table 5.12: The solution for elevator damage at the 4th level.

Problem location	Elevator
Problem	4th level damage
Which Reconfiguration Mech. Block	2, 5 and 7
What Reconfiguration Degree	1 slower

Altitude and vertical speed responses are reliable shown in Figure 5.89. First, for flight level change, vario is limited to 1 (1000 ft./min.). However, after by reconfiguration block-2, vario is limited to 0.5 (500 ft./min.). Besides, elevator movement is decreased by reconfiguration block-5. Airspeed and throttle responses are shown in Figure 5.90.  $\phi$  is at zero and  $\theta$ ,  $\alpha$  are shown in Figure 5.91. Finally, slower reconfiguration degree helps to prevent elevator actuator saturation shown in Figure 5.92.

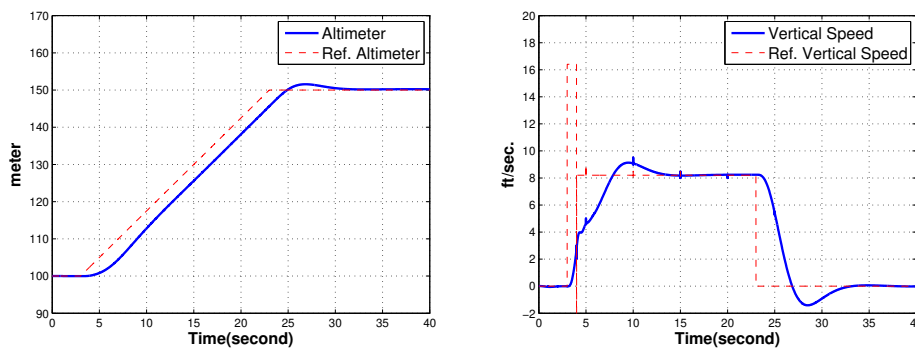


Figure 5.89: Altimeter and vertical speed responses with reconfiguration.

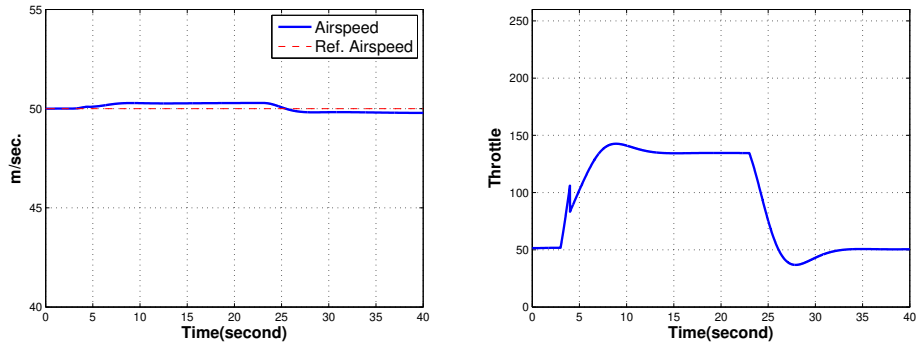


Figure 5.90: Airspeed and throttle responses with reconfiguration.

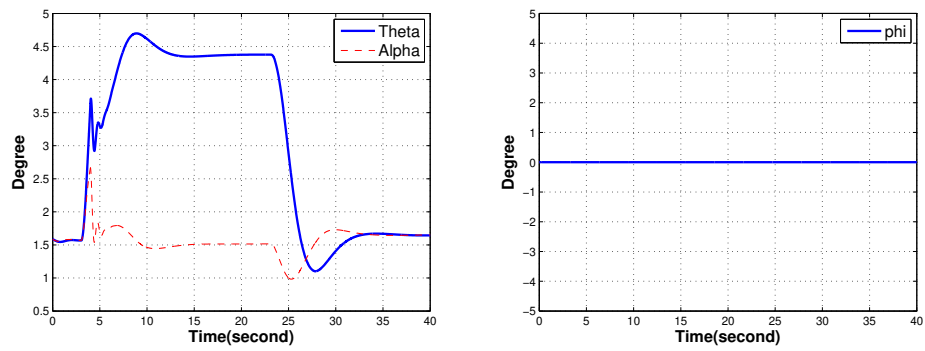


Figure 5.91:  $\theta$ ,  $\alpha$  and  $\phi$  responses with reconfiguration.

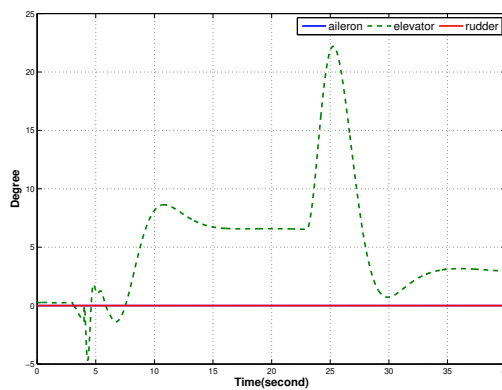


Figure 5.92: Actuator responses with reconfiguration.

### 5.3.3 Rudder Damage

#### 5.3.3.1 The 3rd Level Damage Without Reconfiguration

The 3rd level rudder damage at the 4th second and 40 degree heading change at the 3rd second without reconfiguration:

Without reconfiguration, at the beginning, the UAV can maintain altitude with an  $\alpha$  oscillation, shown in Figure 5.93. Besides, airspeed and throttle oscillate shown in Figure 5.94. However, these oscillations are getting larger and are going to make the UAV unstable. During heading change,  $\psi$  and  $\phi$  oscillate and after heading change is completed,  $\phi$  can not be stabilized shown in Figure 5.95. Rudder and aileron saturate and oscillate shown in Figure 5.96. As a result, without reconfiguration, the incident is going to be LOC-I.

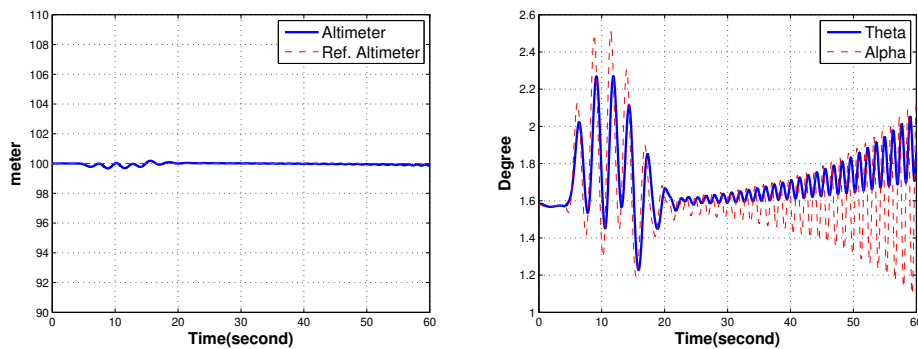


Figure 5.93: Altimeter and  $\theta$ ,  $\alpha$  responses without reconfiguration.

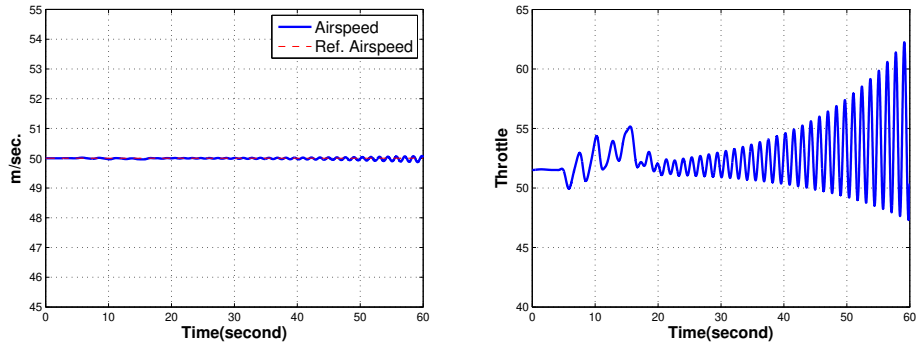


Figure 5.94: Airspeed and throttle responses without reconfiguration.

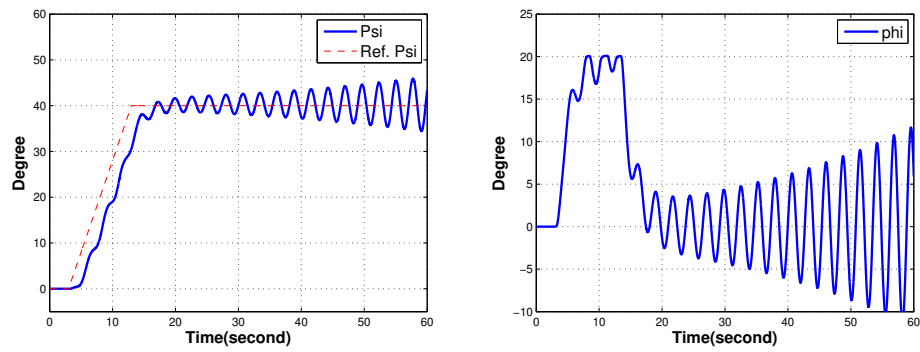


Figure 5.95:  $\psi$  and  $\phi$  responses without reconfiguration.

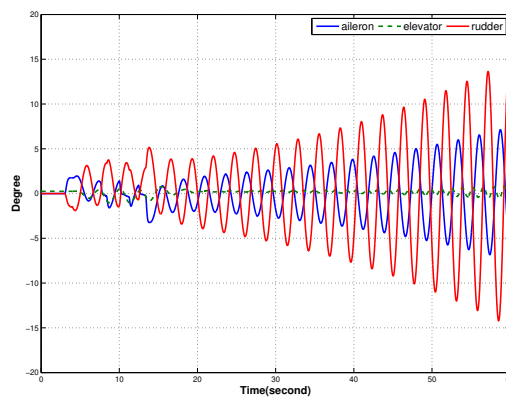


Figure 5.96: Actuator responses without reconfiguration.

### 5.3.3.2 The 3rd Level Damage With Reconfiguration

The 3rd level rudder damage at the 4th second and 40 degree heading change at the 3rd second with reconfiguration: The path for the solution is shown in Table 5.13.

Table 5.13: The solution for rudder damage at the 3rd level.

Problem location	Rudder
Problem	3rd level damage
Which Reconfiguration Mech. Block	1, 5 and 7
What Reconfiguration Degree	1 aileron slower
	0.3 rudder faster

Altitude,  $\theta$ ,  $\alpha$  responses are reliable, shown in Figure 5.97. Besides, airspeed and throttle responses are at desired value, shown in Figure 5.98. By reconfiguration block-5, rudder movement is increased and aileron movement is decreased. By reconfiguration block-1,  $\psi$  limiter slew rate is reconfigured from 4 to 2 and  $\phi$  rate saturation limiter from 20 to 14 degrees, shown in Figure 5.99. Also, this helps to prevent rudder actuator saturation, shown in Figure 5.100, because more deflection is required to minimize  $\beta$  by damaged control rudder surface. If the  $\phi$  and  $\psi$  limiter is not reconfigured, the rudder actuator can saturate. However, with reconfiguration, it is at an approximately 7 degrees deflection, shown in Figure 5.100.

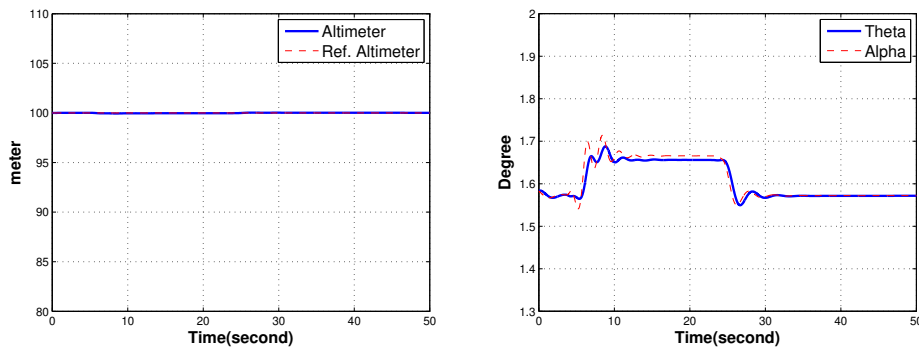


Figure 5.97: Altimeter and  $\theta$ ,  $\alpha$  responses with reconfiguration.

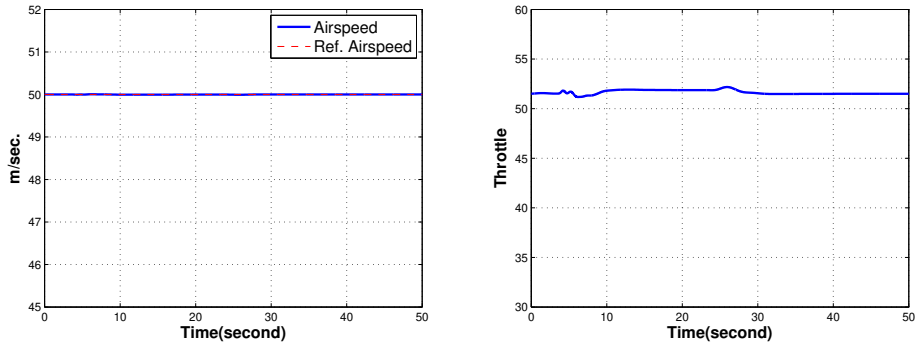


Figure 5.98: Airspeed and throttle responses with reconfiguration.

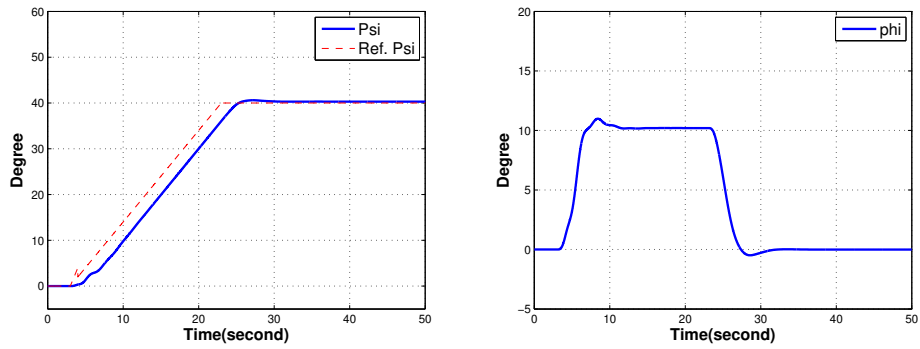


Figure 5.99:  $\psi$  and  $\phi$  responses with reconfiguration.

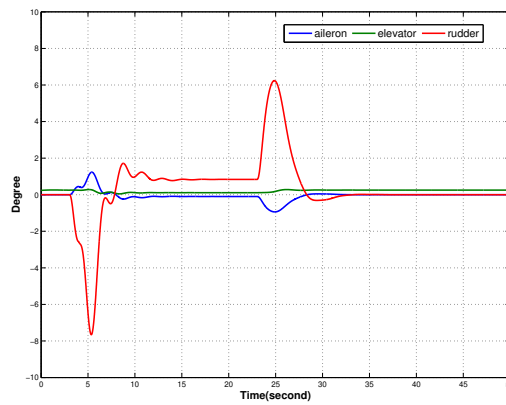


Figure 5.100: Actuator responses with reconfiguration.

### 5.3.3.3 The 4th Level Damage Without Reconfiguration

The 4th level rudder damage at the 4th second and 40 degree heading change at the 3rd second without reconfiguration:

Without reconfiguration, at the beginning, the UAV can maintain altitude with an  $\alpha$  oscillation shown in Figure 5.101. Besides, airspeed and throttle oscillate and sometimes airspeed decreases dangerously low, shown in Figure 5.102. However, these oscillations are getting larger and make the UAV unstable. During heading change,  $\psi$  and  $\phi$  oscillate and  $\phi$  can not be stabilized, shown in Figure 5.103. Rudder and aileron oscillate and saturate, shown in Figure 5.104. It ends with LOC-I.

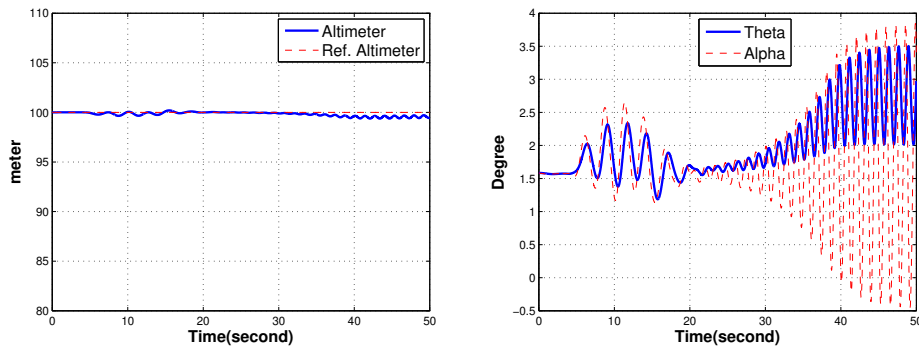


Figure 5.101: Altimeter and  $\theta$ ,  $\alpha$  responses without reconfiguration.

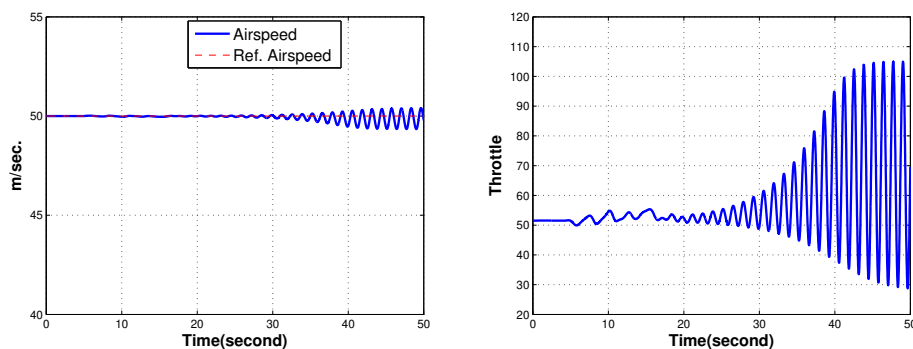


Figure 5.102: Airspeed and throttle responses without reconfiguration.

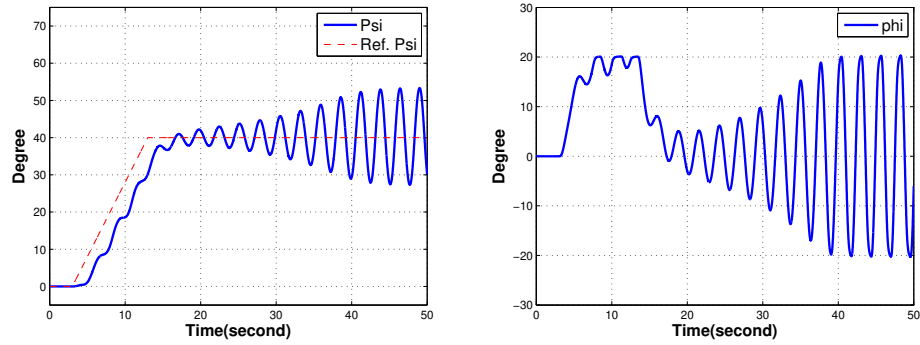


Figure 5.103:  $\psi$  and  $\phi$  responses without reconfiguration.

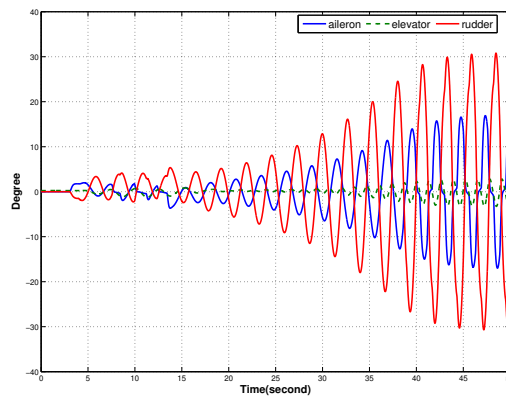


Figure 5.104: Actuator responses without reconfiguration.

### 5.3.3.4 The 4th Level Damage With Reconfiguration

The 4th level rudder damage at the 4th second and 40 degree heading change at the 3rd second with reconfiguration: The path for the solution is shown in Table 5.14.

Table 5.14: The solution for rudder damage at the 4th level.

Problem location	Rudder
Problem	4th level damage
Which Reconfiguration Mech. Block	1, 5 and 7
What Reconfiguration Degree	1 aileron slower
	0.5 rudder faster

Altitude,  $\theta$ ,  $\alpha$  responses are reliable shown in Figure 5.105. Besides, airspeed and throttle responses are at desired values shown in Figure 5.106. By reconfiguration mechanism-5, aileron movement is decreased and rudder movement is increased. By reconfiguration mechanism-1,  $\psi$  rate limiter slew rate is reconfigured from 4 to 2 and  $\phi$  saturation limiter from 20 to 14 degrees, shown in Figure 5.107. Also, this helps to prevent aileron actuator saturation, shown in Figure 5.108 because more deflection is required to reach desired attitude by damaged control surface.

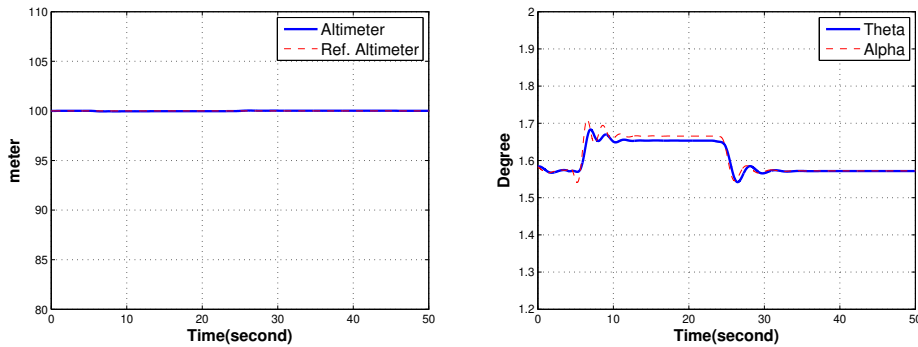


Figure 5.105: Altimeter and  $\theta$ ,  $\alpha$  responses with reconfiguration.

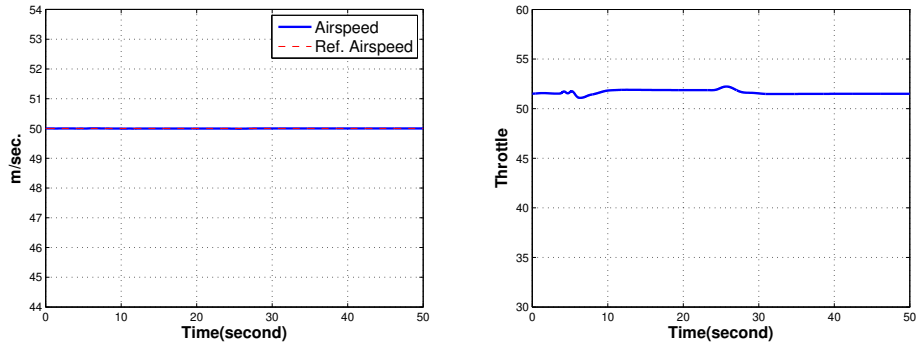


Figure 5.106: Airspeed and throttle responses with reconfiguration.

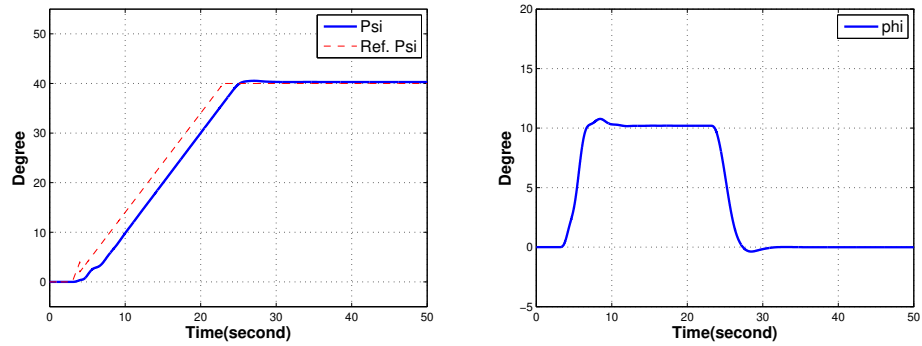


Figure 5.107:  $\psi$  and  $\phi$  responses with reconfiguration.

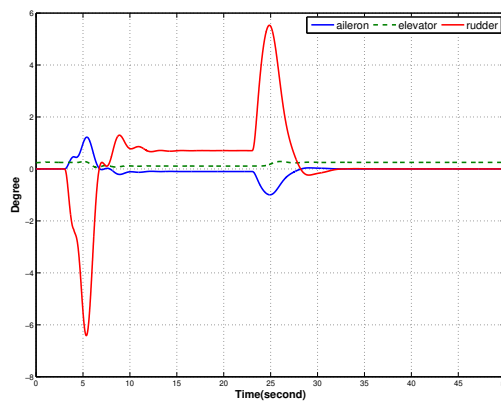


Figure 5.108: Actuator responses with reconfiguration.



## CHAPTER 6

### RESULTS FOR OTHER EMERGENCY SITUATIONS

#### 6.1 Emergency Case-4 Engine Full Shut down :Longitudinal Controller Exchange for Reference Command

##### 6.1.1 Engine Shut down during Level flight

The UAV maintains 100 meters and 50 kt. At the 5th second, engine full shut down failure occurs. After that, reconfiguration mechanism-6 becomes active, depicted in Table 6.1. First, reconfiguration mechanism-6 decreases speed to 35 kt. which is assumed as the best glide speed. Second, when 35 kt. is reached, in reference command, the  $\theta_{ref}$  and  $\delta t$  creator controller-2 becomes active, shown in Figure 4.10.  $\alpha$ ,  $\theta$  and throttle responses are depicted in Figure 6.2. Airspeed, altitude and reference airspeed, altitude responses are depicted in Figure 6.1. Difference between reference airspeed and airspeed is normal because as a safety, approximately 1 kt. is added during reconfiguration. Besides, throttle command  $\delta_t$  is isolated by reconfiguration mechanism-6, due to avoiding undesirable throttle command, shown in Figure 6.2.

Table 6.1: The solution for Engine Full Shut down.

Problem location	Engine
Problem	full shut down
Which Reconfiguration Mech. Block	6
What Reconfiguration Degree	-

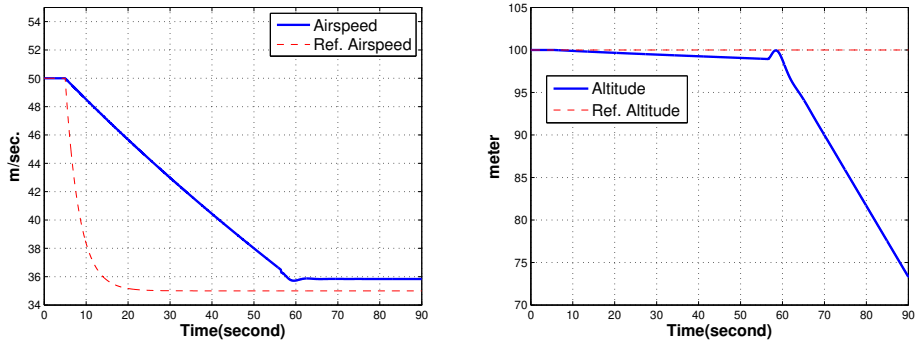


Figure 6.1: Airspeed and altitude responses during level flight for full engine shut down.

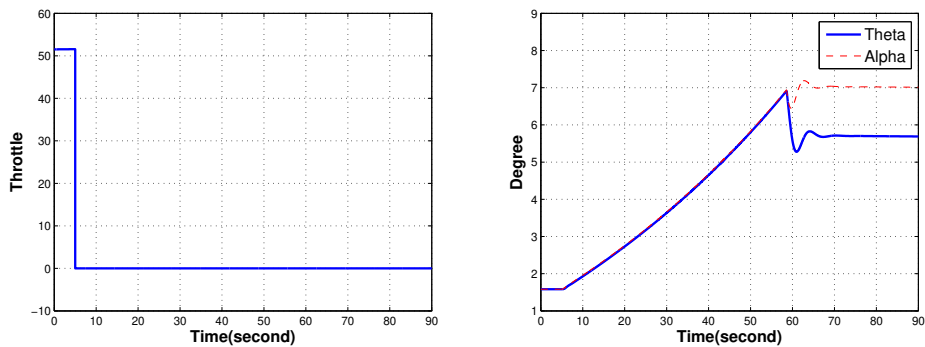


Figure 6.2: Throttle command and  $\alpha$ ,  $\theta$  responses during level flight for full engine shut down.

### 6.1.2 Engine Shut down during Climbing

The UAV starts climbing from 100 meters to 200 meters with the vertical speed at the 3rd second. At the 5th second, engine full shut down failure occurs. After that, reconfiguration mechanism-6 becomes active. The same configuration process for reference command, is depicted respectively in Figure 6.3 and 6.4. One of the difference is when an engine failure occurs at the 5th second, the UAV continues climbing shown in Figure 6.3. It is rational because instead of changing the UAV's attitude, to continue climbing to a higher altitude provides a pilot more time for judgement and

finding the best terrain for emergency landing.

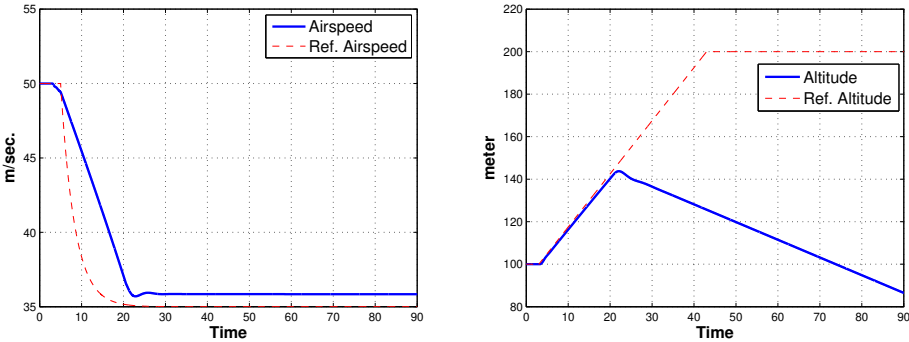


Figure 6.3: Airspeed and altimeter responses during climb for full engine shut down.

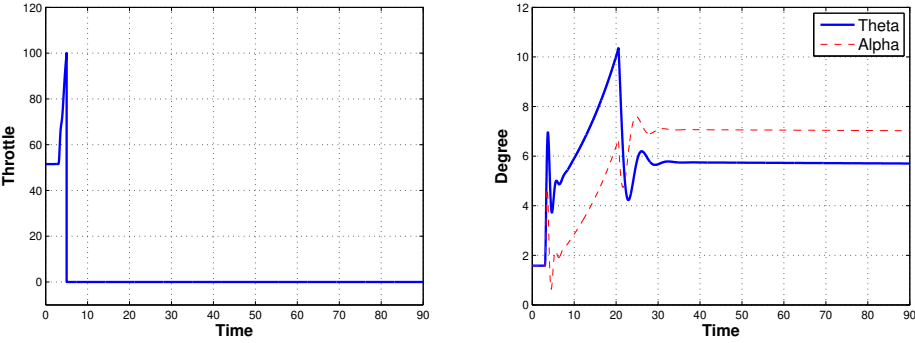


Figure 6.4: Throttle command and  $\alpha$  and  $\theta$  responses during climb for full engine shut down.

### 6.2 Emergency Case-5 Controllability or Observability Problem

Controllability and observability have to be checked online by Simulink Matlab function block in the controller shown in Figure 4.28. As stated in Section 4.3.1, controllability and observability matrices have to be created. However, especially during that process, due to SDC matrices, the system can be uncontrollable or unobservable. Also, in [48], even if eigenvalues of the SDC matrices have negative real parts, global asymptotic stability is not guaranteed for SDRE controllers. In addition, it is also hard to find whether globally asymptotic stable, during or after fault or failure.

Besides, there are several problems with SDRE. As a result, the best way to compensate these problems is to change from the nonlinear controller to the linear controller (LQR/LQT).

### 6.2.1 Controllability fault (1) during climbing about Tracker Controller-2 and without reconfiguration

Controllability Fault is entered to the Tracker controller-2 at the 4th second. Besides, UAV begins climbing from 100 meters to 150 meters. During fault injection, if there is a defect for the  $B(x)$  matrix for the elevator command row, the elevator command cannot be generated. Besides, if there is no changing from SDRE to LQR, the result is nearly a control surface stuck problem. In other words, Regulator controller-2 generates a command but it is useless tracking pilot commands shown in Figure 6.5. Besides, throttle command is normal and so airspeed response, shown in Figure 6.6. Regulator controller-2 generating command means, the UAV wants to return to the equilibrium point again, as depicted for  $\theta$  in Figure 6.5. Actuator and controller responses are respectively depicted in Figure 6.7 and Figure 6.8.

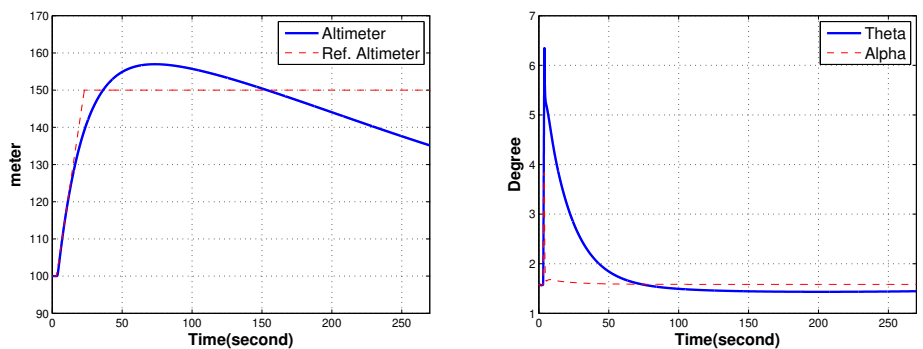


Figure 6.5: Altimeter and  $\theta$ ,  $\alpha$  responses and reconfiguration for algorithm does not occur.

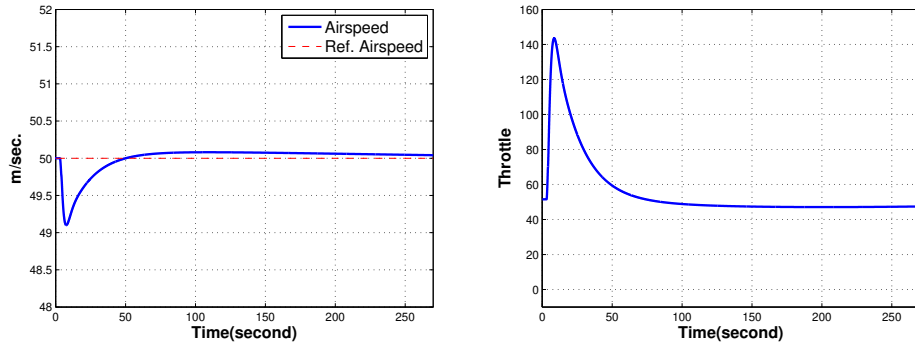


Figure 6.6: Airspeed and throttle responses and reconfiguration for algorithm does not occur.

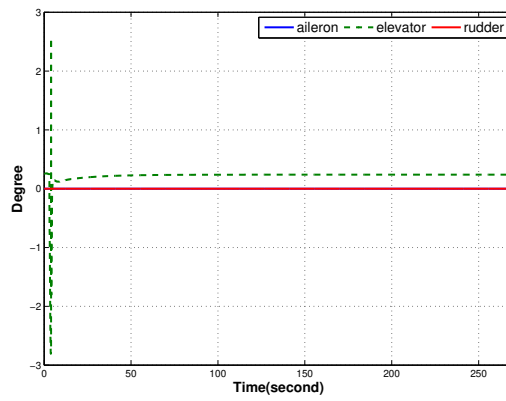


Figure 6.7: Actuator responses and reconfiguration for algorithm does not occur.

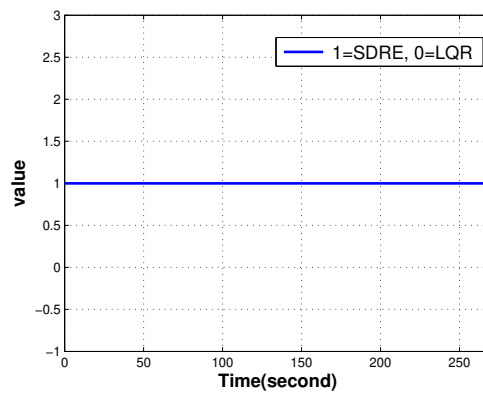


Figure 6.8: The controller algorithm and reconfiguration for algorithm does not occur.

### 6.2.2 Controllability fault (2) during heading change about Tracker Controller-2 and without reconfiguration

Controllability Fault is entered to the Tracker controller-2 at the 4th second. If there is a defect for the  $B(x)$  matrix for aileron and elevator command row, aileron and elevator tracking command cannot be generated. If there is no changing from SDRE to LQR, the result is totally loss of control in air (LOC-I) depicted in Figure 6.9, Figure 6.11 and Figure 6.10, due to mainly rudder oscillation to reach command signal about heading, depicted in Figure 6.12. The controller continues on SDRE controller, depicted in Figure 6.13.

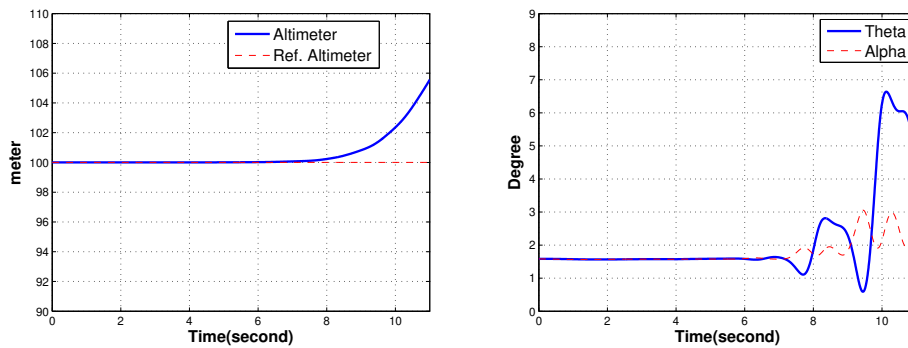


Figure 6.9: Altimeter and  $\theta$ ,  $\alpha$  responses and reconfiguration for algorithm does not occur.

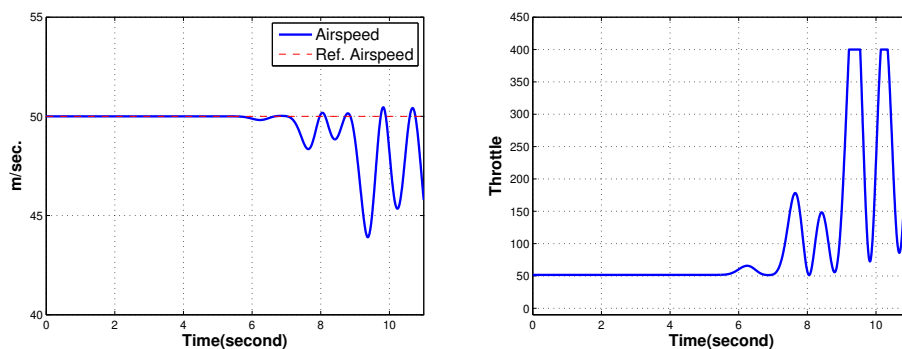


Figure 6.10: Airspeed and throttle responses and reconfiguration for algorithm does not occur.

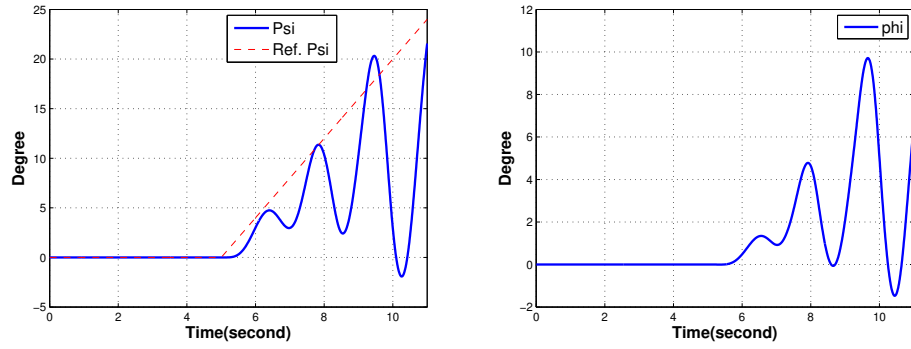


Figure 6.11:  $\psi$  and  $\phi$  responses and reconfiguration for algorithm does not occur.

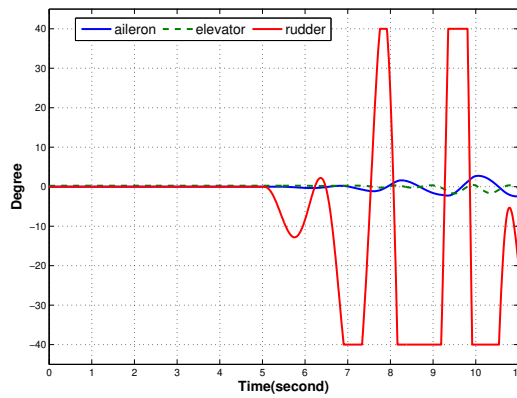


Figure 6.12: Actuator responses and reconfiguration for algorithm does not occur.

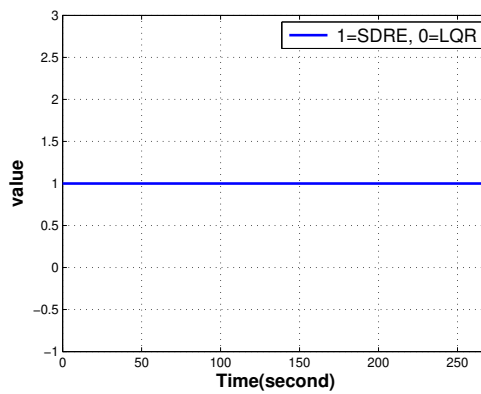


Figure 6.13: The controller algorithm and reconfiguration for algorithm does not occur.

Finally, without changing the controller algorithm from SDRE to LQR, if there is a problem about controllability and observability, the consequence can be fatal due to LOC-I. To achieve safety, which is the crucial criteria in aviation, reconfiguration mechanism changes controller algorithm from SDRE to LQR, wherever the problem occurs. In other words, it is enough to have a problem with any controller (tracker or regulator) for reconfiguration.

### 6.2.3 Controllability fault (1) during climbing about Tracker Controller-2 and with reconfiguration

Controllability Fault is entered to the Tracker controller-2 at the 4th second and the UAV begins climbing from 100 meters to 150 meters. The reconfiguration for the controller occurs at the 4th second, from SDRE to LQR and the solution path is depicted in Table 6.2. The responses are depicted in Figure 6.14 and Figure 6.15. Actuators are working well depicted in Figure 6.16. Finally, reconfiguration occurs at the 4th second shown in Figure 6.17.

Table 6.2: The solution for controllability and observability problem during climbing.

Problem location	The Controller
Problem	uncont. and unobs.
Which Reconfiguration Mech. Block	7
What Reconfiguration Degree	-

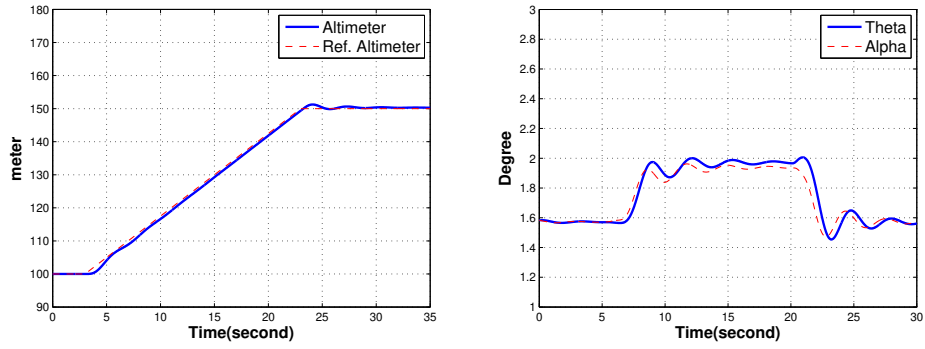


Figure 6.14: Altimeter and  $\theta$ ,  $\alpha$  responses and reconfiguration for algorithm occurs.

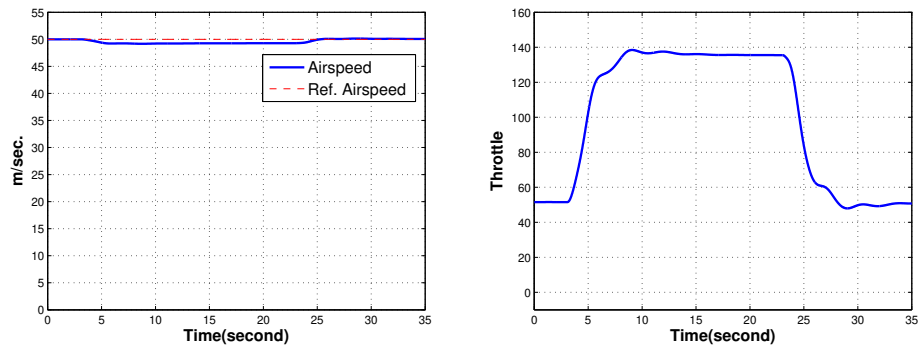


Figure 6.15: Airspeed and throttle responses and reconfiguration for algorithm occurs.

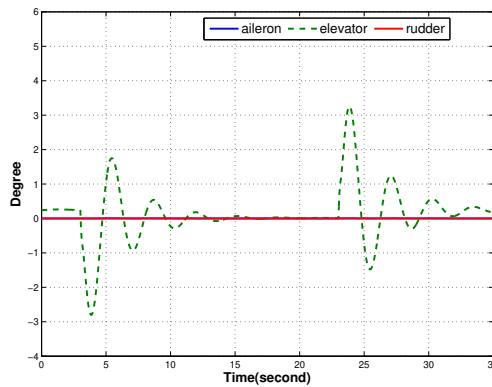


Figure 6.16: Actuator responses and reconfiguration for algorithm occurs.

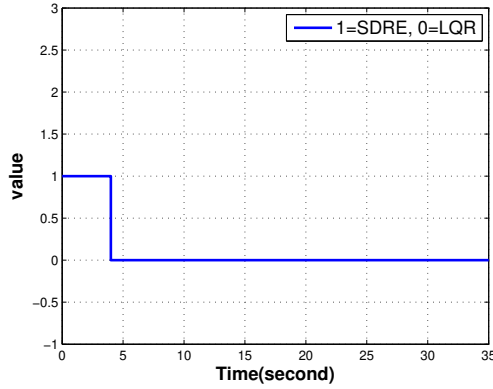


Figure 6.17: Controller algorithm and reconfiguration for algorithm occurs.

#### 6.2.4 Controllability fault (2) during heading change about Tracker Controller-2 and with reconfiguration

Controllability Fault is entered to the Tracker controller-2 at the 4th second and the UAV begins 60 degree heading change. The reconfiguration for controller occurs at the 4th second, from SDRE to LQR and the solution path is depicted in Table 6.2. The responses are depicted in Figure 6.18, Figure 6.19 and Figure 6.20. Actuators are working well, depicted in Figure 6.21. Finally, reconfiguration occurs at the 4th second, shown in Figure 6.22.

Table 6.3: The solution for controllability and observability problem during heading change.

Problem location	The Controller
Problem	uncont. and unobs.
Which Reconfiguration Mech. Block	7
What Reconfiguration Degree	-

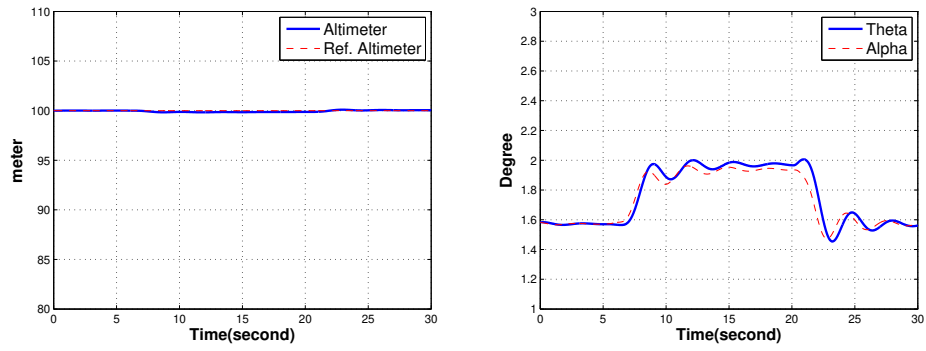


Figure 6.18: Altimeter and  $\theta$ ,  $\alpha$  responses and reconfiguration for algorithm occurs.

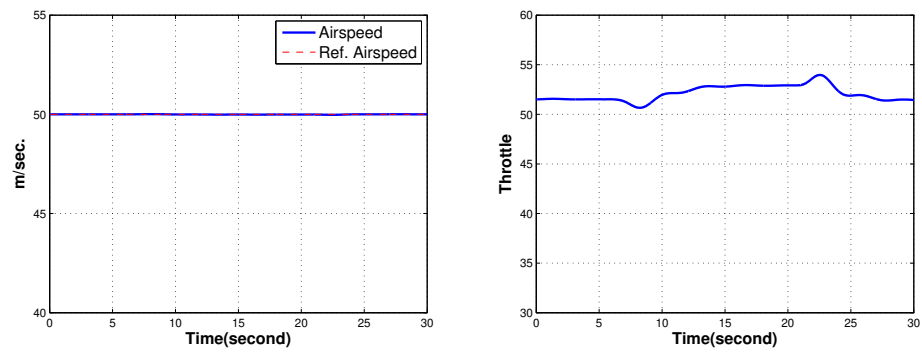


Figure 6.19: Airspeed and throttle responses and reconfiguration for algorithm occurs.

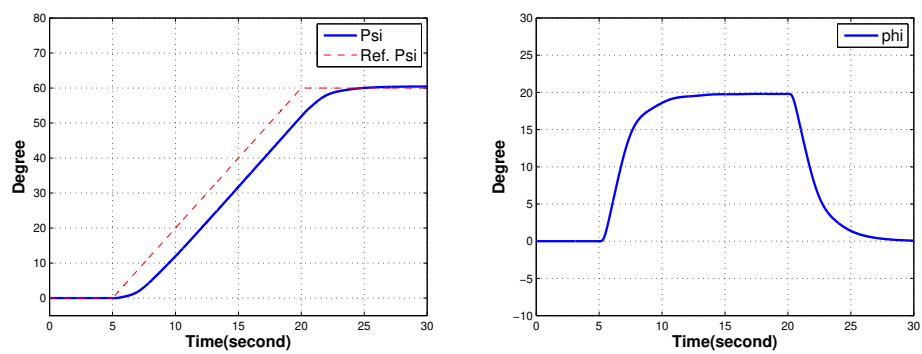


Figure 6.20:  $\psi$  and  $\phi$  responses and reconfiguration for algorithm occurs.

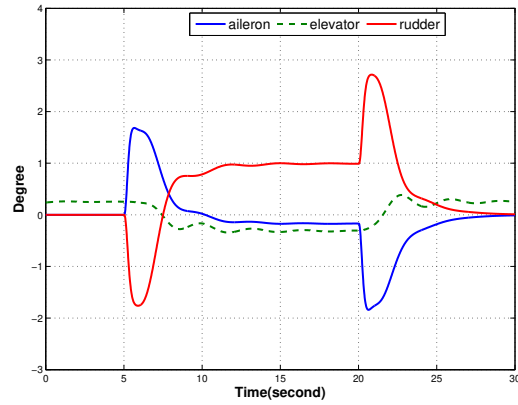


Figure 6.21: Actuator responses and reconfiguration for algorithm occurs.

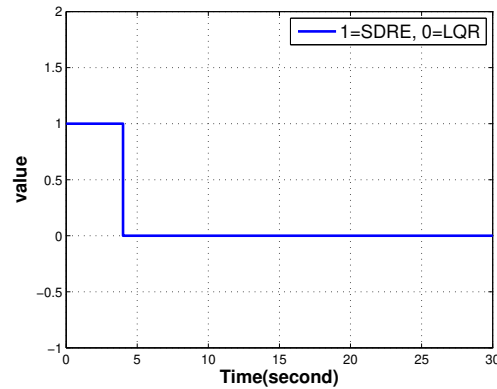


Figure 6.22: Controller algorithm and reconfiguration for algorithm occurs.

### 6.3 Emergency Case-6 Turbulence and Wind gust

#### 6.3.1 Moderate to Severe Turbulence condition and without reconfiguration

Moderate to severe turbulence condition is simulated by the Dryden wind turbulence model in the atmospheric environment model. The controller copes with leveling the UAV, shown in Figure 6.23, Figure 6.24 and Figure 6.25. Without reconfiguration of the controller, control surface movements are too much, shown in Figure 6.26.

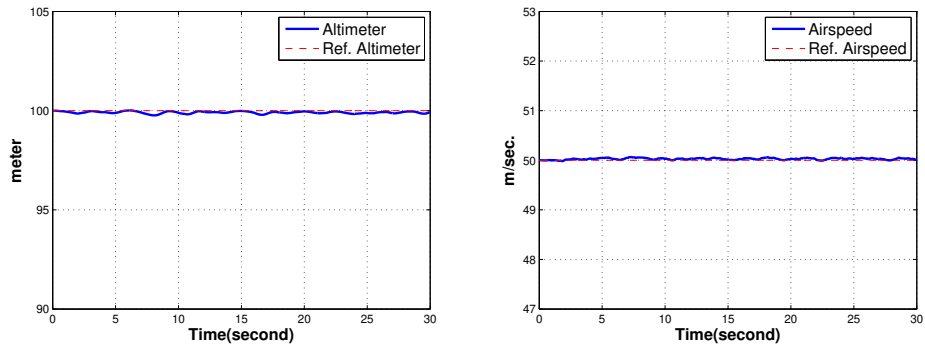


Figure 6.23: Altitude and air speed responses and reconfiguration for algorithm does not occur.

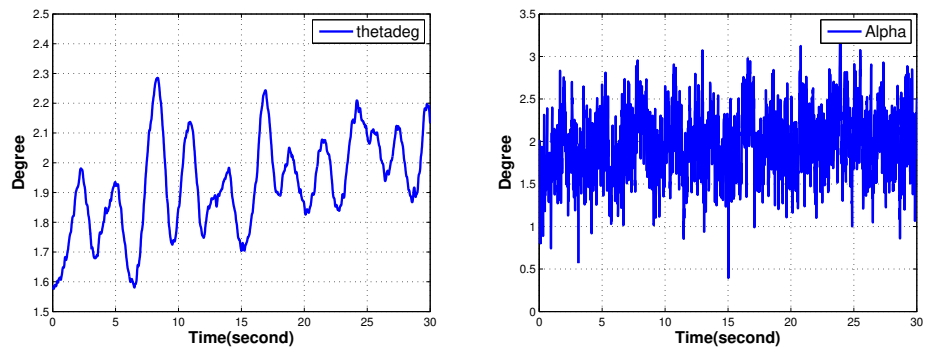


Figure 6.24:  $\theta$  and  $\alpha$  responses and reconfiguration for algorithm does not occur.

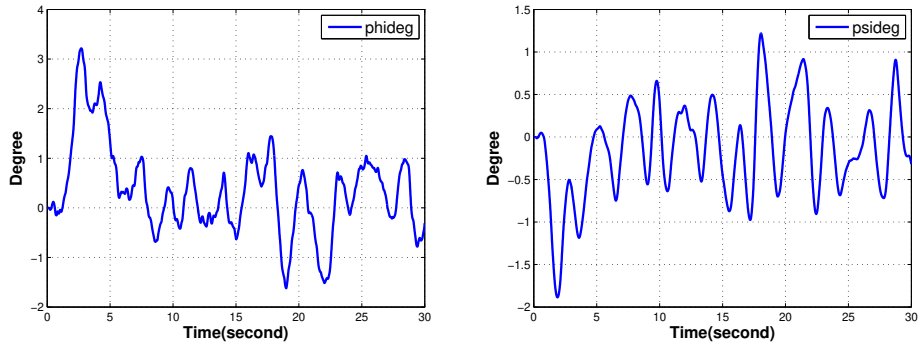


Figure 6.25:  $\phi$  and  $\psi$  responses and reconfiguration for algorithm does not occur.

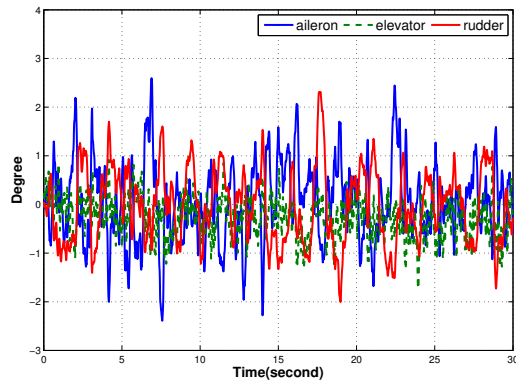


Figure 6.26: Control surface deflection and reconfiguration for algorithm does not occur.

### 6.3.2 Moderate to Severe Turbulence condition and with reconfiguration

The solution path is depicted in Table 6.4. The reconfigured controller copes with leveling the UAV shown in Figure 6.27, Figure 6.28 and Figure 6.29. By reconfiguration mechanism-5, control surfaces movements are made slower, shown in Figure 6.30. Too much G-force is prevented so do structural damage to fuselage, wings, tail. Golden rule can be achieved by this reconfiguration.

Table 6.4: The solution for the turbulence problem.

Problem location	Controller
Problem	turbulence
Which Reconfiguration Mech. Block	5
What Reconfiguration Degree	4 and 0-2000 meters

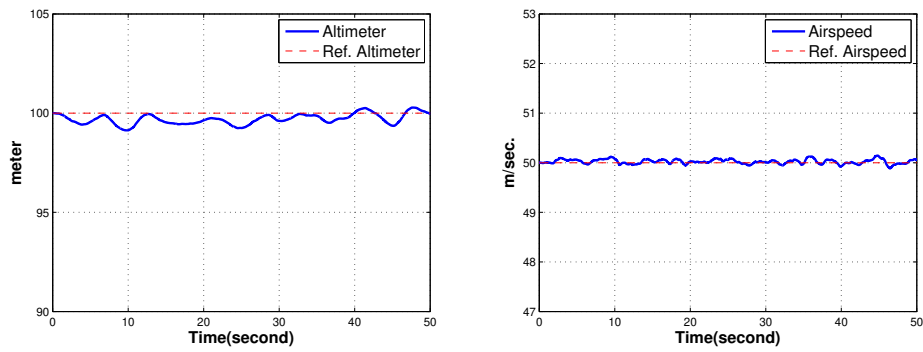


Figure 6.27: Altitude and air speed responses and reconfiguration for algorithm occurs.

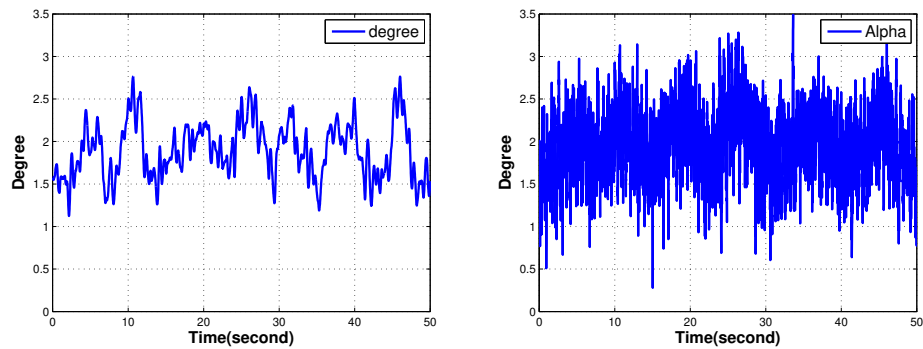


Figure 6.28:  $\theta$  and  $\alpha$  responses and reconfiguration for algorithm occurs.

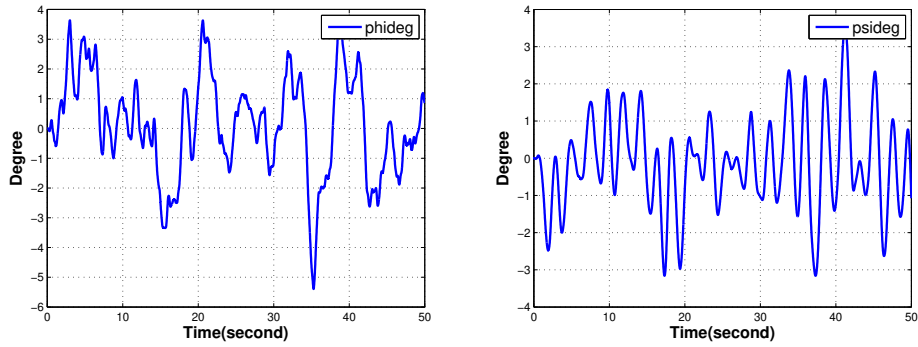


Figure 6.29:  $\phi$  and  $\psi$  responses and reconfiguration for algorithm occurs.

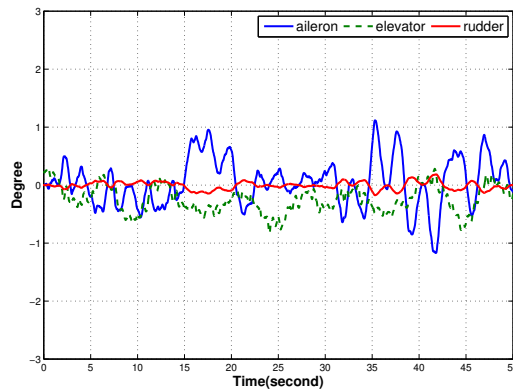


Figure 6.30: Control surface deflection and reconfiguration for algorithm occurs.

The results can be interpreted as: without reconfiguration in Figure 6.26, the movement of control surfaces is changing between maximum -2.5 to 2.5 degrees and there is too much movement. However, with reconfiguration in Figure 6.30, the movement of control surfaces, is changing between maximum -1.1 to 1.2 degree and the movement is in an acceptable level.

## CHAPTER 7

### CONCLUSION

#### 7.1 Conclusion

In this thesis, the 169 kg. UAV is designed in an open source program, XFLR5. The characteristics, aerodynamic derivatives, cg, and cp are taken from this program for simulating in Matlab/Simulink environment. Besides, different faults and failures are injected into the model. Finally, reconfiguration is made in the SDRE algorithm of the FCC.

From simulation results, we arrived at the following conclusions:

- For the autopilot of the UAV, SDRE algorithm is used. Besides, if there is a problem regarding controllability and observability, it will change from SDRE to LQR/LQT algorithm. This feature is very useful for fault-tolerant control. The result shows that the UAV can fly just like nothing happen after reconfiguration.
- There are 7 mechanisms just as a firewall for any emergency in the reconfiguration mechanism. Results show that especially 5th mechanism which is used for reconfiguring of  $Q$  and  $R$  for  $K_{T-2}$  and  $K_{R-2}$ , works well during control surface damage, degradation and stuck. With the help of the different  $Q$  and  $R$  matrices with interpolation tables, the flight control computer (FCC) becomes fault tolerant. Besides, other mechanisms are useful after failure or fault occurs. They work as assistive devices during maneuvers to limit the UAV's autopilot. Results show that support mechanisms are very useful after recovery from emergency situations.
- With the help of the flexible SDRE algorithm design, during different levels

of turbulence, control surface movement can be mitigated. Besides, due to the small size of the UAV's, they can be affected more than airline or transport aircraft. The result shows that the movement of the control surfaces is decreased and it is achieved without chasing airspeed and altitude precisely.

- During full engine shut down, the pilot has to glide with the best glide airspeed and during gliding, maintaining this speed is crucial. The result shows that the autopilot can maintain this airspeed with the airspeed controller which maintains airspeed with the change of  $\theta$  and so does elevator command. This feature is very crucial due to give more time to the pilot or operator for judgement. Besides, reconfiguration mechanism changes controller architecture to this type during full engine shut down.
- Reconfiguration for the aileron is good for recovery and post, but sometimes to some degree, no need to recovery. For level 1 and 2 **damages for the aileron**, reconfiguration is not required. For level 3 damages, reconfiguration is required for the best performance. However, for level 4 damages reconfiguration is mandatory for positive control of the UAV. For level 1 and 2 **degradation for the aileron**, reconfiguration is not required. However, for level 3 and 4 degradation reconfiguration is mandatory for positive control of the UAV. **Stuck for the aileron** is one of the worst cases. To prevent LOC-I, 0.5 degrees stuck is studied and finally, it is said that reconfiguration is mandatory.
- Reconfiguration for the elevator is good for recovery and post, but sometimes to some degree, no need to recovery. For level 1, 2, 3 and 4 **damages for the elevator**, reconfiguration is not essential. However, to prevent actuator saturation, reconfiguration is mandatory. For level 1 and 2 **degradation for the elevator**, reconfiguration is not required. However, for level 3 and 4 degradations, reconfiguration is required for preventing saturation. **Stuck for the elevator** is one of the worst cases. To prevent LOC-I, a new approach has to be used such as Propulsion Controlled Aircraft (PCA).
- Reconfiguration for the rudder is good for recovery and post but sometimes to some degree, no need to recovery. For level 1 and 2 **damages for the rudder**, reconfiguration is not required. However, for level 3 and 4 damages reconfiguration is mandatory for positive control of the UAV. For level 1 and 2 **degradation for the rudder**, reconfiguration is not required. However, for level 3

and 4 degradations, reconfiguration is mandatory for preventing LOC-I. **Stuck for the rudder** is one of the worst cases. To prevent LOC-I, 20 and 40 degrees stuck is studied and finally, it is said that reconfiguration is mandatory.

## 7.2 Future Work

- Fault Detection and Diagnosis (FDD) and Fault Detection and Isolation (FDI) are not modelled for this thesis. However, as future work, they can be modelled with different approaches such as an artificial neural network.
- For the reconfiguration mechanism, especially for  $Q$  and  $R$  matrices, fuzzy logic can be used.
- In the SDRE controller, there is Algebraic Riccati Equation (ARE) solver. This equation is solved by the eigenvalue and eigenvector method. However, Schur decomposition or iterative methods can be used for fast computational time.
- As an emergency case; structural damage, an abrupt center of gravity change can be studied with SDRE algorithm.
- As a meteorological emergency case; wind shear and microburst condition can be studied during approach and landing phase with SDRE algorithm.
- Throttle command can be included in the state space model for SDRE controller. Besides, multi-engine aircraft model can be used to compensate especially yaw moment during aileron or rudder stuck.
- To make control surface movement fast, during evading missile, can be studied with SDRE algorithm.
- In the reconfiguration mechanism; reconfiguration of  $\phi$  and  $\theta$  command filters, reconfiguration of  $Q_1$  and  $R_1$  for  $K_{T-1}$  are developed but it is not used in any emergency case. It can be used for different emergency cases as a backup.
- Rate limiters are used for limiting the first derivative of the signal. As a result, initial conditions are very crucial. During maneuvers, reconfiguration of rate limiters needs further study.
- Detailed actuator model can be constructed.



## REFERENCES

- [1] ICAO, *Loss of Control In-Flight (LOC-I)*. [online] Retrieved from <https://www.icao.int/safety/LOCI/Pages/default.aspx> on May 2018.
- [2] IATA, *Loss of Control In-Flight Accident Analysis Report-2015*. [online] Retrieved from <https://www.iata.org/whatwedo/safety/Documents/LOC-I-1st-Ed-2015.pdf> on May 2018.
- [3] ICAO, *International Civil Aviation Organization Safety Report-2016*. [online] Retrieved from <https://www.icao.int/safety/Documents/Forms/AllItems.aspx> on May 2018.
- [4] D. Briere and P. Traverse, “Airbus a320-a330-a340 electrical flight controls - a family of fault-tolerant systems,” *FTCS-23 The Twenty-Third International Symposium on Fault-Tolerant Computing*, pp. 616–623, 1993.
- [5] C. Edwards, T. Lombaerts, and H. Smaili, *Fault Tolerant Flight Control*. Springer, 2010.
- [6] K. W. Williams, *A Summary of Unmanned Aircraft Accident/Incident Data*. Final Report, FAA, 2004.
- [7] R. Isermann and P. Ballé, “Trends in the application of model-based fault detection and diagnosis of technical processes,” *Control Engineering Practice*, vol. 5, no. 5, pp. 709 – 719, 1997.
- [8] Y. Zhang and J. Jiang, “Bibliographical review on reconfigurable fault-tolerant control systems,” *Annual Reviews in Control*, vol. 32, no. 2, pp. 229 – 252, 2008.
- [9] *The Photos of Airbus A300B4-203(F) flight OO-DLL*. [online] Retrieved from <https://www.jetphotos.com/photo/188116> on May 2018.

- [10] M.Sghairi, A. Bonneval, and Y.Crouzet, "Challenges in building fault-tolerant flight control system for a civil aircraft," *Proceedings of IAENG International Journal of Computer Science*, 35:4, IJCS, 2007.
- [11] C. Edwards, H. Alwi, and C. P. Tan, *Fault Detection and Fault-Tolerant Control Using Sliding Modes*. Springer-Verlag London, 2011.
- [12] *Aircraft Accident Report-USAir Flight 427, Boeing 737-300 , Near Aliquippa, Pennsylvania, September 8, 1994*. NTSB-USA, 1994.
- [13] *Aircraft Accident Report-Netherlands Aviation Safety Board-Netherlands EL AL Flight 1862, Boeing 747-258F 4X-AXG, Bijlmermeer, Amsterdam, october 4, 1992*. Netherlands Aviation Safety Board-Netherlands, 1992.
- [14] E. Sobhani-Tehrani and K. Khorasani, *Fault Diagnosis of Nonlinear Systems Using a Hybrid Approach*. Springer US, 2009.
- [15] K. Valavanis, P. Oh, and L. A. Piegl, *Unmanned Aircraft Systems*. Springer, 2009.
- [16] *Aircraft Accident Report-United Airlines Flight 232, McDonnell Douglas DC-10-10, Gateway Airport, Sioux City, Iowa, July 19,1989*. NTSB-USA, 1989.
- [17] *Aircraft Accident Report-Japan Airlines Co., Ltd., Boeing 747 SR-100, JAA8119 Gunma Prefectura Japan August 12 1985*. Aircraft Accident Investigation Commision Minisrty of Transport-Japan, 1985.
- [18] *Aircraft Accident Report-Final Report On The Accident on 1st June 2009 to the Airbus A330-203 Registered F-GZCP operated by Air France Flight AF 447 Rio de Janeiro - Paris*. BEA-France, 2012.
- [19] J. F.Stewart and T. L.Shuck, *Flight-Testing of The Self-Repairing Flight Control System Using The F-15 Highly Integrated Digital Electronic Control Flight Research Facility*. Springer US, 2009.
- [20] F. W. Burcham, J. J. Burke, T. A. Maine, and C. G. Fullerton, "Development and flight test of an emergency flight control system using only engine thrust on an md-11 transport airplane," 1997.

- [21] J. J. Burken, C. E. Hanso, and J. A. Lee, "Flight test comparison of different adaptive augmentations of fault tolerant control laws for a modified f-15 aircraft," 2009.
- [22] G. J. J. Ducard, *Fault Tolerant Flight Control and Guidance System*. Springer, 2009.
- [23] G. Papageorgiou, K. Glover, G. D'Mello, and Y. Pate, "Taking robust l<sub>p</sub> control into flight on the vaac harrier," *Proceedings of the 39th IEEE Conference on Decision and Control Sydney, Australia December*, pp. 4558–4564, 2000.
- [24] Y. Shtessel, J. Buffington, and S. Banda, "Multiple timescale flightcontrol using reconfigurable sliding modes," *Journal Of Guidance, Control, And Dynamics Vol.22, No.6, November –December*, pp. 873–883, 1999.
- [25] R. A. Hess and S. R. Wells, "Sliding mode control applied to reconfigurable flight control design," *Journal Of Guidance, Control, And Dynamics Vol.26, No.3, May –June*, pp. 452–462, 2003.
- [26] H. Alwi and C. Edwards, "Fault detection and fault tolerant control of a civil aircraft using a sliding mode based scheme," *IEEE Transactions On Control Systems Technology, Vol.1, no.11, April*, pp. 2–12, 2007.
- [27] J. Zhao, B. Jiang, P. Shi, and Z. He, "Fault tolerant control for damaged aircraft based on sliding mode control scheme," *International Journal of Innovative Computing, Information and Control Volume 10, Number 1, February*, pp. 293–302, 2014.
- [28] J. D. Boskovic and R. K. Mehra, "A multiple model-based reconfigurable flight control system design," *Proceedings of the 37th IEEE Conference on Decision Control Tampa, Florida USA December*, pp. 4503–4508, 1998.
- [29] Y. Zhang and J. Jiang, "An interacting multiple-model based fault detection, diagnosis and fault-tolerant control approach," *Proceedings of the 38th Conference on Decision Control Phoenix, Arizona USA December*, pp. 3593–3598, 1999.

- [30] A. B. Milhim, Y. Zhang, and C.-A. Rabbath, "Gain scheduling based pid controller for fault tolerant control of a quad-rotor uav," *AIAA Infotech@Aerospace 2010 20 - 22 April*, pp. 3530–3543, 2010, Atlanta, Georgia.
- [31] J.-Y. Shin, "Gain-scheduled fault tolerance control under false identification," 2005.
- [32] J. Mohammadpour and C. W. Scherer, *Control of Linear Parameter Varying Systems with Applications*. Springer, 2012.
- [33] Z. Liu, C. Yuan, and Y. Zhang, "Adaptive fault-tolerant control of unmanned quadrotor helicopter using linear parameter varying control technique," *International Conference on Unmanned Aircraft Systems (ICUAS) June 7-10*, pp. 980–985, 2016, Arlington, VA US.
- [34] R. Bhattacharya, G. J. Balas, M. A. Kaya, and A. Packard, "Nonlinear receding horizon control of an f-16 aircraft," *Journal Of Guidance, Control, And Dynamics, Vol.25, No.5 ,September –October*, pp. 924–931, 2002.
- [35] J.-F. Magni, S. Bennani, and J. Terlouw, *Robust Flight Control: A Design Challenge*. Springer, 1997.
- [36] Z. Liu, C. Yuan, and Y. Zhang, "Mpc fault-tolerant control case study: Flight 1862," *In:Proceeding of the IFAC Symposium SAFEPROCESS*, pp. 119–124, 2003, WA, USA.
- [37] I. K. Konstantopoulos and P. J. Antsaklis, *Eigenstructure assignment in reconfigurable control systems*. University of Notre Dame, 1996.
- [38] I. D. Landau, R. Lozano, M. M'Saad, and A. Karimi, *Adaptive Control*. Springer, 2011.
- [39] H. M. Nguyen and D. S. Naidu, *Control Systems, Robotics and Automation*. UNESCO EOLSS, 2011.
- [40] M. A. Duarte and K. S. Narendra, "Indirect model reference adaptive control with dynamic adjustment of parameters," *International Journal Of Adaptive Control And Signal Processing, Vol.10,* pp. 603–621, 1996.

- [41] A. Chamseddine, Y. Zhang, C.-A. Rabbath, C. Fulford, and J. Apkarian, "Model reference adaptive fault tolerant control of a quadrotor uav," *Infotech@Aerospace'11*, pp. 1606–1619, 2011, St. Louis, Missouri, USA.
- [42] Y. S. Liu, Q. Li, Z. Ren, and Z. Lv, "A new fault tolerant strategy for commercial aircraft based on adaptive control," *International Conference on Sensing, Diagnostics, Prognostics, and Control*, pp. 377–382, 2017.
- [43] D. Tancredi and Y. G. aand Haiyang Chao, "Fault tolerant formation flight control using different adaptation technique," *International Conference on Unmanned Aircraft Systems (ICUAS)*, pp. 1106–1113, 2013, Grand Hyatt Atlanta, Atlanta, GA.
- [44] A. Fekih and J. B. Hmida, "A self tuning adaptive approach for actuator failure compensation in aircraft systems," *IEEE International Conference on Industrial Technology*, pp. 48–52, 2010.
- [45] D. Naidu, *Optimal Control System*. CRC press, 2003.
- [46] B. D. O. Anderson and J. B. Moore, *Optimal Control System*. Prentice-Hall International, Inc., 1989.
- [47] J. R. Cloutier, "State-dependent riccati equation techniques:an overview," *Proceedings of the American Control Conference Albuquerque, New Mexico June*, pp. 932–936, 1997.
- [48] T. Çimen, "State-dependent riccati equation (sdre) control: A survey," *Proceedings of the 17th World Congress The International Federation of Automatic Control Seoul, Korea, July 6-11*, pp. 3761–3775, 2008.
- [49] H. T. Banks, B. M. Lewis, and H. T. Tranz, "Nonlinear feedback controllers and compensators: A state-dependent riccati equation approach," *Computational Optimization and Applications vol.37*, pp. 177–218, 2007.
- [50] T. Çimen, "Approximate nonlinear optimal sdre tracking control," *IFAC Proceedings, Volume 40, Issue 7*, pp. 147–152, 2007.
- [51] A. Merttopçuoğlu, A. Kahvecioğlu, and T. Çimen, "Sdre control of the control

- actuation system of a guided missile,” *IFAC Proceedings, Volume 40, Issue 7*, pp. 774–779, 2007.
- [52] O. Tekinalp, T. Unlu, and I. Yavrucuk, “Simulation and flight control of a tilt duct uav,” *AIAA Modeling and Simulation Technologies Conference 10-13 August 2009, Chicago, Illinois*, pp. 6138–6153, 2009, Chicago, Illinois.
- [53] A. Bogdanov and E. A. Wan, “State-dependent riccati equation control for small autonomous helicopters,” *Journal of Guidance, Control, and Dynamics* 2007, 30:1, pp. 47–60, 2007.
- [54] K. A. Wise and J. L. Sedwick, “Nonlinear control of agile missiles using state dependent riccati equations,” *Proceedings of the American Control Conference Albuquerque, New Mexico June*, pp. 379–380, 1997.
- [55] R. Guo and J. Chen, “Sdre attitude control with global asymptotic stability for an unmanned helicopter,” *2011 International Conference on Transportation, Mechanical, and Electrical Engineering (TMEE) December 16-18, Changchun, China*, pp. 1044–1049, 2011.
- [56] S. S. Vaddi and P. K. Menon, “Numerical sdre approach for missile integrated guidance - control,” *AIAA Guidance, Navigation and Control Conference and Exhibit, 20 - 23 August*, pp. 6672–6689, 2007, Hilton Head, South Carolina.
- [57] P. K. Menon, T. Lam, L. S. Crawford, and V. H. L. Cheng, “Real-time computational methods for sdre nonlinear control of missiles,” *American Control Conference, 8 - 10 May*, pp. 1–17, 2002, Anchorage, AK.
- [58] H. Voos, “Nonlinear state-dependent riccati equation control of a quadrotor uav,” *Proceedings of the 2006 IEEE International Conference on Control Applications Munich, Germany, October 4-6*, pp. 2547–2552, 2006.
- [59] O. T. Mohammad Mehdi Gomroki, “Relative position control of a two-satellite formation using the sdre control method,” *Advances in the Astronautical Sciences* 152, January, pp. 235–254, 2014.
- [60] D. K. Parrish and D. B. Ridgely, “Attitude control of a satellite using the sdre method,” *Proceedings of the American Control Conference Albuquerque, New Mexico June*, pp. 943–946, 1997.

- [61] F. Liccardo, S. Strano, and M. Terzo, "Optimal control using state-dependent riccati equation (sdre) for a hydraulic actuator," *Proceedings of the World Congress on Engineering 2013 Vol III, WCE 2013, July 3 - 5*, pp. 1–4, 2013, London, U.K.
- [62] G. X. Xu, "Nonlinear fault-tolerant guidance and control for damaged aircraft," Master's thesis, University of Toronto, 2011.
- [63] W. Durham, K. A. Bordignon, and R. Beck, *Aircraft Control Allocation*. Wiley, 2017.
- [64] M. Bodson, "Evaluation of optimization methods for control allocation," *Journal Of Guidance, Control, And Dynamics*, Vol.25, No.4, July –August, pp. 48–52, 2002.
- [65] Y. Zhang, V. S. Suresh, B. Jiang, and D. Theilliol, "Reconfigurable control allocation against aircraft control effector failures," *16th IEEE International Conference on Control Applications Part of IEEE Multi-conference on Systems and Control Singapore, 1-3 October*, pp. 1197–1202, 2007.
- [66] P. Lu, E.-J. van Kampen, C. de Visser, and Q. Chu, "Aircraft fault-tolerant trajectory control using incremental nonlinear dynamic inversion," *Control Engineering Practice, Volume 57, December*, pp. 126–141, 2016.
- [67] L. G. Sun, C. C. de Visser, Q. P. Chu, and W. Falkena, "A hybrid sensor based backstepping control approach with its application to fault-tolerant flight control," *Journal Of Guidance, Control and Dynamics Vol. 37, No. 1, January–February*, pp. 59–71, 2014.
- [68] A. B. Kisabo, F. A. Agboola, C. A. Osheku, M. A. L. Adetoro, and A. A. Funmilayo, "Pitch control of an aircraft using artificial intelligence," *Journal of Scientific Research Reports*, pp. 1–16, 2012.
- [69] K. Krishnakumar and K. Gundy-burlet, "Intelligent control approaches for aircraft applications," tech. rep., National Aeronautics and Space Administration, Ames Research Center, 2001.
- [70] N. Siddique, *Intelligent Control*. Springer, 2014.

- [71] S. H. Almutairi and N. Aouf, "Reconfigurable dynamic control allocation for aircraft with actuator failures," *Royal Aeronautical Society, The Aeronautical Journal, Volume 121, No 1237, March*, p. 341–371, 2017.
- [72] U. Halici, "Artificial neural networks lecture notes," *Middle East Technical University-Electrical and Alectronics Engineering*, 2004.
- [73] A. Paice, "Nonlinear systems and control lecture notes," (*ETH Zurich*) *Swiss Federal Institute of Technology Zurich Automatic Control Laboratory*, 2009.
- [74] S. Haykin, *Neural Network*. Pearson Education, 1999.
- [75] G. C. Mario G. Perhinschi, John Burken, "Comparison of different neural augmentations for the fault tolerant control laws of the wvu yf-22 model aircraft," *Control and Automation, 2006. MED 2006. 14th Mediterranean Conference on 28-30 June*, 2006.
- [76] X. Liu, Y. Wu, and J. Shi, "Adaptive fault-tolerant flight control system design using neural networks," *Industrial Technology, ICIT 2008. IEEE International Conference on 21-24 April*, 2008.
- [77] *XFLR5 Manuel (2013)*. [online] <http://www.xflr5.com/xflr5.htm> on Jan 2018.
- [78] *The USAF Stability and Control DATCOM*. AFFDL-TR-79-3032, US Airforce, 1999.
- [79] A. Turevskiy, S. Gage, and C. Buhr, "Model-based design of a new light-weight aircraft," *AIAA Modeling and Simulation Technologies Conference and Exhibit, 20-23 August*, p. 1–15, 2007.
- [80] A. Murch, "A flight control system architecture for the nasa airstar flight test infrastructure," *AIAA Guidance, Navigation and Control Conference and Exhibit Honolulu, Hawaii, 18-21 August*, p. 1–8, 2008.
- [81] B. Etkin, *Dynamics of Flight*. John Wiley Sons, Inc., 1976.
- [82] J. Roskam, *Airplane Flight Dynamics and Automatic Flight Controls*. DARcorporation, 2001.

- [83] J. R. Raol and J. Singh, *Flight Mechanics Modeling and Analysis*. CRC Press, 2009.
- [84] B. L. Stevens and F. L. Lewis, *Aircraft Control and Simulation*. John Wiley Sons, Inc., 1992.
- [85] A. Kotikalpudi, B. Taylor, C. Moreno, H. Pfer, , and G. J. Balas, “Aerodynamic analysis using xflr-5,” p. 1–12.
- [86] R. M. Bray, “A wind tunnel study of the pioneer remotely piloted vehicle,” Master’s thesis, Naval Postgraduate School, 1991.
- [87] B. Bacon and I. Gregory, “General equations of motion for a damaged asymmetric aircraft,” *AIAA Atmospheric Flight Mechanics Conference and Exhibit, Hilton Head, South Carolina, 20-23 August*, p. 1–13, 2007.
- [88] X. Li and H. H. Liu, “A passive fault tolerant flight control for maximum allowable vertical tail damaged aircraft,” *Journal of Dynamic Systems Measurement and Control* 134, May, 2012.
- [89] G. H. Shah, “Aerodynamic effects and modeling of damage to transport aircraft,” *AIAA Guidance, Navigation and Control Conference and Exhibit Honolulu, Hawaii, 18-21 August*, p. 1–13, 2008.
- [90] A. Marco, E. Duke, and J. Berndt, “A general solution to the aircraft trim problem,” *AIAA Modeling and Simulation Technologies Conference and Exhibit 20 - 23 August*, p. 1–40, 2007.
- [91] R. C. Nelson, *Flight Stability and Automatic Control*. McGrawHill, 1997.
- [92] D. Mclean, *Automatic Flight Control Systems*. Prentice Hall, Inc., 1990.
- [93] A. S. Onen, “Modeling and controller design of a vtol air vehicle,” Master’s thesis, METU, 2015.
- [94] S. Katsev, “Streamlining of the sdre controller algorithm for an embedded implementation,” Master’s thesis, Rochester Institute of Technology, 2006.
- [95] *King Air 350/350C Proline 21 Pilot Training Manuel*. Flight Safety International Inc., 2008.

- [96] AIRBUS, 2018. A318-A319-A320-A321 Flight Crew Operating Manuel-System Description 1.
- [97] *Airframes and Systems*. JEPPESEN, 2015.
- [98] *Pilots Handbook of Aeronautical knowledge*. FAA, 2016.
- [99] K. J. Szalai, C. R. Jarvis, G. E. Krier, V. A. Megna, L. D. Brock, and R. N. O’Donnel, *NASA Fly-by-wire Flight Control Validation Experience*. NASA, 1978.
- [100] *Aircraft Actuation System*, 2014 (last released 2014). <http://cisb.org.br/wiefp2014/presentations/Session>
- [101] *NASA Armstrong Fact Sheet: F-8 Digital Fly-By-Wire Aircraft*, 2014 (last released 2014). <https://www.nasa.gov/centers/armstrong/news/FactSheets/FS-024-DFRC.html>.
- [102] T. Samad and A. Annaswamy, *The Impact of Control Technology*. IEEE Control System Society, 2014.
- [103] *Northrop Grumman RQ-4 Global Hawk Block 40*, 2017 (last released 2014). <https://www.flightglobalimages.com/northrop-grumman-rq-4-global-hawk-block-40/print/3783327.html>.
- [104] Y. Yeh, “Triple-triple redundant 777 primary flight computers,” *Proceedings of IEEE Aerospace Applications Conference, Aspen, CO, USA*, pp. 6293–307, 1996.
- [105] *Statistical Summary of Commercial Jet Airplane Accidents Worldwide Operations 1959 – 2017s*. Aviation Safety Boeing Commercial Airplanes, 2017.
- [106] S. Jacobson, “Aircraft loss of control causal factors and mitigation challenges,” *AIAA Guidance, Navigation, and Control Conference, Guidance, Navigation, and Control and Co-located Conferences*, 2007.
- [107] *Aircraft Accident Report-Final Report On The Accident on 1st June 2009 to the Airbus A330-203 Registered F-GZCP operated by Air France Flight AF 447 Rio de Janeiro - Paris*. BEA-France, 2012.

- [108] B.Kinzig, MacAulay-Brown, and Inc., *Global Hawk Systems Engineering Case Study*. Air Force Institute of Technology, Air Force Center for Systems Engineering, 2010.
- [109] M. Lyu, *Software Fault Tolerant*. John Wiley and Sons Ltd., 1995.



## APPENDIX A

### INTRODUCTION TO FLIGHT CONTROLS

#### A.1 Flight Controls

Flight Control Systems are crucial for controlling the aircraft safely. Aircraft can be controlled with respect to its three axes which are longitudinal, lateral and directional, by flight controls. There are mainly two types of flight controls for aircraft. These are primary and secondary flight controls depicted in Figure A.1.

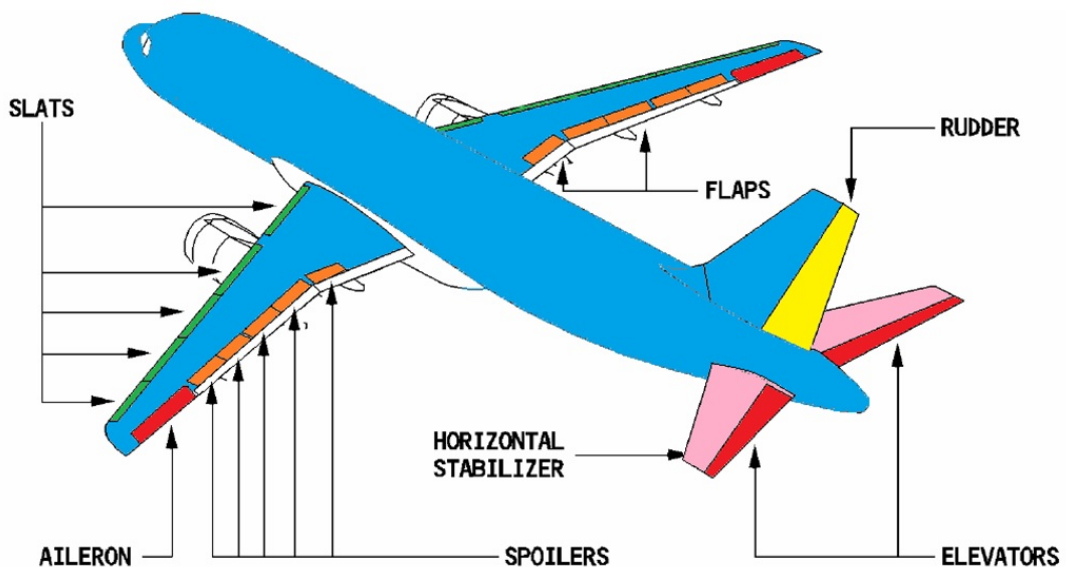


Figure A.1: Aircraft flight controls [96].

Elevators, ailerons and rudders are **primary flight controls**. However, sometimes depending on the aircraft type, elevons (elevator+aileron) which are used for Northrop Grumman B-2 Spirit flight control surfaces, canards, flaperons (flap+aileron), rudder-vator (rudder+elevator) shown in Figure A.2 can be used. On the other hand, flight

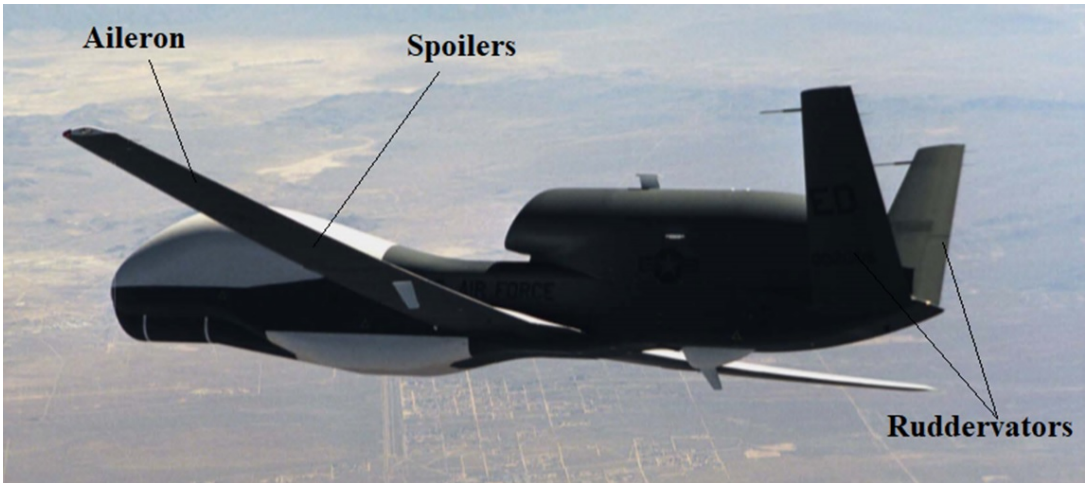


Figure A.2: Global Hawk UAV Flight Controls [15].

and ground spoilers, leading edge high lift devices such as slats and trailing edge high lift devices such as flaps, trim tabs (for example Trimmable Horizontal Stabilizer) are **secondary flight controls** [97]. In the cockpit, these flight controls are controlled by **side stick** used in Airbus aircraft and some of the business jets, **control columns** used in Boeing aircraft and the last **push pull type yoke** is used in small general aviation aircraft. Besides, there are systems between control surfaces and controls. These control surfaces are manipulated by three types of systems. These systems are:

1. Mechanical systems
2. Hydro mechanical systems
3. Fly-by-wire systems(FBW) [98]

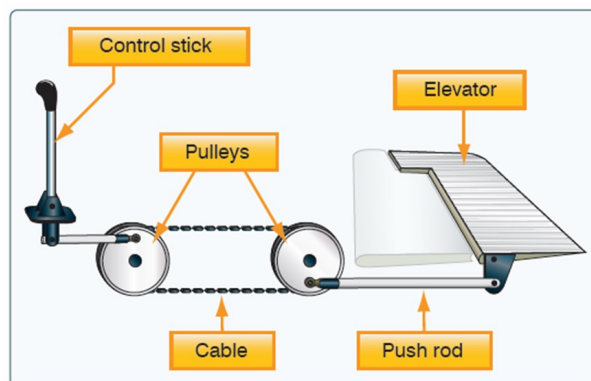


Figure A.3: Mechanical systems [98].

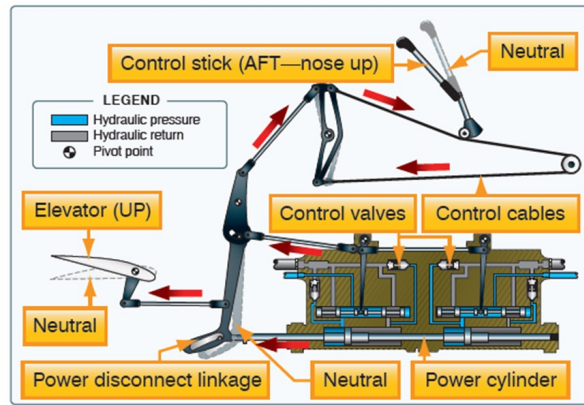


Figure A.4: Hydromechanical systems [98].

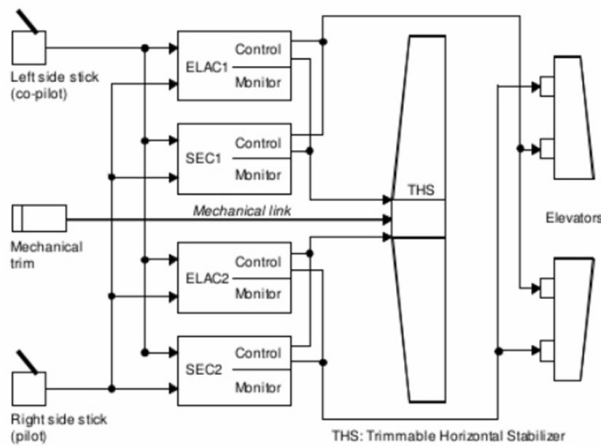


Figure A.5: Fly-by-wire systems (FBW)

First, mechanical systems, depicted in Figure A.3, are used in the early aircraft. Also, they are still used in the light category aircraft such as Cessna 182 Skyhawk, Beechcraft B-200 King Air, which do not need large forces and moments to move control surfaces. Second, due to the increase in size and complexity of the flight controls, hydromechanical systems depicted in Figure A.4, are used. Finally, with the help of electric or mechanical actuators, digital computers, and fiber optic cables, the new type of control connection, Fly-by-wire extensively becomes popular. The physical connection between pilot and control surfaces becomes electrically connected. Between pilot and control surfaces, there are different types of flight control computers which are shown in Figure A.5 [98].

Fly-by-wire (FBW) systems are getting more popular recently because of the reduc-

tion of weight, and other safety reasons. Regarding safety, it has stringent requirements like the critical failure must be less than  $10^{-9}$  per flight hour [99]. Regarding the working principle, first pilot input converted to the electrical signal, after that this signal is transmitted to the flight control computer (FCC). It calculates the required control surface deflection more effective than the human pilot and then transmits it to the actuators. Finally, actuators manipulate control surfaces. These type of actuators are Hydraulic Actuators (HA), Electric Actuators With Hydrostatic Transmission (EHA) and Electric Actuators With Mechanical Transmission (EMA) [100]. For example, Airbus A320/330/340 flight control surfaces electrically controlled and hydraulically moved. Besides, trimmable horizontal stabilizer and rudder can be mechanically moved.

Fly-by-wire maintains stability, in the meantime increases maneuverability and safety. The advantage of the Fly-by-wire (FBW) is considerably greater. It is safer due to redundancies because if there is a failure on the actuator, another actuator can easily continue to operate. Besides, aircraft having full fly-by-wire don't suffer from the hydraulic leak which precludes aircraft control. Aircraft can be flown in the flight envelope with the help of the fly-by-wire. For example, the pilot can't decrease the aircraft speed below the stall speed. As a result, fly-by-wire increases maneuverability and safety due to the effective calculation of the aircraft control surface deflection. It is more efficient because of weight reduction of the hydraulic lines and pumps. Finally, maintenance costs are decreased [101].

Historically, the Canadian Avro CF-105 Arrow interceptor was the first aircraft which has an analog flight control computer. Also, Lockheed Martin F-16 has an analog flight control computer which entered the service in the late 1970s. Now, F-16 has a Digital Fly-By-Wire (DFBW). After that, in 1972, the first Digital Fly-By-Wire (DFBW) aircraft with no mechanical backup whose model name was F-8 Crusader, was tested in Flight Research Center, Edwards, CA (now Armstrong Flight Research Center). In 1982, A310, A300-600; in 1987, A320 are the first commercial using the Digital Fly-By-Wire (DFBW) for flight control computer. Nowadays, It has been used in different types of spacecraft, space launch vehicles such as, Boeing Inertial Upper Stage (IUS) which used to launch Ulysses, Galileo and Magellan, different types of aircraft such as Airbus A320, B-2 Stealth Bomber, Boeing 777, Boeing 787,

Dassault Falcon 7X, Joint Strike Fighter X35, V-22 Osprey, AH-64 Apache, NH-90, Sikorsky S-92, and several unmanned aerial vehicles (UAVs) [101, 102, 5]. One of the examples for civil UAV, the Volcan UAV uses stability augmented Fly-by-wire [15]. Moreover, for Global Hawk UAV, ruddervators are controlled by electrically [103]. Besides, there is a disadvantage of the fly-by-wire (FBW) systems. Due to electromagnetic interference, cables have to be shielded heavily. Also, the pilot can't feel the controls directly, so artificial feel feedback systems are designed. Because of electrical system failures or sensor failures, fly-by-wire (FBW) systems are directly affected [97].

As a result, the challenging part for controlling aircraft is Flight Control Computers (FCC). These computers are important for flight safety. For example, in the Airbus A330, there are five flight computers. This aircraft has three flight control primary computers and two flight control secondary computers. Each flight computer interacts together. Also, each flight computer has two independent units which control each other. Besides, these computers are different from each other, because different manufacturers, software, computer languages, teams are used. For this reason, if there is an error in one of the computer, another does not suffer from this error due to diversity [5]. As regards designing flight control computer, there is a different philosophy between Airbus and Boeing companies. It can be extremely useful philosophies for unmanned aerial vehicle flight control computers.

## **A.2 Airbus versus Boeing Philosophies about Flight Control Computer**

Airbus A320 has seven flight control computers. Each of them has two different and independent computers which are called channel. These channels are monitoring and control shown in Figure A.6. The task of the monitoring channel is checking the control channel and ensuring it to work properly. If there is a difference between these channels in one of the computer, it separates itself from the line. Different from the Airbus A340, Airbus A320 has two Elevator and Aileron Computers (ELAC), three Spoiler and Elevator Computers (SEC) and two Rudder Control Computers (FAC). Each of these computers is made by different manufacturers to make it fault tolerant. Besides, each channel for computers and each type of computers have different soft-

ware. Dissimilarity can be achieved in this way. For example, Spoiler and Elevator Computers (SEC) and Elevator and Aileron Computers (ELAC) are different in terms of software [4]. In Airbus A320, ELAC's, SEC's and FAC's are manipulated for roll, pitch and yaw control, shown in respectively in Figure A.7, in Figure A.8 and in Figure A.9. Besides, there are two actuators for each aileron, two for each elevator, two for trimmable horizontal stabilizer and three for the rudder.

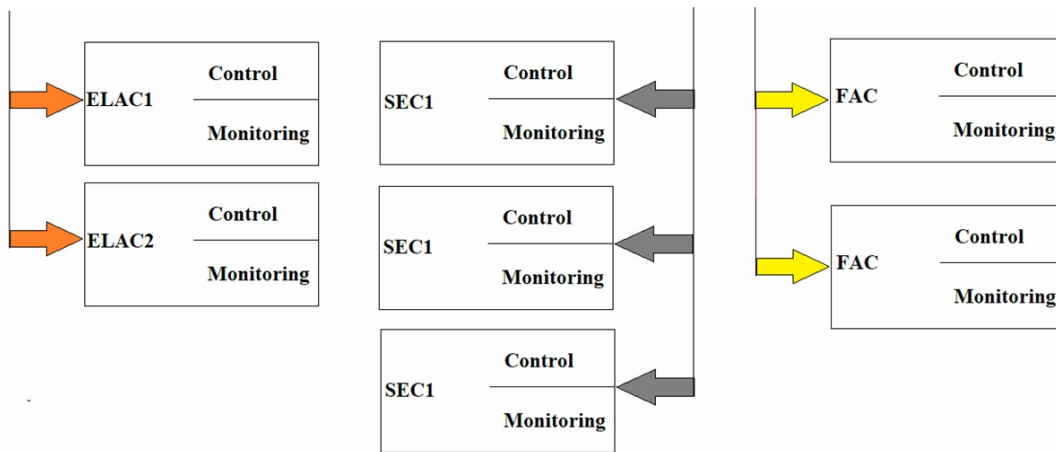


Figure A.6: Flight Control Computers for A320

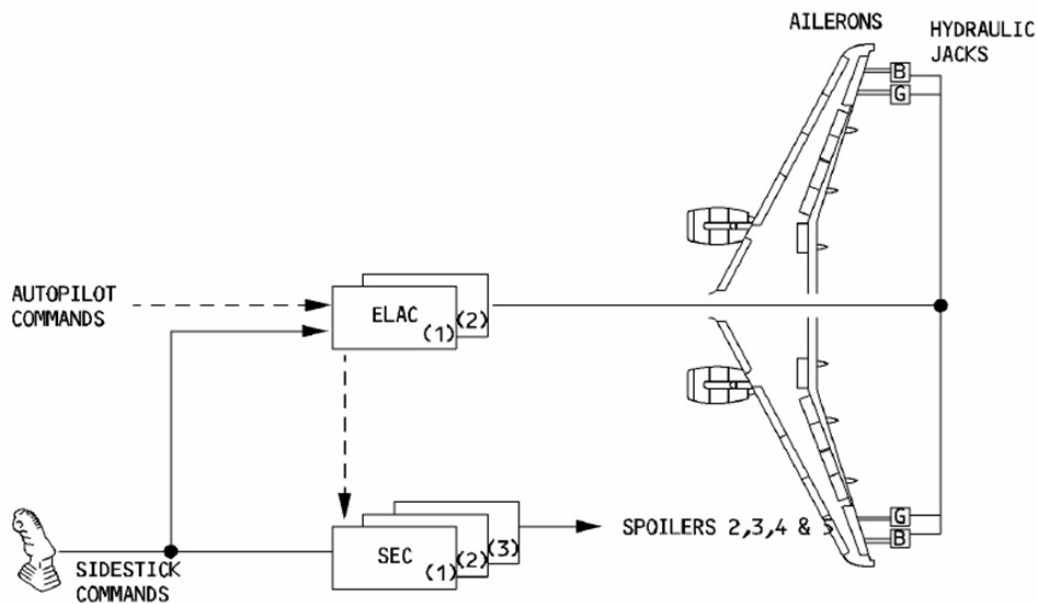


Figure A.7: Roll Control for Airbus A320 [96].

In Boeing 777, there is a triple-triple redundancy for primary flight control. There

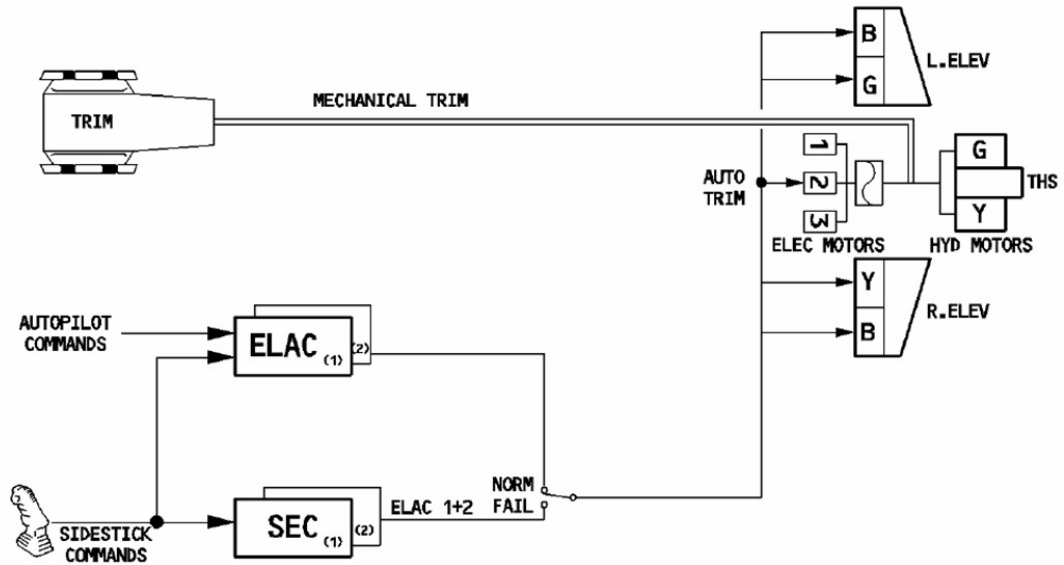


Figure A.8: Pitch Control for Airbus A320 [96].

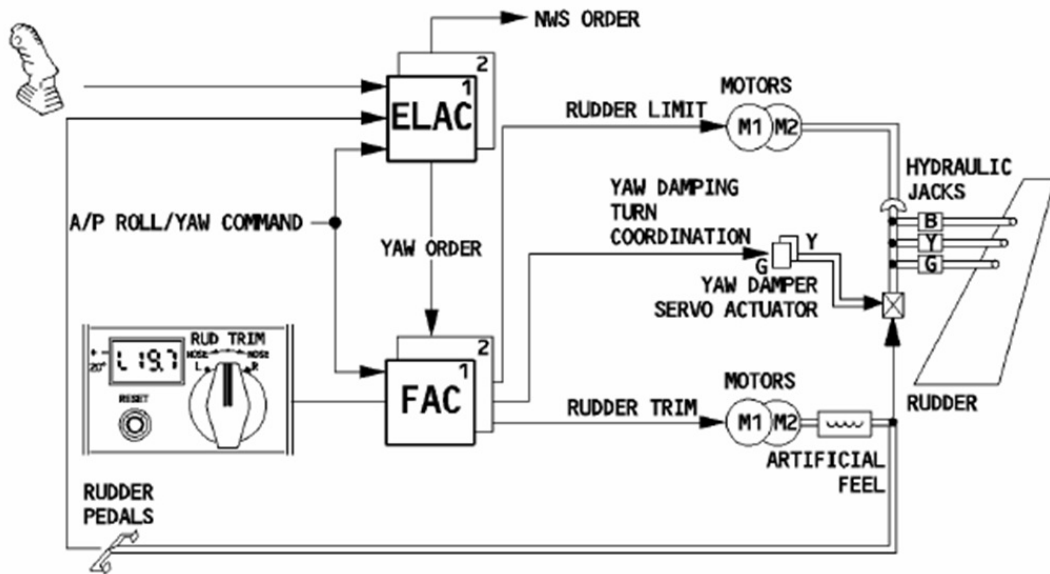


Figure A.9: Yaw Control for Airbus A320 [96].

are three similar Primary Flight Computer (PFC). Regarding PFC, there are three similar channels. Besides, other than channels, there are three dissimilar computation lanes in PFC which take all three different flight control signals. Each lane has a different microprocessor. Their names are AMD 29050, Motorola 68040 and Intel 80486 which have different compilers and hardware, shown in FigureA.10. Their

outputs are connected to a voter. A voter selects the correct signal by majority voting [104].

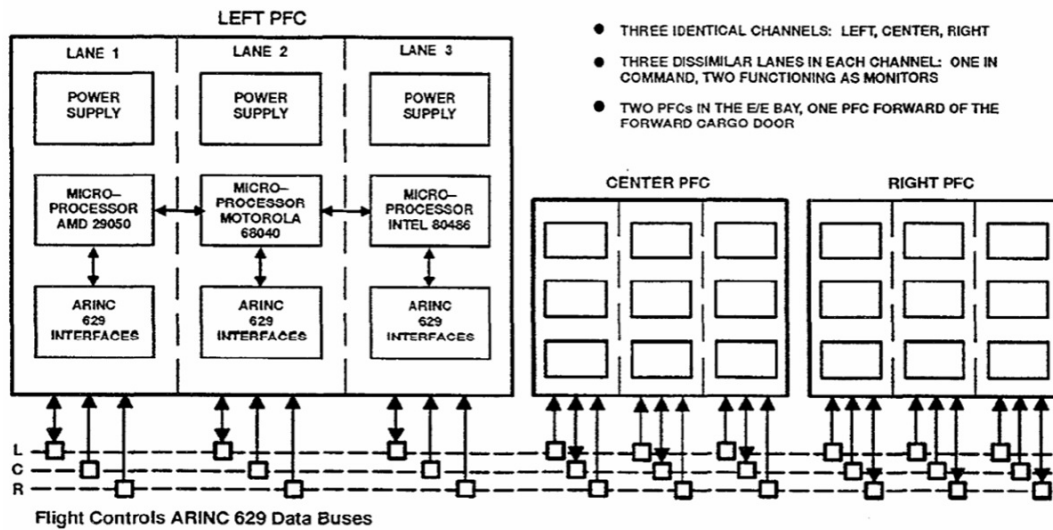


Figure A.10: Flight Control Computers for B777 [104].

### A.3 Loss-of-Control In-Flight (LOC-I)

Before explaining Fault Tolerant Control Systems, the loss of control in-flight (LOC-I) and related accidents have to be known because they can be prevented by Fault Tolerant Control Systems.

If there is a problem with the control of the aircraft due to a failure or fault, flight controls take more attention for preventing control related accidents. For these accidents, one of the main accident categories is Loss of Control In-flight (LOC-I). It has the highest percentage for the number of Fatal accidents between 2010 and 2014 [3]. The meaning of the LOC-I is “the flight crew was unable to maintain control of the aircraft in flight, resulting in an unrecoverable deviation from the intended flight path.” [1]. Due to LOC-I, fatal accidents for worldwide commercial jet fleet approximately doubled compared with the Controlled Flight into Terrain (CFIT) accidents and in connection with the LOC-I, 14 accidents, 1129 onboard fatalities, have occurred between 2008-2017 for Worldwide Commercial Jet Fleet [105]. The most important causal factors are:

1. Human-induced loss of control
2. System-induced loss of control
3. Environmentally-Induced Loss of Control [106]

Human-induced loss of control is directly related to interaction problems between automation and pilots. The relevant accident was Air France 447 disaster on May 31, 2009. Due to ice crystals in highly specific climate conditions, all three pitot tubes were blocked which was not supposed to be because of pitot heating. However, aircraft could have manipulated by hand. Also, autopilot disengaged automatically and the fly-by-wire system operated on alternate law. After accumulation of the ice crystals finished, right seated the first officer unintentionally and unexpectedly pulled back the side stick and climbed from 35.000 ft. to 38.000 ft. As a result, airspeed decreased dangerously. Despite stall warnings, aircraft lost approximately 10.000 ft. in a minute. After 3 to 4 minutes, aircraft crashed to the Atlantic Ocean and distressingly all crew and passengers were lost their life [107].

As previously stated, for flight control computers, stringent standards are in force. However, accidents due to system-induced loss of control related to flight control malfunctions continue to occur. Causal factors associated with systems-induced loss of control can be a loss of control power, authority, or effectiveness of the control system.

#### **A.4 Aircraft Accidents Related to Loss-of-Control In-Flight (LOC-I)**

There are numerous aircraft accident examples related to Loss of Control In-flight (LOC-I) [5].

In the first accident, American Airlines widebody Mc-Donnell Douglass DC-10-10, Flight AA191 crashed after takeoff on May 25, 1979. Due to improper maintenance procedures, aircraft's No:1 engine and pylon tore from entirely from the aircraft during the takeoff roll. After takeoff, during climbing, because of the damaged wing, hydraulic fluid leaked from the line in the same wing leading edge slats. Therefore, some of the slats are extended but some of them retracted. Rolling began to the left and aircraft crashed with a 112 degree bank angle and 21 degree pitch down angle.

In National Transportation Safety Board (NTSB) Final report, the accident cause was explained as “The probable cause of this accident was the asymmetrical stall and the ensuing roll of the aircraft because of the uncommanded retraction of the left wing outboard leading edge slats and the loss of stall warning and slat disagreement indication systems resulting from maintenance-induced damage leading to the separation of the No:1 engine and pylon assembly at a critical point during takeoff. The separation resulted from damage by improper maintenance procedures which led to the failure of the pylon structure.” [18].

In the second accident, Japan Airlines Boeing 747SR-100, Flight JL123 crashed on August 12, 1985. A tail strike which had occurred seven years before the accident affected the rear pressure bulkhead. It was repaired but the bulkhead due to explosive decompression was blown off. Also, the vertical fin was almost blown off. The most dangerous part was all hydraulics lost. The crew had no controls except four engines. They coped with taking control of the aircraft with differential thrust. However, aircraft was crashed into the mountainous area and all crew and passengers died. Recommendation about the airworthiness of the aircraft by Aircraft Accident Investigation Commission in Japan was “In this accident, ruptures of the fuselage tail, vertical fin, and hydraulics flight control systems were caused as a chain reaction by flow out of the pressurized air due to rupture of aft pressure bulkhead. To prevent the recurrence of such situations, a study should be initiated on the addition to the airworthiness criteria of the provisions concerning the fail-safe capability of peripheral structures, functional systems etc. against rupture of pressurized structural components such as the aft pressure bulkhead on a large aircraft.” [17].

In the third accident, United Airlines Mc-Donnell Douglas DC-10-10, Flight UA232 crashed on July 19, 1989. During an enroute flight, the fan disk of engine number two which was placed at the beginning of the vertical tail disintegrated. During disintegration, horizontal stabilizer was damaged. Also, three independent hydraulic systems were lost so do flight controls. The crew coped with taking control of the aircraft with differential thrust. The crew remarkably controlled the aircraft and managed to a hard landing on the ground. Despite the dramatic end, 111 of 296 people died. Recommendation to Federal Aviation Administration (FAA) by National Transportation Safety Board (NTSB) was “Encourage research and development of backup flight

control systems for newly certificated wide-body airplanes that utilize an alternative source of motive power separate from that source used for the conventional control system.” [16].

In the fourth accident, EL AL Cargo Boeing 747-200F, LY1862 crashed on October 4, 1992. During climbing No:3 engine pylon damaged and broke off. After that, no:4 engine also damaged. In the meantime, hydraulic systems 3 and 4 stopped functioning. Partial hydraulics were available so crew managed to control the aircraft to some degree. The crew decided to steer the aircraft to the airport. Due to asymmetric thrust, changing aerodynamic behavior, crippled controls resulted from partial hydraulics, the large size of the aircraft, it was crashed to the apartments. Recommendation by Netherlands Aviation Safety Board was “Review flight control design to ensure that flight control surfaces do not contribute adversely to airplane control in case of loss of power to a control surface.” [13].

In the fifth accident, United Airlines Boeing 737-200, N999UA crashed on March 3, 1991. During going around from the runway, the crew coped with controlling the aircraft but after several minutes aircraft hit to the ground with 200 kt. airspeed. The aircraft was totally destroyed. After the NTSB (National Transportation Safety Board) investigation, final report about the accident was not gotten through. However, a malfunction on the rudder PCU was determined.

In the sixth accident, USAir flight 427 Boeing 737-300, N513AU crashed on September 8, 1994. The crashed occurred during an approach to the runway. During the approach, aircraft began abrupt roll and slammed to the ground. After that, the same malfunction is determined about rudder PCU in the investigation. The final report says due to the movement of the rudder surface to its blowdown limit because of malfunction, pilots cannot control the aircraft. NTSB made recommendations to the Federal Aviation Administration (FAA). One of them is “Amend 14 Code of Federal Regulations Section 25.671(c)(3) to require that transport-category airplanes be shown to be capable of continued safe flight and landing after jamming of a flight control at any deflection possible, up to and including its full deflection, unless such a jam is shown to be extremely improbable. (A-99-23)” [12].

In the seventh accident, DHL Airbus A300B4-203F freighter, OO-DLL was hit by

the surface-to-air missile on November 22, 2003. The missile hit the left wing and destroyed some of the parts. Besides, all three hydraulics were lost and there was a fuel leakage for the left engine on the left wing due to damage. Primary flight controls were not manipulated by the pilots. Besides flaps, slats and spoilers did not move. However, the crew professionally controlled the aircraft only with the throttle. Finally, they unbelievably managed to land the aircraft. [5].

In [108], there are accidents related to Global Hawk UAV.

These are accidents directly related to aircraft and the UAV flight control systems. Besides, there are numerous accidents related to system-induced loss of control due to malfunction in the flight control system, surfaces, actuators or due to structural damage. Finally, after interpreting these disastrous accidents, designing or reconfiguring flight control system is a vital and life preserver for avoiding these type of accidents.

## APPENDIX B

### COMPARISON FOR THE UAV AND PIONEER UAV

#### B.1 The Difference With Regard to Aerodynamic Stability Derivatives Between The UAV and Pioneer UAV

In Table B.1, the difference between the UAV and Pioneer UAV with regard to stability derivatives, is found by Equation B.1.

$$Aero_{Difference} = Aero_{UAV} - Aero_{Pioneer} \quad (B.1)$$

Table B.1: The Difference With Regard to Aerodynamic Stability Derivatives Between The UAV and Pioneer UAV.

	$C_D$	$C_L$	$C_y$	$C_l$	$C_m$	$C_n$
$\alpha$	-0.3012	0.7976	0	0	0.9195	0
$\beta$	0	0	0.6184	0.0077	0	-0.0431
$p$	0	0	-0.0302	-0.0917	0	0.0406
$q$	0	1.6510	0	0	17.4971	0
$r$	0	0	0	-0.1453	0	0.1538
$\delta_a$	0	0	0	-0.0421	0	0.0195
$\delta_e$	0.0266	0.1096	0	0	-0.0005	0
$\delta_r$	0	0	-0.1339	0.0042	0	0.0715
	$C_{D_o}$	$C_{L_o}$	$C_{y_o}$	$C_{l_o}$	$C_{m_o}$	$C_{n_o}$
	-0.05	-0.0335	0	0	-0.1582	0



## APPENDIX C

### DEFINITIONS

#### C.1 Definitions of Fault-Tolerant

Definitions about system and state are given:

1. Faults: “An unpermitted deviation of at least one characteristic property or parameter of the system from the acceptable, usual, standard condition.”
2. Failure: “A permanent interruption of a system’s ability to perform a required function under specified operating conditions.”
3. Error: “A deviation between a measured or computed value (of an output variable) and the true, specified or theoretically correct value.”
4. Residual: “A fault indicator, based on a deviation between measurements and model equation based computations.”
5. Disturbance: “An unknown (and uncontrolled) input acting on a system.”

Definitions about functions are given:

1. Fault Detection : “Determination of the faults present in a system and the time of detection.”
2. Fault Isolation : “Determination of the kind, location and time of detection of a fault. Follows fault detection.”
3. Fault Identification : “Determination of the size and time-variant behaviour of a fault. Follows fault isolation.”
4. Fault Diagnosis : “Determination of the kind, size, location and time of detection of a fault. Follows fault detection. Includes fault isolation and identification.”

Definitions about models are given:

1. Quantitative model : “Use of static and dynamic relations among system variables and parameters in order to describe a system’s behaviour in quantitative mathematical terms.”
2. Qualitative model: “Use of static and dynamic relations among system variables and parameters in order to describe a system’s behaviour in qualitative terms such as causalities or if-then rules.”
3. Analytical redundancy: “Use of two or more (but not necessarily identical) ways to determine a variable, where one way uses a mathematical process model in analytical form.”

Definitions about System Properties are given:

1. Reliability: “Ability of a system to perform a required function under stated conditions, within a given scope, during a given period of time.”
2. Safety: “Ability of a system not to cause danger to persons or equipment or the environment.”
3. Availability: “Probability that a system or equipment will operate satisfactorily and effectively at any point of time.”
4. Dependability: “A form of availability that has the property of always being available when required. It is the degree to which a system is operable and capable of performing its required function at any randomly chosen time during its specified operating time, provided that the item is available at the start of that period.”

## **C.2 Definitions of Fault-Tolerant Techniques**

### **C.2.1 Redundancy**

Redundancy is basically using parts more than one. There are two types of redundancy, direct (hardware) and analytic (software) redundancy. Direct redundancy is about hardware [10]. For example, using two or three sensors for measuring the same thing. During a fault, a voting system can be used to find which one is the degraded

sensor shown in Figure C.1. In other words, for example, sensor-1 and sensor-2 send an accurate signal but sensor-3 sends faulty one. The Voting mechanism finds sensor-3 is not analogous with others. Also, in terms of control surfaces, using at least two actuators for one control surface is a good example of direct redundancy. For Airbus A320, these actuators are two for each aileron, two for each elevator and three for rudder shown in Figure C.2 [11].

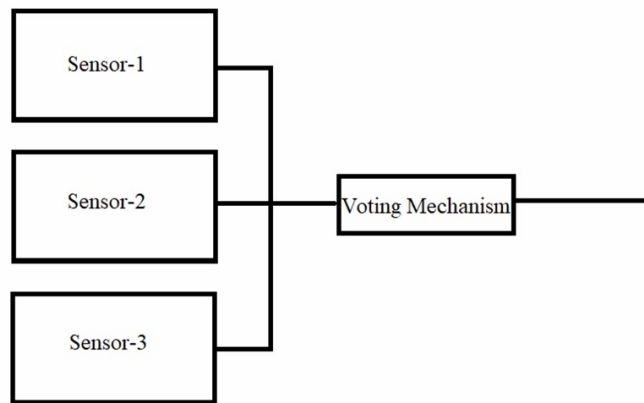


Figure C.1: Sensor direct (hardware) redundancy and Voting System for Sensors

On the other hand, analytic redundancy is related to software. Sometimes analytic redundancy is known as diversity [10]. Instead of using lots of hardware; some algorithms, mathematical models or observers can be used for analytic redundancy which is useful for cost and weight reduction [11]. Analytic redundancy is explained under the title of diversity.

For large aircraft, direct (hardware) redundancy can be achieved for flight control surfaces, flight control computers, sensors. An example of redundancy is an Airbus A320 which has two generators for electrical power which are supplied by engines. As stated before Airbus A320 is electrically controlled, hydraulically actuated. Because hydraulic power is also very important if the two engines shut down there is also a Ram Air Turbine (RAT) which is like a Cessna 172 propeller and extended automatically under aircraft's fuselage. It provides hydraulics power to flight control actuators. There are three hydraulics systems which identified by colour (green, blue and yellow) despite the fact that one of them is enough for safe flight shown in FigureC.2. Also, flight control computers are redundant in Airbus A320. As stated

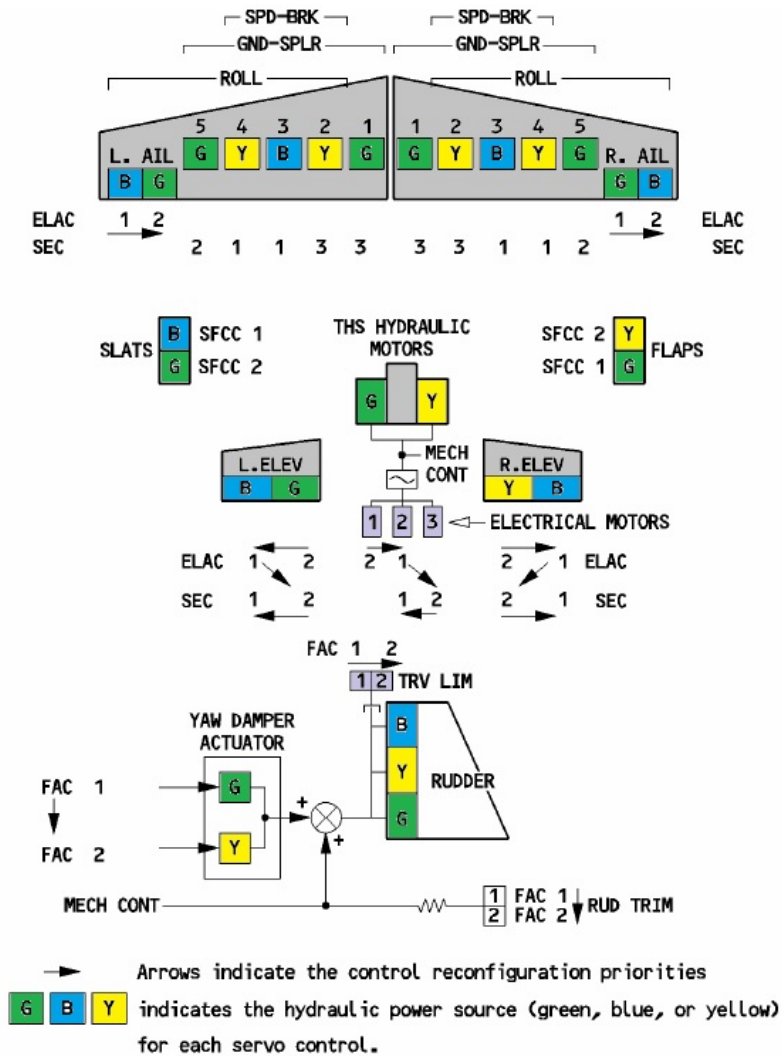


Figure C.2: Actuator direct (hardware) redundancy for control surfaces [96].

before it has two Elevator and Aileron Computers (ELAC), three Spoiler and Elevator Computers (SEC) and two Rudder Control Computers (FAC) [4]. Another example for redundancy is in Boeing 777 which has a triple-triple redundant Primary Flight Computers (PFC). To explain it in another way, Triple modular redundancy (TMR) concept is used for hardware redundancy, N-version dissimilarity concept is used for software redundancy or diversity in Boeing 777 [104].

## C.2.2 Diversity

Sometimes software redundancy referred to as diversity [10]. Three main forms of software diversity to achieve dependability:

1. N self-Checking: Software checks its own behaviour.
2. N-version Programming: There are N different programmes which do the same task but in a different way. Each of them sends a signal to a voter and by majority checking, the best signal is chosen and a faulty one can be found [10].
3. Recovery Blocks: Variant Execution Scheme is sequencing. The consistency of the input data is implicit and based on backward recovery. Error detection is done by acceptance tests [109]. If the primary block finds the output of the block is erroneous by acceptance test, the same input entered to the alternate block. The sequence is continued in this manner shown in Figure C.3.

Diversity and redundancy are interlocked in terms of flight control computers because there is more than one computer and each computer has a different software or different lane.

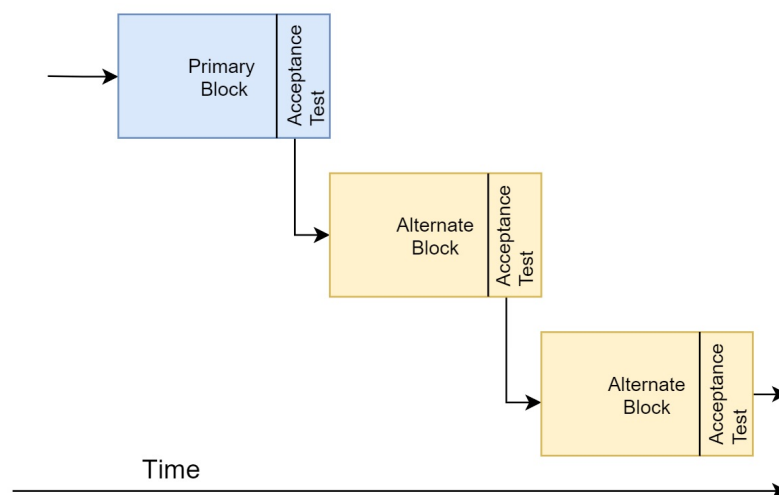


Figure C.3: Recovery Blocks

### **C.2.3 Segregation**

Segregation is related to isolation and separation of each redundant system [10]. For example, large body aircraft have separated three hydraulic lines.